2020-01-01

Fluvial Interactions of the Jurassic Salt Wash Member of the Morrison Formation with the Gypsum Valley Salt Diapir, CO

Clair Henry Bailey
University of Texas at El Paso

FLUVIAL INTERACTIONS OF THE JURASSIC SALT WASH MEMBER

OF THE MORRISON FORMATION WITH THE

GYPSUM VALLEY SALT DIAPIR, CO

CLAIRE H. BAILEY

Doctoral Program in Geological Sciences

APPROVED:

Richard P. Langford, Ph.D., Chair

Katherine A. Giles, Ph.D., Co-Chair

Benjamin Brunner, Ph.D.

Terry L. Pavlis, Ph.D.

Gary Weissmann, Ph.D.

Stephen L. Crites, Jr., Ph.D.
Dean of the Graduate School

Dedication

For Mom and Dad. For always believing I could be anything I put my heart into.

FLUVIAL INTERACTIONS OF THE JURASSIC SALT WASH MEMBER OF THE MORRISON FORMATION WITH THE GYPSUM VALLEY SALT DIAPIR, CO

by

CLAIRE H. BAILEY, B.S., M.S.

DISSERTATION

Presented to the Faculty of the Graduate School of

The University of Texas at El Paso

in Partial Fulfillment

of the Requirements

for the Degree of

DOCTOR OF PHILOSOPHY

Department of Geological Sciences

THE UNIVERSITY OF TEXAS AT EL PASO

May, 2020

Acknowledgements

First, I would like to thank my family. Mom thank you for being my rock always. For believing that I was stronger than I ever believed. For watching me fall over and over again and reminding me get up and keep it moving. For supporting me not only emotionally on this journey but also financially. To my sister Liz, thanks for always cheering me on and bringing me smiles when I needed them most. To my pup Penny, thank you for being the bright spot in each and every day. To my father, I carry your spirit, your light, and love with me always.

This work is possible through the support of the Institute of Tectonic Studies Salt-Sediment Interaction Research Consortium at The University of Texas at El Paso and its industry sponsors. Current sponsors BHP Billiton, BP, Chevron, ConocoPhillips, ExxonMobil, Hess, Kosmos, Repsol, and Total USA. Thank you for your financial support and feedback on consortium presentations throughout my time as a student. Additional funding for field and laboratory work was generously provided by the Geological Society of America Research Grant, ExxonMobil Research Grant and Tech Scholarship, the American Association of Petroleum Geologists Southwest Section Research Scholarship, SIPES Foundation Earth Science Scholarship, West Texas Geological Society Scholarship, and from the UTEP Department of Geological Sciences. Other forms of support were received from the NSF GK-12 graduate fellowship.

To the numerous field assistants, I have had throughout my research Nathan Beck, Samantha Ramirez, Elizabeth Heness, Itza Fong, Keith Barnes, Raphael Delfin, and Jennifer Dixon thank you for your time, the company on death marches, ideas, laughs, and most of all for carrying rocks. Also important are all the friends who watched Penny while I was out in the field or attending conferences: Jim Rutkofske and Lorraine Negron. A special thank you to Nila Matsler for logistical support over the course of my time as a student apart of S-SIRC.

To all the friends who've become family along my journey at UTEP each one of the following of your friendships has meant the world to me and I am excited to call y'all colleagues and friends. Rachel Slank thank you for supporting me through this journey. Whether that meant flying to be right by my side when I needed it most or over the phone. To Jim Rutkofske, John Olgin, Amanda Labrado, Austin Hill, Elizabeth Heness, Jade Brush, Tai Subia, Valeria Hurtado, Kristen Gonzalez, Kat Salas, Anna Mwangi, Loraine Negron, Gail Arnold, and Evey Gannaway-Dalton thank you for the laughter, memes, hugs, and words of encouragement. I would like to thank Amanda Owen, Sharon McMullen, Tim Demko, and William Esch for their advice and passionate discussions about the Salt Wash. To my geology brothers Darryl Reano and Ben Linzmeier for all the helpful tips, proof reading, and discussions of our shared love for geology. To Lisa White, Karen Grove, and Jim Neiss without whom I would have never discovered my love and passion for geology. Thank you three for taking a girl from the Bayview and opening her eyes to a new way of looking at the world. The moment I met you three my life changed. To Laura Serpa and Terry Pavlis for being part of the group that has watched me grow since high school. Thank you for the mentorship and push to come to UTEP.

I would like to thank my Committee Benjamin Brunner, Terry Pavlis, and Gary Weissmann for challenging me as a scientist, mentoring, for the awesome discussions on my research, and most of all edits!

Last but most important are my advisors Rip Langford and Kate Giles. I am so incredibly lucky to have such passionate advisors. Kate thank you for your support, advice, encouragement, and pushing me to work at my best. Rip thank you for the support, edits, weekends, but most of all thank you for sharing your passion for the field and stratigraphy of the Colorado Plateau with me. It was a pleasure to learn from you both.

Abstract

Gypsum Valley diapir in Gypsum Valley Colorado is an ideal location to investigate the interaction between a fluvial system and a diapir going through late stage collapse and rise. The outcrop exposures in Gypsum Valley allow for the analysis in changes of the fluvial system of the Salt Wash Member of the Morrison Formation as it gets redirected by the salt wall and deposits sediment on top of, on the margins, and in the Disappointment and Dry Creek minibasins. Previous work has focused on understanding and predicting how fluvial systems react when they encounter a salt diapir, but all the analysis and data collected focuses on what the stacking patterns are like in the adjacent minibasins which are still far from even the margin of the salt diapir. This dissertation is a field-based study that uses a stratigraphic and petrographic analysis of the Salt Wash Member of the Morrison Formation to document and describe deposition of fluvial sandstones on top of, on the margin, and in the adjacent minibasins of the Gypsum Valley diapir.

Gypsum Valley is located within the Paradox Basin and is the southernmost northwest trending salt diapir within the basin. Gypsum Valley can be broken into two regions during deposition of the Salt Wash Member: Little Gypsum Valley is the northern region of the diapir that was subsiding during Salt Wash deposition, which overlies the Summerville and Entrada Formations, which overlie the diapiric caprock. The southern region is Big Gypsum Valley which formed enough of a topographic high during early deposition of the Salt Wash Member to restrict fluvial deposition to the margins of the diapir. The Salt Wash Member crops out around the periphery of the diapir and overlying the salt caprock in small outcrops Big Gypsum Valley, as well as overlying the Summerville Formation on top of the diapir in Little Gypsum Valley.

The Salt Wash Member at Gypsum Valley can be broken into four stratigraphic units: 1) interbedded sandstone channels and mudstones (ISCM), 2) amalgamated sandstone channels (ASC), 3) isolated sandstone channels (ISC), and 4) laterally stacked sandstone channels (LSSC). Each of these units was mapped throughout Gypsum Valley to determine how stacking patterns varied around the diapir to document thinning, erosion, onlap, and truncation of Salt Wash Member strata during deposition of each of the stratigraphic units. Changes in the fluvial fairways around and across, as they interacted with the Gypsum Valley diapir were also mapped. These relationships were used to determine the timing and relative rate of subsidence, diapir rise, and how this impacted change in sediment supply.

These observations led to the conclusion that the stratigraphic relationships documented represent wedge style halokinetic sequences and suggests that sedimentation of the fluvial Salt Wash Member was able to keep up with the local accommodation created by the Gypsum Valley Salt Diapir. When the diapir was a topographic high it was a zone of bypass or erosion creating truncation. This research also shows that fluvial systems can be influenced by salt movement at different scales and that deposition can be abundant on the flanks of diapirs.

Petrographic analysis of the Salt Wash Member suggests that the more quartzose and rounded signature of the analyzed minerals suggests there was possibly recycling of sediment from older eolian stratigraphy. In LGV, the main authigenic cement present are calcite cements. Ferroan dolomite and dolomite cements are mainly only present in BGV where there is the presence of deep structures like the megaflap and radial faults. Analysis of the distribution of authigenic cements and porosity show that there are no major stratigraphic changes between units of the Salt Wash Member. The analysis also suggests there are not observable changes with proximity to the diapir. Instead differences in authigenic cements from LGV to BGV are due to

the presence of deep structures that can bring basinal fluids to the surface in BGV. Whereas older structures of shoulders prevent this process in LGV.

One specific area studied in detail is ‘the Hat’ syndepositional syncline, that is composed of strata mainly from the Salt Wash Member. This study focuses on documenting stratigraphic changes within the syncline and describing how the fluvial system fills a subsiding minibasin over the top of a diapir. There are 3 marked growth sequence boundaries that represent changes in the rate of subsidence of the minibasin. The Salt Wash Member is the thickest at this location and is a very muddy stratigraphic section. Sandstone strata are present in their typical thicknesses; however, the intervening mudstones thicken into the syncline. Sandstones onlap underlying sequence boundaries. This indicates that the subsiding minibasins trapped fluvial fines otherwise would have bypassed the diapir.

The results of this dissertation contribute to understanding stacking patterns and potential diagenetic alteration of the sandstones deposited around diapirs. This has important implications for understanding reservoir distribution and quality around diapirs as well as other components of the hydrocarbon system such as seal and trap formation.

Table of Contents

List of Tables

List of Figures

Chapter 1: Introduction

This dissertation is a study of the interactions between the Salt Wash Member of the Jurassic Morrison Formation and Gypsum Valley Salt diapir, which was in its final stages of deformation during Morrison Deposition (Stokes and Phoenix, 1948; Trudgill, 2011). The dissertation is broken into three chapters. Chapter two describes the interactions of the fluvial Salt Wash Member of the Morrison Formation around the Gypsum Valley salt diapir. Chapter three focuses on understanding the diagenetic changes in the sandstones of the Salt Wash Member and how it is related to near-diapir fluid flow. Chapter four documents and interprets the fluvial architecture of the Salt Wash Member deposited over the crest of the Little Gypsum Valley diapir at 'The Hat' syncline.

The main objectives of this research are to better understand the interaction of fluvial systems with salt diapirs. This research focuses on documenting and interpreting the fluvial architecture, stacking patterns, facies distribution, and diagenetic changes of the Salt Wash Member of the Morrison Formation on top of, proximal, and adjacent to the Gypsum Valley Diapir. Previous work on this topic focuses on understanding fluvial systems kilometers away from the diapir margin in the adjacent minibasins and the models created to try and predict fluvial behavior are based on those depositional stacking patterns. This study is one of the few that documents significant deposition by a fluvial system on top of and on the margins of dynamic salt diapir movement.

To better understand the dynamic between these two systems, this outcrop study focused on analyzing changes in thickness, facies, and sand to mud ratios around the diapir. Twenty-four composite stratigraphic sections were measured adjacent to the diapir margin, within Little Gypsum Valley on top of the diapir, and distally away from the diapir margin into the adjacent

Disappointment and Dry Creek minibasins in order to describe the quality and distribution of potential reservoir sandstones. The Salt Wash Member at Gypsum Valley can be broken into four stratigraphic units: 1) Interbedded sandstone channels and mudstones 2) amalgamated sandstone channels 3) isolated sandstone channels, and 4) laterally stacked sandstone channels. Stratigraphic units and key beds were mapped using a combination of QGIS and panoramic photos to understand the lateral changes, stratigraphic relationships, and to document onlap, truncation, and erosional relationships with older strata and the diapir. Samples were collected from each stratigraphic unit throughout measured sections. These samples were made into thin sections stained and impregnated with blue epoxy for petrographic analysis. All samples were analyzed, and 75 samples were point counted 300 points per slide for detailed analysis to document and map the distribution of authigenic cements and porosity changes in proximity to the Gypsum Valley Diapir.

1.1 BACKGROUND

Gypsum Valley is located within the Paradox Basin and is the southernmost of the northwest-trending salt diapirs within the basin. Gypsum Valley is 40 km long and 3-5 km wide and exposes strata that range from the Pennsylvanian through the Cretaceous. Gypsum Valley can be broken into two regions. To the north is Little Gypsum Valley. In Little Gypsum Valley the diapir was subsiding during deposition of the Salt Wash Member and is therefore exposes Salt Wash Member strata across the top of the diapir. In this study Little Gypsum Valley was studied in two regions ‘the Hat’ and Grassy Hill. Big Gypsum Valley is the southern region of the diapir where Permian salt is exposed. There is thinning, erosion, onlap, and truncation of the Salt Wash Member, and exposures are restricted to the margins of the salt diapir, except for deformed synclines around the margins of the valley. For the purposes of this study, Big Gypsum

Valley exposures were grouped into four different study areas: 1) Anderson Mesa, 2) the southeastern margin of Big Gypsum Valley, 3) the southwestern margin of Big Gypsum Valley, and 4) the Megaflap (Figure 1.1).

This study subdivides the Salt Wash Member at Gypsum Valley into four stratigraphic units: 1) interbedded sandstone channels and mudstones (ISCM), 2) amalgamated sandstone channels (ASC), 3) isolated sandstone channels (ISC), and 4) laterally stacked sandstone channels (LSSC). The variations in thickness, sandstone percentages, paleocurrent directions, and structural, and stratigraphic relationships with older strata of each of these units was mapped and documented throughout Gypsum Valley.

1.2 SIGNIFICANCE AND IMPLICATIONS

This dissertation is one of the first to document and describe changes of a fluvial system as it deposits sediment on top of and on the margins of a dynamic salt diapir. This study adds to the literature that attempts to address and predict fluvial stacking patterns and flow surrounding a salt diapir. The results contradict previous studies, which suggest that fluvial channels are concentrated in the centers of the intervening minibasins (Elston and Landis, 1960; Hazel, 1994; Prochnow et al., 2006; Matthews et al., 2007; Banham and Mountney, 2013b; Venus et al., 2015). Previous studies have focused on documenting and predicting the stacking patterns and flow pathways as fluvial systems interact with salt diapirs (Banham and Mountney, 2013b, 2013a). These bodies of work focus on deposition of fluvial systems in adjacent minibasins and rarely address what happens to those fluvial systems as they deposit sediment on the margins and on top of salt diapirs (Elston and Landis, 1960; Hazel, 1994; Prochnow et al., 2006; Matthews et al., 2007; Banham and Mountney, 2013b; Venus et al., 2015). The previous work done to understand fluvial systems predict that within the adjacent minibasins a consistent rate of

subsidence and a consistent rate of sediment supply fluvial systems will deposit dominantly amalgamated sandstone packages of sediment (Banham and Mountney, 2013b, 2013a). In addition, the models built assume that salt diapirs act uniformly along strike, and don't account for depocenters that can occur on top of or along the margins. The results of this study indicate the interaction between these two systems can be much more dynamic. Fluvial deposition can occur on top of the diapir and along the margins as well as in the minibasins.

This study supports the theory that subsidence rate is an important driver to the stacking pattern of the fluvial system, but the rate of subsidence can vary, even over a short amount of time. It also can vary spatially over very short distances (<1 km). Deposition of amalgamated sandstone packages vs more interbedded muddy floodplain facies can vary based on diapir rise or subsidence and variation in diapirism can occur over kilometers.

This study can serve as an outcrop analog for similar fluvial salt interactions in other salt basins throughout the world where there is hydrocarbon development. In these basins it is important to understand and be able to predict where the thickest and best quality reservoir sandstones might be located on top of diapirs, along the margins of diapirs, or in adjacent minibasins. It is also important to understand whether the other components of a hydrocarbon system are in place. For example, the muddy facies deposited on top of a stacked fluvial package can act as a seal.

1.3 SUMMARY OF CHAPTERS

The first two papers are in chapters 2 and 3. They focus on understanding the interaction between the fluvial system of the Salt Wash Member with the Gypsum Valley Diapir at a larger scale, around the periphery of Gypsum Valley. The fourth chapter focuses on the formation of

the ‘the Hat’ syncline formed within the minibasins formed over the top of the diapir within Little Gypsum Valley.

1.3.1 Chapter 2: Halokinetic Influence on Fluvial Depositional Patterns in the Salt Wash Member of the Jurassic Morrison Formation, Gypsum Valley Salt Wall, Paradox Basin, Colorado

The fluvial systems of the Jurassic Salt Wash Member of the Morrison Formation were deposited throughout Gypsum Valley and within the adjacent minibasins. In Little Gypsum Valley the Salt Wash Member was deposited on top of the diapir as it subsided. In Little Gypsum Valley two areas (Grassy Hill and ‘The Hat’) both form synclines on top of the diapir during deposition of the Salt Wash Member. Subsidence over the top of the diapir at these two locations leads to thickening of the Salt Wash Member. Changes in thickness and sandstone percentage mark changes in the rates of subsidence throughout deposition of the Salt Wash Member and controlling the resulting stacking patterns. In Big Gypsum Valley, the opposite occurs during deposition of the Salt Wash Member. There is thinning, pinch out, truncation, onlap, and erosion of each of the stratigraphic units of the Salt Wash Member. These relationships seen within the Salt Wash Member, with older stratigraphy, and with the diapir are evidence of wedge style halokinetic sequences which suggests that the diapir was sometimes a topographic high and a zone of bypass but mostly enough of a topographic low that deposition by the fluvial system was able to keep up with local accommodation.

1.3.2 Chapter 3: Diagenetic Changes Within the Jurassic Fluvial Salt Wash Member Sandstones of the Morrison Formation Related to Fluid Interactions with the Gypsum Valley Salt Diapir, Paradox Basin, CO

This study aims to add to the body of knowledge in Gypsum Valley and throughout the literature to understand the distribution of authigenic cements and how they vary on top of a diapir,

on the margin, and distal within adjacent minibasins. Sandstones deposited throughout Gypsum Valley by the Salt Wash Member are quartz arenites composed mostly of quartz minor amounts of feldspars, lithics, and other accessory minerals. These sandstones have evidence of alteration by fluids flowing around the diapir by authigenic cements. Within Little Gypsum Valley porosity is highest in samples over the top of the diapir, calcite cements are common, and quartz over growths are at high amounts. In Big Gypsum Valley porosity is lower, calcite cements are less abundant and dolomite cements are abundant. The differences in cement types from Little Gypsum Valley to Big Gypsum Valley are likely related to the presence of structures in Big Gypsum Valley that carry basinal fluids to the surface.

1.3.3 Chapter 4: Fluvial Architecture of a Top Salt Minibasin; Jurassic Salt Wash Member of the Morrison Formation at "The Hat" Syncline, Gypsum Valley Salt Wall, Colorado

The Hat is a syncline that formed syndepositionally within a minibasin over the top of the Gypsum Valley diapir during Salt Wash Member deposition. As a result of the subsidence of this minibasin over the top of the diapir the Salt Wash Member forms a thickened muddy stratigraphic section. During deposition of the Salt Wash Member there are three marked periods of subsidence defined by onlap and truncation of Salt Wash Member channels deposited across the structure. Each of these marked events represents a change in the rate of subsidence during deposition of the Salt Wash Member. The first marked event defines the initiation of subsidence at 'the Hat' and the subsequent one defines an increase in subsidence rate, and the last represents a decrease in subsidence and filling of the basin. This study is one of the first to describe deposition of a fluvial system within a minibasin over the top of a diapir.

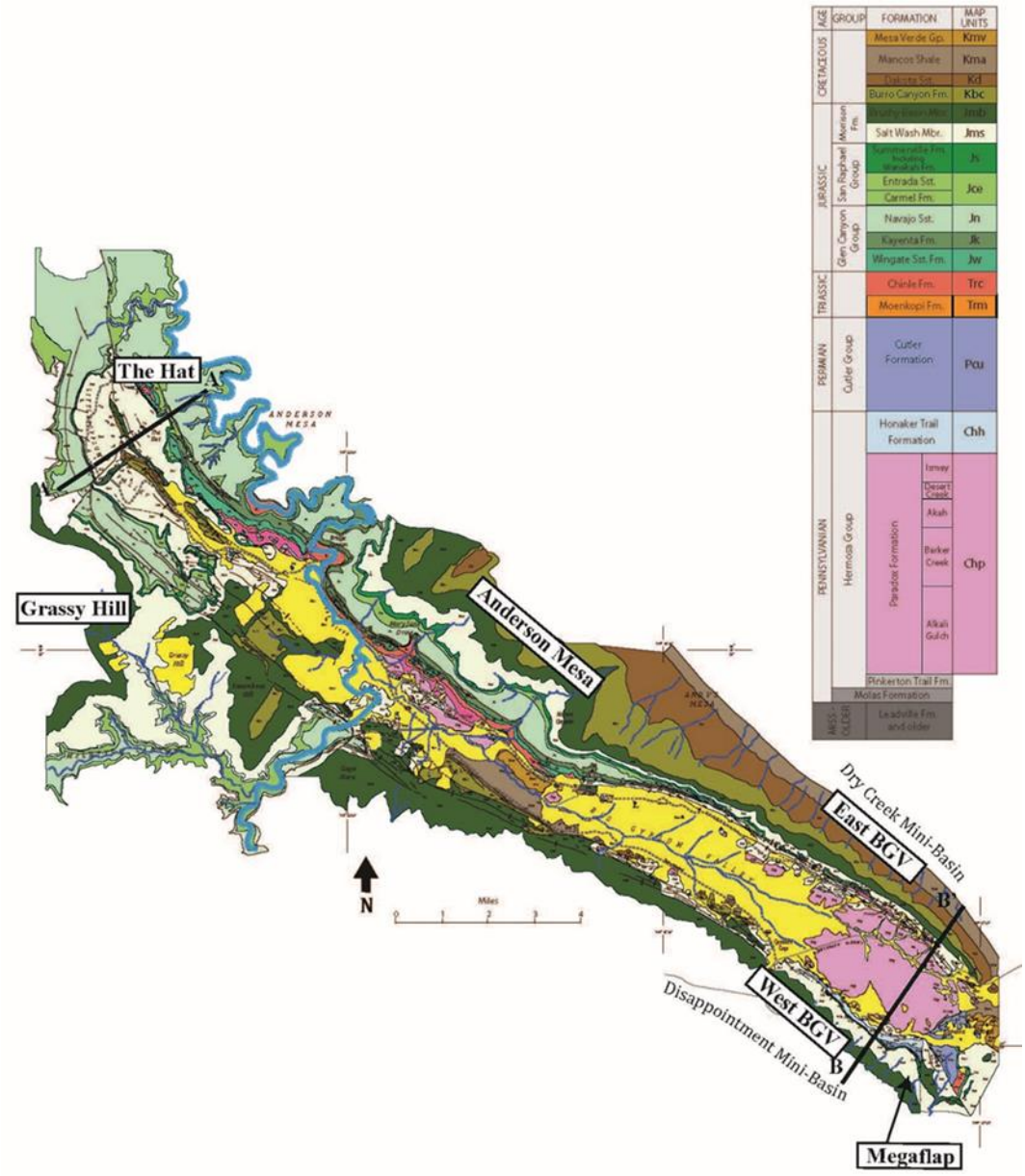

Figure 1.1: Geologic Map of Gypsum Valley

Chapter 2: Halokinetic Influence on Fluvial Depositional Patterns in the Salt Wash Member of the Jurassic Morrison Formation, Gypsum Valley Salt Wall, Paradox Basin, Colorado

Introduction

Previous studies addressing the interaction between fluvial depositional systems and passive salt diapirs document the stacking patterns and fluvial architecture primarily in the adjacent mini-basins, which can be kilometers away from the salt diapir (Elston and Landis, 1960; Hazel, 1994; Prochnow et al., 2006; Matthews et al., 2007; Banham and Mountney, 2013; Venus et al., 2015). These studies infer probable depositional patterns on the flank or overlying the diapir from trends documented within the adjacent minibasin. However, studies of strata from other depositional systems along diapir contacts suggests that dramatic changes in depositional environment may occur immediately adjacent to the diapir (Giles and Lawton, 2002; Giles and Rowan, 2012). This study specifically documents how fluvial systems behave when they are proximal to or overtop a salt diapir. It compares the fluvial architecture and depositional trends around and over the top of a salt wall as well as out into the adjacent flanking minibasins. Understanding the distribution of fluvial sandstones around diapirs can help predict the location of the thickest potential reservoirs for hydrocarbon development. Further we can better understand the potential to have a seal or trap in place.

In the Paradox Basin of the Colorado Plateau, Gypsum Valley exposes strata ranging in age from Triassic through latest Jurassic that can be observed in depositional contact with the Gypsum Valley salt wall (Stokes and Phoenix, 1948; Shawe, 1968; Heness, 2016; Escosa et al., 2018). The youngest of the strata, with exposed depositional relationships adjacent to and overlying the northwestern end of the salt wall is the Latest Jurassic Morrison Formation (Stokes

and Phoenix, 1948; Escosa et al., 2018). This exposure offers an unparalleled opportunity to study how passive diapirism effects fluvial depositional systems. In this study, we document and interpret the fluvial architecture of the Salt Wash Member of the Jurassic Morrison Formation deposited on top of, proximal, and distal to the Gypsum Valley salt diapir. We document the following in the Salt Wash Member: 1) fluvial depositional facies and architecture stacking patterns and stratigraphic distribution, 2) the thickness changes in the Salt Wash Member, and 3) changes in flow paths of the fluvial system. We then relate the depositional trends documented to spatial and temporal variations in subsidence and uplift along the length of the Gypsum Valley salt wall.

Geologic Background

The Paradox Basin is a Late Paleozoic foreland basin that extends across eastern Utah and southwestern Colorado (Figure 2.1) and contains nine northwest trending salt walls exposed by Neogene erosion of the Colorado Plateau (Shoemaker et al., 1958, 1958; Elston and Landis, 1960; Elston et al., 1962; Hite et al., 1972; Barbeau, 2003). The diapirs are flanked by synclinal minibasins formed by withdrawal of the underlying salt, which feeds the adjacent diapirs (Trudgill et al., 2004; Hudec et al., 2009; Trudgill, 2011). The Paradox Basin subsided during the Middle Pennsylvanian to Permian due to flexural loading by thrusts along the SW flank of the Uncompahgre Uplift (Barbeau, 2003) associated with Ancestral Rocky Mountains tectonism (Dickinson and Lawton, 2003; Trudgill, 2011) (Figure 2.1). The basin was largely filled by the middle Permian (Elston et al., 1962; Hite et al., 1972; Barbeau, 2003; Kluth and DuChene, 2009). During the Pennsylvanian, fluctuation of glacioeustatic sea level resulted in cyclic deposition of approximately 2500 m of interbedded evaporites, dolomite and shale that form the Paradox Formation (Borden, 1952; Hite and Gere, 1958; Hite et al., 1972; Hite and Buckner, 1981).

Differential sediment loading of the Paradox Formation by the prograding Permian Cutler Group derived from the Uncompahgre Uplift initiated passive diapirism and growth of the salt walls (Ge et al., 1997; Trudgill et al., 2004; Trudgill, 2011). Salt wall rise was most rapid in the Permian with decreased activity into the Triassic (Shoemaker et al., 1958; Lawton and Buck, 2006; Trudgill, 2011; Escosa et al., 2018). In the Mesozoic, minibasins adjacent to salt walls throughout the Paradox Basin largely filled and passive diapirism concluded by the end of the Jurassic (Cater and Craig, 1970; Shawe, 1970; Ge et al., 1997). Diapirism waned in the Triassic in the northern Paradox Basin (Trudgill, 2011), and in the Late Jurassic in the southern Paradox Basin (Trudgill et al., 2004; Rowan et al., 2016; Escosa et al., 2018). Across the areal extent of the Paradox Basin, Jurassic Salt Wash Member strata are not thought to be affected by salt tectonics except at Gypsum Valley and Paradox Valley salt walls (Elston and Landis, 1960; Vogel, 1960; Cater and Craig, 1970; Trudgill, 2011; Rowan et al., 2016).

Gypsum Valley

Gypsum Valley, located in southwestern Colorado, is the southernmost exposed northwest-trending salt wall in the Paradox Basin and is approximately 35 km long and 2-3.5 km wide (Landis, 1961; Escosa et al., 2018) (Figure 2.2). To the northeast of the Gypsum Valley salt diapir is flanked by the Dry Creek salt withdrawal minibasin and to the southwest by Disappointment Valley minibasin. Salt flowing from beneath the sinking minibasins fed passive growth of the salt diapirs (Trudgill, 2011). Passive diapirism, which is syndepositional growth of a diapir whose exposed crest rises as sediments accumulate around it, began in the Permian and continued into the Cretaceous in Gypsum Valley (Donald C. Barton (2), 1933; Nelson and Fairchild, 1989; Vendeville and Jackson, 1991; Rowan et al., 2016; Escosa et al., 2018). Within Gypsum Valley there are large regions of exposed diapiric caprock composed primarily of

gypsum, but locally contain inclusions of dolomite and black shale. Strata from Late Pennsylvanian to Cretaceous age dip away from the diapir and thicken into the adjacent minibasins. Typically, older strata dip more steeply than younger strata (Stokes and Phoenix, 1948; Escosa et al., 2018).

Gypsum Valley can be divided into two geomorphic areas: Little Gypsum Valley forms the narrower northwest end and Big Gypsum Valley forms the wider southeast end of the valley (Figure 2.2) (Stokes and Phoenix, 1948; Escosa et al., 2018). On the southwestern margin of Big Gypsum Valley, Pennsylvanian- Permian age strata form a megaflap; a panel of steeply dipping to vertical strata extend several kms along the side of a diapir (Rowan et al., 2016; Escosa et al., 2018). During the Jurassic the megaflap was exposed and formed a topographic high that was onlapped/overlapped by the Morrison Formation (Figure 2.2, 2.3) (Escosa et al., 2018). At its northern end, the megaflap is buried beneath the Morrison Formation, which overlies the megaflap in angular unconformity (Figure 2.2, 2.3). Along strike to the south the megaflap decreases in dip and is terminated by a pair of radial faults (Escosa et al., 2018). Continuing along the southwestern flank of Big Gypsum Valley, the Salt Wash and Brushy Basin Members of the Morrison Formation are not present along the margin of the diapir. Several minor faults offset these units which also exhibit minor folding parallel to the diapir margin.

On the northeastern flank of Big Gypsum Valley, seismic and well logs establish that a counterregional fault accommodated a greatly thickened Pennsylvanian to Early Permian section (Rowan et al., 2016; Escosa et al., 2018) (Figure 2.3). The Gypsum Valley diapir terminates to the southeast in a moderately plunging nose of salt in the footwall of the counterregional fault (Escosa et al., 2018). In the northeastern hanging wall of the fault, Cretaceous strata are exposed at the surface along the southern termination of the diapir. To the northeast, along the diapir

margin, onlap and erosional truncation result in a thin Mesozoic section that dips away from the diapir. The Chinle, Kayenta and Entrada Formations thin towards the southwest along this margin, with the uppermost Entrada Sandstone dipping at approximately 30 degrees away from the diapir (Figure 2.2). The Salt Wash Member of the Morrison Formation onlaps the older strata and, near the southern end extends onto the Paradox caprock of the diapir. Dips range from 3 to 9 degrees to the northeast. Along the diapir margin, the flanking minibasin strata are offset along a fault that increases in displacement to a point approximately 2 km southeast of the Dolores River (Figure 2.2). This forms a topographic high, Anderson Mesa. Dips decrease along the mesa, until they are essentially flat in Little Gypsum Valley (Figure 2.2).

In Little Gypsum Valley, the exposed halokinetic deformation is more symmetrical, and Late Jurassic strata are less deformed. Langford et al. (2018) show that the diapir began to be constricted and partially buried, beginning in the Triassic. The Triassic Chinle Formation and overlying Jurassic Glen Canyon Group form "salt shoulders" that bury the margins of the Gypsum Valley Salt Diapir (Langford et al., 2018). The Entrada Sandstone covered most of Little Gypsum Valley in the Late Jurassic and typically underlies the Jurassic Summerville Formation and the Salt Wash Member of the Morrison Formation (Langford et al., 2018). The result of this progressive diapir-burial history is that the Salt Wash Member of the Morrison Formation is exposed along and within most of the periphery of the Gypsum Valley diapir. It is buried along the southeastern margin of Big Gypsum Valley, and near the counter regional fault (Figure 2.2). It is eroded from along the diapir margin along the northern flank of Little Gypsum Valley (Figure 2.2). However, complete sections of the Salt Wash Member can be measured around the diapir, and within the diapir in 'the Hat' syncline, a syndepositional syncline formed

above the diapir (Figure 2.2). Another complete section can be measured west of 'the Hat' syncline, on the Grassy Hills, flanking a second syncline (Figure 2.2).

Morrison Formation Stratigraphy

The Late Jurassic Morrison Formation was deposited by distributive fluvial systems across the western interior of North America (Craig, 1955a; Turner and Peterson, 2004; Owen et al., 2015c, 2015b). It covers an area of 150,000km^2 from the Sevier foreland eastward to the Rio Grande rift and Front Range of Colorado (Turner and Peterson, 2004; Dickinson and Gehrels, 2008) (Figure 2.1). The maximum thickness of the Morrison Formation, where it is not affected by salt tectonism is found in the Henry Mountains where it measures 237m. However, it reaches a thickness of over 340 m in the Disappointment Valley syncline adjacent to the Gypsum Valley salt wall, where it thickens into the salt withdrawal minibasins (Shawe, 1968). The Morrison Formation includes ten formal members, which are best known on the Colorado Plateau, where they consist entirely of terrestrial depositional systems (Craig, 1955a; Peterson, 1984; Turner and Peterson, 2004). In the Gypsum Valley area only two members are recognized, the Salt Wash Member overlain by the Brushy Basin Member (Figure 2.2). The Salt Wash Member consists of interbedded tan sandstones and purple, green, and red shales. The overlying Brushy Basin Member contains thick mudstones with isolated coarse-grained and gravelly channels fills.

The main source of sediment for the Morrison Formation in the Late Jurassic has been inferred to lie to the south along the uplifted rift shoulders of the Mogollon Highlands, which were associated with the late stages of active rifting along the Bisbee Basin from 165-145 Ma (Craig, 1955a; Dickinson and Gehrels, 2008; Owen et al., 2015a) (Figure 2.1). The Morrison Formation was deposited in a low accommodation backbulge basin produced by thrusting in the

Sevier thrust belt located to the west and north of the Colorado Plateau (DeCelles and Currie, 1996; Currie, 1998).

Geologic evidence and numerical models run by several researchers confirm that the climate in the southern United States during the Late Jurassic was dry (Moore et al., 1992; Valdes and Sellwood, 1992). Models present warmer temperatures in the summer months (40-45° C) with cooler temperatures (20° C) in the winter months (Moore et al., 1992). Models suggest that evaporation rates were significant year-round within an overall semi-arid climate (Moore et al., 1992; Valdes and Sellwood, 1992).

Salt Wash Member Stratigraphy

The Salt Wash Member is the most extensively exposed member of the Morrison Formation spanning central Utah, west-central Colorado, northeast Arizona, and northwestern New Mexico (Craig, 1955a; Mullens and Freeman, 1957a; Turner and Peterson, 2004). The Salt Wash Member has been described as an eastward prograding distributive fluvial system (Craig, 1955a; Mullens and Freeman, 1957a; Weissmann et al., 2010; Owen et al., 2015a, 2015c). Several workers have described and characterized the Salt Wash Member as amalgamated, vertically stacked sandstone fluvial channel packages interbedded with floodplain siltstones and mudstones (Stokes, 1944; Craig, 1955a; Mullens and Freeman, 1957a; Peterson, 1984; Turner and Peterson, 2004; Dickinson and Gehrels, 2008; Owen et al., 2015b).

Several authors argue their data suggests a single source area for Salt Wash Member detritus (Craig, 1955a; Mullens and Freeman, 1957a; Tyler and Ethridge, 1983; Owen et al., 2015a). Owen et al. (2015), using a statistical projection of paleocurrent data suggested the apex of the Salt Wash source is in northeastern Arizona supporting previous work suggesting the sole source of sediment is from the Mogollon highlands (Mullens and Freeman, 1957b; Dickinson

and Gehrels, 2008). Paleocurrents indicate flow to the north and the northeast (Stokes, 1944; Turner and Peterson, 2004; Dickinson and Gehrels, 2008) (Figure 2.1).

As a distributive fluvial system, the Salt Wash Member can be described as progradational with distal facies at the base of section and more proximal facies higher in the succession (Craig, 1955a; Weissmann et al., 2010; Owen et al., 2015c, 2015b). This allows for prediction of the type of facies seen in proximity to the source of sediment (Weissmann et al., 2010; Owen et al., 2015c, 2015b). In most areas, the Salt Wash Member overlies the marine and marginal marine deposits of the Summerville Formation (Craig, 1955a; Peterson, 1984). In areas south and west of the study area, the Salt Wash Member rests on the distal shallow ephemeral lake facies of the Tidwell Member (Peterson, 1984; Owen et al., 2015c). The Tidwell Member is considered to be the distal component of the Salt Wash Member distributive fluvial system (Peterson, 1984; Owen et al., 2015c). It is composed of floodplain facies interbedded with gypsiferous wetland deposits, along with a finely crystalline carbonate wackestone containing gastropods and charophytes, and clastic ephemeral lake deposits that are composed dominantly of horizontally laminated muds and wave-rippled sandstones (Peterson, 1984; Owen et al., 2015c).

The medial part of the Salt Wash Member distributive system is described as having channel belt deposits separated by laterally extensive floodplain packages (Weissmann et al., 2010; Owen et al., 2015c). This part of the system is described as having 40-70% sandstone. Floodplain facies are described as dominantly mudstone, siltstone, and sandstone (Mullens and Freeman, 1957b).

The proximal part of the distributive fluvial system is dominated by amalgamated channel belt facies with pockets of floodplain muds. Typically, the channels are 70-100% coarse-grained

sandstone. Both meandering and braided fluvial elements have been described and documented throughout the Salt Wash Member (Stokes, 1944; Peterson, 1984; Kjemperud et al., 2008; Owen et al., 2015c). The top of the Salt Wash Member transitions into the fluvio-lacustrine deposits of the Brushy Basin Member of the Morrison Formation (Stokes, 1944; Craig, 1955b; Peterson, 1984).

Salt Wash Member in the Gypsum Valley Area

In far western Colorado, including Gypsum Valley the Salt Wash Member records a fluvial system with highly variable paleocurrent directions and a maximum exposed thickness of 335 meters (Shawe, 1968; Cater and Craig, 1970). In the axis of the Disappointment Valley syncline the Morrison Formation total thickness is enhanced by salt withdrawal subsidence and is over 340 m thick. The Salt Wash here is like other exposures of the medial part of the distributive fan and is composed of channel deposits composed of interbedded lenticular cross-bedded sandstones and floodplain deposits that contain tabular thin and flat bedded mudstones and sandstones (Figure 2.4).

Shawe et al. (1968) subdivided the Salt Wash Member, in this area, into three stratigraphic units based on sand mud ratios and stacking patterns of sandstone and mudstone lithofacies. His work described below formed the starting point for stratigraphic analysis in this study. Thicknesses are variable due to the salt tectonism that is the focus of this study, Shawe et al., (1968) measured sections that range from 24 m to 125 m thick.

The lower unit of the Salt Wash Member is 20 to 42 m thick, is a steep ledge former, and consists of thick laterally discontinuous sandstone packages. These packages that make up 75% of the section and range from 6 to 37 m thick separated by thinner discontinuous mudstones that range from partings to 10 m thick. The sandstones in this lower unit exhibit low angle cross-

bedding, horizontal bedding, and massive bedding. The middle unit is a 30 to 60 m thick slope former and consists primarily of mudstone and siltstones with dispersed isolated lenses of sandstone. The mudstones and siltstones average 24 meters thick. The sandstones have a maximum observed thickness of 20 m, but most commonly are 1 to 2 m thick and consist of thin beds that exhibit ripple cross-strata. The upper unit consists of a thick basal cliff, up to 30 m thick, that may extend for up to 6 km in outcrop. The cliff consists of laterally and vertically stacked large channel fills, with individual channels up to 10 m, thick. Along strike, the cliff may split into several ledges separated by thin layers of mudstone.

Shawe et al. (1968) also collected paleo current information from the region south and west of Gypsum Valley and were able to map channel slope in the upper unit. They inferred easterly and southeasterly transport within the upper unit, with an approximate channel slope of 0.00095.

Methods

Twenty-one composite stratigraphic sections were measured throughout Gypsum Valley. These have been grouped for ease of description into the following six areas (Figure 2.5): 'the Hat', Grassy Hill, Anderson Mesa, Big Gypsum Valley-eastside, Big Gypsum Valley -westside, and the Megaflap. Four complete sections were measured at 'the Hat' (HT 1-4, four at Grassy Hill (GH-1, GH-2, GH-4, BGH-1, five at Anderson Mesa (HM-1, HM-2, HM-3, HM-5, HM-6, HM-7), two at Big Gypsum Valley -Eastside (BGV-1, BGV-2), 4 at Big Gypsum Valley-westside (GG-1, GG-3, GG-4, GG-5 and 2 at the Megaflap (MF-1 and MF-2) (Figure 2.5). Stratigraphic sections were used to characterize facies and changes in thickness, stratigraphy and facies distribution. Paleocurrents were taken throughout Gypsum Valley in the Salt Wash Member where parting lineations and trough cross strata are evident. However, exposures of these features are restricted to a few units. Therefore, paleocurrent data are patchy and may not

be robust at some locations. Panoramic outcrop photos and geologic mapping in the field using both satellite imagery and aerial photos from Google Earth were used to map and track lateral changes in stratigraphy, facies, geometry, and to tie locations of stratigraphic sections. Key beds were correlated to highlight the effects of diapiric tectonism by walking between sections in the field. For simplicity, sections were correlated primarily using facies associations. In addition, measurements of grain size, sedimentary structures, paleocurrents, and channel geometries were collected to help analyze the differences in fluvial architecture, stacking patterns, sand percentage, and direction of flow as the Salt Wash Member was deposited throughout Gypsum Valley. Maps were compiled using QGIS open-source GIS software. Thickness and sandstone percentage maps were created using data collected from stratigraphic sections and created in Adobe Illustrator.

Results

Salt Wash Member Stratal Architecture Heading

The Salt Wash Member in the Gypsum Valley area is subdivided here into four stratigraphic units based on the stratal architecture of the sandstone channels (Figure 2.4). The basal ledgy unit is termed the interbedded sandstone channels and mudstones (ISCM). The overlying prominent cliff and ledge former is termed the amalgamated sandstone channels (ASC). The two lower units correspond to the “Lower” unit of Shawe et al. (1968). The ASC unit is overlain by a slope former with thicker shales termed the isolated sandstone channels (ISC), which corresponds to Shawe et al. (1968) “middle” unit. The uppermost unit is termed the laterally stacked sandstone channels (LSSC). This contains the thick cliff-forming sandstone described by Shawe et al. (1968) as the “Upper” unit, but also includes an overlying mudstone, which they mapped as basal strata of the overlying Brushy Basin Member of the Morrison

Formation. This mudstone interval was mapped as Salt Wash Member LSSC here because the encased sandstones within the mudstone dominated unit are lithologically similar to the Salt Wash sandstones and not to the dark, pebbly coarse-grained sandstones of the Brushy Basin Member.

Interbedded Sandstone Channels and Mudstones (ISCM)

The ISCM forms a basal ledgy unit below the cliff-forming Amalgamated Sandstone Channels Unit (ASC). ISCM is present on top of the diapir and on the margin at Grassy Hill. ISCM is also present on the flank and in the minibasin on Anderson Mesa. Where present, the ISCM crops out as a series of ledges composed of 1- to 2-m high sandstone cliffs separated by nearly horizontal "steps" (Figure 2.6A). The sandstones are typical Salt Wash Member buff -colored sandstones and are composed of fine-medium grained, well sorted, rounded-subrounded sandstones. Sandstones are horizontally bedded, trough cross-bedded with dominantly ripple cross-strata, undulatory bedding, and local bioturbation. These sandstones are interpreted to be channels that grade laterally into sandy crevasse splay deposits (Figure 2.6). This sandy crevasse splay grades into a brown bioturbated mudstone with white reduction zones around burrows.

Amalgamated Sandstone Channels (ASC)

The ASC forms a prominent cliff or steep set of ledges across most of Gypsum Valley where it forms the base of the Salt Wash Member outcrops. The unit exhibits discontinuous lenticular beds dominantly composed of laterally and vertically amalgamated channel fills (Figure 2.7). The amalgamated channel fill consists of light gray to white sandstone beds that have coarse-grained sandstone bases commonly containing rip-up clasts as well as granules and pebbles of limestone, feldspar, and chert clasts. These grade upward into trough cross-stratified

fine to medium-grained sandstones and then into ripple cross-stratified and horizontally laminated fine-grained sandstones. Bed tops commonly exhibit bioturbation (Figure 2.7).

Tyler and Ethridge (1983) interpreted the ASC strata in the Gypsum Valley area to be the deposits of straight-channel streams with low braiding indices, based on the relatively simple internal geometries of channel fills, the low dispersion of paleocurrents, and the large, and unidirectional preserved trough cross strata. They inferred that the channels had vegetated banks based on the presence of common crevasse splay strata. Smaller channel fills in this unit were interpreted as meandering tributaries based on better defined upward-fining trends and greater dispersion of paleocurrent indicators (Tyler and Ethridge, 1983). Chesley and Leier (2018) described similar amalgamated channel beds in Central Utah, and concluded, similarly to Tyler and Etheridge (1983), the larger channels within the unit were braided and the smaller were straight channel and meandering streams.

Isolated Sandstone Channels (ISC)

The ISC unit forms a ledgy recessive slope above the ASC cliffs. This unit exhibits sandstone channel fills interbedded with reddish brown to greenish gray mudstones that are interpreted to be floodplain facies (Figure 2.8). Channel fills range up to 3.5 m thick, and 60 m wide in outcrop, but commonly are smaller. Channel fill sandstones are upward fining from medium to fine grained, rusty dark reddish-brown sandstones that have sharp and erosional bases with granule to pebble sized rip-up clast conglomerates that grade up into subhorizontally laminated sandstones. These beds often exhibit soft-sediment deformation consisting of flame and slump structures and convoluted bedding (Figure 2.8). These beds are often overlain by massive to ripple cross-stratified to bioturbated beds.

The floodplain facies consist of reddish-brown, red, and greenish-gray mudstones and siltstones that when well exposed are thinly bedded (Figure 2.8). Generally, these facies is poorly

exposed and is more commonly a slope former between isolated channel fill ledges (Figure 2.8). Thin interbeds of wave-rippled or bioturbated sandstones are common in mudstone to siltstone outcrops. When exposed these beds can be laterally extensive for about five meters but more commonly pinch out laterally. Thin limestones (< 30 cm thick) are found in this unit in the southern part of Gypsum Valley, which outcrop over an area up to 5 km^2 and are most common in the lower third of the ISC unit. Limestones are occasionally laminated.

Laterally Stacked Sandstone Channels (LSSC)

The unit consists of a 5-30-meter-thick, cliff-forming sandstone that is not present everywhere, but is continuous over 5-10 km in outcrop. The thick stacked sandstones are visible on both flanks of Little Gypsum Valley salt wall as well as along the southern half of the northeast flank of the salt wall (Figure 2.9; 2.10). This unit is dominantly composed of laterally stacked channel fills (Figure 2.9). The channel fills within this unit are similar to those described for ISC (Figure 2.9;2.8). The beds within individual channel fills are typically 1.5 to 8 meters thick. Shawe et al. (1968), noted the lateral changes within this unit that are characteristic of amalgamated fluvial channel units. One distinguishing feature, first noted by Shawe et al. (1968), is the presence of abundant carbonized and petrified wood. This indicates a generally reduced environment within the channel fills during and after deposition. The cliff-former is overlain by a thick slope-forming mudstone with thin isolated channel sandstones that extend to the basal Brushy Basin Member channels. This mudstone interval has been mapped as part of the Brushy Basin Member by (Shawe et al., 1968), however, it is included in the LSSC here, based on the outcrop appearance and petrology of the sandstones within the interval.

The LSSC unit is interpreted as channels within the Morrison DFS, that flowed through a vegetated setting. The channel gradient was moderate (Shawe, 1968). Shawe et al., (1968) calculated a gradient of 0.0009 to the east and southeast.

Depositional Trends in the Salt Wash Member Stratigraphic Units

The thickness, sandstone percentage, and channel paleocurrent orientations of the Salt Wash Member stratigraphic units vary spatially and temporally/stratigraphically across the Gypsum Valley area (Figures 2.10; 2.11). The following section describes the changes within the Salt Wash Member at each location.

Interbedded Sandstone Channels and Mudstones (ISCM)

The ISCM unit is not present at all Salt Wash Member outcrops around Big Gypsum Valley (BGV) (Figure 2.10; 2.12), however, it is present in Little Gypsum Valley. ISCM thickens dramatically into Little Gypsum Valley (LGV) at Grassy Hill but is not present at 'the Hat'. A thick section forms the recessive slope above the Summerville Formation at Grassy Hill, which pinches out approximately 5 km north along the rim of the diapir. The unit can also be traced into a syncline that extends along Grassy Hill (Figure 2.12) where it thickens to 55 m in the axis of the syncline (GH-1) from 20 m on the flank of the syncline, at the margin of the diapir at GH-2 and distal to the diapir at BGH-1 (Figure 2.12). The lack of ISCM at 'the Hat' is due to either non-deposition, complete erosion prior to deposition of overlying units, or intertonguing with and becomes indistinguishable from the overlying ASC facies. The nature of the contact cannot be determined because it is buried under younger units within LGV. However, since ISCM was deposited at Grassy Hill it indicates that there was local accumulation space available for this unit to be preserved.

The ISCM is much sandier on the margin (81%) at Grassy Hill where it is dominantly composed of sandy crevasse splay and channel fill with thin floodplain mudstones separating them. When deposited on top of the diapir at Grassy Hill it is much thicker, less sandy (24%), and composed of more floodplain mudstones deposited in between sandy crevasse splay and channel fill (Figure 2.12).

The ISCM is also identified on Anderson Mesa, where it is exposed along the Dolores River Canyon, and in Hamm Canyon (Figure 2.12). The unit is thin .5km from the margin of the diapir (5m at HM-5) and thickens to approximately 15 m at HM-6 and HM-7, 2.8 km from the diapir margin on the flank of the Dry Creek minibasin. This unit is visible in the field and in aerial and satellite imagery to be present at sections HM-6 and HM-7, which were inaccessible from the ground. The ISCM on Anderson Mesa is like the unit deposited on the margin and is also composed of sandy crevasse splay and channel fills with a sandstone percentage of 27% (Figure 2.12). On Anderson Mesa ISCM is exposed for 3.5 km along the flank of the diapir and is truncated to the south by erosional truncation by channels of the overlying ASC (Figure 2.12).

During deposition of the ISCM in LGV accommodation space was created over the top of the diapir as it subsided allowing this unit to be preserved. The opposite is true in BGV where the pinchout of this unit and its truncation by the overlying ASC into BGV indicates that diapirism and subsidence of the Dry Creek minibasin resulted in its erosion along the diapir margin, although erosion did not notably thin the underlying Summerville Formation. As a topographic high, the diapir prevented deposition of this unit along the margin in BGV and possibly redirected its channels to deposit sediment into the adjacent Dry Creek minibasin, which is why this unit appears to thicken distal to the diapir margin (Figure 2.12). Without paleocurrent data for this unit it is difficult to be certain the direction of channel flow and deposition.

Amalgamated Sandstone Channels (ASC)

The ASC unit forms the lower cliff of the Salt Wash Member and is exposed around Gypsum Valley and on the diapir in the Grassy Hill and 'the Hat' synclines in Little Gypsum Valley (Figures 2.13). The ASC unit varies more in thickness around Gypsum Valley (5-69 m) than in other regional studies, where it has been reported as 20-43 m thick (Shawe et al., 1968). The unit is thickest in 'the Hat' syncline, at 69 m. Much of this thickening is accomplished by intercalations of clay beds that increase in thickness into the synclines (Figure 2.10A). Dramatic exposures along the flanks of these synclines show mudstones pinching out as the intercalated sandstones onlap and merge with the ASC (Bailey, 2020-Chapter 4). ASC is the thickest (15-69 meters) and the least sandy (24%) in the axis of 'the Hat' syncline (Figure 2.13) (Bailey, 2020-Chapter 4). The truncation of ASC and resulting pinch out of the intervening mudstones increases the sandstone percentage over a very short distance from the axis of the syncline to the margin (Figure 2.13).

The ASC unit overlies ISCM at Grassy Hill and in Anderson Mesa. In LGV ASC is thick at 'the Hat' (69m), but thin in the Grassy Hills syncline at 9 meters (Figure 2.13). It thickens dramatically southwest into the Disappointment Valley minibasin in section BGH-1 to 48.3 meters and the sandstone percentage is high 45-65% (Figure 2.13). Paleocurrents taken from troughs in this area show channels of the unit flowing to the northwest along the margin of the diapir (Figure 2.13).

ASC in Anderson Mesa truncates the underlying ISCM unit just south of HM-5. The ASC unit is thinnest at Anderson Mesa, where it ranges from 5 to 7-m-thick, except where it scours out the underlying Summerville Formation, forming a prominent valley fill (Figure 2.13). ASC thins to the south along the margin at Anderson Mesa until it pinches out by truncation and

erosion along an angular unconformity between it and the overlying ISC unit just south of Hamm Canyon in Big Gypsum Valley (Figure 2.13). On the east side of Big Gypsum Valley, the Summerville Formation is eroded below in an unconformity where it overlies the Wingate Formation. The contact with the overlying ISC unit is an intertonguing and gradational contact as the uppermost ASC channels pinch out into flanking mudstones.

In Little Gypsum Valley and Anderson Mesa, paleoflow directions are variable (Figure 2.13). Southwest, south, and northeast directions are the most common (Figure 13). Paleoflow at Anderson Mesa was to the southwest, and at 'the Hat', generally south, oblique to the axis of the syncline (Figure 2.13). The overall pattern of flow is into LGV.

ASC, along with the entire Salt Wash Member is covered by younger strata along the western flank of Big Gypsum Valley, from Gypsum Gap, northwest for 10 km. On the southwestern margin the Salt Wash Member emerges from where it is truncated between angular unconformities (Figure 2.13). ASC along the western margin of BGV is variable in thickness and ranges from 4 meters at GG-5 and 31 meters at GG-3 and the sandstone percentages range from 49% at GG-3 to 78% at GG-5. At the Megaflap the thickness is also variable, and the thickness is measured to be 11.4 meters at MF-1 and 29.1 meters at MF-2 with the ASC unit being much sandier at 42% at MF-1 and 30% at MF-2. In Big Gypsum Valley, flow is toward the southeast, along the diapir (Figure 2.13). This is subparallel to the regional flow directions described by (Shawe et al., 1968 and Tyler and Etheridge, 1983). The ASC onlaps the northeast side of BGV and is not exposed, so no information is available on this side of the valley. However, it is likely, that the BGV diapir formed a barrier to flow of the ASC channels and directed them to the southeast, around the diapir.

The unconformities observed in ASC throughout Gypsum Valley are interpreted to be tapered composite halokinetic sequence boundaries of a wedge sequence (Giles and Rowan, 2012). Wedge sequences are described as having broad and gentle drape-fold geometries (Giles and Rowan, 2012). These are interpreted to be tapered and composite halokinetic sequences because they exhibit low angle unconformities and because thinning towards the diapir occurs over a wide zone.

Isolated Sandstone Channels (ISC)

The ISC unit is the third stratigraphic unit and is exposed throughout Gypsum Valley (Figure 2.4, 2.14). The ISC forms a more shaley slope between the cliffs of the ASC and LSSC (Figure 2.4). This unit overlies ASC except for on the southeastern margin of BGV, where the lower two units are not present due to erosion below the ISC. The ISC overlies older strata along the western side of BGV where it onlaps the older strata folded against the diapir (Figure 2.10D). Around the margins of BGV, it rests depositionally on the Paradox diapiric salt (Figure 2.2). The lower contact of the ISC appears conformable with the ASC in LGV, and in southwestern BGV. Along the northwestern flank of BGV, it rests in gentle angular unconformity on older strata. Its upper contact with the overlying LSSC everywhere appears to be conformable and, in many places gradational, where more and thicker sands are present below the LSSC. In areas where no obvious LSSC cliff is evident, the upper boundary of the ISC is uncertain.

The ISC varies locally in thickness around Gypsum Valley. This can be ascribed to three factors. First, the uncertain upper boundary of the ISC results in varying thickness measurements. Second, thickening of units into the minibasins that flank the diapir. Thirdly, local salt tectonic sequences allow thickening within and along the margins of the diapir. The most obvious halokinetic sequences are observed in ‘the Hat’ syncline, and along the

southwestern margin of BGV, where prominent angular unconformities are located below the top of the ISC (Figures 2.10A).

ISC is thick in the axis of ‘the Hat’ and in the Grassy Hill synclines (GH-1), where it is dominantly composed of floodplain muds. At ‘the Hat’ this unit is thick in the axis of the syncline where it ranges from 65.4 meters thick at HT-2 to 74 meters at HT-3 and HT-4. ISC is the thinnest on the margin of the diapir, on the northeast flank of ‘the Hat’ syncline (Figure 2.14) where it thins dramatically to 25 meters at HT-1 onto the margin of the syncline. The sandstone percentage of the unit increases to 46% through thinning and onlap of the mudstones against the flanks of the syncline onto growth sequence boundary B (Figure 2.10A; 2.14) (Bailey, 2020-Chapter 4). However, erosion of the top of the unit by truncation of the overlying LSSC limits accurate thickness estimates in this area. Paleocurrents of this unit at ‘the Hat’ show that channels flowed to the south/southeast (Figure 2.14).

At Grassy Hill there are sections of the ISC unit that are located on top of the diapir, on the margin, and away and the thickness is relatively consistent. This unit on top of the diapir at Grassy Hill is 32 meters at GH-1. On the margin ISC is at 44 meters at GH-2 and 43 meters at GH-1. At BGH-1 ISC thickens into the Disappointment minibasin to 47 meters and gets sandier at 42% compared to 25% on top of the diapir.

ISC at Anderson Mesa ranges in thickness from 31-55 meters (Figure 2.14). Generally, ISC thins to the south into BGV. ISC is the least sandy on Anderson Mesa at 4% where the unit is thick with very few channels and mostly composed of floodplain facies. This unit truncates and erodes the top of the underlying ASC unit south of Hamm Canyon. The paleocurrents from troughs in this unit show channels were flowing in multiple directions to the northeast, southeast, and southwest.

ISC on the eastern margin of BGV is thick with a high sand percentage (Figures 2.14). The unit is the sandiest at 52% where the unit thins to 27 meters in the sections closest to the diapir (Figure 2.14). The paleocurrent data in this area show that the channels of the ISC flowed dominantly to the west across the diapir (Figure 2.14). This implies that the area was a fairway through which channels were focused during ISC deposition.

In addition to the synclines, the ISC unit is thick along the southwest margin of Big Gypsum Valley, where it reaches a maximum of 112 m at GG-1 (Figure 2.14), however, this may include some thickness of unidentified LSSC. This unit is also thick at the other measured sections along the southwest margin where it is 93 meters at GG-3 and GG-5 and 44 meters at GG-4. This unit is the sandiest at GG-5 at 40% but is 21-34% sandy at GG-1,3, and 4. In proximity of the megaflap this unit is also thick at 57 meters at MF-1 and 87 meters at MF-2 with a relatively low sand percentage around 25%.

Laterally Stacked Sandstone Channels (LSSC)

The LSSC is the uppermost unit of the Salt Wash Member stratigraphy, is the second most sandy unit, and is present at all locations except on the southwestern margin of BGV (Figure 2.15). This unit everywhere overlies the ISC unit in apparent gradational conformity. The top of the unit is also gradational, and was placed at either the lowest dark, pebbly sandstone of the Brushy Basin Member or at the transition between reddish brown mudstones of the Salt Wash Member and the greenish gray mudstones of the Brushy Basin Member (Figure 2.15).

LSSC is thickest in ‘the Hat’ where it is 105 meters thick and has the lowest sandstone percentage at 15% and the thickest mudstone interval in the axis of the syncline compared to other locations throughout Gypsum Valley (Figure 2.15). On the northeast margin of ‘the Hat’ syncline, the LSSC has been removed by erosion. The prominent cliff-forming sandstone of the LSSC forms well-defined axial fluvial fairways but does not appear to thicken or thin in response

to syncline formation. The mudstone interval with isolated channels that forms the upper part of the unit thickens and thins in response to diapirism (Figures 2.15). Paleocurrents of channels at 'the Hat' flow dominantly to the west, across the diapir (Figure 2.15).

The LSSC in the adjacent Grassy Hills syncline is thinner than the section at 'the Hat' (Figures 2.15). LSSC is 28 meters on top of the diapir at GH-1 and 28 meters at GH-2 and 45 meters at GH-4. The LSSC does not thicken into the adjacent Disappointment minibasin at BGH-1 where it is 19 meters thick. The sandstone percentage of this unit at Grassy Hill is the least sandy on top of the diapir at GH-1 (45%) and the sandiest into the Disappointment minibasin at BGH-1 (85%). The sandstone here may be part of a fairway and is very thick, and therefore, sandstone percentage is high into the minibasin (Figure 2.15).

On the northern flank of Big Gypsum Valley, on Anderson Mesa, the unit thickens to the southeast along the margin of the diapir (Figure 2.15). LSSC ranges in thickness from 10 meters to 48 meters at Anderson Mesa. This unit is thin around 10 meters at HM-6 but is thickest on Anderson Mesa at 48 meters around HM-1. It is also the sandiest at these two locations. The paleocurrent data from trough cross bedding throughout this unit at Anderson Mesa indicates channel flow predominately to the southwest and northwest. Paleocurrent data from troughs throughout this unit at Anderson Mesa show flow to the southwest and northwest, parallel to the diapir margin.

Further southeast, in Big Gypsum Valley, the LSSC unit maintains a more consistent thickness (Figure 2.15). LSSC on the eastern margin of BGV is the thinnest and mostly composed of stacked channel sandstone fill (Figure 2.15). This unit at BGV-1 is 18 meters and 10 meters at BGV-2. The sandstone percentage of LSSC at this location is at a high of 98% (Figure 2.15).

LSSC is not present on the southwestern margin of the diapir, where it was either not deposited because it depositionally pinches out or is eroded away. It is also possible that here the LSSC and the underlying ISC are indistinguishable from one another and the contact was not determined. The contact is not exposed along the margin between Grassy Hill and the southwestern margin of BGV because it is buried by younger stratigraphy.

The thinned ASC unit, that scours into the Summerville Formation and the diapir-margin parallel paleocurrents indicate the diapir formed a topographic barrier to sand and along the northeast margin, a topographic high, that extended from southeast from Anderson Mesa (Figures 2.16). The ASC unit pinching out at Hamm Canyon presents a geologic problem because the underlying Summerville Formation is not completely eroded on the northeastern margin. Although the ASC maintains a 20-30 m thick section in southeastern Big Gypsum Valley, the southwesterly directed paleocurrents suggest that the diapir was high enough to redirect these channels around the diapir.

Variations in the thickness of this unit away from the diapir margin could be related to local variations in topography changing the amount of accumulation space available for the unit to be preserved (Figure 2.16). The changes could also be related to erosion of the unit but there was not extensive evidence of this in outcrop. This unit is the thinnest over the top of the diapir at GH-1 and this variation could be due to changes in subsidence rate during deposition decreasing the potential accumulation space needed for preservation of the unit (Figure 2.16).

In Little Gypsum Valley, the thickness patterns and paleocurrent data suggest a complicated and active deformation of the top and flanks of the diapir. Both minibasins were subsiding (Figure 2.16). However, the Disappointment minibasin was subsiding adjacent to the diapir, resulting in greater thicknesses along the southwest flank of the diapir (Figure 2.16).

Along the northeast flank, sections were thinner, and suggesting lower rates of subsidence. 'The Hat' syncline subsided rapidly and filled with a much muddier ASC interval that contained abundant floodplain mudstones (Figure 2.13). However, the Grassy Hills syncline did not subside during deposition of the ASC, although it had been very active during ISCM deposition.

The thickened and muddy sections on 'the Hat' and Grassy Hills synclines suggest subsidence of the diapir crest, in which additional floodplain muds accumulated, but which did not focus the flow of channels. Thickened and sandy intervals in sections BGH-1 and HM-6 and HM-8 indicate that channels did flow along the diapir, as the two minibasins subsided (Figures 2.11). Big Gypsum Valley exhibits one or two major channel fairways through which later truncated streams flowed across the diapir (Figure 2.16). It is unclear whether one fairway flowed to the east, into the diapir, and then exited farther north, between BGV-1 and BGV-2, or whether these represent two fairways, with one fairway on the southwest of the diapir, flowing east, past its southern end, and a second that flowed west into the diapir at BGV-2 that exited the diapir east of this section, in the area now covered by younger strata (Figure 2.16).

At 'the Hat' the channels of ISC are truncated by and onlap onto growth sequence boundary C (Bailey, 2020-Chapter 4). Deposition of this unit at 'the Hat' is interpreted to mark a decrease in subsidence and filling of 'the Hat' minibasin. The Grassy Hills syncline seems to record a similar, reduced subsidence during LSSC deposition. The westward trending channels and flow suggest that in LGV, the large streams that formed the LSSC were not affected by salt tectonism. It is likely that the rate of sedimentation by the LSSC channel greatly exceeded the rate of subsidence into the synclines. The overlying muddy interval, however maintained sedimentation rates sufficient enough, so that facies did not change across the synclines. However, the interval thickens dramatically due to subsidence of the diapir crest (Figures 2.16).

The flanking minibasins show a reduced rate of subsidence during this interval, and the section does not thicken appreciably (Figure 2.16).

LSSC is not present on the southwestern margin of the diapir (Figure 2.15). The LSSC was either not deposited or pinches out to the southeast, however this relationship is not exposed as these strata are buried beneath younger strata. The thinning of the LSSC on the eastern side of the diapir along with its regional continuity suggests that salt tectonism in Big Gypsum valley may have diverted channels into the Disappointment Valley minibasin to the southeast and thinned the LSSC on the northeastern side of the diapir.

Discussion

We propose that variations in thickness, sandstone percentage, and paleocurrent directions are due to differential salt tectonic movement of the Gypsum Valley salt diapir in the Late Jurassic. Halokinetic subsidence or uplift of salt resulted in either: 1) non-deposition, thinning, or thickening of the unit, 2) removal by erosional truncation or onlap, or 3) facies changes. The interaction of the Gypsum diapir with the deposition of the Salt Wash Member presents a complex and intriguing story that involves dramatic local changes as well as the interplay of the diapir with the fluvial system. Overall, the Big Gypsum Valley area can be divided into the diapir, and the flanking minibasins, Dry Creek to the northeast, and Disappointment to the southwest. The diapir can be divided into an area centered in Little Gypsum Valley that exhibited variable subsidence during Salt Wash deposition, and Big Gypsum Valley that generally exhibits evidence of diapiric rise and subsidence of adjacent minibasins.

Regionally in the Slick Rock district the Salt Wash Member has been described to be 75 to 125 meters thick (Tyler and Ethridge, 1983). Locally within the Disappointment mini-basin

the Salt Wash Member has been measured from wells to be a similar thickness of 122 meters thick (Shawe, 1968). This indicates that minibasin subsidence continued throughout Morrison deposition.

Two factors can cause variation in apparent subsidence rate. The rate of deformation can vary with local subsidence thickening units, and uplift creating pinchouts through thinning, onlap and erosion beneath angular unconformities. The rate of sediment influx can increase or decrease. More rapid deposition creates intervals that exhibit lower apparent rates of deformation. Slower deposition superimposed on diapiric deformation, would present a picture with more dramatic changes in thickness and higher apparent deformation rates. For our analysis, we inferred that the rate of deposition was controlled by the position of Gypsum Valley in the Salt Wash distributive fan (Owen et al., 2015c). The rate of deposition of the Salt Wash Member was probably relatively consistent. A more local control would be proximity to an axial drainage, which would be expected to be aggrade more rapidly than areas more distal and fed by minor tributaries.

The Summerville Formation, which underlies the Salt Wash Member is a good example of a unit deposited quickly, over a short period of time. The Summerville Formation is present throughout the study area and has the consistent thicknesses of 12-15 meters. The Summerville Formation therefore indicates that at the beginning of Salt Wash Member deposition, the Gypsum Valley area was an exposed, relatively flat surface of a former tidal flat and there was little or no diapir -related topography. It also suggests that in most of Gypsum Valley there was enough accumulation space for the Salt Wash Member to be deposited and preserved.

Overlying the Summerville Formation is the basal ISCM unit along the part of the diapir, and in Dry Creek minibasin (Figure 2.12). The thickening of the ISCM in these areas indicates

areas of localized subsidence and a rate of deposition that was slow enough relative to deformation so that thickness variation was important. The dramatic thickening of the ISCM into the Grassy Hills syncline marks the first Salt Wash Member age local subsidence of the diapir crest (Figure 2.12). Thickening into the minibasins and observed truncation of the ISCM on an angular unconformity north of the Grassy Hills indicates a possible slight lowering of base level that removed the thinner ISCM intervals but did not erode the underlying Summerville Formation. This interpretation is tentative, and the lack of Summerville Formation erosion is difficult to interpret in this context.

The ASC unit, with its abundant stream channels varies less in thickness than do the other units of the Salt Wash Member (Figure 2.13). The dramatic thickening of the ASC into 'the Hat' syncline suggests rapid and very local subsidence of this part of the diapir crest at this time. Thickening of the ASC in the Grassy Hills area indicates a faster subsidence of the Disappointment Valley syncline and a general subsidence of the northwestern diapir margin (Figures 2.13). The Dry Creek minibasin on the northeastern side of the diapir, does not show any thickening during this time. Thicknesses from the Anderson Mesa to the southeast, reflect erosion on an overlying unconformity in the ISC interval rather than depositional changes during ASC deposition. The ASC unit is thin along the southwestern margin of BGV (Figure 2.13). Paleocurrents that are subparallel to the diapir margin suggest that the channels were diverted around the southern end of the diapir (Figure 2.13).

The ASC marks the first interval where paleocurrents indicate flow into the diapir (Figure 2.13). In this instance, Little Gypsum Valley, along with similar flow into Big Gypsum Valley in the ISC, suggests that parts of the diapir were topographic lows, and perhaps more rapid erosion of the diapir created accumulation space on the diapir (Figure 2.14). During deposition of

the Salt Wash Member the diapir in LGV was subsiding, creating topographic lows for the fluvial system to cover and deposit sediment. This is supported by increases in thickness of several units deposited on top of the diapir and paleocurrents indicating flow across the diapir in LGV.

The ISC marked increased response to diapiric deformation and more greatly varying thicknesses suggest that the ISC, containing smaller distributary channels, was deposited more slowly. Continued flow into LGV, indicates that this area continued to form a topographic low. An angular unconformity in the lower ISC truncates the underlying units, the depth and angularity increase into BGV and correlate with deformation around the diapir. This is interpreted to be a tapered composite halokinetic sequence in the terminology of Giles and Rowan (2012). The ISC onlaps the diapiric margin and overlies the diapir caprock in BGV (Figure 2.14). The cliff-forming channel complexes of the LSSC probably reflect a return to more rapid deposition, and thickness changes largely represent the locations of channel sandstone fairways (Figures 2.15). The shale that marks the tops of the LSSC unit accommodates most of the thinning and thickening related to diapiric deformation and may mark a return to slower rates of deposition.

Throughout Salt Wash Member deposition, Little Gypsum Valley was marked by subsidence and little associated minibasin subsidence, whereas, BGV exhibits subsidence of the minibasins and thinning over the diapir suggesting continued diapiric rise. Subsidence of the diapir in LGV could be due to several factors including: 1) that radial faults in LGV of the diapir are no longer active, suggesting there was no longer any diapir rise. 2) Salt was no longer moving from the adjacent Dry Creek and Disappointment minibasins feeding the Gypsum Valley diapir at LGV. 3) There could have been some dissolution of salt beneath LGV contributing to

subsidence. Radial faults at the northern end of LGV have been observed not cutting through the Jurassic strata of the Salt Wash Member and younger indicating that diapiric doming had ceased by the Jurassic in that area. The Cretaceous and younger strata show little thickening between Gypsum Valley and the Paradox salt wall to the north. This suggests that by Morrison time, the salt had welded out in the adjacent minibasins in the northern part of Gypsum Valley. Without a source of salt to feed the diapir in LGV, less salt was available in LGV and it began to subside. Therefore, the fluvial system of the Salt Wash Member was able to flow across the diapir and deposit sediment on top of the diapir in the available accumulation space.

In BGV the dynamic between the Gypsum Valley diapir and the fluvial Salt Wash Member was very different from LGV and much more complex. There was source of deep salt that continued diapir movement in BGV. The radial faults at this end of the diapir were active and continue to be active until the late Cretaceous. The Cretaceous strata thicken and fill the minibasins (Escosa et al., 2018). The megaflap formed a vertical topographic high on the southwestern margin of the Gypsum Valley diapir that acted as a barrier or changed the flow of the Salt Wash Member (Escosa et al., 2018). The diapir itself was also a topographic high at different stratigraphic intervals during Salt Wash Member deposition and this was variable across the diapir. Tapered composite halokinetic sequence boundaries described in the ASC and ISC are evidence of wedge style halokinetic sequences which suggests that within BGV overall sediment accumulation rate adjacent to the diapir exceeded diapir-rise rate (Giles and Rowan, 2012). This interpretation supports the idea that there were times where the diapir topography was low to non-existent allowing the Salt Wash Member sedimentation to keep up with local accommodation and deposit sediment on top of the diapir. When the diapir is slightly higher, it becomes a zone of bypass or erosion creating truncation.

Conclusion

Thickness trends and paleoflow directions indicate that deposition of the Salt Wash Member around the Gypsum Valley salt wall was influenced by changes in the rate of sedimentation and varying diapiric deformation around the diapir and in the adjacent minibasins. In general, sandier intervals show less impact of diapirism and are inferred to have been deposited more rapidly.

Each part of the system was active at different times and at different rates. LGV, had rapid rates of subsidence in synclines on the crest of the diapir during most of Salt Wash Member deposition. In contrast, BGV continued passive diapiric rise and minibasin subsidence throughout Salt Wash Member deposition (Figure 2.16). Streams were diverted parallel to the diapir margin and deposited abundant sandstone along and across the diapir. This contrasts with current models of the interaction of fluvial sandstones and salt tectonism, which typically show channels directed along the axes of the minibasins. This study indicates that sandstones are restricted to the subsiding salt withdrawal minibasins but can be more abundant on diapir flanks and crests than previously thought. Diapirism can vary substantially along diapirs probably due to varying rates of salt availability from adjacent sources.

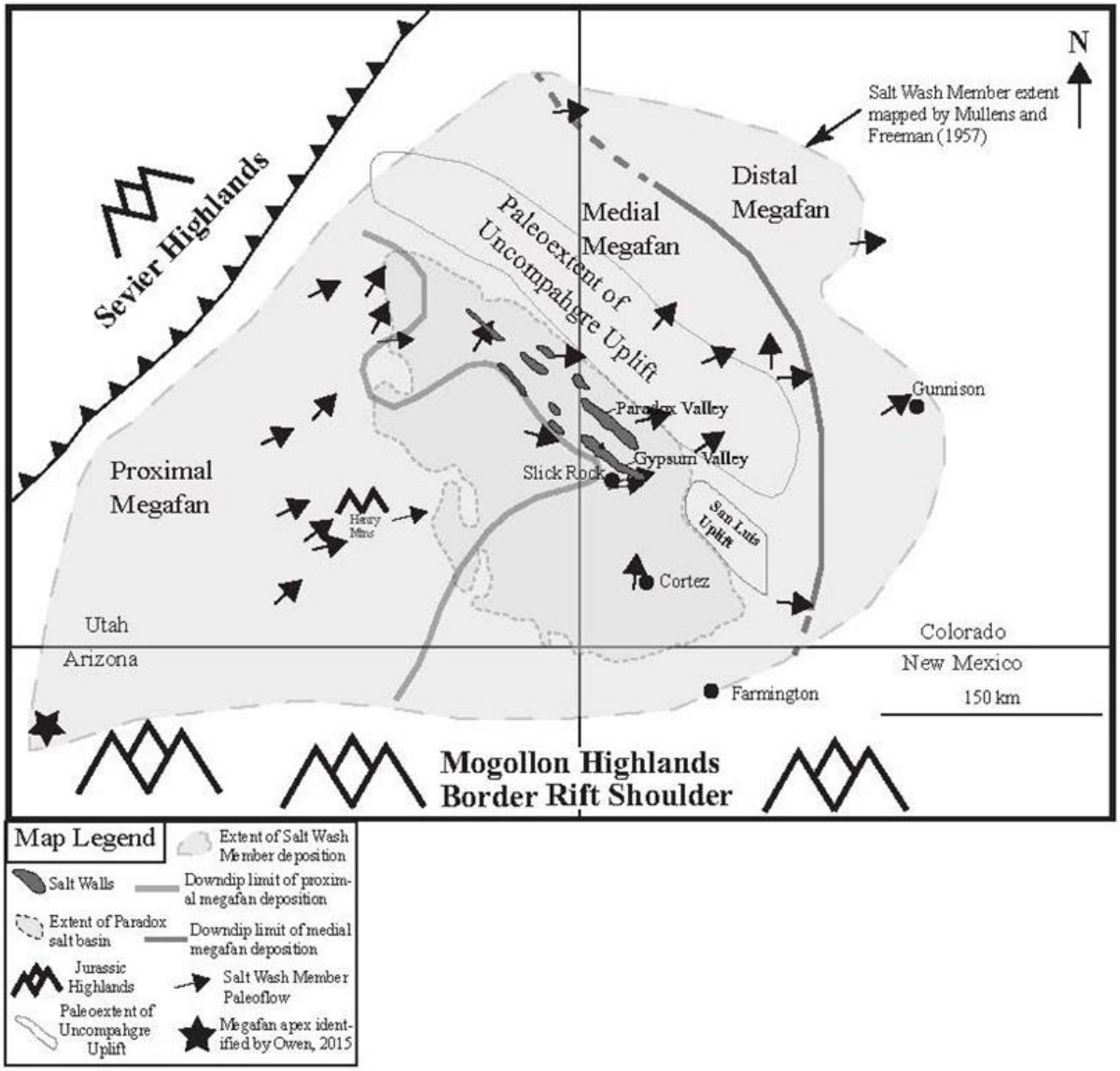

Figure 2.1: Regional map of Jurassic Salt Wash Member of the Morrison Formation depositional system and areal extent of Paradox Basin deposition.

Fluvial system paleoflow of the Salt Wash Member from Owen et al. (2015) is indicated by gray arrows and the extent of the fluvial system from Mullens and Freeman (1957) is a dashed outline. Paradox Basin salt walls are outlined with dark infill gray. (Figure altered after Barbeau, 2003; Trudgill, 2011; Owen et al., 2015)

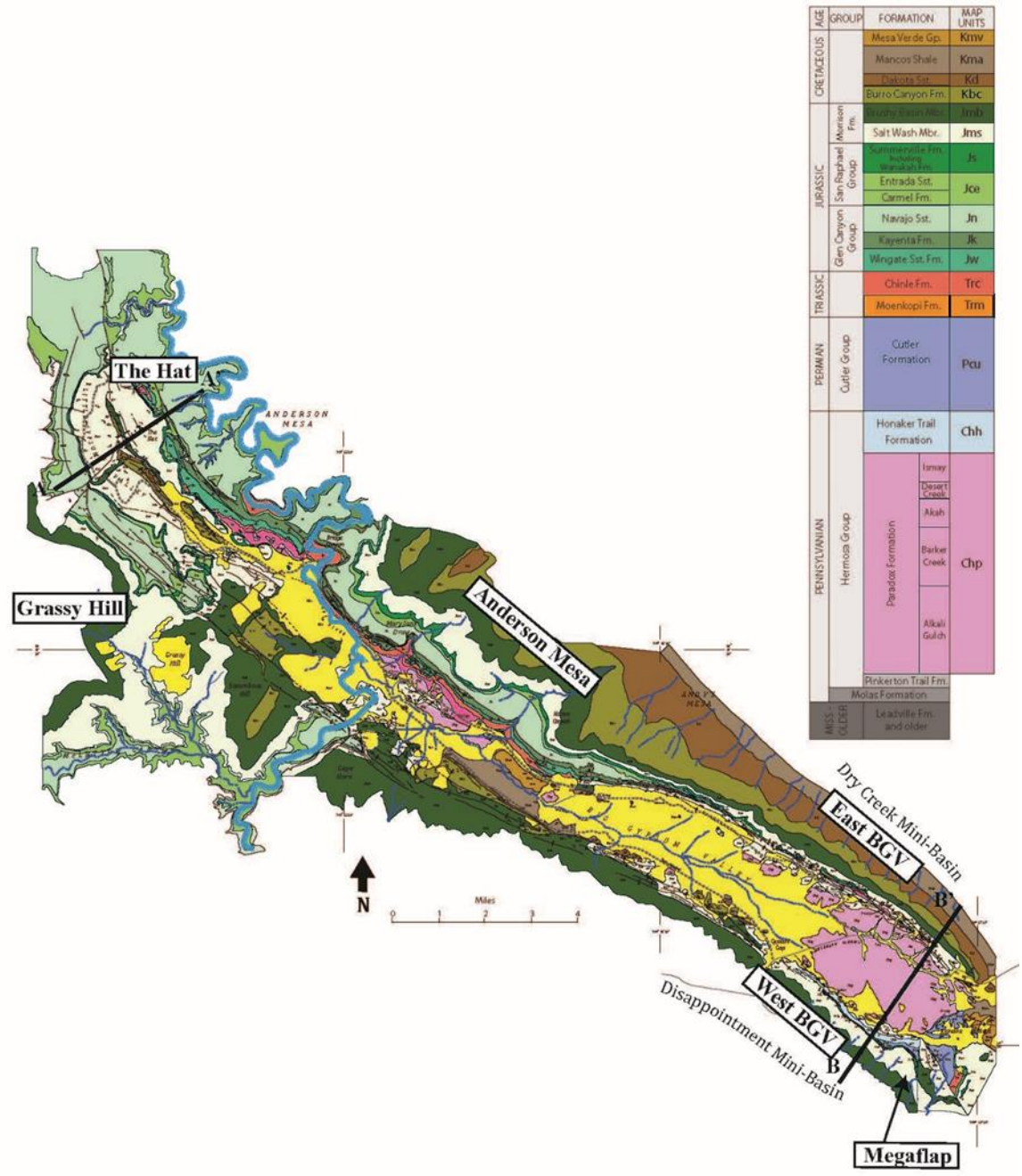

Figure 2.2: Colored Geologic Map of Gypsum Valley

Map includes stratigraphic units outcropping in Gypsum Valley, the Dolores River that cuts through Gypsum Valley, different study areas covered in this paper, and the location of the cross-sections in figure 5.

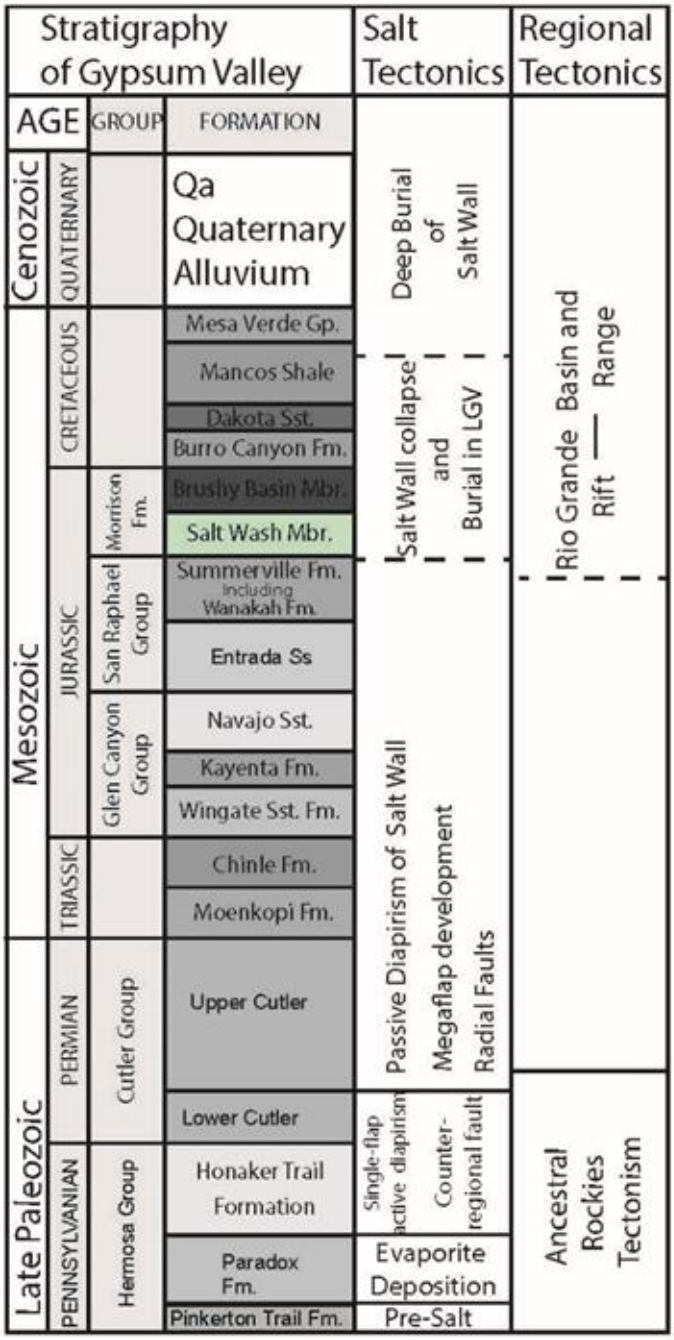

Figure 2.3: Stratigraphy and tectonic history of Gypsum Valley Area.

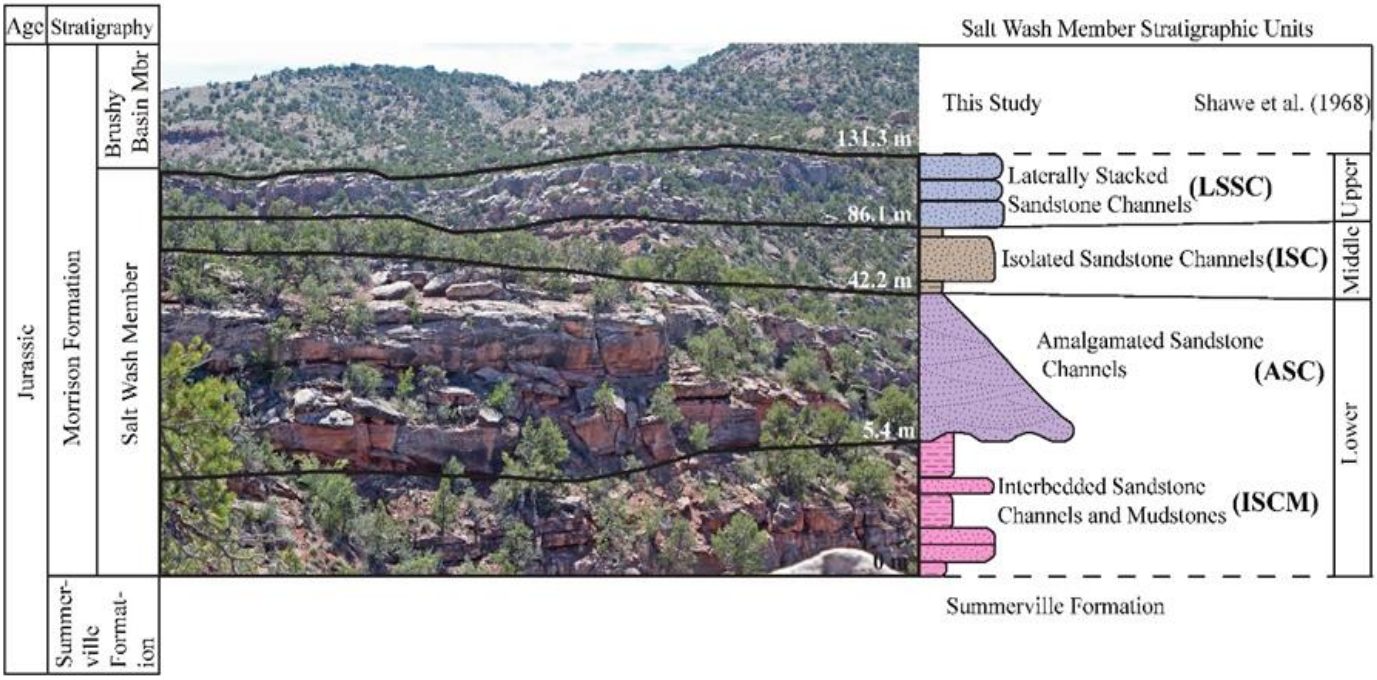

Figure 2.4: Outcrop photo of complete section of Salt Wash Member, Morrison Formation at Grassy Hill on the SW side of Little Gypsum Valley.

The column on the right side identifies units described in this study and correlation to Shawe et al. (1968). Their lower unit contains ISCM and ASC, Middle unit is ISC, and Upper Unit is LSSC. The approximate thickness of the Salt Wash Member at this location is 131.3 meters thick.

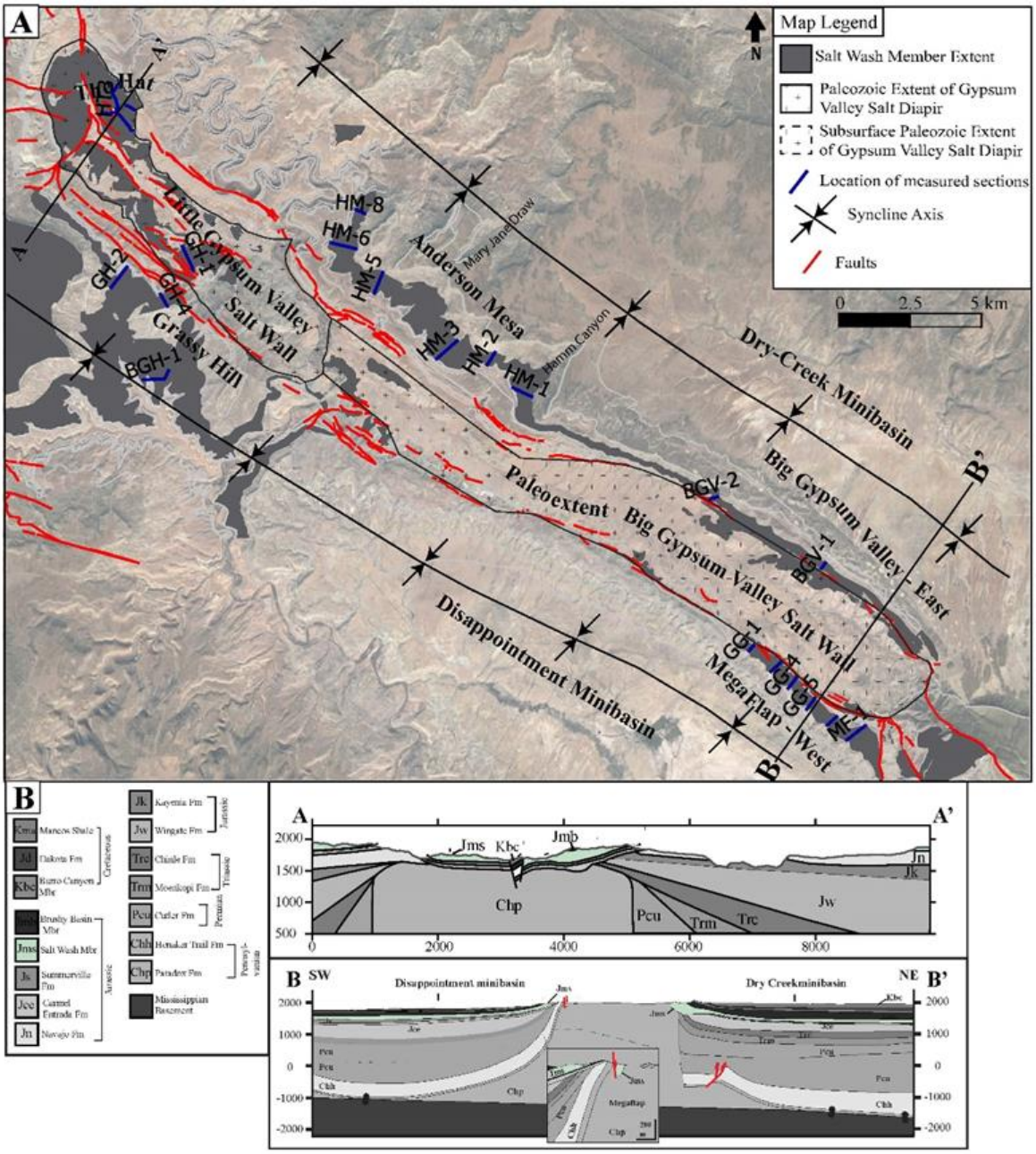

Figure 2.5: Paleoextent of Gypsum Valley and the Salt Wash Member

A. Map showing the outcrop extent of the Salt Wash Member as well as the surface and subsurface extent of the Gypsum Valley salt wall during deposition of the Salt Wash Member, faults, location of the Dry-Creek and Disappointment minibasin, and location of of crosssections A-A' and B-B'. B. Crossections A-A' across Little Gypsum Valley and B-B' (from Escosa et al., 2018) Big Gypsum Valley.

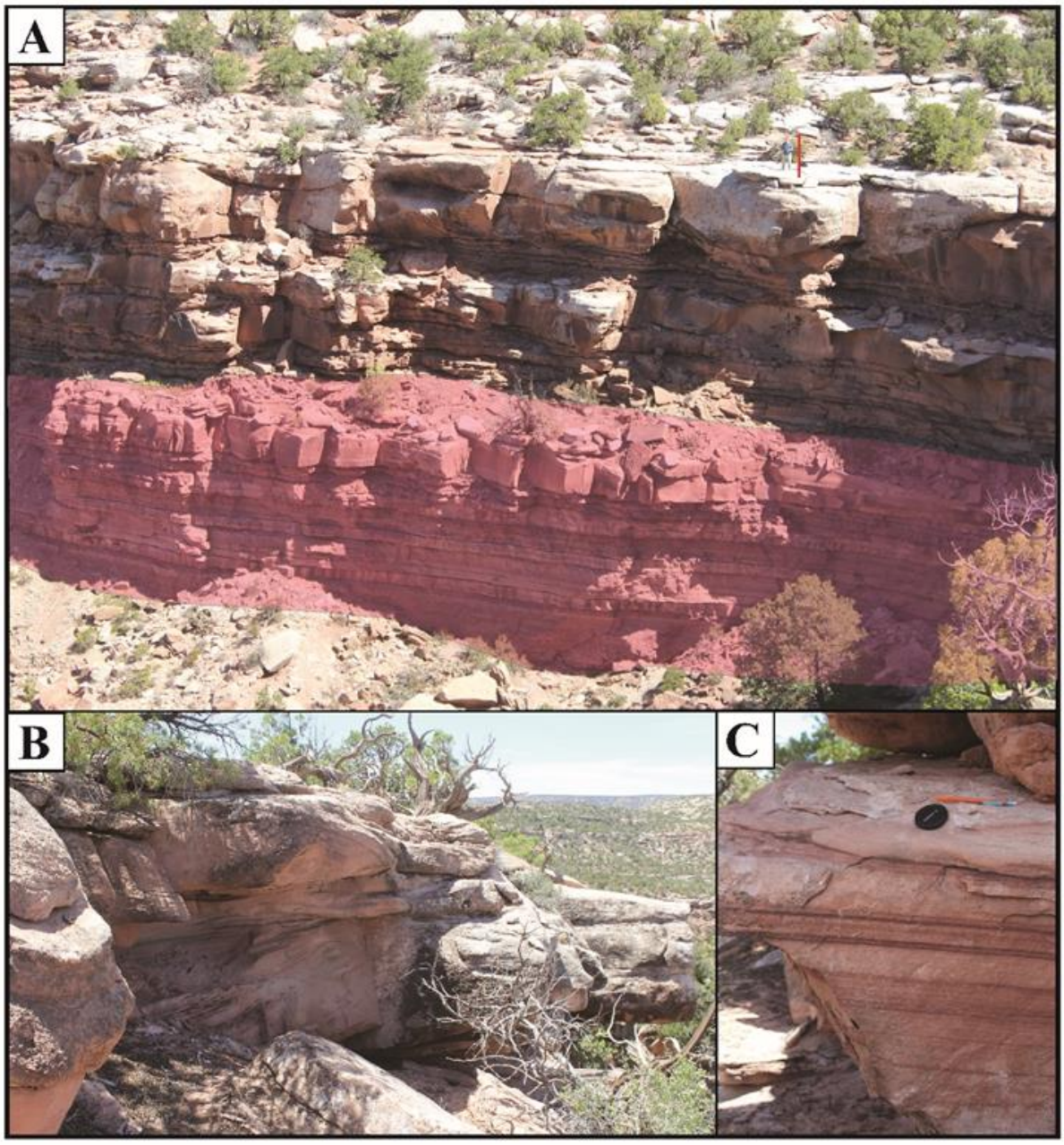

Figure 2.6: Outcrop photos of Interbedded Sandstone Channels and Mudstone.

A. Thick deposit of Interbedded Sandstone channels and mudstones. Highlighted in pink with capped by the Amalgamated sandstone channels. Unit is approximately 15 m thick in this photo at Anderson Mesa. B. Sandy Crevasse Splay with rough crossbedding at 2 meters thick. C. Sandy Crevasse Splay with laminated bedding channel is 1 m thick.

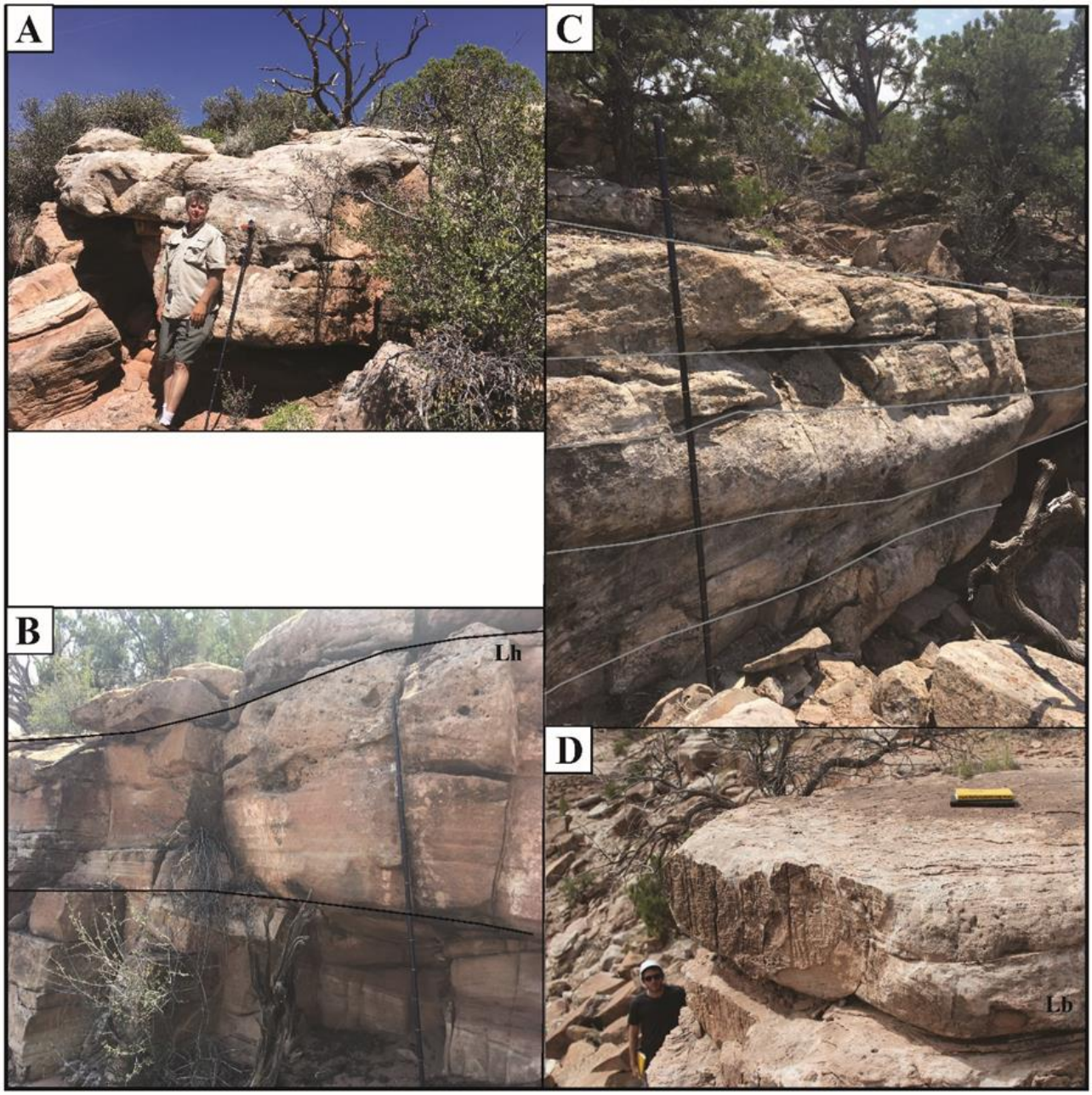

Figure 2.7: Outcrop photos of the Amalgamated Sandstone Channels (ASC)

A. Laminated to trough crossbedded channel sandstone. B. Laminated sandstone channel fill. C. Trough crossbedded channel sandstones E. Laminated to ripple cross-stratfied sandstones with bioturbation throughout the uppermost part of the bed.

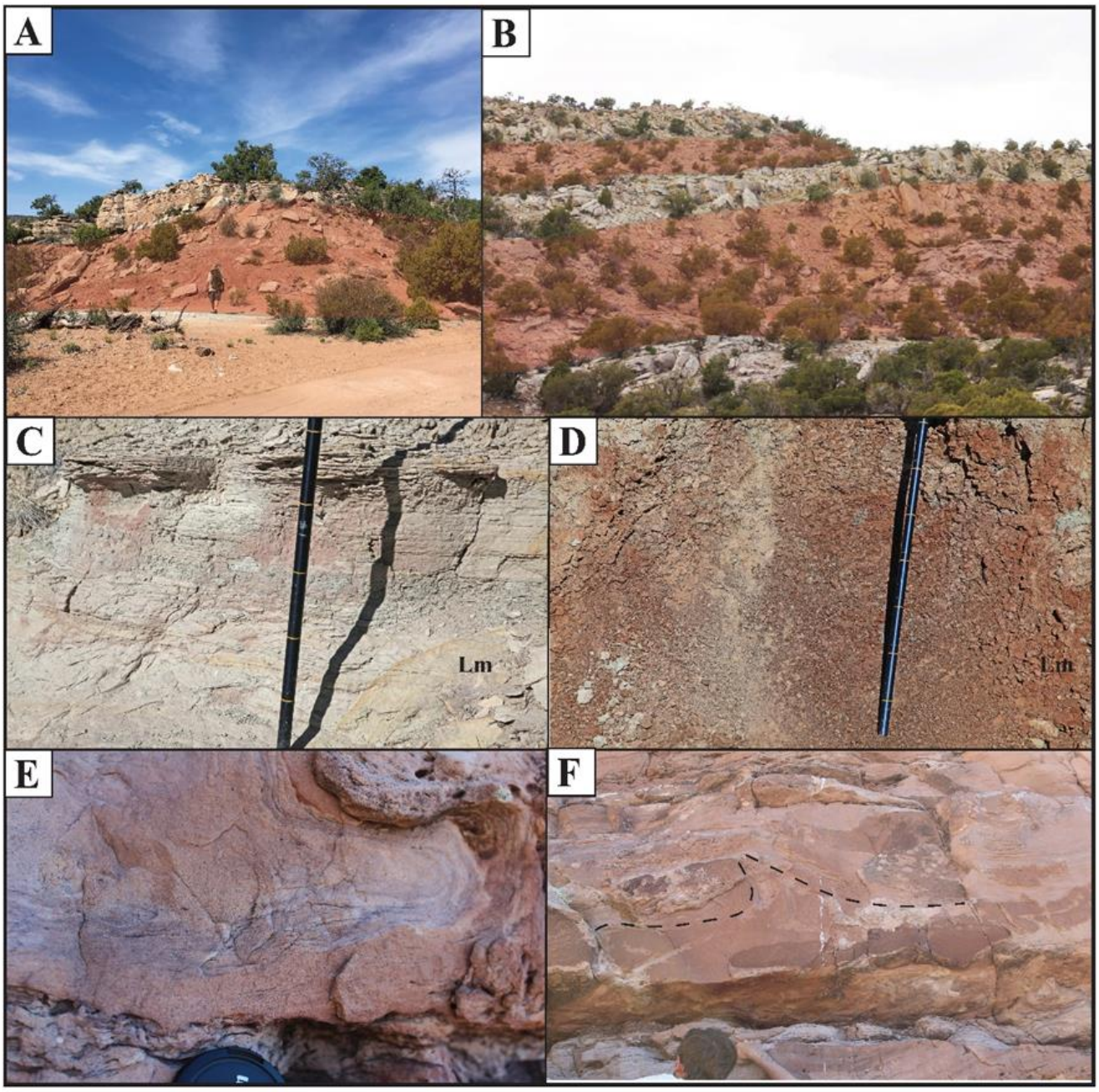

Figure 2.8: Outcrop photos of the Isolated Sandstone Channel (ISC).

A. Isolated sandstone channels interbedded with reddish brown to greenish gray siltstones and mudstones. Red highlighting mudstones in outcrop. B. Red highlighting mudstones interbedded with sandstone channels. C. Greenish gray floodplain mudstones/siltstones D. Reddish brown mudstones/siltstones E. Convoluted bedding in channel fill. F. Flame structure in channel fill.

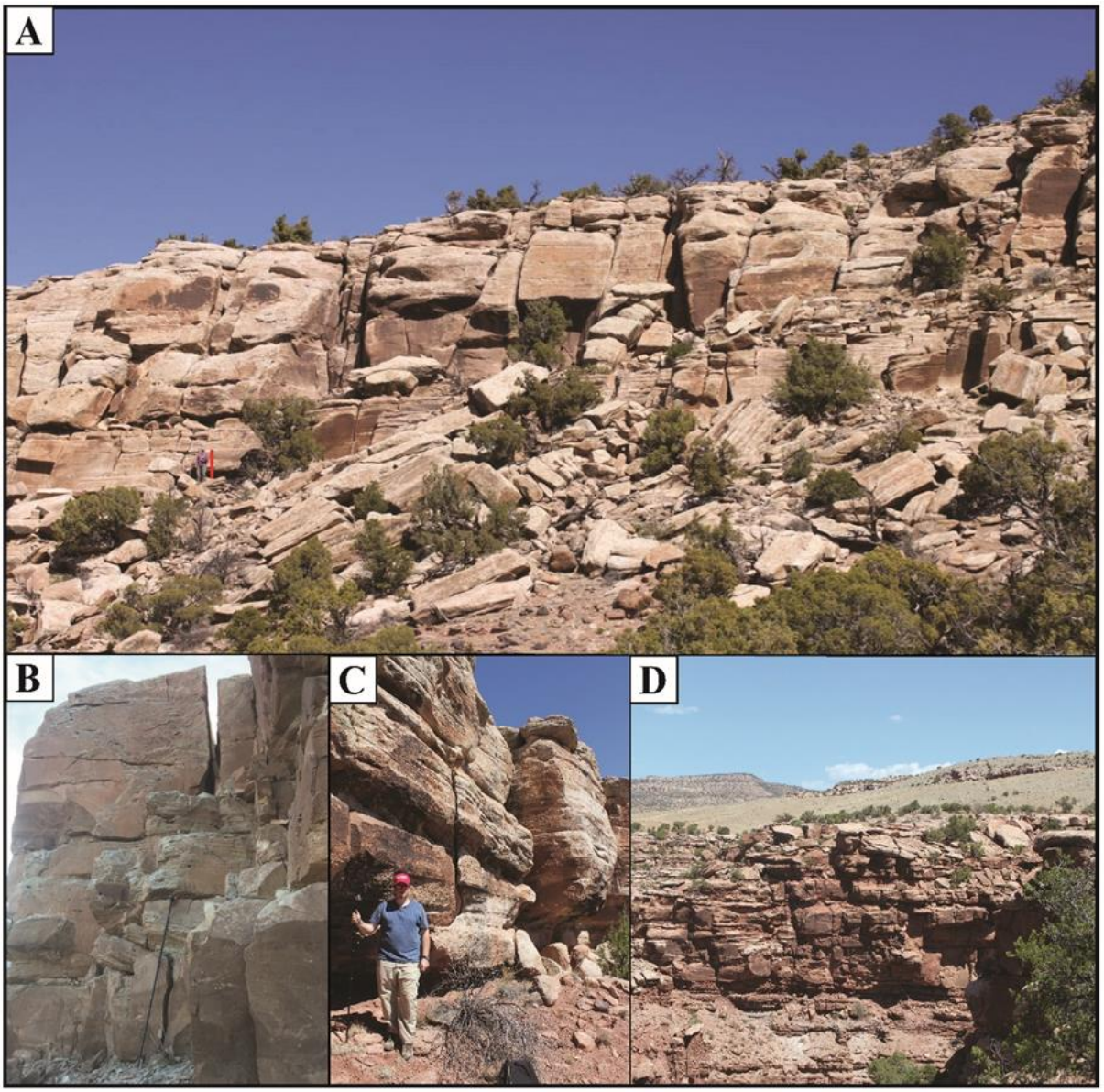

Figure 2.9: Outcrop photos of the laterally stacked sandstone channels (LSSC).

A. Laterally Stacked Sandstone channels 6-10 m thick with dominantly subhorizontal bedding. B. LSSC with dominantly massive to subhorizontal bedding. C. Subhorizonal bedding in channel fill. D. LSSC at the distal section of Grassy Hill.

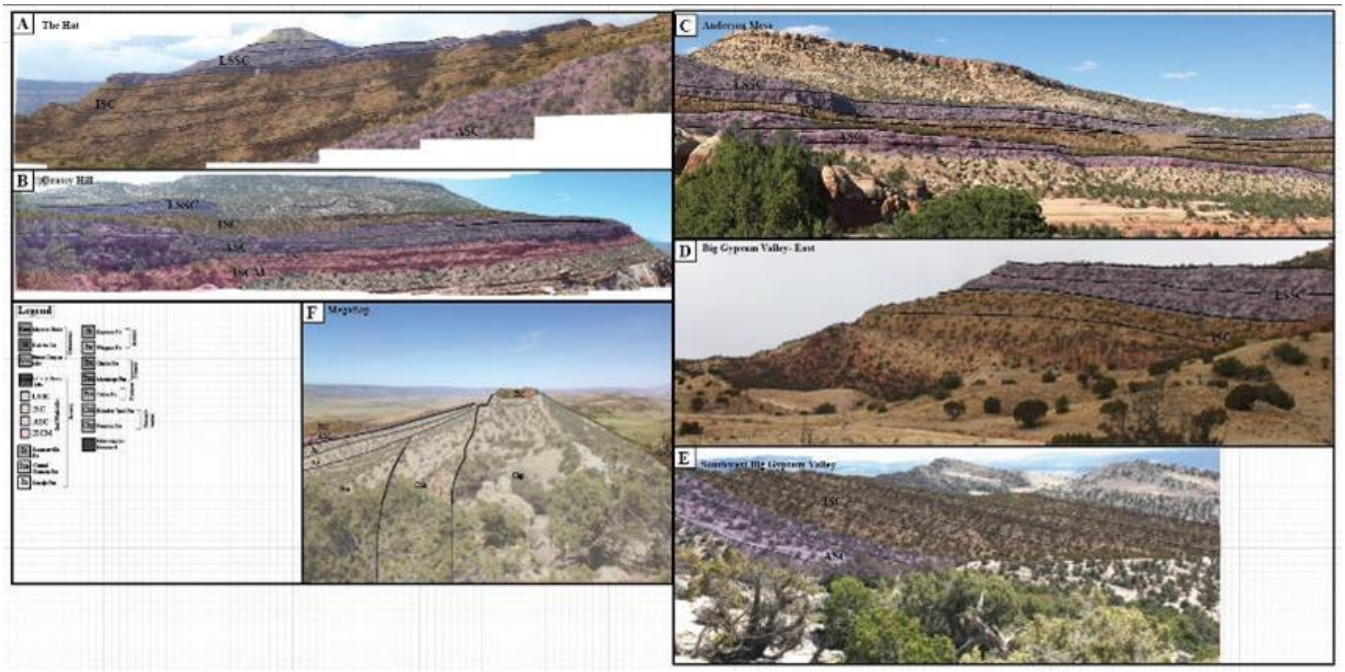

Figure 2.10: Panoramic photos of the stratigraphy at each location throughout Gypsum Valley.

Refer to Figure 2 for the location within Gypsum Valley A. The Hat B. Grassy Hill C. Anderson Mesa D. Southeastern Big Gypsum Valley E. Southwestern Big Gypsum Valley F. MegaFlap.

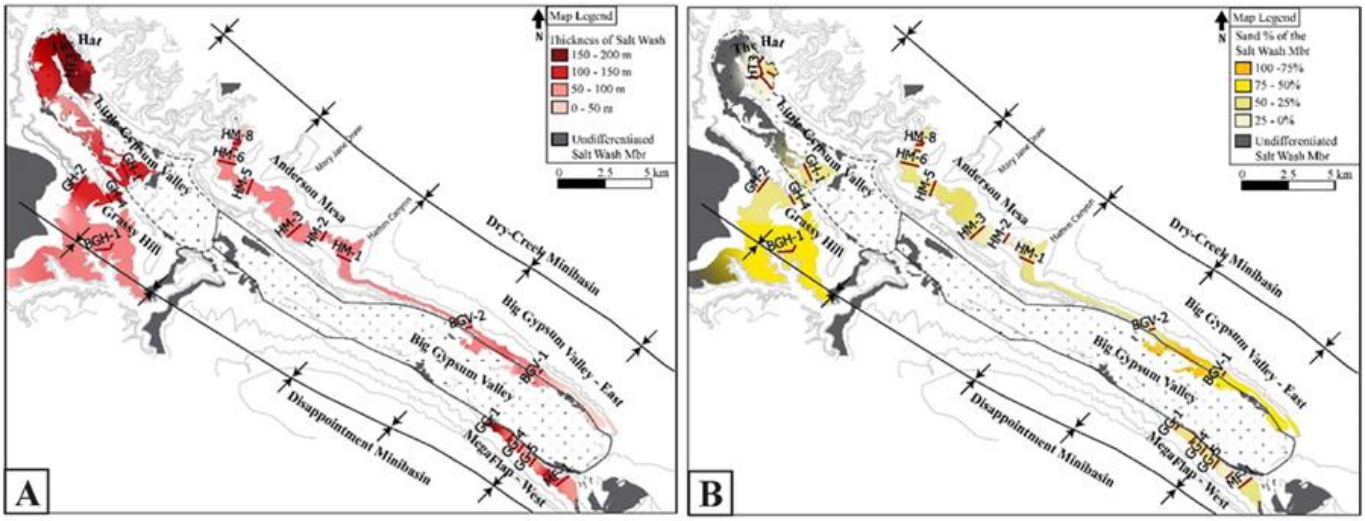

Figure 2.11: Changes in the Salt Wash Member

A. Thickness changes within the entire Salt Wash Member in Gypsum Valley. B. Sandstone percentage changes throughout the entire Salt Wash Member throughout Gypsum Valley.

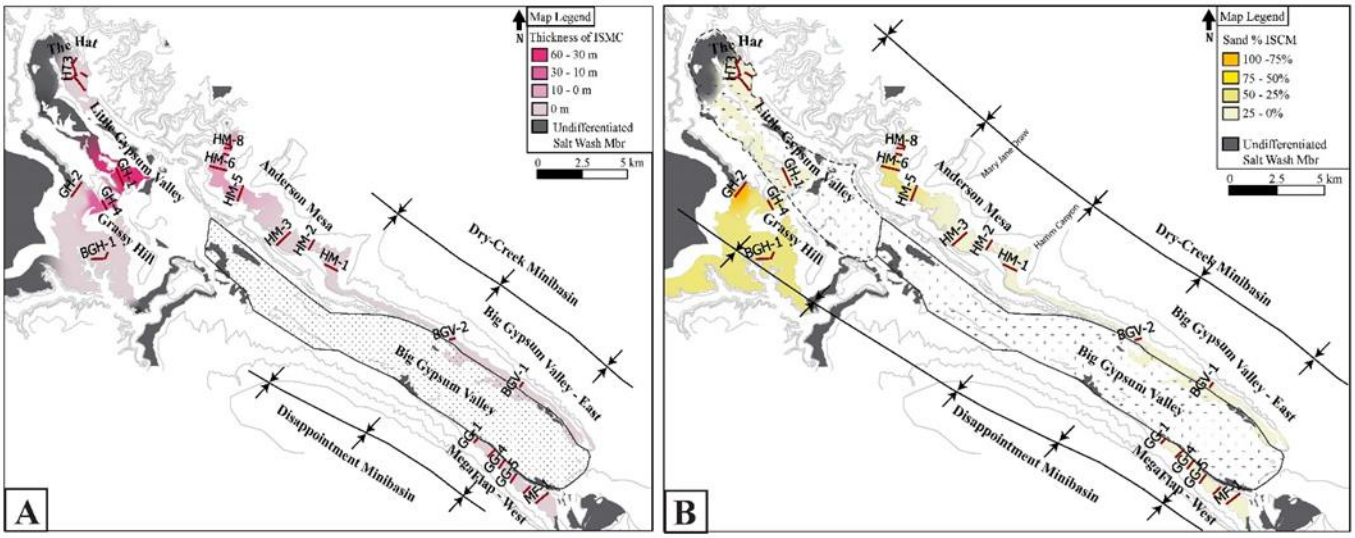

Figure 2.12: Changes in ISCM

A. Thickness changes within the ISCM in Gypsum Valley. B. Sandstone percentage changes throughout the ISCM throughout Gypsum Valley.

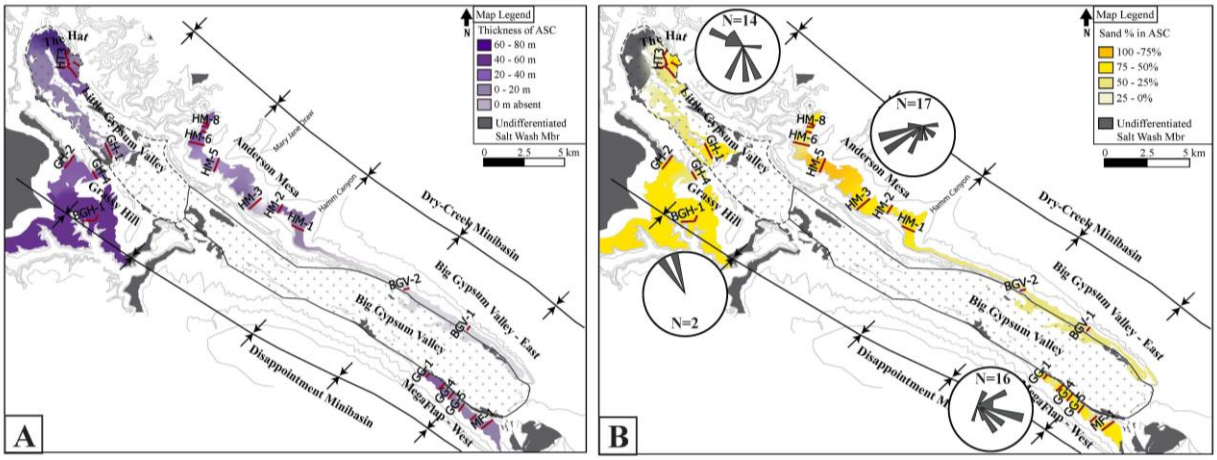

Figure 2.13: Changes in ASC

A. Thickness changes within the ASC in Gypsum Valley. B. Sandstone percentage changes throughout the ASC throughout Gypsum Valley.

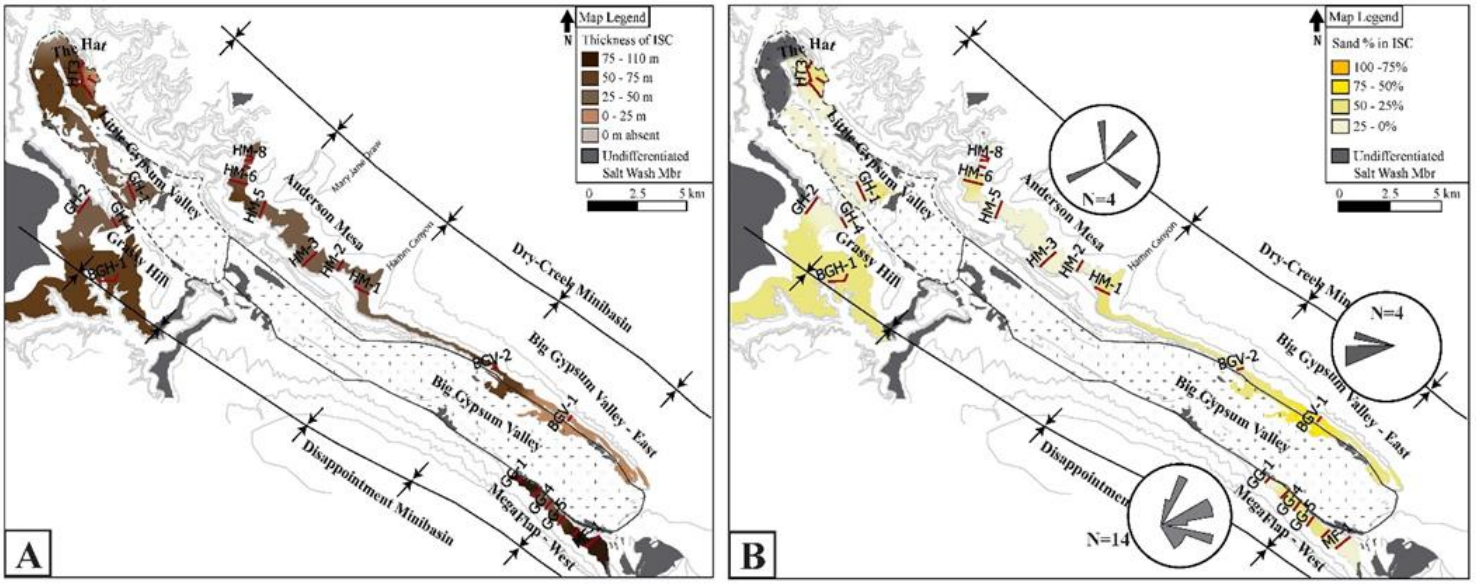

Figure 2.14: Changes in ISC

A. Thickness changes within the ISC in Gypsum Valley. B. Sandstone percentage changes throughout the ISC throughout Gypsum Valley.

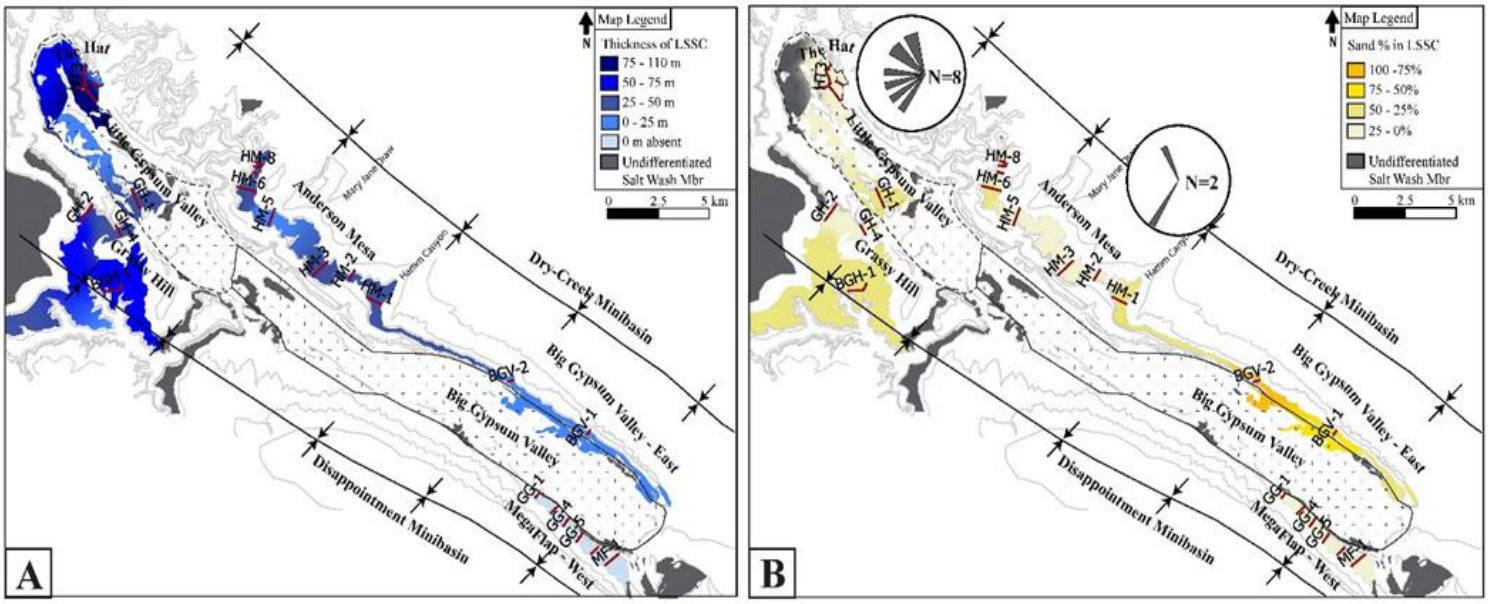

Figure 2.15: Changes in LSSC
A. Thickness changes within the LSSC in Gypsum Valley. B. Sandstone percentage changes throughout the LSSC throughout Gypsum Valley.

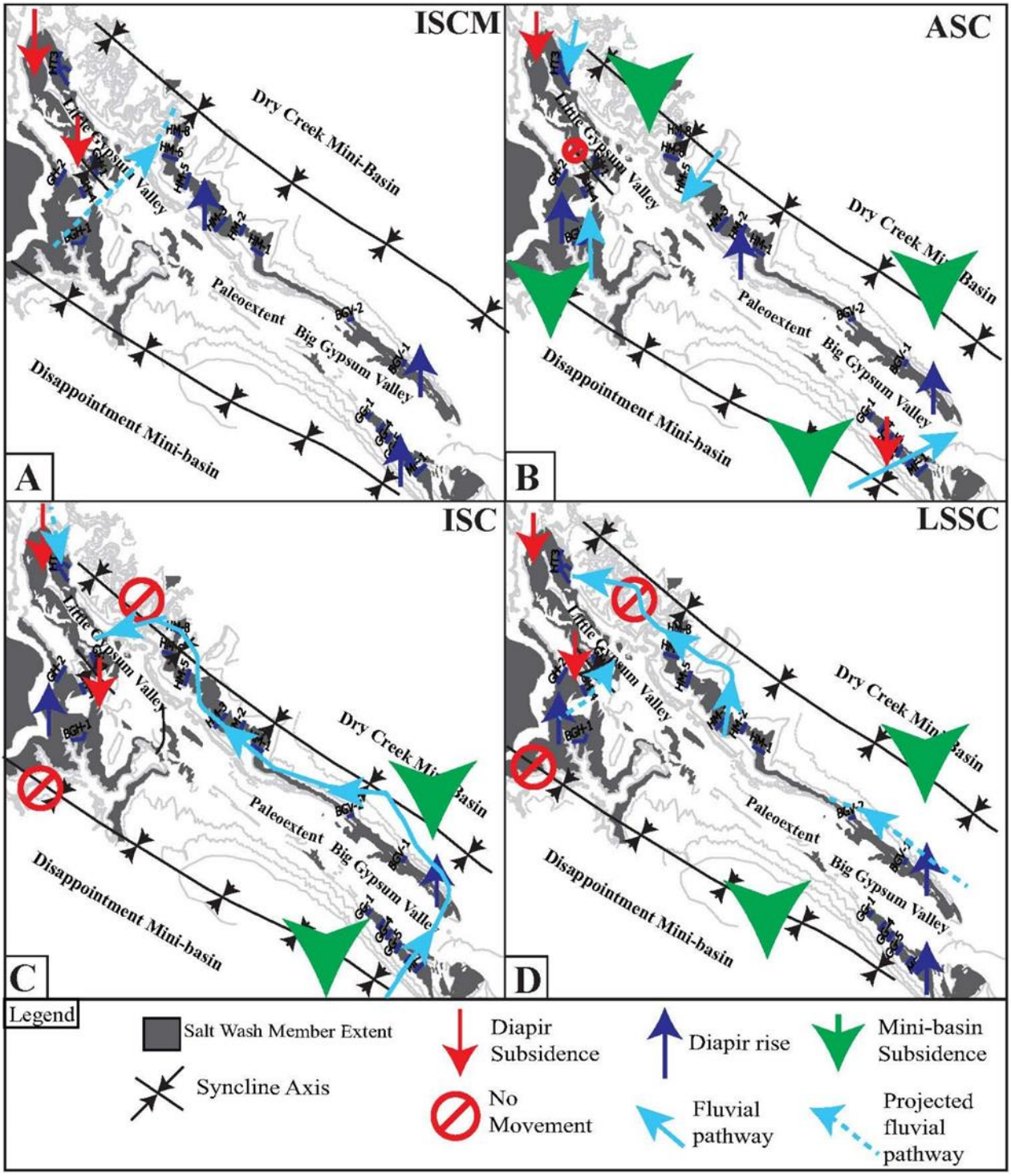

Figure 2.16: Summary of Events

Summary of diapir subsidence, rise, or no movement around Gypsum Valley throughout Salt Wash Member deposition. Figure also shows movement in adjacent Dry Creek and Disappointment minibasins.

References

Andrie, J.R., Giles, K.A., Lawton, T.F., and Rowan, M.G., 2012, Halokinetic-sequence stratigraphy, fluvial sedimentology and structural geometry of the Eocene Carroza Formation along La Popa salt weld, La Popa Basin, Mexico: Geological Society, London, Special Publications, v. 363, p. 59–79, doi:10.1144/SP363.4.

Banham, S.G., and Mountney, N.P., 2013a, Controls on fluvial sedimentary architecture and sediment-fill state in salt-walled mini-basins: Triassic Moenkopi Formation, Salt Anticline Region, SE Utah, USA: Basin Research, v. 25, p. 709–737, doi:10.1111/bre.12022.

Banham, S.G., and Mountney, N.P., 2013b, Evolution of fluvial systems in salt-walled mini-basins: A review and new insights: Sedimentary Geology, v. 296, p. 142–166, doi:10.1016/j.sedgeo.2013.08.010.

Blum, M.D., and Törnqvist, T.E., 2000, Fluvial responses to climate and sea-level change: a review and look forward: Fluvial responses to climate and sea-level change: Sedimentology, v. 47, p. 2–48, doi:10.1046/j.1365-3091.2000.00008.x.

Cater, F.W., 1970, Geology of the Salt Anticline Region in Southwestern Colorado: , p. 84.

Cater, F.W., and Craig, L.C., 1970, Geology of the Salt Anticline region in southwestern Colorado, with a section on stratigraphy.: Geol. Quad. U.S. Geol. Survey PP-637, 84 p.

Craig, L.C., 1955, Stratigraphy of the Morrison and Related Formations, Colorado Plateau Region: A Preliminary Report: U.S. Government Printing Office, 50 p.

Cross, T.A., 1986, Tectonic Controls of Foreland Basin Subsidence and Laramide Style Deformation, Western United States - Foreland Basins - Wiley Online Library:, https://onlinelibrary.wiley.com/doi/abs/10.1002/9781444303810.ch1 (accessed September 2019).

DeCelles, P.G., 2004, Late Jurassic to Eocene evolution of the Cordilleran thrust belt and foreland basin system, western U.S.A.: American Journal of Science, v. 304, p. 105–168, doi:10.2475/ajs.304.2.105.

DeCelles, P.G., and Currie, B.S., 1996, Long-term sediment accumulation in the Middle Jurassic–early Eocene Cordilleran retroarc foreland-basin system: Geology, v. 24, p. 591, doi:10.1130/0091-7613(1996)024<0591:LTSAIT>2.3.CO;2.

DeCelles, P.G., Lawton, T.F., and Mitra, G., 1995, Thrust timing, growth of structural culminations, and synorogenic sedimentation in the type Sevier orogenic belt, western United States: Geology, v. 23, p. 699, doi:10.1130/0091-7613(1995)023<0699:TTGOSC>2.3.CO;2.

Dickinson, W.R., and Gehrels, G.E., 2008, Sediment delivery to the Cordilleran foreland basin: Insights from U-Pb ages of detrital zircons in Upper Jurassic and Cretaceous strata of the

Colorado Plateau: American Journal of Science, v. 308, p. 1041–1082, doi:10.2475/10.2008.01.

Dickinson, W.R., and Lawton, T.F., 2003, Sequential intercontinental suturing as the ultimate control for Pennsylvanian Ancestral Rocky Mountains deformation: Geology, v. 31, p. 609–612, doi:10.1130/0091-7613(2003)031<0609:SISATU>2.0.CO;2.

Dickinson, W.R., and Lawton, T.F., 2001, Tectonic setting and sandstone petrofacies of the Bisbee basin (USA–Mexico): Journal of South American Earth Sciences, v. 14, p. 475–504, doi:10.1016/S0895-9811(01)00046-3.

Elston, D., and Landis, E., 1960, Pre-Cutler unconformities and early growth of the Paradox Valley and Gypsum Valley salt anticlines, Colorado, *in* Short papers in the geological sciences: US Geol. Survey Prof. Paper 400B, p. B261–B265.

Escosa, F.O., Rowan, M.G., Giles, K.A., Deatrick, K.T., Mast, A.M., Langford, R.P., Hearon, T.E., and Roca, E., 2018, Lateral terminations of salt walls and megaflaps: An example from Gypsum Valley Diapir, Paradox Basin, Colorado, USA: Basin Research, doi:10.1111/bre.12316.

Ge, H., Jackson, M.P.A., and Vendeville, and B.C., 1997, Kinematics and Dynamics of Salt Tectonics Driven by Progradation: AAPG Bulletin, v. 81, p. 398–423.

Hazel, J.E., 1994, Sedimentary response to intrabasinal salt tectonism in the Upper Triassic Chinle Formation: US Geological Survey Bulletin 2000-F, 30 p.

Heller, P.L., Bowdler, S.S., Chambers, H.P., Coogan, J.C., Hagen, E.S., Shuster, M.W., Winslow, N.S., and Lawton, T.F., 1986, Time of initial thrusting in the Sevier orogenic belt, Idaho-Wyoming and Utah: Geology, v. 14, p. 388, doi:10.1130/0091-7613(1986)14<388:TOITIT>2.0.CO;2.

Heller, P.L., and Paola, C., 1989, The paradox of Lower Cretaceous gravels and the initiation of thrusting in the Sevier orogenic belt, United States Western Interior: GSA Bulletin, v. 101, p. 864–875, doi:10.1130/0016-7606(1989)101<0864:TPOLCG>2.3.CO;2.

Hite, R.J., and Buckner, D.H., 1981, Stratigraphic Correlations, Facies Concepts, and Cyclicity in Pennsylvanian Rocks of the Paradox Basin: , p. 13.

Kjemperud, A.V., Schomacker, E.R., and Cross, T.A., 2008, Architecture and stratigraphy of alluvial deposits, Morrison Formation (Upper Jurassic), Utah: AAPG Bulletin, v. 92, p. 1055–1076, doi:10.1306/03250807115.

Landis, E.R., Shoemaker, E.M., and Elston, D.P., 1961, Early and late growth of the Gypsum Valley salt anticline, San Miguel County, Colorado: Short papers in the geologic and hydrologic sciences: US Geol. Survey Prof. Paper, p. C131–136.

Langford, R., Giles, K.A., Thompson, J.A., and Rowan, M.G., 2018, Shoulder Formation in the Paradox Basin: A Record of Progressive Diapir Narrowing and Minibasin Expansion,

http://www.searchanddiscovery.com/abstracts/html/2018/ace2018/abstracts/2855342.html (accessed June 2019).

Lawton, T.F., and Buck, B.J., 2006, Implications of diapir-derived detritus and gypsic paleosols in Lower Triassic strata near the Castle Valley salt wall, Paradox Basin, Utah: Geology, v. 34, p. 885–888.

Lawton, T.F., González-León, C.M., Lucas, S.G., and Scott, R.W., 2004, Stratigraphy and sedimentology of the upper Aptian–upper Albian Mural Limestone (Bisbee Group) in northern Sonora, Mexic: Cretaceous Research, v. 25, p. 43–60, doi:10.1016/j.cretres.2003.09.003.

Matthews, W.J., Hampson, G.J., Trudgill, B.D., and Underhill, J.R., 2007, Controls on fluviolacustrine reservoir distribution and architecture in passive salt-diapir provinces: Insights from outcrop analogs: AAPG bulletin, v. 91, p. 1367–1403.

Mullens, T.E., and Freeman, V.L., 1957, Lithofacies of the Salt Wash Member of the Morrison Formation, Colorado Plateau: Geological Society of America Bulletin, v. 68, p. 505–526, doi:10.1130/0016-7606(1957)68[505:LOTSWM]2.0.CO;2.

Owen, A., Jupp, P.E., Nichols, G.J., Hartley, A.J., Weissmann, G.S., and Sadykova, D., 2015a, Statistical Estimation of the Position of An Apex: Application To the Geological Record: Journal of Sedimentary Research, v. 85, p. 142–152, doi:10.2110/jsr.2015.16.

Owen, A., Nichols, G.J., Hartley, A.J., and Weissmann, G.S., 2015b, Vertical trends within the prograding Salt Wash distributive fluvial system, SW USA: Basin Research, p. n/a-n/a, doi:10.1111/bre.12165.

Owen, A., Nichols, G.J., Hartley, A.J., Weissmann, G.S., and Scuderi, L.A., 2015c, Quantification of a Distributive Fluvial System: The Salt Wash DFS of the Morrison Formation, SW U.S.A.: Journal of Sedimentary Research, v. 85, p. 544–561, doi:10.2110/jsr.2015.35.

Peterson, F., 1984, Fluvial sedimentation on a quivering craton: Influence of slight crustal movements on fluvial processes, upper Jurassic Morrison formation, western Colorado plateau: Sedimentary Geology, v. 38, p. 21–49, doi:10.1016/0037-0738(84)90073-3.

Prochnow, S.J., Atchley, S.C., Boucher, T.E., Nordt, L.C., and Hudec, M.R., 2006, The influence of salt withdrawal subsidence on palaeosol maturity and cyclic fluvial deposition in the Upper Triassic Chinle Formation: Castle Valley, Utah: Sedimentology, v. 53, p. 1319–1345.

Ronson, R.B., 2018, Facies Changes Associated with Formation of an Extensive Salt Shoulder by the Coastal and Eolian Carmel and Entrada Formations, Gypsum Valley, Colorado [M.S.]: The University of Texas at El Paso, 142 p., https://search.proquest.com/docview/2111273760/abstract/B4ECC5C697AE4A86PQ/1 (accessed June 2019).

Rowan, M.G., Giles, K.A., Hearon IV, T.E., and Fiduk, J.C., 2016, Megaflaps adjacent to salt diapirs: AAPG Bulletin, v. 100, p. 1723–1747, doi:10.1306/05241616009.

Shawe, D.R., 1968a, Geological investigations in the Slick Rock district, San Miguel and Dolores Counties, Colorado: G.P.O.

Shawe, D.R., 1968b, Petrography of sedimentary rocks in the Slick Rock district, San Miguel and Dolores Counties, Colorado: U.S. Geol. Survey Prof. Paper 576-B, 34 p.

Shoemaker, E.M., Case, J.E., and Elston, D.P., 1958, Salt Anticlines of the Paradox Basin, *in* Guidebook to the Geology of the Paradox Basin, Ninth Annual Field Conference, Utah Geological Survey, p. 39–59, http://archives.datapages.com/data/uga/data/008/008001/39_ugs80039.htm (accessed November 2017).

Stokes, W.L., 1944, Morrison formation and related deposits in and adjacent to the Colorado Plateau: Geological Society of America Bulletin, v. 55, p. 951–992, doi:10.1130/GSAB-55-951.

Stokes, W.L., and Phoenix, D.A., 1948, Geology of the Egnar-Gypsum Valley area, San Miguel and Montrose Counties, Colorado: US Geological Survey Oil and Gas Investigations Map OM-93.

Trudgill, B.D., 2011, Evolution of salt structures in the northern Paradox Basin: controls on evaporite deposition, salt wall growth and supra-salt stratigraphic architecture: Basin Research, v. 23, p. 208–238, doi:10.1111/j.1365-2117.2010.00478.x.

Turner, C.E., and Peterson, F., 2004, Reconstruction of the Upper Jurassic Morrison Formation extinct ecosystem—a synthesis: Sedimentary Geology, v. 167, p. 309–355, doi:10.1016/j.sedgeo.2004.01.009.

Tyler, N., and Ethridge, F.G., 1983, Depositional setting of the Salt Wash Member of the Morrison Formation, Southwest Colorado: Journal of Sedimentary Research, v. 53, p. 67–82, doi:10.1306/212F8157-2B24-11D7-8648000102C1865D.

Venus, J.H., Mountney, N.P., and McCaffrey, W.D., 2015, Syn-sedimentary salt diapirism as a control on fluvial-system evolution: an example from the proximal Permian Cutler Group, SE Utah, USA: Basin Research, v. 27, p. 152–182, doi:10.1111/bre.12066.

Vogel, J.D., 1960, Geology and ore deposits of the Klondike Ridge area, Colorado: U.S. Geological Survey], Open-File Report USGS Numbered Series 60–145, http://pubs.er.usgs.gov/publication/ofr60145 (accessed February 2019).

Weissmann, G.S., Hartley, A.J., Nichols, G.J., Scuderi, L.A., Olson, M., Buehler, H., and Banteah, R., 2010, Fluvial form in modern continental sedimentary basins: Distributive fluvial systems: Geology, v. 38, p. 39–42, doi:10.1130/G30242.1.

Yingling, V.L., and Heller, P.L., 1992, Timing and record of foreland sedimentation during the initiation of the Sevier orogenic belt in central Utah: Basin Research, v. 4, p. 279–290, doi:10.1111/j.1365-2117.1992.tb00049.x.

Chapter 3: Diagenetic Changes within the Jurassic Fluvial Salt Wash Member Sandstones of the Morrison Formation Related to Fluid Interactions with the Gypsum Valley Salt Diapir, Paradox Basin, CO

Abstract

This study documents variability in the grain composition, porosity, and distribution of authigenic cements of sandstones in the Salt Wash Member of the Morrison Formation in proximity to the Gypsum Valley salt diapir. In Gypsum Valley the Salt Wash Member was deposited in microbasins that formed on top of the salt while other parts of the salt wall were still diapirically rising and adjacent minibasins were subsiding. The impact of the near-diapir diagenetic processes is pivotal for the understanding of the porosity and permeability trends of salt-related hydrocarbon reservoirs. This 'transitional position' serves as a potential pathway for diapir-adjacent fluid flow, making the Morrison Formation a model for a critical player in hydrocarbon systems.

The Salt Wash Member sandstones from multiple locations around Gypsum Valley are predominantly quartzarenites and to a lesser extent sublitharenites, with porosities in a range from 11-20% with grains) the lowest being in Big Gypsum Valley and the highest in Little Gypsum Valley. Lithic components include chert, siltstone, claystone, limestone, dolostone, metamorphic, and igneous rock fragments. Most of the porosity, including porosity that was later occluded by cements, is attributed to secondary porosity created by the dissolution of lithic chert grains, feldspar, and early carbonate cements. Quantitatively, quartz overgrowth cements dominate, followed by calcite cements. Occasional nonferroan and ferroan dolomite cements are present. Pyrite and barite, two authigenic minerals that previously have been found in the Salt Wash

Member are absent in the study area. No indicators for hydrocarbon migration (e.g. dead oil or rock bleaching) were observed.

We interpret these observations as the result of mixing of saline fluids derived from diapir halite dissolution by meteoric water – potentially driven by convection fueled by heat flux from the salt diapir – which strongly impacted sandstone diagenesis. Oxygen-rich meteoric waters enabled oxidation of organic matter and production of carbonic acid, which favored the dissolution of early carbonate cements and feldspar, whereas fluid flow and complexation of carbonate and sulfate by sodium ions and complexation of calcium and magnesium by chloride limited the precipitation of carbonate and barite cements. The implication of this finding is that in passive diapiric systems, near-diapir fluid flow constitutes a mechanism that enhances and maintains porosity and permeability in sandstones, which is critical for the emplacement of hydrocarbon migration conduits. Secondary porosity formed by near diapir diagenetic fluids enhanced porosity. Sample porosity ranged from 11-20%, Double the 5.4% average in samples farther from the diapir (Breit and Goldhaber, 1996).

Introduction

Very few experimental or field-based studies have focused on understanding how sandstones are diagenetically altered by fluids that interact with salt diapirs. Understanding the diagenetic changes in sandstone packages adjacent to salt diapirs is critical because mineral dissolution and cement precipitation can either increase or reduce porosity and permeability, thereby degrading or improving the reservoir potential and changing hydrocarbon migration pathways (McManus and Hanor, 1988, 1993a; Esch, 1995). Previous studies documented the presence/absence of authigenic minerals and cements, mapped their distribution around salt diapirs, and aimed to understand the role of faults and fractures that carry fluids (McManus and

Hanor, 1988; Posey and Kyle, 1988; Breit et al., 1990; Esch, 1995; Breit and Goldhaber, 1996; Heness, 2016; Ronson, 2018). They quantified the amount of halite dissolved by fluids required to later create the observed cements and, the amount of fluids required to dissolve halite (McManus and Hanor, 1993b). Other studies focused on understanding transport pathways of these fluids and the thermohaline convective flow of the fluid systems around salt (McManus and Hanor, 1988; Breit et al., 1990; Esch, 1995). Today, the work to map and identify the authigenic minerals that are precipitated as a result of fluids that have interacted with an adjacent salt diapir, comprises only a little more than a handful of studies (McManus and Hanor, 1988; Posey and Kyle, 1988; Breit et al., 1990; Esch, 1995; Breit and Goldhaber, 1996; Heness, 2016; Ronson, 2018). This study aims to significantly add to that body of knowledge by documenting and interpreting the grain composition, porosity, and distribution of authigenic cements of sandstones from the Jurassic Salt Wash Member of the Morrison Formation from multiple sites in and near Gypsum Valley in the Paradox Basin, Colorado from distal, to proximal, to on top roof-position relative to the Gypsum Valley salt diapir (Figure 3.1, 3.2).

Targeting the Salt Wash Member of the Morrison Formation at the Gypsum Valley salt diapir is important for two reasons: First, the Morrison Formation was locally deposited in microbasins that formed on top of the salt while other parts of the salt wall were still rising, forming a ‘transitional position’ that serves as a potential pathway for circum-diapir fluid flow (Bailey, 2020: Chapter 4). As such, the Morrison Formation is a model for hydrocarbon conduits, which are critical players in hydrocarbon systems. It is important to understand the impact of the near-diapir diagenetic processes on the porosity and permeability of this conduit. Second, the fluvial sandstones of the Salt Wash Member have been studied extensively because they host significant vanadium-uranium deposits, including a study that focused on the diagenesis of this member in

the Paradox Basin by Breit and Goldhaber (1996). That study attributed some of the observed diagenetic features, in particular the precipitation of calcite, dolomite and barite cements to salty brines that moved from the Pennsylvanian Paradox Formation upward along faults. The Paradox Formation is the source for the salt walls in the Paradox Basin, including the Gypsum Valley diapir, but the study by Breit and Goldhaber (1996) did not attribute any diagenetic features directly to the interaction between diapiric salt and the Salt Wash Member, despite the fact that in some locations this member is in contact with the salt. The absence of this information constitutes a critical gap in knowledge: is the diagenesis of near-salt sandstones proximal to salt diapirs fundamentally different from distal locations?

Impact of Fluid Flow at Salt Diapirs on Diagenesis

Movement of fluids that interact with salt alter salt diapir-flanking sandstones through dissolution and precipitation of authigenic minerals (McManus and Hanor, 1988; Esch, 1995). Evaporites that make up salt diapirs are very soluble and have a high thermal conductivity, which results in complex thermohaline convective flow systems characterized by steep temperature and salinity gradients (Fischer, 2013). McManus and Hanor (1988), suggested that the addition of sodium (Na^+) and chloride (Cl^-) ions from halite dissolution into formation waters could activate diagenetic reactions within the stratigraphy adjacent to salt domes. Subsequent work traced the origin and temperature of fluids flowing through formations to local salt diapirs by using strontium (Sr), carbon (C), oxygen (O), and sulfur (S) isotopic compositions of authigenic minerals such as carbonates, barite, and pyrite (McManus and Hanor, 1988; Breit et al., 1990; McManus and Hanor, 1993b; Breit and Goldhaber, 1996; Fischer et al., 2013). These contributions demonstrated that calcium ions (Ca^{2+}) and S were derived from the dissolution of salt, and carbonate was produced by oxidation of methane (CH_4) and sulfate (SO_4^{2-}) reduction (McManus and Hanor, 1993). These

reactions and transport by fluids resulted in the precipitation of cements such as authigenic calcite, pyrite, dolomite, barite, and pyrrhotite (McManus and Hanor, 1988; Breit et al., 1990; Esch, 1995; Breit and Goldhaber, 1996). Fluids that interact with the salt diapir preferentially flow through welds or faults and fractures concentrated in the flanking stratigraphy. Thus, diagenetic alteration caused by the presence of the fluids can be focused around these structures (Breit et al., 1990; Hudson and Hanson, 2010; Fischer et al., 2013). Fluids that flow through diapir-flanking sandstones have been documented to impact sandstone diagenesis up to at least one kilometer away from the diapir margin (McManus and Hanor, 1993b). Cementation by the aforementioned suite of minerals is most pervasive closest to the salt-sediment interface and also occurs preferentially at the base of sandstone beds (McManus and Hanor, 1988, 1993b; Esch, 1995).

Diagenesis Studies in the Paradox Basin

For the Paradox Basin studies that specifically address aspects salt dissolution-related diagenesis are available for four topics, which will in the following briefly introduced here.

A study at the Onion Creek salt diapir focused on understanding the spatial and temporal variability of the paleofluids that flowed through faults and fractures (Figure 3.1; Fischer et al., 2013). Fluids from the Onion Creek Diapir were divided into three types, namely meteoric, moderate, and high salinity fluids, the latter probably originating from Pennsylvanian and Permian evaporites (Fischer et al., 2013). Intense mixing of shallow meteoric and deep brine fluids were likely the cause that no significant stratigraphic segregation of fluids could be detected (Fischer et al., 2013).

In Gypsum Valley, the diagenetic alteration of sandstones and the distribution of the different types of cements proximal and distal to the diapir margin were studied for the fluvio-lacustrine Triassic Chinle Formation (Heness, 2016) and the coastal and eolian Jurassic Carmel

and Entrada Formations (Ronson, 2018). Heness (2016) compared diagenetic features from the Chinle Formation on the southeastern margin of Gypsum Valley at Bridge Canyon with a location at Summit Canyon, which is 10 km away from the Gypsum Valley diapir (Figure 3.2). The major authigenic cements found at all locations within the Chinle Formation were hematite, calcite and dolomite, whereby hematite cementation is early in the paragenetic history and can inhibit subsequent calcite cementation. Dolomite cement was present in almost all samples. It forms early in the paragenetic sequence, is replaced by calcite, and forms again late in the history by replacing calcite (Heness, 2016). Samples with either only calcite or dolomite cements were found on the diapir margin and samples containing both calcite and dolomite were found away from the salt diapir (Heness, 2016). Proximal to the diapir margin authigenic cements filled pore spaces resulting in decreased porosity. Distal to the diapir, at Summit Canyon, porosity was the highest of all samples at 12-20% (Heness, 2016). Ronson (2018) compared diagenetic features from the Carmel and Entrada formations in Little Gypsum Valley on the northeastern margin of the diapir to a location at Slick Rock Canyon distal to the diapir margin. Similar to the study by Heness (2016), Ronson (2018) found that the major authigenic minerals within these lithologies are hematite, calcite, and dolomite. On the diapir margin iron oxide cementation was early followed by calcite cementation, compaction, void filling calcite, partial dissolution of calcite cement, and late stage localized dolomite cementation (Ronson, 2018). Distal to the diapir at Slick Rock Canyon iron oxide cementation was similar with a complete late stage dolomitization of calcite followed by partial dissolution of dolomite and calcite cements, and a late stage of iron cementation (Ronson, 2018). All samples studied had relatively high porosity (7-20%) but the highest was found on the diapir margin in Little Gypsum Valley (Ronson, 2018). Calcite cements were found on the diapir margin and dolomite cements distal to the diapir (Ronson, 2018). While both studies

found that porosity was secondary, and the result of dissolution of cements and/or grains (Heness, 2016; Ronson, 2018), the histories of cementation and porosity occlusion appear to be in stark contrast between the Chinle Formation (highest porosity distal from Gypsum Valley Diapir) and the Entrada and Carmel formations (highest prosity proximal to Gypsum Valley Diapir).

In the Paradox Basin, diagenesis of the Salt Wash Member is the most extensively studied (Breit and Goldhaber, 1989, 1996; Breit et al., 1990). The Salt Wash Member within the Slick Rock district displays several assemblages of authigenic minerals including albite, barite, calcite, chlorite, chalcedony, dolomite, hematite, illite-smectite, kaolinite, pyrite, quartz overgrowths, and smectite, where calcite is most abundant (Breit and Goldhaber, 1996). Breit and Goldhaber (1996) found the paragenetic sequence to be: (1) precipitation of calcite, chlorite-smectite, ferric oxides, pyrite, and chalcedony precipitated during shallow burial (<400 m), (2) formation of quartz overgrowths, chlorite, and illite-smectite during deep burial (1 to 4 km), (3) migration of brines derived partly from bedded salts in the Pennsylvanian Paradox Formation along faults into Morrison sandstones, followed by meteoric waters resulting in the precipitation of calcite, dolomite, and barite, (4) Late Tertiary erosion of structurally elevated areas resulting in dissolution of chlorite and plagioclase, and the precipitation of kaolinite. Interestingly, the study by Breit and Goldhaber (1996) didn't attribute any diagenetic features directly to the interaction between diapiric salt and the Salt Wash Member, despite the fact that in some locations this member is in contact with the salt. As the studies by Heness (2016) and Ronson (2018) demonstrated, diagenesis proximal and distal to the diapir margin can be significantly different, and this information is missing for the Salt Wash Member of the Morrison Formation.

Salt Wash Member of the Morrison Formation

The Salt Wash Member is the most aerially extensive exposed member of the Morrison Formation spanning central Utah, west-central Colorado, northeast Arizona, and northwestern New Mexico (Craig, 1955; Mullens and Freeman, 1957; Turner and Peterson, 2004). The Salt Wash Member has been described as an eastward prograding distributive fluvial system (Craig, 1955; Mullens and Freeman, 1957; Weissmann et al., 2013). Several workers have described and characterized the Salt Wash Member as amalgamated, vertically stacked sandstone fluvial channel packages interbedded with siltstones and mudstones of floodplain deposits (Stokes, 1944; Craig, 1955; Mullens and Freeman, 1957; Peterson, 1984; Turner and Peterson, 2004; Dickinson and Gehrels, 2008; Owen et al., 2015). A single source area for the sediments of the Salt Wash Member has been proposed (Craig, 1955; Mullens and Freeman, 1957; Tyler and Ethridge, 1983; Owen et al., 2015). Using a statistical projection of paleocurrent data Owen (2015) suggested the apex of the Salt Wash to be located in northeastern Arizona, which supported previous work proposing a sole source of sediment in the Mogollon highlands (Mullens and Freeman, 1957; Dickinson and Gehrels, 2008). Paleocurrents indicate flow to the north and the northeast (Stokes, 1944; Turner and Peterson, 2004; Dickinson and Gehrels, 2008) (Figure 3.1). Today, there is a consensus that the sediments of the Salt Wash Member of the Morrison are mainly derived from Paleozoic-age sediments recycled from Jurassic eolianites uplifted in the Mogollon highlands and the Sevier thrust belt with minor input from igneous or metamorphic sources (Craig, 1955; Dickinson and Gehrels, 2008).

The sandstones of the Salt Wash Member have been classified as sublitharenites that are medium to fine grained, moderately to well sorted, and subrounded to subangular (Craig, 1955; Dickinson and Gehrels, 2008). The sandstones of the Salt Wash Member are mainly composed of

detrital sand grains and minor amounts of silt or clay grains (Craig, 1955). The detrital sand grains are quartz, feldspars (orthoclase and albite), chert, gypsum, calcite, dolomite, and heavy minerals like zircon, tourmaline, garnet, rutile, anatase, staurolite, biotite, spinel, and apatite (Craig, 1955; Dickinson and Gehrels, 2008). Quartz and quartz overgrowths make up most of the sandstone at about 86% (Craig, 1955; Dickinson and Gehrels, 2008). Calcite cements have also been found in minor amounts (Craig, 1955).

Methods

Twenty-four composite stratigraphic sections were measured at five study locations throughout Gypsum Valley: The Hat, Grassy Hill, Anderson Mesa, Southeast Big Gypsum Valley, and the MegaFlap. Location of sections were chosen to analyze samples that are taken on top of the diapir, diapir margin/proximal, and distally away from the diapir. Samples were taken from sandstones throughout each stratigraphic section and located with GPS coordinates. A total of 116 rock samples were collected, 10 samples were collected from The Hat, 24 samples from Grassy Hill, 39 samples from Anderson Mesa, 10 samples from the southeastern margin of Big Gypsum Valley, and 33 samples from the southwestern margin of Big Gypsum Valley.

Rock samples were brought back to the lab, cut into billets, and sent to Spectrum Petrographic Inc., Vancouver, Washington be made into thin sections. Thin section samples were stained for calcite, ferroan calcite, ferroan dolomite, feldspar, and impregnated with blue-dyed epoxy for identification of porosity. Samples were petrographically analyzed using a Leica microscope. All samples were analyzed to determine the presence of minerals, cement types, porosity types, and compaction. Petrofacies were determined based on mineral presence, cement types, and porosity present within samples. The common types of porosity (e.g. intergranular, partial dissolution, oversized pores and floating grains, and moldic) were identified by comparison

to guidebooks (Schmidt et al., 1977; Ulmer-Scholle et al., 2015). The dominant porosity types seen indicate that most of the porosity in samples is secondary with lesser amounts of preserved primary porosity (Schmidt, 1977; Ulmer-Scholle et al., 2014). The paragenetic sequence was inferred from thin section observations of cross-cutting relationships and superposition of cements. Point counts were conducted at 300 points per slide on a total of 75 samples to determine mineralogy, cement, and porosity percentages. Nine samples were counted at The Hat, 19 samples were counted at Grassy Hill, 26 samples were counted from Anderson Mesa, 11 samples were counted from southwestern Big Gypsum Valley, and 10 on the southeastern margin of Big Gypsum Valley.

Results and Discussion

Overall Composition and Sandstone Texture

The sandstone texture is the same for all samples and does not vary stratigraphically or from site to site. Samples range in grain size from low fine to low medium. Sorting in almost all samples ranges from moderately to well sorted. Sand grain rounding is dominantly subrounded to subangular. Typically, sandstones of fluvial origin are sub-angular to angular grains and thus, the more rounded grains in the study suggests that there is local recycling of the older eoalian formations like the Wingate and Carmel Entrada contributing to the sediment budget of the Salt Wash Member.

Compositionally, all samples fall into the quartzarenite and sublitharenite classification (Folk, 1980). The grain composition falls in a range of 72-95% quartz, 0.5-2.5% feldspar, and 0.6-25% lithics (Figure 3.3). Other components are accessory minerals such as minor amounts of muscovite, chalcedony, tourmaline, zircon, opaques, and glauconite, as well as cements. Quartz is present mainly as monocrystalline quartz but there is also a minor amount of polycrystalline quartz. Feldspars include plagioclase and potassium feldspar. The feldspar grains are often partially to

almost completely dissolved with ghost remnants of the grains replaced by authigenic calcite. Lithic grains are also common with a range of 0.6-25%. The lithic grains include chert, siltstone, claystone, limestone, dolostone, metamorphic, and igneous rock fragments, with chert grains being the most common lithic fragment. Chert grain fabrics are dominantly microcrystalline, but a few grains also exhibited a coarser grain fabric mixed with the microcrystalline fabric. As for the feldspar, chert grains are often observed to be partially dissolved grains that are replaced by authigenic minerals like calcite. Siltstone grains are the second most common lithic component. These grains are dominantly siliciclastic siltstone fragments composed of rounded to subangular quartz and opaque minerals with hematite cement. More rarely observed and not counted in point counts are siltstone grains containing bioclasts. Rarely, other lithic grains are observed, including shale, claystone, limestone, dolostone, metamorphic, and igneous rock fragments.

Cements are common and make up 17-20% of samples and are interpreted to be authigenic cements. The dominant cements are quartz overgrowths, followed by calcite, and then ferroan dolomite, and hematite cements. Ferroan calcite and non-ferroan dolomite cements are rarely observed. Quartz overgrowths occur at all locations and represent in most samples 20% to 40% of the cements and porosity. These overgrowths are most commonly found on monocrystalline quartz grains and appear to grow relatively early in the diagenetic history if pore space is not filled by earlier dolomite and/or ferroan dolomite cements. Calcite cements are the second most abundant, ranging from 19% to 39%. They are precipitated late in the history of the sandstones and are found filling secondary porosity created by dissolution of dolomite/ferroan dolomite or feldspars and chert grains. Ferroan calcite is also precipitated in the late stages of deposition replacing dolomite cements, dissolved grains, or filling intergranular porosity. Dolomite cements occupy a range of 10% to 23% and are formed early in the diagenetic history just after deposition.

Porosity makes up a range of 28% to 62% of the samples. This calculated percentage did not include this compared to grain components. Since grains make up 50-60% of the sandstone composition the component was taken out to see the significant changes there are in porosity throughout Gypsum Valley. When compared to the grain component porosity ranges from 11-20% in samples. Porosity observed in samples includes intergranular, partial dissolution, oversized pores and floating grains, and moldic porosity. The dominant porosity types indicate that most of the porosity in samples is of secondary origin and that only little primary porosity is preserved. Based on these observations, the secondary porosity formed primarily from the dissolution of feldspar and chert grains and the dissolution of early ferroan dolomite cements. No indicators for hydrocarbon migration (e.g. dead oil or rock bleaching) were observed.

Distribution of cements

The types of cements vary throughout the stratigraphy of the Salt Wash Member and by location. No patterns were found that would indicate that certain cement types are only present in one stratigraphic unit. Quartz overgrowths are present within most samples and abundant at each location (Figure 3.4). Calcite cements are also present at most locations throughout Gypsum Valley but decrease in abundance toward the southeastern margin of Big Gypsum Valley (Figure 3.4). Dolomite cements are present only in Little Gypsum Valley up against the Gypsum Valley Salt diapir on both the southeastern and southwestern margins and at Grassy Hill (Figure 3.4).

Paragenetic Sequence

All samples recorded the same sequence of diagenetic processes. However, the extent/pervasiveness of the processes likely varied, as evidenced by variations in the amount of cement and dominant cement types from sample to sample and throughout the stratigraphy. The paragenetic sequence is as follows (Figure 3.5): (1) precipitation of early ferroan dolomite cements

(Figure 3.6), (2) growth of quartz overgrowths filling pore space (Figure 3.7), (3) compaction (Figure 3.7.), (4) dissolution of early dolomite cements, feldspar, and chert grains forming secondary porosity and enlarged pores, (Figure 3.8) (5) precipitation of calcite and in lesser amounts ferroan calcite that fills secondary pores and fills dissolved grains (Figures 3.5, 3.9).

Interpretation

The most striking diagenetic feature observed in the sandstones of the Salt Wash Member of the Morrison Formation at Gypsum Valley is the creation of secondary porosity, and its incomplete occlusion by formation of later cements, which is critical for the interpretation of the Salt Wash Member as a model for a critical component in hydrocarbon migration. Such dissolution has not been described for the Salt Wash Member in more distal positions from the salt (Breit and Goldhaber, 1996), but has been documented for the the fluvio-lacustrine Triassic Chinle Formation (Heness, 2016) and the coastal and eolian Jurassic Carmel and Entrada formations (Ronson, 2018) in proximity to the Gypsum Valley salt diapir. Sample porosity ranged from 11% to 20%. Double the 5.4% average in samples farther from the diapir (Breit and Goldhaber, 1996). While it appears that generation of secondary porosity is a common denominator for near-diapir diagenesis of sandstones, there are differences for the subsequent filling of this pore space. For the Chinle Formation, it was observed that proximal to the diapir margin, authigenic cements filled pore spaces resulting in decreased porosity, whereas distal to the diapir authigenic cements did not completely occlude porosity and porosity was the highest (Heness, 2016). In the case of the Jurassic Carmel and Entrada formations (Ronson, 2018) and the Salt Wash Member in this study, infilling of pore space with cements appears to have been more pronounced distal to the diapir. Indeed, barite and pyrite, cements observed for the Salt Wash Member by Breit and Goldhaber (1996) are absent in the proximity of the Gypsum Valley salt dome. This observation agrees with

the fact that the barite content in samples from the Salt Wash Member decreased proximal to the diapir (Breit and Goldhaber, 1996). We hypothesize that the majority of these patterns can be explained by different fluid flow patterns and chemistries at different relative distances from the diapir, as well as at different stages in diapir evolution. We believe that three components play important roles: convective flow above salt diapirs, upward flow of deep fluids along faults, and different stages of salt diapirism and hydrocarbon migration.

Convective Fluid Flow

Proximal, and in particular in crestal position to the diapir, heat flow is expected to be elevated due to the high thermal conductivity of salt (O'Brien and Lerche, 1988; Evans et al., 1991; Canova et al., 2018). Thus, it is likely that in permeable sediments, such as sandstones, convection cells are established. These cells will drive upwelling of saline waters from halite dissolution, and downwelling of oxygenated meteoric waters. The presence of dissolved oxygen in waters will: 1) inhibit sulfate reduction, and thus prevent pyrite formation, and 2) drive the oxidation of organic matter, which results in the genesis of carbonic acid. The slightly acidic conditions enhance feldspar weathering (Blum, 1994), favor quartz overgrowth precipitation, and impede the precipitation of carbonates. Moreover, the presence of dissolved salts, i.e. sodium and chloride ions, lower the activity of carbonate, sulfate, calcium, barium and magnesium ions via complexation, which further limits the precipitation of carbonate minerals and barite. Thus, convective fluid flow above the diapir provides a mechanism that satisfies the observation of genesis of secondary porosity generation, quartz cement precipitation, and limited or absent generation of carbonate, barite, and pyrite cements.

Upward Flow of Deep Fluids Along Faults

Precipitation of authigenic minerals from brines that move upward along faults have been observed for the distal portions of the Salt Wash Member (Breit and Goldhaber, 1996), but it is reasonable to assume that such processes also contribute to locations more proximal to the Gypsum Valley Salt diapir, as is evident by the presence of faults and other structural features (i.e. Megaflap, Figure 3.2). Overall, porosity appears to be somewhat higher in Little Gypsum Valley than for the south-eastern end of Big Gypsum Valley, where two radial faults and a counter regional fault offset stratigraphy from the Pennsylvanian to the Cretaceous (Escosa et al., 2019). The Megaflap, which includes steeply upturned strata belonging to the uppermost part of the Paradox Formation (Mast, 2016) and these deep fault structures are expected to serve as conduits for basinal fluids. In Little Gypsum Valley such deep structures are absent, which may explain the higher porosity and the extremely low abundance of dolomite and ferroan dolomite.

Different Stages of Salt Diapirism and Hydrocarbon Migration

Different stages of salt diapirism and hydrocarbon migration may be the cause for why the Chinle Formation authigenic cements filled pore spaces proximal to the diapir margin, whereas this is not the case for the Carmel and Entrada Formations (Ronson, 2018) and the Salt Wash Member in this study. The Chinle Formation contains clasts of carbonate caprock that were derived from the Gypsum Valley salt diapir (Heness, 2016; Lerer, 2017; Poe, 2018). The formation of the carbonate caprock, which as slightly earlier or contemporaneous to the deposition of the Chinle Formation was caused by the migration of hydrocarbons into the crest of the salt diapir, where its oxidation coupled to sulfate reduction resulted in the replacement of gypsum from the caprock of diapir with carbonates. Such carbonate-rich fluids could have contributed to the cementation of sandstones of the Chinle Formation in the most proximal position to the diapir margin, a process

that is known as genesis of “false caprock” (Prikryl et al., 1988). No carbonate caprock is associated with the Salt Wash Member, and no indication for hydrocarbon migration (e.g. rock bleaching or dead oil) have been observed in this study, which may explain the considerable difference in cementation to the sandstones of the Chinle Formation.

Conclusions

The diagenesis of the Salt Wash Member of the Morrison Formation in Gypsum Valley is a model for the understanding of the impact of near-salt fluid circulation on the porosity and permeability of critical hydrocarbon conduits. The Salt Wash Member paragenetic sequence of diagenetic events is as follows: (1) precipitation of early ferroan dolomite cements, (2) growth of quartz overgrowths filling pore space, (3) compaction, (4) dissolution of early dolomite cements, feldspar, and chert grains forming secondary porosity and enlarged pores, (5) precipitation of calcite and in lesser amounts ferroan calcite that fills secondary pores and fills dissolved grains. There are no distinct patterns that would indicate a segregation of cements to certain stratigraphic units of the Salt Wash Member, however, there are geographic differences where higher contents of ferroan dolomite and dolomite cements can be attributed to the proximity of the sites to major structures, such as faults and the Megaflap in Big Gypsum Valley. This means that locally, such structures can impact the permeability of a sandstone unit. However, for the role of such sandstone units as conduits for hydrocarbon migration, different stages of salt diapir evolution and concomitt and hydrocarbon migration into the crest of a diapir and convective fluid flow above the diapir driven by heat flux from the diapir may be more important. Hydrocarbon migration can lead to cementation of pore space, as proposed for the Chinle Formation, while convective mixing of saline fluids derived from halite dissolution with meteoric water established secondary porosity in the Salt Wash Member and maintained this porosity in a range from 28% to 62%. This means that

near-diapir fluid flow constitutes a mechanism that enhances and maintains porosity and permeability in sandstones, which is critical for the emplacement of hydrocarbon migration conduits.

Figures

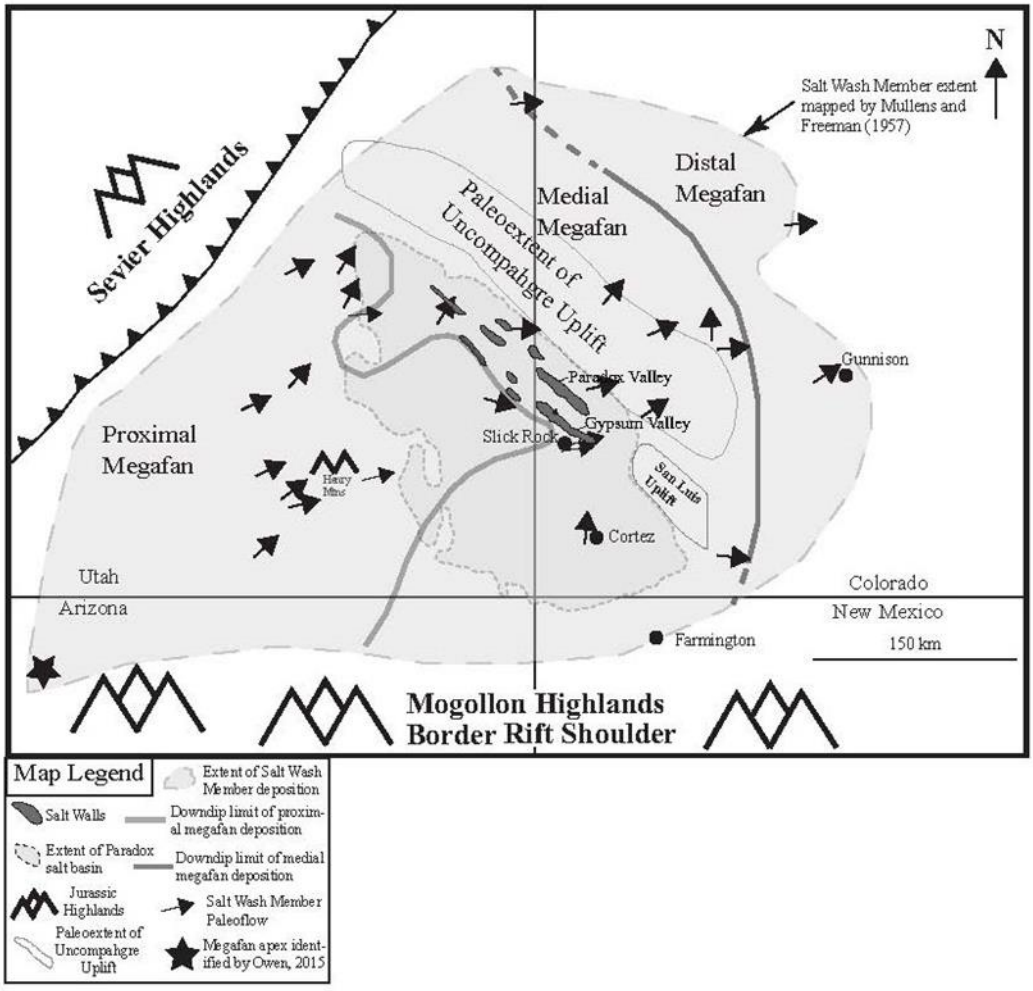

Figure 3.1: Regional map of Jurassic Salt Wash Member of the Morrison Formation depositional system and areal extent of Paradox Basin deposition.

Fluvial system paleoflow of the Salt Wash Member from Owen et al. (2015) is indicated by gray arrows and the extent of the fluvial system from Mullens and Freeman (1957) is a dashed outline. Paradox Basin salt walls are outlined with dark infill gray. (Figure altered after Barbeau, 2003; Trudgill, 2011; Owen et al., 2015)

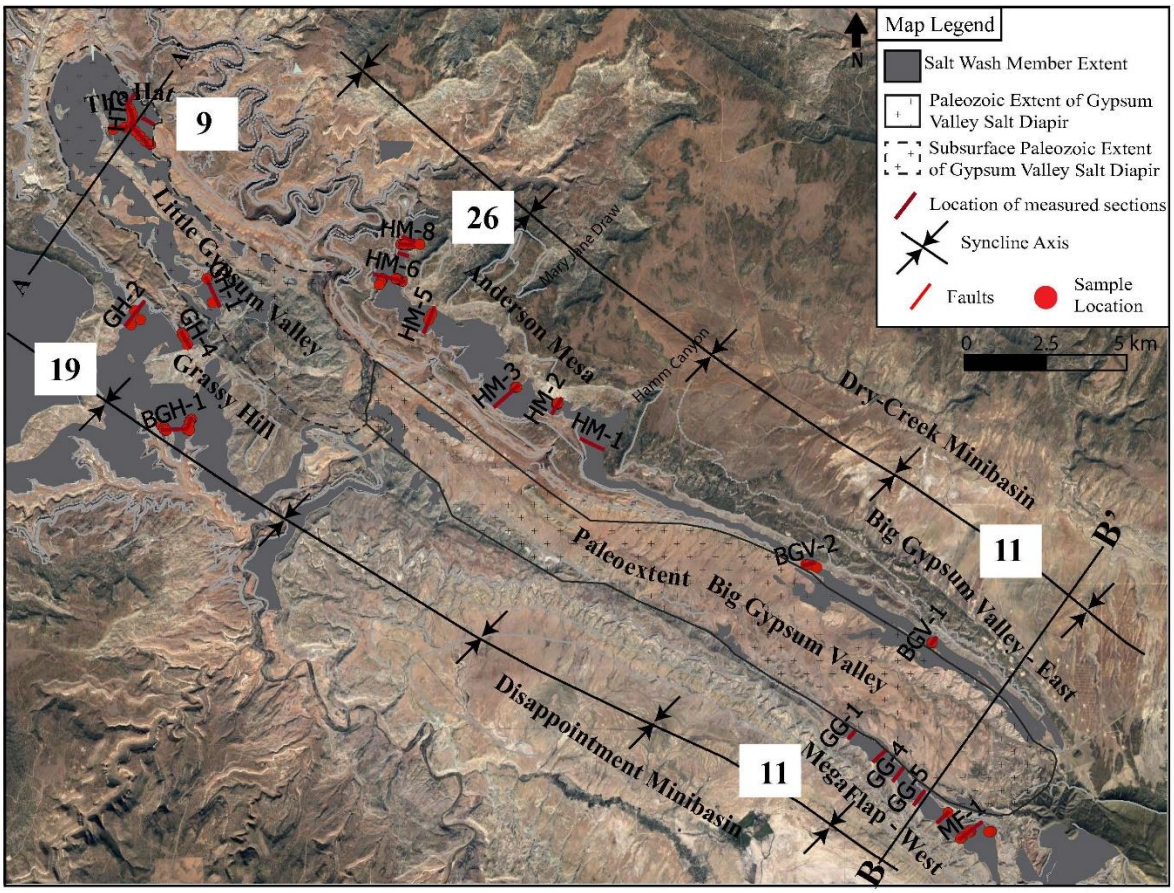

Figure 3.2: Map of present day Salt Wash Member outcrop in and ar ound Gypsum Valley.

The hatched pattern represents the estimated extent of the salt diapir that was exposed at the surface at the beginning of Salt Wash Member deposition. By the end of deposition all, or almost all of the diapir had been buried by Salt Wash Member strata. These have largely been removed by erosion, except for isolated remnants resting on the salt. To the northeast and southeast of the diapir, The Salt Wash Member has been buried under younger strata. In Little Gypsum Valley, the Salt Wash Member and younger strata are faulted by late Tertiary faults. The red dots show the locations of petrographic samples.

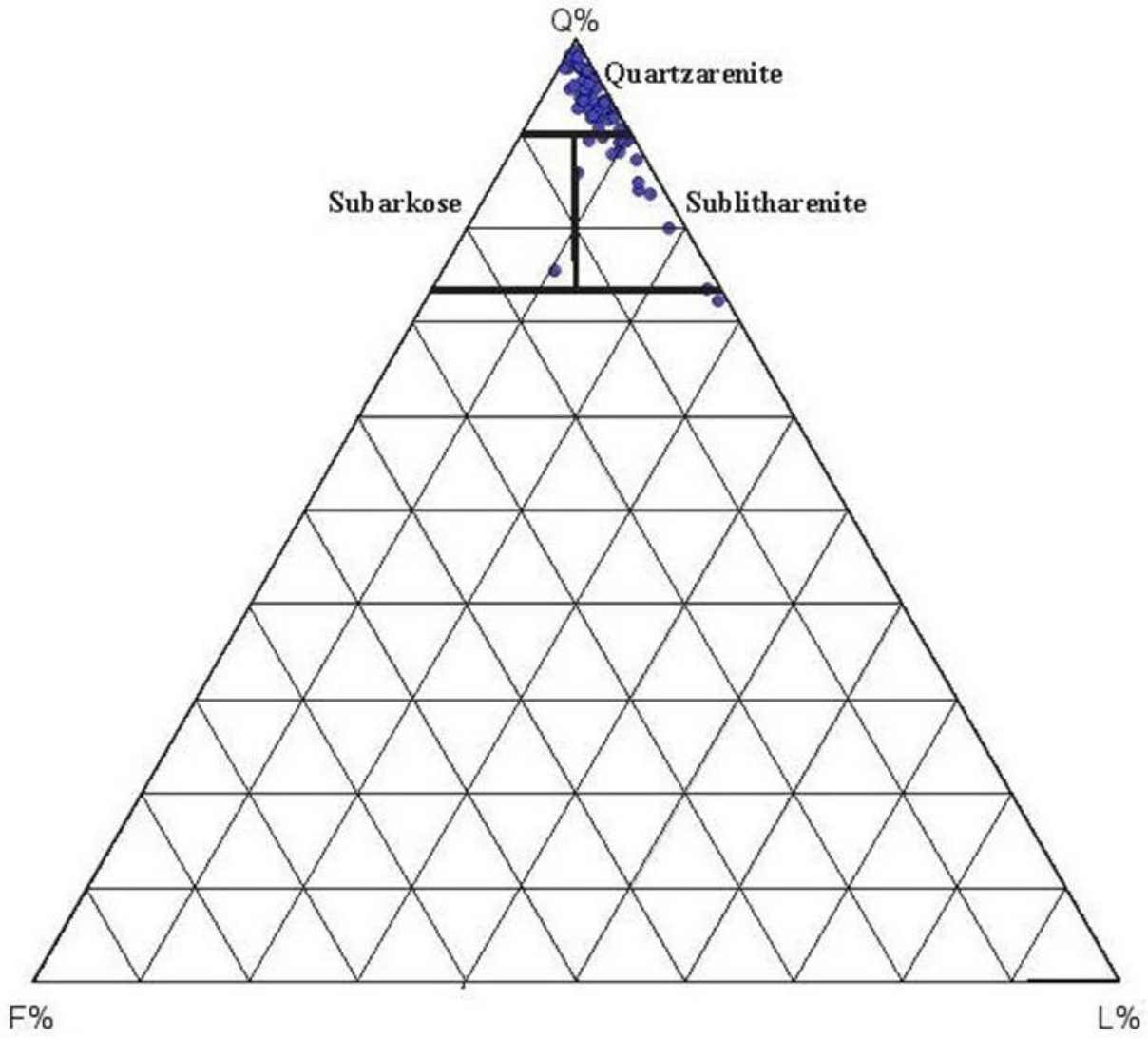

Figure 3.3: QFL Ternary sandstone composition diagram Folk (1980).

Blue dots indicate all samples point counted in the study. Most samples fall into the quartzarenite and sublitharenite classification.

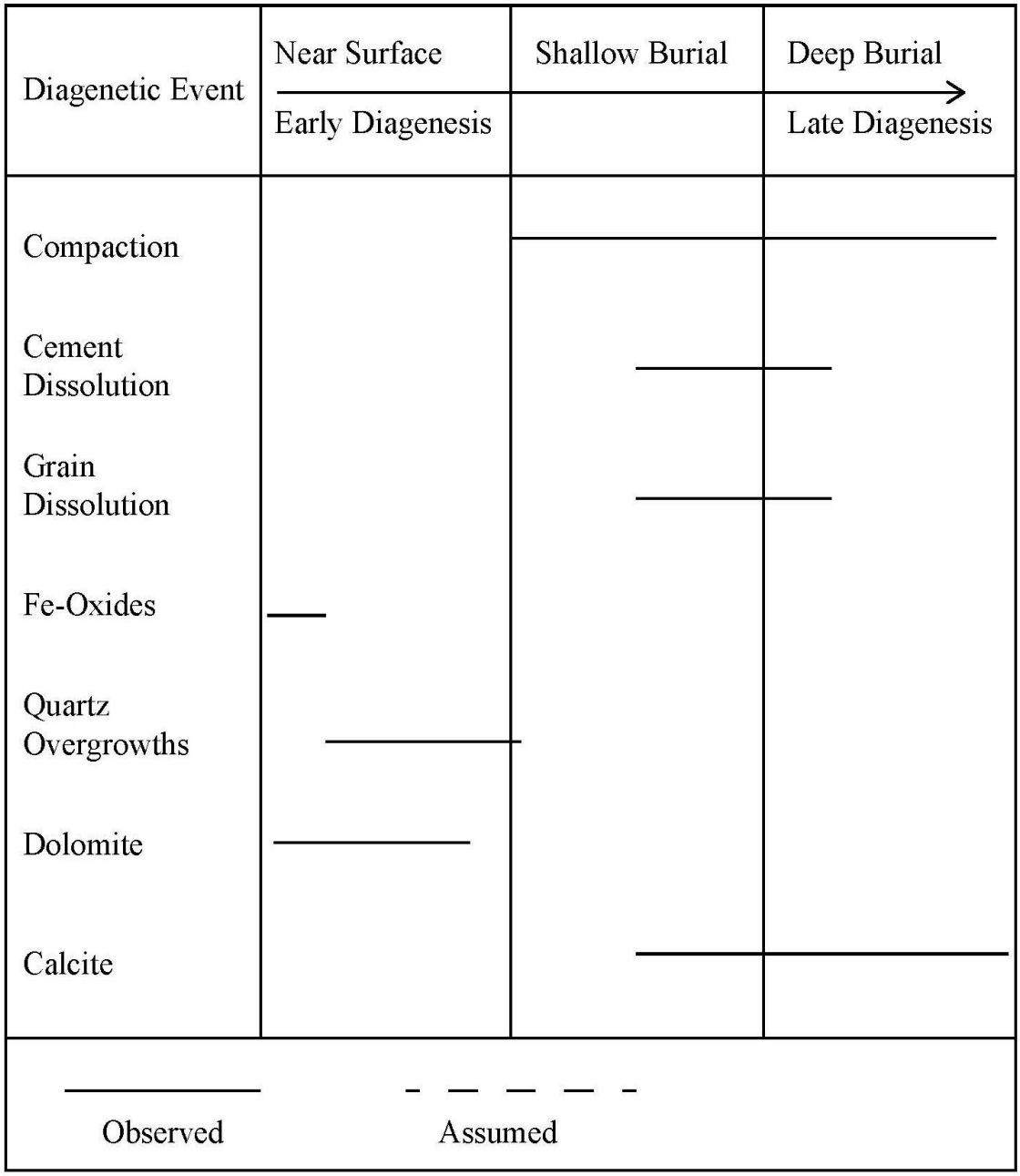

Figure 3.4: Diagenetic Event Chart for Sandstone samples throughout Gypsum Valley in the Salt Wash Member

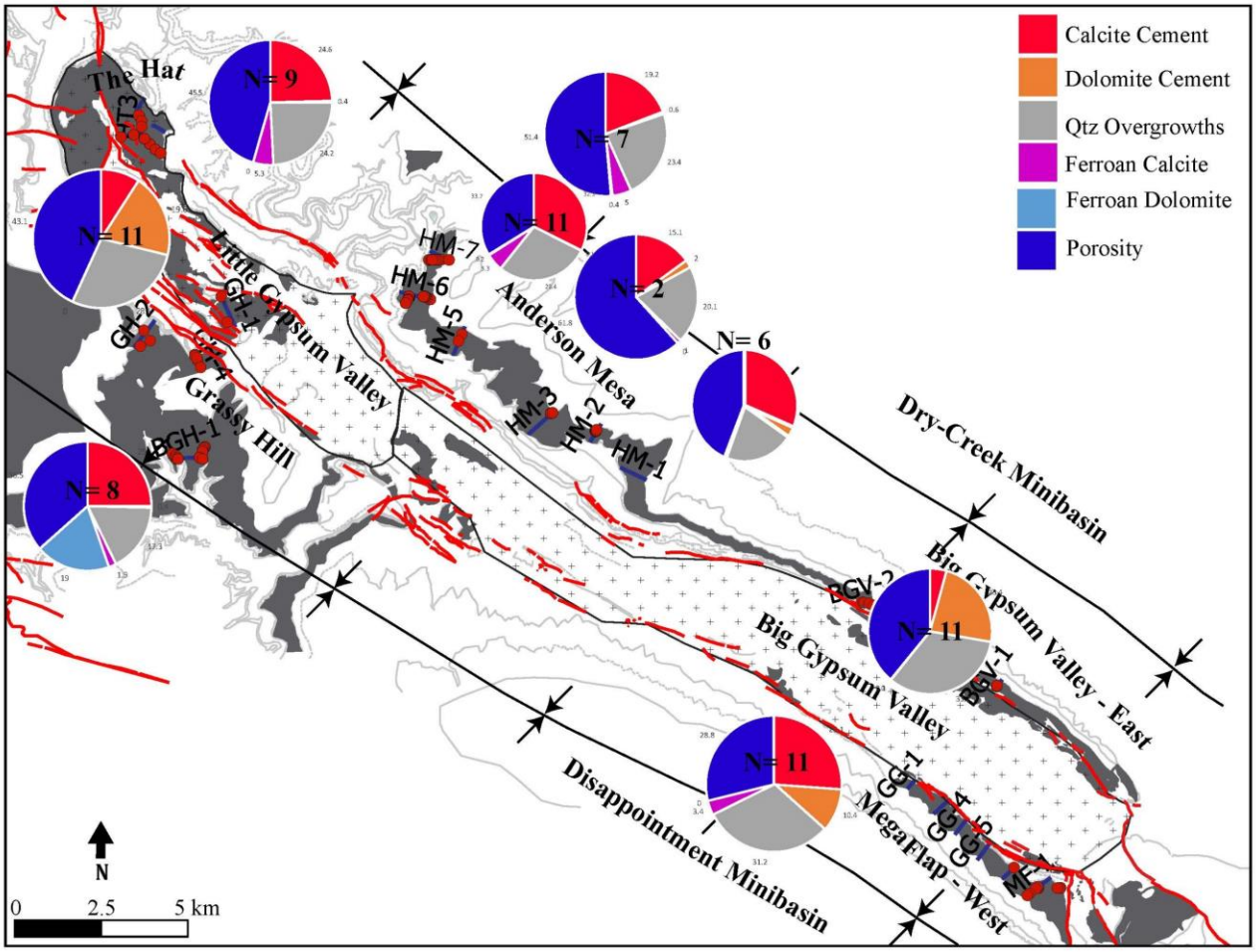

Figure 3.5: Map of distribution of cements throughout Gypsum Valley.

Cement percentages are presented in the form of a pie chart. Pie charts were placed where the group of samples are located Gypsum Valley.

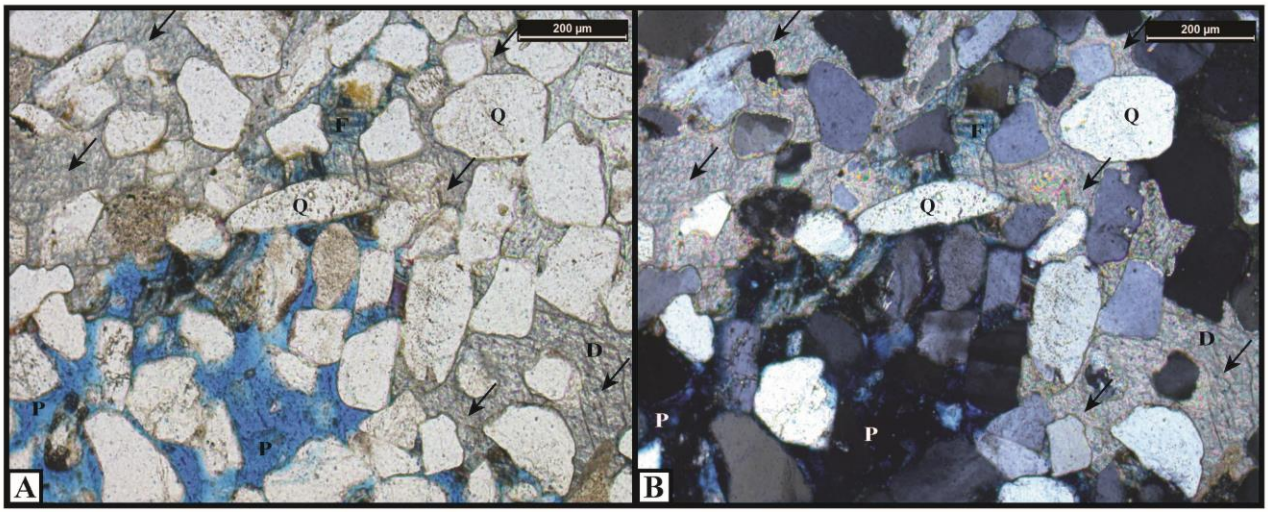

Figure 3.6: Petrographic images of sample showing paragenetic sequence step 1

Precipitation of early dolomite cements. Left side images are in PPL and right side images are in XPL. Key grains are labeled: Q-Quartz, F-Feldspar, C-Calcite, D-Ferroan Dolomite, P- Pore space. Blue epoxy in images represent pore space. Arrows in images highlight the early ferroan dolomite cement that is filling the pore space. There is an absence of quartz overgrowths and calcite cements that are in the latter part of the paragenetic sequence.

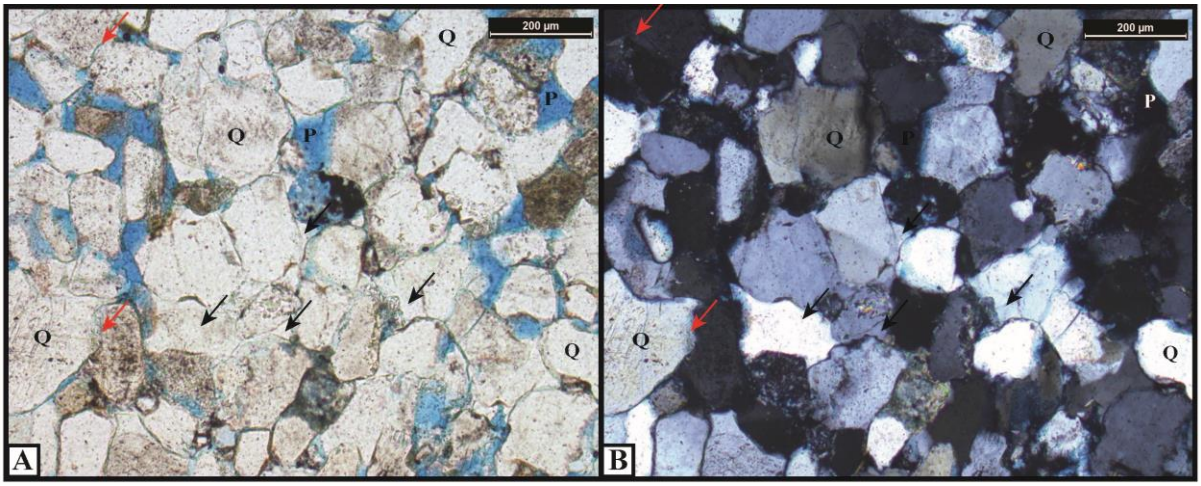

Figure 3.7: Petrographic images of sample showing paragenetic sequence step 2

Growth of quartz overgrowths filling pore space and compaction. Left side images are in PPL and right side images are in XPL. Key grains are labeled: Q-Quartz, F-Feldspar, C-Calcite, D-Dolomite, and P-Pore Space. Black arrows in images highlight quartz over growths and red arrows highlight grain boundaries of compaction.

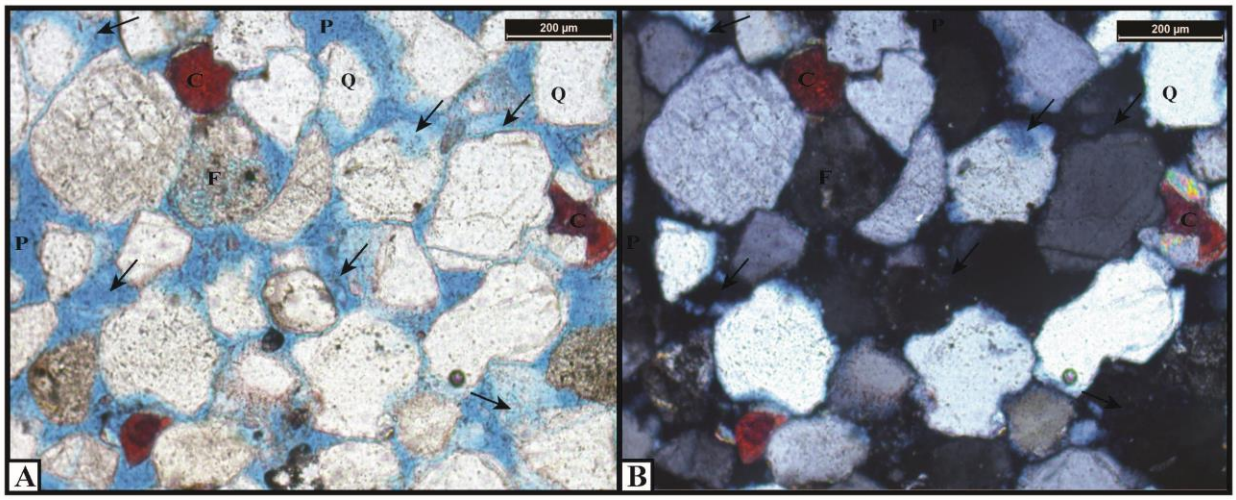

Figure 3.8: Petrographic images of sample showing paragenetic sequence step 3

Dissolution of grains forming secondary porosity and enlarged pores. Left side images are in PPL and right side images are in XPL. Key grains are labeled: Q-Quartz, F-Feldspar, C-Calcite, D-Dolomite, and P-pore space. Black arrows in images highlight grains that are dissolving and ghost grains that have been almost entirely dissolved creating pore space. In thin section dissolved grains are often observed to be cements and feldspar grains.

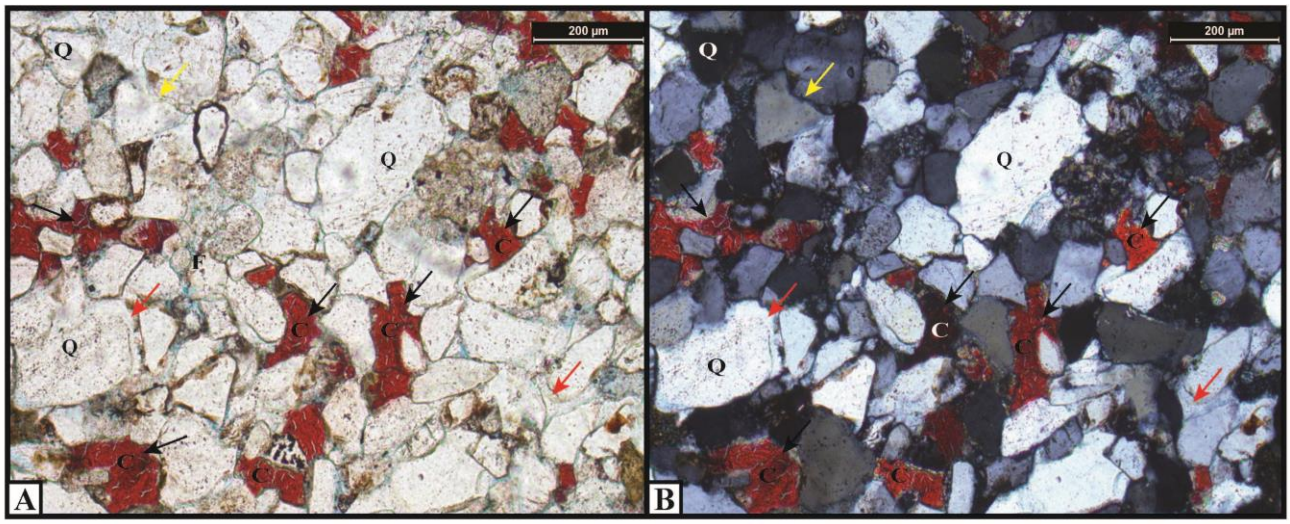

Figure 3.9: Petrographic images of sample showing paragenetic sequence step 4

Precipitation of calcite that fills secondary pores and fills grains.Left side images are in PPL and right side images are in XPL. Key grains are labeled: Q-Quartz, F-Feldspar, C-Calcite,

D-Dolomite, and P-Pore space. Black arrows in images highlight precipitation of calcite within pore space after the previous steps of the paragenetic sequence have taken place. For reference quartz overgrowths are hightlighted by red arrows, compaction by yellow arrows, and note the absence of ferroan dolomite in this paragenetic sequence.

References

Blum, A.E., 1994, Feldspars in Weathering, *in* Parsons, I. ed., Feldspars and their Reactions, Dordrecht, Springer Netherlands, NATO ASI Series, p. 595–630, doi:10.1007/978-94-011-1106-5_15.

Breit, G.N., and Goldhaber, M.B., 1996, Diagenesis of Sandstones in the Morrison Formation within the Paradox Basin: , p. 197–210.

Breit, G., and Goldhaber, M., 1989, Hematite-enriched sandstones and chromium-rich clays-Clues to the origin of vanadium-uranium deposits in the Morrison Formation, southwestern Colorado and southeastern Utah, USA: No. IAEA-TECDOC--500. in, Uranium Resources and Geology of the United States, Proceedings of a Technical Committee Meeting held in Saskatoon Canada. September 1987.

Breit, G.N., Goldhaber, M.B., Shawe, D.R., and Simmons, E.C., 1990, Authigenic barite as an indicator of fluid movement through sandstones within the Colorado Plateau: Journal of Sedimentary Research, v. 60, p. 884–896, doi:10.1306/D426763B-2B26-11D7-8648000102C1865D.

Canova, D.P., Fischer, M.P., Jayne, R.S., and Pollyea, R.M., 2018, Advective Heat Transport and the Salt Chimney Effect: A Numerical Analysis: Hindawi Geofluids, doi:10.1155/2018/2378710. 10p.

Craig, L.C., 1955, Stratigraphy of the Morrison and Related Formations, Colorado Plateau Region: A Preliminary Report: U.S. Government Printing Office, 50 p.

Dickinson, W.R., and Gehrels, G.E., 2008, Sediment delivery to the Cordilleran foreland basin: Insights from U-Pb ages of detrital zircons in Upper Jurassic and Cretaceous strata of the Colorado Plateau: American Journal of Science, v. 308, p. 1041–1082, doi:10.2475/10.2008.01.

Esch, W., 1995, Effects of Salt Dome Dissolution on Sediment Diagenesis: An Experimental and Field Study.: LSU Historical Dissertations and Theses, https://digitalcommons.lsu.edu/gradschool_disstheses/6095, 220 p.

Escosa, F.O., Rowan, M.G., Giles, K.A., Deatrick, K.T., Mast, A.M., Langford, R.P., Hearon IV, T.E., and Roca, E., 2019, Lateral terminations of salt walls and megaflaps: An example from Gypsum Valley Diapir, Paradox Basin, Colorado, USA: Basin Research, v. 31, p. 191–212, doi:10.1111/bre.12316.

Evans, D.G., Nunn, J.A., and Hanor, J.S., 1991, Mechanisms driving groundwater flow near salt domes: Geophysical Research Letters, v. 18, p. 927–930, doi:10.1029/91GL00908.

Fischer, M.P., Kenroy, P.R., and Smith, A.P., 2013, Fluid Systems around Salt Diapirs: Search and Discovery Article #50902, p. 29.

Folk, R.L., 1980, Petrology of sedimentary rocks: Hemphill Publishing Company.

Heness, E.A., 2016, Salt tectonic controls on facies and sequence stratigraphy of the Triassic Chinle Formation, Gypsum Valley Salt Wall, Colorado [M.S.]: The University of Texas at El Paso, 156 p., https://search.proquest.com/docview/1805065474/abstract/796FEE4CB252404APQ/8 (accessed April 2019).

Hudson, S.M., and Hanson, A.D., 2010, Thermal maturation and hydrocarbon migration within La Popa Basin, northeastern Mexico, with implications for other salt structures: AAPG Bulletin, v. 94, p. 273–291, doi:10.1306/07130907012.

Lerer, K., 2017, Gypsum, Calcite, and Dolomite Caprock Fabrics and Geochemistry from the Gypsum Valley Salt Diapir, Paradox Basin, Southwestern Colorado [M.S.]: The University of Texas at El Paso, 177 p., https://search.proquest.com/docview/2008155128/abstract/3A2E93E346B34F1CPQ/1 (accessed April 2019).

Mast, A.M., 2016, The origin of anomalous carbonate units outcropping at the salt sediment interface of the southern end of Gypsum Valley Salt Wall, Paradox Basin, southwest Colorado [M.S.]: The University of Texas at El Paso, 199 p., https://search.proquest.com/docview/1876050813/abstract/AE792941A9CF465CPQ/1 (accessed April 2019).

McManus, K.M., and Hanor, J.S., 1988, Calcite and iron sulfide cementation of Miocene sediments flanking the West Hackberry salt dome, southwest Louisiana, U.S.A.: Chemical Geology, v. 74, p. 99–112, doi:10.1016/0009-2541(88)90148-9.

McManus, K.M., and Hanor, J.S., 1993a, Diagenetic evidence for massive evaporite dissolution, fluid flow, and mass transfer in the Louisiana Gulf Coast: Geology, v. 21, p. 727–730, doi:10.1130/0091-7613(1993)021<0727:DEFMED>2.3.CO;2.

McManus, K.M., and Hanor, J.S., 1993b, Diagenetic evidence for massive evaporite dissolution, fluid flow, and mass transfer in the Louisiana Gulf Coast: Geology, v. 21, p. 727–730, doi:10.1130/0091-7613(1993)021<0727:DEFMED>2.3.CO;2.

Mullens, T.E., and Freeman, V.L., 1957, Lithofacies of the Salt Wash Member of the Morrison Formation, Colorado Plateau: GSA Bulletin, v. 68, p. 505–526, doi:10.1130/0016-7606(1957)68[505:LOTSWM]2.0.CO;2.

O'Brien, J.J., and Lerche, I., 1988, Impact of Heat Flux Anomalies Around Salt Diapirs and Salt Sheets in the Gulf Coast on Hydrocarbon Maturity: Models and Observations: v. 38, http://archives.datapages.com/data/gcags/data/038/038001/0231.htm (accessed November 2019).

Owen, A., Jupp, P.E., Nichols, G.J., Hartley, A.J., Weissmann, G.S., and Sadykova, D., 2015, Statistical estimation of the position of an apex: Application to the geological record: Journal of Sedimentary Research, v. 85, p. 142–152, doi:10.2110/jsr.2015.16.

Peterson, F., 1984, Fluvial sedimentation on a quivering craton: Influence of slight crustal movements on fluvial processes, upper Jurassic Morrison formation, western Colorado plateau: Sedimentary Geology, v. 38, p. 21–49, doi:10.1016/0037-0738(84)90073-3.

Poe, P.L., 2018, Characterization and Geochemistry of Carbonate Caprock Associated with the Gypsum Valley Salt Wall, Paradox Basin, Colorado: Implications for Understanding Lateral Caprock Emplacement [M.S.]: The University of Texas at El Paso, 119 p., https://search.proquest.com/docview/2174055007/abstract/303499E668C14A71PQ/1 (accessed April 2019).

Posey, H.H., and Kyle, J.R., 1988, Fluid-rock interactions in the salt dome environment: An introduction and review: Chemical Geology, v. 74, p. 1–24, doi:10.1016/0009-2541(88)90143-X.

Prikryl, J.D., Posey, H.H., and Kyle, J.R., 1988, A petrographic and geochemical model for the origin of calcite cap rock at Damon Mound salt dome, Texas, U.S.A.: Chemical Geology, v. 74, p. 67–97, doi:10.1016/0009-2541(88)90147-7.

Ronson, R.B., 2018, Facies Changes Associated with Formation of an Extensive Salt Shoulder by the Coastal and Eolian Carmel and Entrada Formations, Gypsum Valley, Colorado [M.S.]: The University of Texas at El Paso, 142 p., https://search.proquest.com/docview/2111273760/abstract/4841851E56454385PQ/1 (accessed April 2019).

Schmidt, V., McDonald, D.A., and Platt, R.L., 1977, Pore Geometry and Reservoir Aspects of Secondary Porosity in Sandstones: Bulletin of Canadian Petroleum Geology, v. 25, p. 271–290.

Stokes, W.L., 1944, Morrison formation and related deposits in and adjacent to the Colorado Plateau: GSA Bulletin, v. 55, p. 951–992, doi:10.1130/GSAB-55-951.

Turner, C.E., and Peterson, F., 2004, Reconstruction of the Upper Jurassic Morrison Formation extinct ecosystem—a synthesis: Sedimentary Geology, v. 167, p. 309–355, doi:10.1016/j.sedgeo.2004.01.009.

Tyler, N., and Ethridge, F.G., 1983, Depositional setting of the Salt Wash Member of the Morrison Formation, Southwest Colorado: Journal of Sedimentary Research, v. 53, p. 67–82, doi:10.1306/212F8157-2B24-11D7-8648000102C1865D.

Ulmer-Scholle, D.S., Scholle, P.A., Schieber, J., and Raine, R.J., 2015, A Color Guide to the Petrography of Sandstones, Siltstones, Shales and Associated Rocks: American Association of Petroleum Geologists, 512 p., doi:10.1306/M1091304.

Weissmann, G. et al., 2013, Prograding distributive fluvial systems: geomorphic models and ancient examples: New Frontiers in Paleopedology and Terrestrial Paleoclimatology: SEPM, Special Publication, v. 104, p. 131–147.

Chapter 4: Fluvial Architecture of a Top Salt Minibasin; Jurassic Salt Wash Member of the Morrison Formation at "The Hat" Syncline, Gypsum Valley Salt Wall, Colorado

Introduction

Most studies of the interactions between fluvial systems and salt diapirs use outcrops in the adjacent salt-withdrawal mini-basins, kilometers from the diapir (Hazel, 1994; Prochnow et al., 2006; Matthews et al., 2007; Andrie et al., 2012; Banham and Mountney, 2013b, 2013a; Venus et al., 2015). These studies lack documentation of stratal architecture and depositional interaction of fluvial systems that directly overlie salt domes. Additionally, no documentation exists of minibasins developed on top of vertically-rising salt diapirs and the resulting stratigraphy from these minibasins, leaving critical gaps in the interpretation of fluvial architecture in near-salt environments. This study fills the gap in knowledge by the documenting the fluvial architecture in a minibasin on top of a diapir. We seek to understand whether the same results documented for mini-basins adjacent to the diapir also apply on top or whether depositional patterns are different?

The accommodation space generated that preserves the stratigraphy of fluvial system architecture in salt tectonic settings can be very dynamic and it is important to understand not only the space generated to accumulate sediments but also the controls on how the fluvial system fills that space with sandstones, mudstones or a combination of the two. The main controls on fluvial deposition outside of and within salt tectonic settings have been widely described and studied. It is clear that regional climate and tectonics play a major role in stream power and sediment supply, which also contributes to the ability of the fluvial system to aggrade or erode (Hazel, 1994; Blum and Törnqvist, 2000; Matthews et al., 2007; Banham and Mountney, 2013b). Tectonics controls the space available for sediment accumulation and preservation of sediments.

In the case of this study local movement of salt from beneath minibasins creates local abrupt increases in accommodation space in the minibasins adjacent to, on the margins, and even on top of salt diapirs (Hazel, 1994; Matthews et al., 2007; Banham and Mountney, 2013b). These studies find that fluvial systems typically flow to the topographic lows of subsiding minibasins away from topographic highs of passively- rising salt diapirs, leading to drainage capture or diversion resulting in reduced local sediment deposition and relocation of sedimentation to primarily minibasins (Matthews et al., 2007; Banham and Mountney, 2013b).

Many studies describe fluvial systems and the resulting stratigraphic architecture when they interact with salt diapirs (Hazel, 1994; Prochnow et al., 2006; Matthews et al., 2007; Andrie et al., 2012; Banham and Mountney, 2013b; Venus et al., 2015). Banham and Mountney (2013b) summarized a great body of the work on fluvial depositional patterns within minibasins and found that sediment supply rate and subsidence rate are two of the most important factors in predicting stacking patterns of sandstones. Generally, when subsidence rates and sediment supply rates are similar, stacking patterns result in interbedded sandy well-connected channels (Banham and Mountney, 2013b).When subsidence rates are high and sediment supply rates are low, poorly connected channels interbedded with fine-grained lacustrine or marine deposits form (Banham and Mountney, 2013b).

In this study we document and interpret the fluvial architecture of Salt Wash Member of the Jurassic Morrison Formation deposited over the crest of the Gypsum Valley Salt Diapir. We focus on the NE end of the salt wall where Salt Wash Member strata are folded into a syncline in a geomorphic area referred to as ‘the Hat’. We (1) document the syndepositional timing of subsidence of the “The Hat” syncline, (2) characterize the syndeformational fluvial architecture, stacking patterns, and facies distributions within the syncline and compare them to those directly

outside of the syncline, and (3) discuss the possible explanations as to why the top salt minibasin fill fluvial architecture, which is dominantly composed of muddy facies that fill a relatively high accommodation space does not follow the predicted consistent subsidence and sediment supply trends that result in high sandstone channel content as described by others. We believe this contribution, which focuses on the Jurassic Salt Wash Member of the Morrison Formation at 'The Hat' syncline, Gypsum Valley Salt Diapir, Colorado is the first documented top salt minibasins.

Geologic Background

The Paradox Basin extends across eastern Utah and southwestern Colorado and contains nine northwest-southeast trending salt walls (Shoemaker et al., 1958) (Figure 4.1). The basin subsided from the Middle Pennsylvanian to Permian due to flexural loading by the Uncompahgre Uplift (Barbeau, 2003), which was associated with Ancestral Rocky Mountains tectonism (Dickinson and Lawton, 2003; Trudgill, 2011) (Figure 4.1). During the Pennsylvanian, glacioeustatic sea level fluctuation resulted in cyclic deposition of approximately 2500 m of interbedded evaporites, shale, and carbonates that formed the layered evaporite sequence of the Paradox Formation (Hite and Buckner, 1981). The Paradox Formation serves as the source of salt for the salt walls in the basin.

Differential sediment loading of the Paradox Formation by Late Paleozoic clastics derived from the Uncompahgre Uplift initiated passive diapirism and growth of the salt walls (Ge et al., 1997). Salt wall rise and minibasin subsidence rates decreased at the beginning of the Mid-Mesozoic (Shoemaker et al., 1958; Lawton and Buck, 2006; Trudgill, 2011; Escosa et al., 2018). Across the areal extent of the Paradox Basin, Jurassic Salt Wash Member strata are widely thought not to be affected by salt tectonics except at Gypsum Valley and Paradox Valley salt walls (Elston and Landis, 1960; Vogel, 1960; Cater and Craig, 1970; Trudgill, 2011; Rowan et al., 2016).

Gypsum Valley

Gypsum Valley, located in southwestern Colorado, is underlain by the southernmost salt wall in the Paradox Basin, which is approximately 35 km long and 2-3.5 km wide (Landis et al., 1961; Escosa et al., 2018) (Figure 4.2). Within Gypsum Valley, large regions of exposed modern gypsic caprock containing minor remnant inclusions of dolomite and black shale derived from the Pennsylvanian Paradox Formation are present. The Gypsum Valley salt wall is bounded on either side by salt withdrawal minibasins; Dry Creek to the northeast and Disappointment to the southwest (Figure 4.2). Salt flowing away from beneath the sinking minibasins fed passive growth of the adjacent salt diapir (Trudgill, 2011). Strata ranging from Late Pennsylvanian to Cretaceous age dip away from the diapir and thicken into the minibasins; typically, older strata are deeply buried and dip more steeply than younger strata (Stokes and Phoenix, 1948; Escosa et al., 2018).

Gypsum Valley has been divided into two geomorphic regions: Little Gypsum Valley forms the narrower northwest end and Big Gypsum Valley forms the wider southwest end of the valley (Figure 4.2) (Stokes and Phoenix, 1948). Presently the boundary between these two regions of the salt diapir are separated by the Dolores River (Figure 4.2). Big Gypsum Valley is asymmetrical in cross section (Figure 4.2B). On the southwestern margin of Big Gypsum Valley, Pennsylvanian through Permian strata thin and upturn to near-vertical alongside the diapir, forming a megaflap (Rowan et al., 2016; Escosa et al., 2018). On the northern flank of Big Gypsum Valley, a counterregional fault is thought to be responsible for the greatly expanded Pennsylvanian and Early Permian section observed in seismic and well logs (Rowan et al., 2016; Escosa et al., 2018). The Jurassic Morrison Formation, which is the focus of this study, is found

in both depositional and fault contact with upturned older strata as well as the Pennsylvanian Paradox Evaporites that form the salt diapir, in this area (Figure 4.2).

In Little Gypsum Valley, the salt diapir is more symmetrical than in Big Gypsum Valley and Late Jurassic strata are less deformed. Here, the diapir began to be buried in the Triassic (Langford et al., 2018). Older units of the Chinle Formation and Glen Canyon Group form "shoulders" that bury the margins of the Gypsum Valley Salt Diapir (Langford et al., 2018). The Entrada Sandstone covered most of the little Gypsum Valley salt wall in the Late Jurassic and typically underlies the Jurassic Summerville Formation and the Salt Wash Member of the Morrison Formation in this area (Figure 4.3; 4.4) (Langford et al., 2018).

Morrison Formation

The Late Jurassic Morrison Formation was deposited by distributive fluvial systems across the western interior of North America (Craig, 1955; Turner and Peterson, 2004; Owen et al., 2015c, 2015b). It covers an area of 150,000km^2 from the Sevier foreland eastward to the area Rio Grande rift and Front Range of Colorado (Turner and Peterson, 2004; Dickinson and Gehrels, 2008) (Figure 4.1). Where not affected by salt tectonism, the maximum thickness of the Morrison Formation is found in the Henry Mountains where it measures 237m. However, it reaches a thickness of over 300 m in the Disappointment minibasin adjacent to Gypsum Valley diapir, where it has been thickened by syndepositional salt withdrawal (Shawe, 1968a). In the Gypsum Valley area only two members of the Morrison Formation are recognized, the Salt Wash Member overlain by the Brushy Basin Member (Figure 4.3). This study mainly focuses on the Salt Wash Member of the Morrison Formation.

The main source of sediment for the Morrison Formation in the Late Jurassic was located to the south of, the uplifted rift shoulders of the Mogollon Highlands, which were associated

with the late stages of active rifting along the Bisbee Basin from 165-145 Ma (Craig, 1955; Dickinson and Gehrels, 2008; Owen et al., 2015c, 2015b) (Figure 4.1). In the Mid-Mesozoic the Sevier foreland basin was flanked to the south by the Mogollon highlands that formed the northern rift shoulder of the Bisbee Basin, which was in the late stages of rifting (Figure 4.1) (Dickinson and Lawton, 2001). The Sevier thrust belt marked the western margin of the foreland basin (Figure 4.1) (Lawton et al., 2004). Timing of the thrusting during the Sevier orogeny is contentious but is considered to have begun either late in the Early Cretaceous or earlier in the Late Jurassic (Cross, 1986; Heller et al., 1986; Yingling and Heller, 1992; DeCelles et al., 1995). If Sevier thrusting began later, then Morrison Formation deposition began before thrusting, but if it began earlier it means that the Morrison Formation was deposited in a subdued backbulge basin (Heller and Paola, 1989; DeCelles and Currie, 1996; DeCelles, 2004).

Salt Wash Member

The Salt Wash Member is an aerially extensive exposed member of the Morrison Formation spanning central Utah, west-central Colorado, northeast Arizona, and northwestern New Mexico (Craig, 1955; Mullens and Freeman, 1957; Turner and Peterson, 2004). The Salt Wash Member is generally described as amalgamated, vertically-stacked, fluvial channel sandstone packages interbedded with floodplain deposits of siltstones and mudstones of (Stokes, 1944; Craig, 1955; Mullens and Freeman, 1957; Tyler and Ethridge, 1983; Peterson, 1984; Turner and Peterson, 2004; Kjemperud et al., 2008; Dickinson and Gehrels, 2008; Owen et al., 2015c, 2015b). Both meandering and braided fluvial channel interpretations have been made for the Salt Wash Member (Stokes, 1944; Peterson, 1984; Kjemperud et al., 2008; Owen et al., 2015b). Paleocurrents indicate flow to the north and the northeast (Stokes, 1944; Turner and Peterson, 2004; Dickinson and Gehrels, 2008; Owen et al., 2015a) (Figure 4.1). Several workers

have argued their data suggests a single source area for the sediments of the Salt Wash Member (Craig, 1955; Mullens and Freeman, 1957; Tyler and Ethridge, 1983; DeCelles, 2004; Owen et al., 2015a). Owen et al., (2015a) using a statistical projection of paleocurrent data suggested the apex of the Salt Wash deposition is in northeastern Arizona (Figure 4.1), supporting previous work suggesting the sole source of sediment is from the Mogollon highlands (Mullens and Freeman, 1957; Dickinson and Gehrels, 2008).

The Salt Wash Member has been interpreted regionally as a north-eastward prograding distributive fluvial system (DFS) within a megafan with a distal fan facies at the base and more proximal fan facies higher in the succession (Craig, 1955; Mullens and Freeman, 1957; Weissmann et al., 2010; Owen et al., 2015c, 2015b). This allows for prediction of the type of facies seen in proximity to the source of sediment (Weissmann et al., 2010; Owen et al., 2015c, 2015b). In most areas, the Salt Wash Member overlies the marine and marginal marine deposits of the Summerville Formation (Craig, 1955; Peterson, 1984). In areas south and west of the study area, the Salt Wash Member rests on the distal facies of the Tidwell Member of the Morrison Formation (Peterson, 1984; Owen et al., 2015b). The Tidwell Member is considered to be the distal fan component of the Salt Wash Member DFS and is composed of floodplain facies interbedded with gypsiferous wetland deposits that have a bladed texture interlayered with finely-crystalline carbonate wackestone containing gastropods and charophytes. The clastic ephemeral wetland deposits that are composed dominantly of horizontally laminated muds and wave-rippled sandstones (Peterson, 1984; Kjemperud et al., 2008; Owen et al., 2015b).

The medial part of the DFS is described as having channel belt deposits separated by laterally extensive floodplain packages (Weissmann et al., 2010; Owen et al., 2015c, 2015b). This part of the system is described as having 40-70% sandstone. Floodplain facies are described

as dominantly mudstone, siltstone, and sandstone (Mullens and Freeman, 1957; Owen et al., 2015c, 2015b). The area of Gypsum Valley falls within the DFS medial fan facies belt (Figure 4.1). The proximal part of the DFS is dominated by amalgamated channel belt facies with pockets of floodplain muds. Typically, the channels are dominantly 70 -100% coarse-grained sandstone.

In the Slick Rock district, including Gypsum Valley, the Salt Wash Member displays highly variable paleocurrent directions and a maximum exposed thickness of 335 meters thick (Shawe, 1968a; Cater, 1970). In the axis of the Disappointment Valley syncline, the entire Morrison Formation including the Salt Wash and Brushy Basin Members are enhanced by salt tectonism and is over 300 m thick. Here the Salt Wash Member is composed of channel deposits that are lenticular cross-bedded sandstones and floodplain deposits that are tabular thin and flat bedded mudstones and sandstones (Shawe, 1968a) (Figure 4.5).

Shawe (1968) subdivided the Salt Wash Member into three stratigraphic units based on different internal stacking patterns of sandstone and mudstone lithofacies (Figure 4.5). The lower cliff-forming unit consists thick (5-37 m), laterally discontinuous sandstone packages separated by thin discontinuous mudstones (Shawe, 1968a) (Figure 4.5). The sandstones in this lower unit exhibit low angle cross-bedding, horizontal, and massive bedding (Shawe, 1968a). The slope- and ledge-forming middle unit consists primarily of mudstone and siltstones with dispersed unconnected lenses of sandstone. The mudstones and siltstones average 24 meters thick. The sandstones in this unit are up to 18 meters thick, are horizontally thinly bedded, and ripple cross-stratified. The upper unit consists of laterally amalgamated lenses of sandstone, forming a prominent cliff that in a few locations forms a single unit and in others are separated by thin layers of mudstone (Figure 4.5). Paleocurrents indicate east and southeast dispersal in the area

south and west of Gypsum valley (Shawe, 1968b). The sandstones in this unit are 1.5 to 19.5 meters thick and are dominantly cross-bedded and horizontally laminated with scour and fill structures. An additional shale unit is included in the Salt Wash in this paper, because the sandstone lenses within it are medium-grained light tan sandstones, easily distinguished from the overlying dark, pebbly Brushy Basin sandstones.

Methods

Four composite stratigraphic sections (HT1, HT2, HT3, HT4) and twenty-four partial sections were measured around the synclinal structure of 'The Hat' (Figure 4.4). In addition, a composite section was measured at the southern margin of Little Gypsum Valley at Grassy Hill for basis of comparison (Figure 4.2). Stratigraphic correlation diagrams document fluvial facies distribution laterally across the syncline and vertically during fill. Panoramic photos and geologic mapping from Google imagery have been used to map and track lateral changes in channel thickness, facies, geometry, and to tie locations of stratigraphic sections and samples. Key beds were correlated using QGIS in the field using an Asus tablet to highlight the effects of diapiric tectonism. In addition, measurements of grain size, sedimentary structures, paleocurrents, and channel geometries were collected to document the differences in fluvial architecture and stacking patterns of the Salt Wash within the Hat syncline.

Results

'The Hat' syncline in Little Gypsum Valley

'The Hat' syncline in Little Gypsum Valley, the subject of this study, is located on the crest of the former passive diapir. Its name is based on the geomorphic shape of a central outcrop that resembles a conical hat (Stokes and Phoenix, 1948) (Figure 4.4). The exposed remnant of the Hat syncline is 1.75 km wide and 0.8 km long with an axis oriented to the north-northwest,

oblique to the NW-SE axis of the salt wall. The syncline rests entirely on Summerville Formation and Entrada Formation strata, that in turn rest on diapiric salt of the Paradox Formation (Figure 4.4). Along its northeastern flank older units of the Kayenta, Wingate and Chinle Formations are exposed beneath the Entrada and are folded into the syncline. Salt is exposed beneath these strata 1.5 km to the southeast, and, to the northwest in a window (The Nubbin) eroded through these same strata. Figure 4.2 shows a structural cross section of the Hat syncline and surrounding area and illustrates these relationships. The northeastern flank of 'the Hat' syncline runs very close to the margin of the diapir (Figure 4.2). The anticline that flanks 'the Hat' syncline to the northeast is interpreted to bound subsidence into the Dry Creek Minibasin to the Northeast, and subsidence into the diapir in 'the Hat' syncline (Figures 4.2;4.4).

The syncline displays excellent exposures of the Salt Wash Member of the Morrison Formation (Figure 4.4). This study provides a detailed analysis of local variations in the Salt Wash Member stratigraphy at Little Gypsum Valley, specifically focusing on changes in fluvial architecture within the syncline.

Facies Assemblages

Three main facies assemblages are identified throughout the study area that make up the stratigraphic stacking patterns described within the Salt Wash Member. The facies assemblages were described and identified based on the lithofacies present (Table 4.1). Two types of channel fill are observed throughout the stratigraphy in Gypsum Valley and are described in detail below, as well as floodplain facies with dominantly mudstones, and sandy crevasse splay deposits.

Channel Fill

The first type of channel fill (Type 1) consists of light gray to white sandstone beds. These beds are typically 1-2 m thick forming packages 2-5 m thick in the axis of the syncline

that thin toward the margin of the syncline where they are 1-2 m thick. These channels have coarse-grained bases often with rip-up clast conglomerates composed of angular, granule to pebble sized and are composed of the underlying reddish brown to greenish gray mudstones and siltstones. These coarse grain bottoms also contain lesser amounts of limestone, feldspar, and chert clasts. They are dominantly trough cross-stratified with rippled and bioturbated tops (Figure 4.6). Less often these beds have laminations and are massive (Figure 4.6). This channel fill is differentiated from the second type of channel fill because typically these channels are amalgamated with internal scouring (Figure 4.6).

The second type of channel fill (Type 2) consists of rusty, dark reddish-brown sandstone beds. This channel fill has sharp and erosional bases with granule to pebble sized rip-up clast conglomerates, that grade into subhorizontal laminations (Figure 4.7; 4.8). These beds often have soft-sediment deformation consisting of flame and slump structures and convoluted bedding (Figure 4.7; 4.8). These beds are overlain by massive to ripple cross-stratified to bioturbated beds (Figure 4.7; 4.8). The channel fill fines upward. Lateral accretion sets and beds with lenticular geometry are locally present.

Floodplain

This facies assemblage is commonly poorly exposed, poorly lithified, and forms slopes between sandstone channel fill ledges (Figure 4.7). It is composed of poorly lithified mudstone and siltstone beds that range in thickness from 1 to 28 meters. Where it is exposed this facies, assemblage is typically composed of the poorly lithified mudstone and siltstone lithofacies that is typically fine-grained, dark reddish-brown color or greenish- grey color. The mudstones and siltstones when well exposed are thinly bedded. Thin beds of wave rippled or bioturbated sandstones are common in mudstone outcrops. When exposed these beds can sometimes be

laterally extensive but more commonly pinch out laterally. These facies often are erosionally-capped by channel fill and are tabular. The mudstones and siltstones also can exhibit a mottled texture with a mix of colors from light reddish brown to dark reddish brown with greenish grey (Figure 4.7). This facies assemblage is interpreted to be floodplain deposits.

Crevasse Splay

This facies assemblage is composed of fine-medium grained, well sorted, rounded-subrounded sandstones. It is typically composed of horizontally bedded, trough cross-bedded, ripple cross-strata, and episodic bioturbated lithofacies. The sandy crevasse splay grades into a brown bioturbated mudstone with white reduced zones around burrows. These sandstones are interpreted to be sandy crevasse splay deposits.

Stratigraphy of the Salt Wash Member at 'The Hat'

In this study the Salt Wash stratigraphy was divided into four units that were mapped throughout the study area: 1) interbedded sandstone channels and mudstones (ISCM), 2) amalgamated sandstone channels (ASC), 3) isolated sandstone channels (ISC), and 4) laterally-stacked sandstone channels (LSSC) (Figure 4.5). For the basis of comparison, the sections measured at 'The Hat' were correlated and compared to the nearest complete section outside the syncline located on the opposite side of Gypsum Valley to the southwest, at Grassy Hill (Figure 4.2). The ASC correlates to Shawe (1968) upper part of the Lower stratigraphic unit, ISC to the middle, and LSSC to the upper unit, although the LSSC defined here includes mudstone strata included in the Brushy Basin by Shawe (1968) (Figure 4.5). The lowermost unit described in this study (ISCM) was observed by Shawe, 1968 and is only seen at a few locations around Gypsum Valley (Bailey, 2020-Chapter 2).

The Salt Wash Member exposed at ‘the Hat’ is thicker and contains a higher proportion of mudstone units than the Salt Wash Member measured in other locations in Gypsum Valley (Figure 4.9). A comparison of measured sections HT-2 and GH-2 show the mudstone content increases in the axis of the syncline and has a notable concentration of sand along the diapir margin (Figure 4.9). The ISC and LSSC units have increased mud content compared to the section measured at Grassy Hill (Figure 4.9). The measured section HT-2 at ‘the Hat’ has a total of 77% mud compared to 54% mud at the section measured at Grassy Hill. The Salt Wash Member section measured in the axis of ‘the Hat’ syncline is 49-23% thicker than sections measured locally around Gypsum Valley from this study and 49% thicker than sections measured more regionally (Shawe, 1968a; Cater, 1970).

Interbedded Sandstone Channels and Mudstones (ISCM)

The ISCM unit is the lower most unit of the Salt Wash Member documented at Grassy Hill but is not present at ‘the Hat’. This unit was primarily deposited in sandy crevasse splays and other floodplain environments. It is exposed locally in Little Gypsum Valley at Grassy Hill where it is 5.4 meters thick. Unit 1 is likely not exposed at ‘the Hat’ because it was either never deposited, eroded away prior to deposition of the overlying units, or intertongues with and becomes indistinguishable with the overlying amalgamated sandstone channels of Unit 2 ASC. The relationship remains uncertain because the Salt Wash Member in the center of Gypsum Valley is buried under younger units.

Amalgamated Sandstone Channels (ASC)

The ASC unit overlies the ISCM unit at Grassy Hill and is present at the base of the Salt Wash Member at ‘the Hat’ syncline, overlying the Jurassic Summerville Formation (Figure 4.6). ASC sandstones were primarily deposited by the type 1 channel fill facies assemblage. The unit

is 24 meters thick in the axis of ‘the Hat’ syncline, 14.5 meters thick on the margin of the syncline, and 37 meters thick at Grassy Hill (Figure 4.6).

The ASC forms a broad ledge on the rim of the "Hat" geomorphic feature (Figure 4.4). The basal channel system is 1.15 meters thick and laterally extensive across the syncline of ‘the Hat'. Individual channels in this unit extend laterally for 0.82 kilometers. Channelized beds have erosional bases with the Summerville Formation below and the isolated channel facies above, are typically 1-3m thick and are 70-200m wide. The channels are an amalgamated package of lenticular, internally scoured channel fill (Figure 4.4). Above the basal channel of this unit, four younger channels of the ASC onlap the basal channel (Figure 4.4). The younger channels are truncated by the overlying ISC unit (Figure 4.4). Paleocurrent data show that these channels flow dominantly to the southwest (Figure 4.4), which is similar to regional Salt Wash flow directions (Figure 4.1).

The ASC unit in the axis of ‘the Hat’ syncline differs from the section measured at Grassy Hill in thickness and mud content. At Grassy Hill it is 36.8 meters thick compared to 25.3 meters in the axis of the syncline and 14.5 on the margin (Figure 4.9). ASC channels at ‘the Hat’ are thinner and contain more mud between packages. This unit consists of 56% sandstone on the rim of the syncline, 47% sandstone in the axis of the syncline compared to 60% at Grassy Hill (Figure 4.9). The section at Grassy Hill is thicker and sandier compared to the sections of amalgamated sandstone channels at ‘the Hat’.

Isolated Sandstone Channels

The ISC overlies the ASC and is present at all studied locations. This unit is 66.3 meters thick in the axis of ‘the Hat’ syncline, 25.2 on the margin of the syncline, and 43.9 meters thick at Grassy Hill (Figure 4.9). It is primarily composed of the type 2 channel fill and floodplain facies assemblages. Mudstones of the floodplain assemblage are thickest within the axis of the

syncline, 30 m as opposed to 15-10 meters on the margin. The floodplain mudstones thin and pinch out onto the margin of the diapir away from 'the Hat' syncline. The beds of channel fill are 5 to 13 meters thick. Total packages of channel fill are 4 to 9.3 meters thick. Paleocurrents show that these channels are flowing to the northwest.

The ISC unit differs from the same unit seen at Grassy Hill in thickness and sand content. This unit is much thinner at Grassy Hill at a thickness of 43.9 meters at Grassy Hill compared to 65.4 meters in the axis of 'the Hat' syncline and 25.2 meters on the rim of the syncline (Figure 4.9). The percent sandstone on the exposures nearest the syncline rim is 15% compared to 18% in the axis of the syncline, and 17% at Grassy Hill. This unit is thickest and sandiest in the axis of the syncline.

Laterally Stacked Sandstone Channels (LSSC)

The LSSC is the uppermost unit identified in the Salt Wash Member and is present at all studied locations. It is 105.3 meters thick in the axis of 'the Hat' syncline compared to 45.2 meters thick at Grassy Hill. This unit is primarily composed of type 2 channel fill that is more laterally stacked than the channel fills found in the underlying ISC (Figure 4.6). The channels are laterally extensive approximately 0.87 km meters across 'the Hat' structure. These channels exhibit lateral accretion sets, are lenticular, and are distinct ledge formers. Channel fills in the laterally-stacked sandstones unit are continuous across most of the axial part of the syncline, making a prominent cliff (Figure 4.8). The dip of the beds within this unit are almost flat with shallow dips at about 12° indicating that filling of the basin is almost completed by the end of Salt Wash deposition (Figure 4.7). The overlying Brushy Basin Member strata are nearly flat, exhibiting a gentle southwestern dip. Paleocurrents show that these channels were north-south and northwest flowing.

The LSSC unit is also different from the same unit at Grassy Hill because of thickness and mud content. This unit at Grassy Hill contains less mud with a sand percentage of 58% compared to 21% in the axis of 'the Hat' syncline (Figure 4.9). The sandstone channels at this location are much more vertically stacked and continuous along the margin of the diapir at Grassy Hill. The Grassy Hill section of this unit is only 45.2 meters thick compared to 105.3 meters at 'the Hat' in the axis of the syncline (Figure 4.9).

Structure and Salt Tectonic Sequences

Today, the Salt Wash Member of the Morrison Formation at 'the Hat' forms a syncline flanked by two associated shorter wavelength anticlines with axes oriented to the north-northwest at an azimuth of 110 degrees (Figure 4.4). The syncline exhibits growth strata with the upper beds being less deformed so that the contact with the overlying Brushy Basin Member dips at only 8 degrees. The exposed uneroded remnant of the syncline is 1.75 km wide and 0.8 km long (Figure 4.4).

In 'the Hat' syncline, as in most of Little Gypsum Valley, the Morrison Formation and underlying Summerville Formation rests on the Late Jurassic Entrada Sandstone, which in turn locally either rests unconformably on Paradox diapiric caprock or with angular unconformity on Early Jurassic Kayenta and Navajo formation strata (Figure 4.4). The Entrada Sandstone exhibits 150 m wavelength syndepositional folds, that are filled with Entrada-age growth strata (Ronson, 2018) (Figure 4.4).

The Summerville Formation appears to have a consistent thickness. Five sections were measured through the Summerville Formation in the axis and on the flanks of 'the Hat' syncline that ranged from nine to twelve meters thick (Figure 4.4). This relatively consistent thickness of the Summerville Formation indicates that formation of the Hat syncline had not commenced, and

the Summerville Formation and basal Salt Wash Member were deposited across a low relief surface. The basal ASC unit of the Salt Wash Member does not erode deeply into the Summerville Formation, but the little bit of erosion accounts for most of the stratigraphic thickness variability of the Summerville Formation.

Growth in accommodation space at 'the Hat' syncline resulted in two syndepositional patterns: (1) beds thicken into the axis of the syncline and (2) there is onlap and truncation within the Salt Wash Member that define synsedimentary growth sequence boundaries (Figure 4.4; 4.9). Four salt tectonic growth sequences have been recognized: GS1, GS2, GS3, GS4 and are defined by growth sequence boundaries that are marked by onlap and truncation of channels mapped across the structure (Figure 4.4; 4.9; 4.10). It is important to note that the growth sequence boundaries described below do not coincide with the Salt Wash Member stratigraphic unit contacts. The growth sequence boundaries GS-B and GS-C cross stratigraphic unit boundaries. Both boundaries are described below and where this is apparent on the southside of 'the Hat' with growth sequence boundary B is highlighted in figure 4.9.

Syndepositional growth sequence GS1 comprises the basal ASC channel and the underlying Summerville Formation (Figure 4.4; 4.9; 4.10). Within this growth sequence the basal channel is conformable with the underlying Summerville Formation and does not exhibit growth into the syncline (Figure 4.4; 4.9; 4.10). The growth sequence boundary between growth sequences GS1 and GS2 is found approximately 5 m above the base of the Morrison/Summerville contact within ASC, which is marked by onlapping strata of ASC (Figure 4.4; 4.10). Growth sequence boundary A is defined by the onlapping of six ASC channel beds that have been traced on the south side of 'the Hat', and four onlapping intervals on the north side of 'the Hat' (Figure 4.4; 4.10). This marks initiation of deformation of 'the Hat' syncline.

Syndepositional growth sequence GS2 contains strata from both ASC and ISC. It is found on both the south and north side of 'the Hat' syncline (Figure 4.4; 4.10). The top of this salt tectonic growth sequence is defined on the south side of the syncline by truncation of three channels within ISC and one channel in ASC (Figure 4.4; 4.10). Above this boundary is defined by onlap of two channels within ISC (Figure 4.4; 4.10). It is marked above by onlap of two ISC channels (Figure 4.4;4.10). On the northside of 'the Hat' syncline this boundary is defined by onlap of three channels within ISC (Figure 4.4;4.10). At this location on both the south and north side the boundary crosses both ASC and ISC where it truncates both channels within ASC and ISC and is primarily onlapped by channels within ISC (Figure 4.4;4.11).

Syndepositional growth sequence GS3 contains partial lithostratigraphic units from both ISC and LSSC (Figure 4.4; 4.10). The growth sequence boundary that defines the upper boundary of this growth sequence is characterized by truncation of two channels within LSSC on the south side of the structure and truncation of two channels within ISC on the northside of the structure. It is also defined by onlap of channels within LSSC on both sides of the structure (Figure 4.4; 4.10). The top of this growth sequence also includes the Brushy Basin Member. This boundary also does not coincide with stratigraphic unit boundaries. This is apparent on both the north and south sides of the syncline (Figure 4.4; 4.11).

Discussion

This study demonstrates that the Salt Wash Member of the Morrison Formation was deposited on thin strata that were previously deposited on salt caprock. Morrison deposition was accompanied by deformation and slow continuous subsidence and provides a new model for both diapirism in the Paradox Basin and for deposition on mobile salt in general. Furthermore, the patterns of deposition at 'the Hat' offer a better constrained model that contrasts with previous

models of deposition around salt diapirs. Deformation of 'the Hat' syncline during Salt Wash Member deposition is most likely related to salt deformation rather than regional tectonism because the timing does not match known deformation events in the Colorado Plateau, which do not commence until 75 Mya.

The Salt Wash Member at 'the Hat' exposes two cliff-forming units containing amalgamated channel sandstones, the ASC, and the lower, cliff-forming interval of the LSSC (Figures 4.9). Gypsum Valley lies within the medial part of the distributive Salt Wash Member system (Owen et al., 2015c), thus sediment supply could be variable during deposition of each stratigraphic unit depending on where the main fan is depositing sediment (Figure 4.1) (Mullens and Freeman, 1957; Owen et al., 2015c). The ASC exhibits the most dramatic changes in facies within the syncline. On the flanking anticline and at Grassy Hills, the ASC is a sandstone ledge, 14.5 to 5 m thick. Within 'the Hat' syncline, the ASC thickens as shales onlap the lowest channel fills and thicken into the syncline (Figure 4.9). The overlying ISC thickens dramatically but shows little change in sandstone percentage of channel thickness within the syncline.

The most reasonable interpretation of the facies change within the ASC is that the larger channels were carrying abundant sediment. However, most of this sediment, especially the mudstones were carried beyond Gypsum Valley, or were re-eroded and transported past Gypsum Valley by younger channels of the ASC. Subsidence of the syncline resulted in trapping of mudstones within the syncline.

In contrast, the rate of sediment influx into the Gypsum Valley areas was likely much slower during ISC deposition. Because much of the sediment in the more distal part of the Salt Wash Member 'the Hat' syncline. However, deposition was enhanced resulting in the accumulation of a much thicker ISC section. The ISC and overlying LSSC show the greatest

thickening in ‘the Hat’. The ISC unit is 21.5 meters and the LSSC unit is 50.1 meters thicker in the axis of the syncline when compared to the Grassy Hill sections. This may have been due to a slower rate of sedimentation, which allowed for greater deposition, or the syncline may have been subsiding more rapidly during ISC deposition.

The channel sandstones in the lower part of the LSSC probably carried large sediment loads. The lack of thickening and facies change suggest that this unit was deposited quickly, and therefore there was not much time for the subsidence of ‘the Hat’ syncline to cause changes in this unit.

Previous studies also discuss subsidence rate as the most important factors controlling the stacking patterns of fluvial systems within a given accumulation space (Hazel, 1994; Matthews et al., 2007; Banham and Mountney, 2013b). This study points to subsidence rate of the microbasin on top of the Gypsum Valley salt diapir as a main factor shaping thickness patterns and depositional style. However, the stacking patterns of the fluvial system are also the opposite of what previous works suggests should be deposited in the available accommodation space. Banham and Mountney (2013b) describe in a series of models largely based on observations in the Paradox Basin and a few other locations that a low subsidence and low sediment supply rate and a high subsidence and high sediment supply rate results in sandy well-connected channels packages filling a subsiding basin.

The results presented demonstrate there are discrepancies between the stratigraphic units identified and the growth sequence boundaries throughout ‘the Hat’ syncline. These growth sequence packages and boundaries represent periods of subsidence, and erosion during deposition of the Salt Wash Member. However, the fact that they do not follow along the same boundaries as the identified stratigraphy presents a problem. This relationship could be showing

that the depositional facies of the Salt Wash Member are controlled by regional conditions and are not specifically tied to local subsidence events. However, the increase in mud content within those lithostratigraphic units at 'the Hat' suggests a local control stemming from the syncline subsidence.

Most models of fluvial deposition related to diapirism suggest that channels are usually found in the axes of the minibasins. However, it is there is little evidence for this in 'the Hat' syncline. This is not likely because it is thought that the Disappointment and Dry Creek minibasins are no longer feeding salt into the diapir in Little Gypsum Valley at the time of Salt Wash Member deposition (Bailey, 2020-Chapter 2). No thinning of the Salt Wash Member is evident as the Salt Wash Member transitions from the minibasins to the diapir. Furthermore, the Morrison and underlying Summerville Formation dip at only a few degrees away from the diapir into the minibasins. In, contrast, the Morrison thins dramatically and is folded in big Gypsum Valley to the southeast. The basin probably best fits into the well-connected sandy channels end member of Banham and Mountney (2013), where the rate of sediment transport greatly exceeds the rate of deformation.

Previous models of fluvial systems in salt basins have focused on depositional patterns of sediments kilometers away from the salt diapirs within the adjacent minibasins and don't address what deposition might be like along the margins or even on top of a salt diapir (Matthews et al., 2007; Banham and Mountney, 2013b). Those previous studies assume that salt withdrawal results in subsidence of salt walled mini-basins creating accommodation space for fluvial systems to deposit sediment and preferentially flow to the topographic lows of subsiding minibasins and away from topographic highs of uplifted salt walls (Matthews et al., 2007; Banham and Mountney, 2013b). Flow of these fluvial systems to minibasins or other topographic

lows (rim synclines, secondary mini-basins) can lead to drainage capture or diversion that results in the reduction of sediment to other locations like on the margins or on top of the diapir (Matthews et al., 2007; Banham and Mountney, 2013b). In the case of this study, the salt walled minibasins are no longer subsiding or creating accommodation space for fluvial systems to be redirected and thus are not depositing all the sand sediment load in to the adjacent minibasins. Throughout Gypsum Valley, the flow patterns during the deposition of the Salt Wash Member were altered by the active Gypsum Valley salt diapir but were not influenced significantly enough to be restricted sand deposition to adjacent mini-basins (Figure 4.4; 2.16) (Bailey, 2020-Chapter 2). The fluvial system carried sediment across the Gypsum Valley salt diapir and deposited sediment on top of the subsiding salt syncline at 'the Hat'.

'The Hat' is best represented by a model of fluctuating subsidence rate and rates of deposition. Lower rates of deposition are marked by growth sequence boundaries and thickening into the syncline. Onlap of strata onto growth sequence boundaries and thickening into the syncline. Onlap of strata onto growth sequence boundaries indicates that the flanks of the syncline were at the surface, and possibly even forming subtle topographic highs. Higher rates of deposition and slower subsidence are reflected in the continuous sandstone beds that extend across the syncline (Figures 4.4).

Conclusion

'The Hat' syncline formed on top of the Gypsum Valley salt diapir during deposition of the Salt Wash Member. Subsidence began after the first channels of the fluvial Salt Wash Member were deposited. Onlap and truncation of the channels of the Salt Wash Member within 'the Hat' basin resulted in four growth sequences separated by 3 growth sequence boundaries that represent periods of growth and erosion during the deposition of the Salt Wash Member.

Subsidence of ‘the Hat’ syncline is thought to result from decreased input of salt from the adjacent Disappointment and Dry Creek minibasins and movement of salt laterally along the axis of the diapir and/or deep dissolution of the salt, allowing relatively slow subsidence over the top of the Little Gypsum Valley Salt diapir. Little, or no subsidence in the adjacent minibasins means that the fluvial systems of the Salt Wash Member were able to cross the diapir, and fill accumulation space in ‘the Hat’ syncline. The result of this subsidence over the top of the diapir is a significant increase in thickness and floodplain facies within the top two stratigraphic units ISC and upper part of the LSSC. These two shale-rich intervals probably were parts of the Morrison fan system, that were fairly remote from contemporaneous depocenters. The slower depositional rate resulted in greatly thickened sections. There are few apparent facies changes within these two intervals, and they are interpreted to have filled the syncline throughout deposition. The ASC and basal LSSC intervals represent main distributary fairways that were deposited much more rapidly. The LSSC does not appreciably thicken or change facies within the syncline and must have been deposited much faster than deformation of the syncline. The ASC interval incorporates additional mudstones between the sandstone. Syncline subsidence is interpreted to have allowed accumulation of floodplain muds that were stripped away by erosion of younger channels in surrounding areas.

Table

Table 4.1: Lithofacies

Table 1- Lithofacies						
Lithofacies Code	Lithofacies	Lithofacies Assemblage	Grain/Clast Size	Sorting/Rounding	Description	Distribution/ Geometry/Thickness
St	Trough cross-bedded sandstone	Type 1 and type 2 channel fill	Low medium - upper fine sand	Well to moderately sorted, subrounded to rounded	White to tan colored beds.	Abundant throughout ASC. Laterally continuous. 0.6-2 m thick.
Scr	Ripple cross-stratified sandstone	Type 1 and crevasse splay channel fill	Very fine - fine sand	Well sorted and Well rounded	Reddish brown to tan and white colored beds.	Abundant throughout all channels. Laterally discontinuous. 0.1- 0.6 m thick
Sh	Subhorizontally laminated sandstone	Type 1, type 2 and crevasse splay channel fill	Fine - low medium sand	Well to moderately sorted, subrounded to rounded	Low angle cross-bedding and horizontal laminations.	Abundant throughout all channels. Laterally continuous for 1-6 m. 0.5 - 4.5 m thick.
Sc	clast conglomerate	Type 1 channel fill	Pebble and granule sized clasts in a upper fine sandy matrix	Angular, subrouned clasts and poorly sorted	Composed of rip-up clasts of reddish brown to greenish grey siltstone and mudstines.Clasts are also chert and limestone.	Not common found typically at the base of channels. Laterally discontinuous.
Sm	Massive sandstone	Type 1 and Type 2 channel fill	Very fine - fine sand	Well sorted, subrounded to rounded	Lack apparent sedimentary structures.	Found throughout each unit. Laterally continuous. 0.2-2 m thick.
Sb	Bioturbated sandstone	Type 1, type 2, and crevasse splay channel fill	Low fine - upper medium sand	Well to moderately sorted, rounded	Ichnofacies associated with the burrows identified in outcrop are interpreted to be from digger wasps (Hymenoptera: Sphecidae)	Abundant throughout each unit. Laterally continuous for 1-4 m. Bioturbated beds 1 m thick.
Ssd	Soft sediment deformed sandstone	Type 1 and type 2 channel fill	Upper very fine to medium sand	Well sorted and rounded	Is composed of flame and slump structures and conute bedding.	Moderately abundant within LSSC. Laterally discontinuous
Fm	Poorly lithified mudstones and siltstones	Floodplain	Dominantly composed of mudstones and siltstones	—	Dark reddish-brown or greenish grey color. Thinnly bedded and can be found with burrows and mottled texture.	Abundant throughout each unit. Slope former, thick layers that pinch out laterally. Thickness ranges from 1-28 m.

Figures

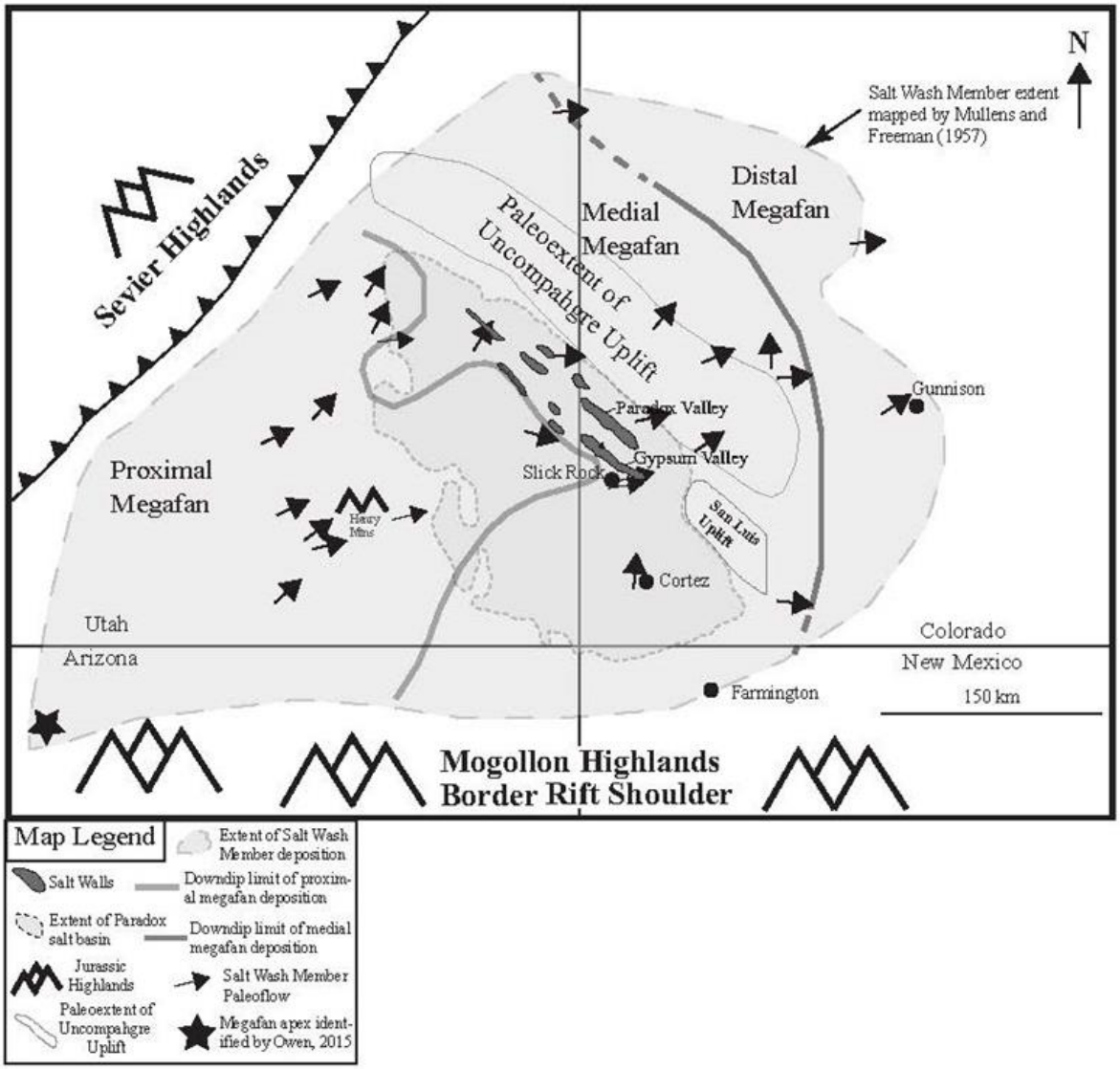

Figure 4.1: Regional map of Jurassic Salt Wash Member of the Morrison Formation depositional system areal extent of Paradox Basin deposition.

Fluvial system paleoflow of the Salt Wash Member from Owen et al. (2015) is indicated by gray arrows and the extent of the fluvial system from Mullens and Freeman (1957) is a dashed outline. Paradox Basin salt walls are outlined with dark infill gray. (Figure altered after Barbeau, 2003; Trudgill, 2011; Owen et al., 2015)

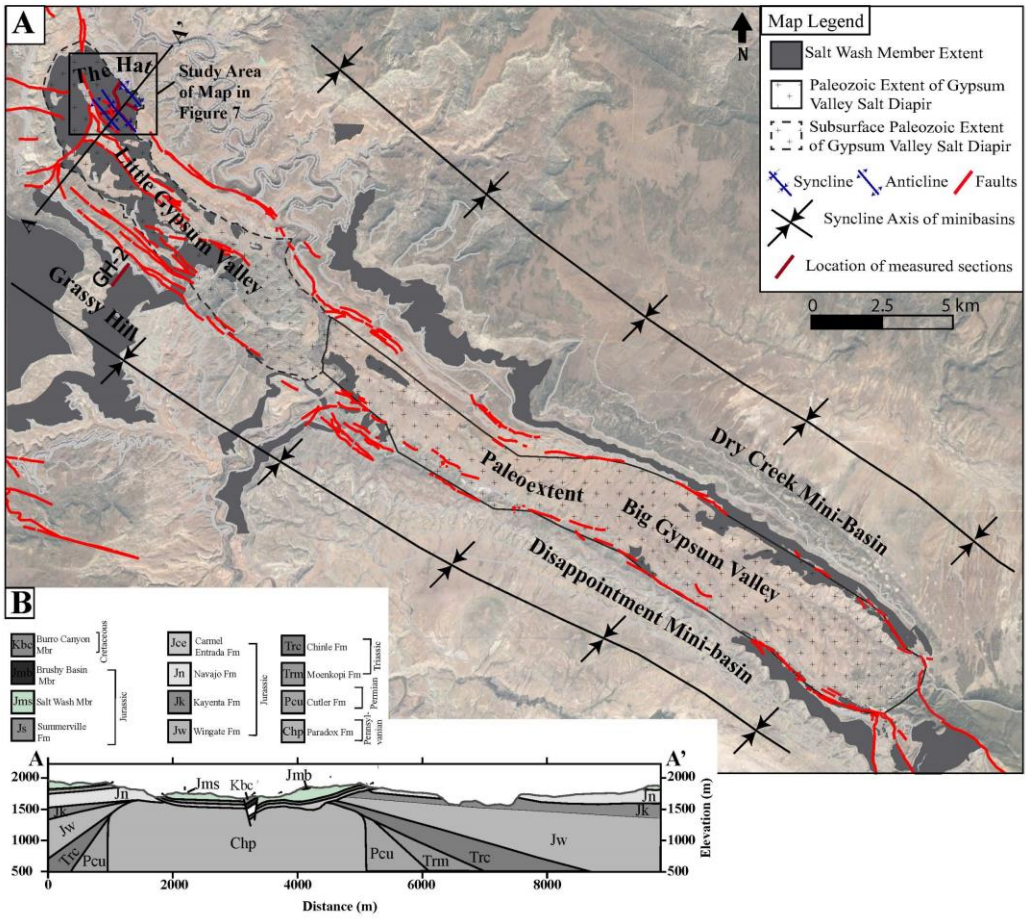

Figure 4.2: Extent of Gypsum Valley Salt Diapir and Salt Wash Member

A. Map showing the extend of the outcrop of the Salt Wash Member in green. Map also shows the extent of the Gypsum Valley Salt Diapir during deposition of the Salt Wash Member. B. Crossection across Little Gypsum Valley. Stratigraphy and tectonic history of Gypsum Valley Area.

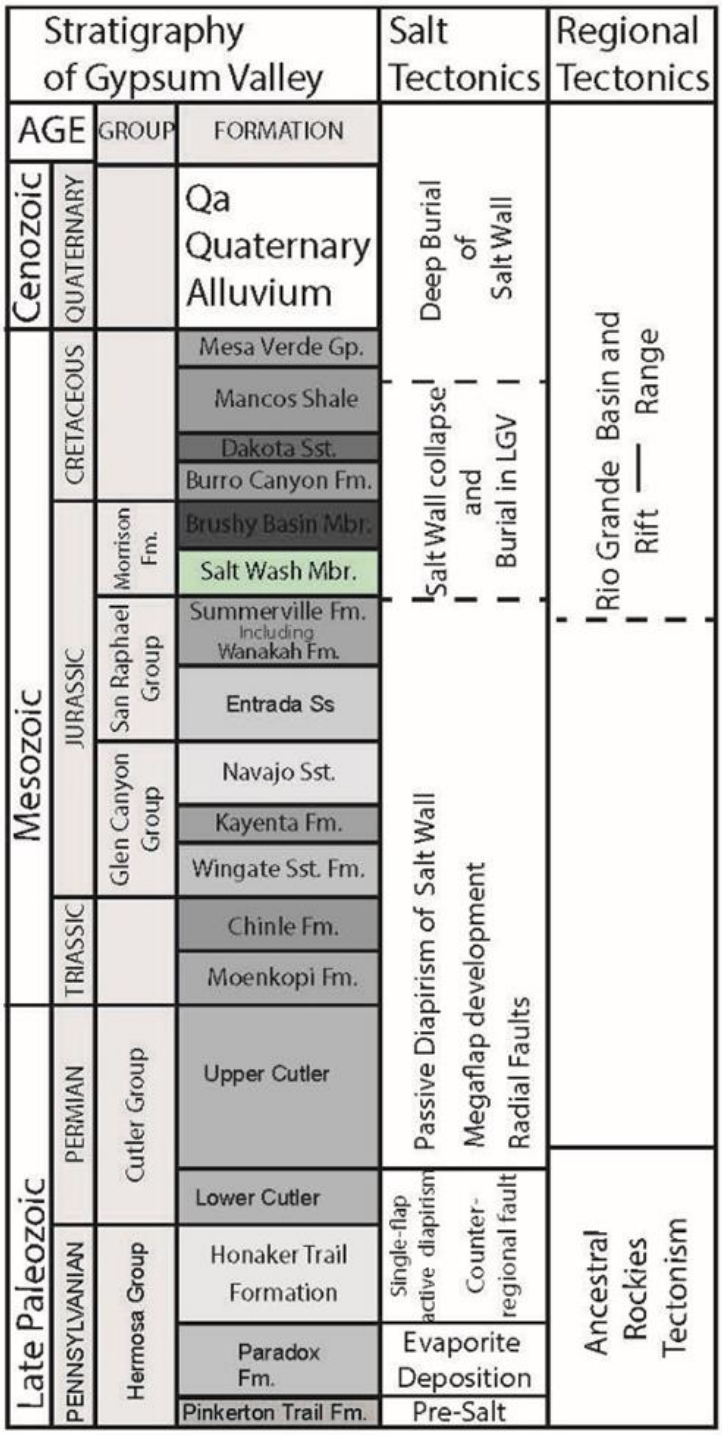

Figure 4.3: Stratigraphy and tectonic history of Gypsum Valley Area.

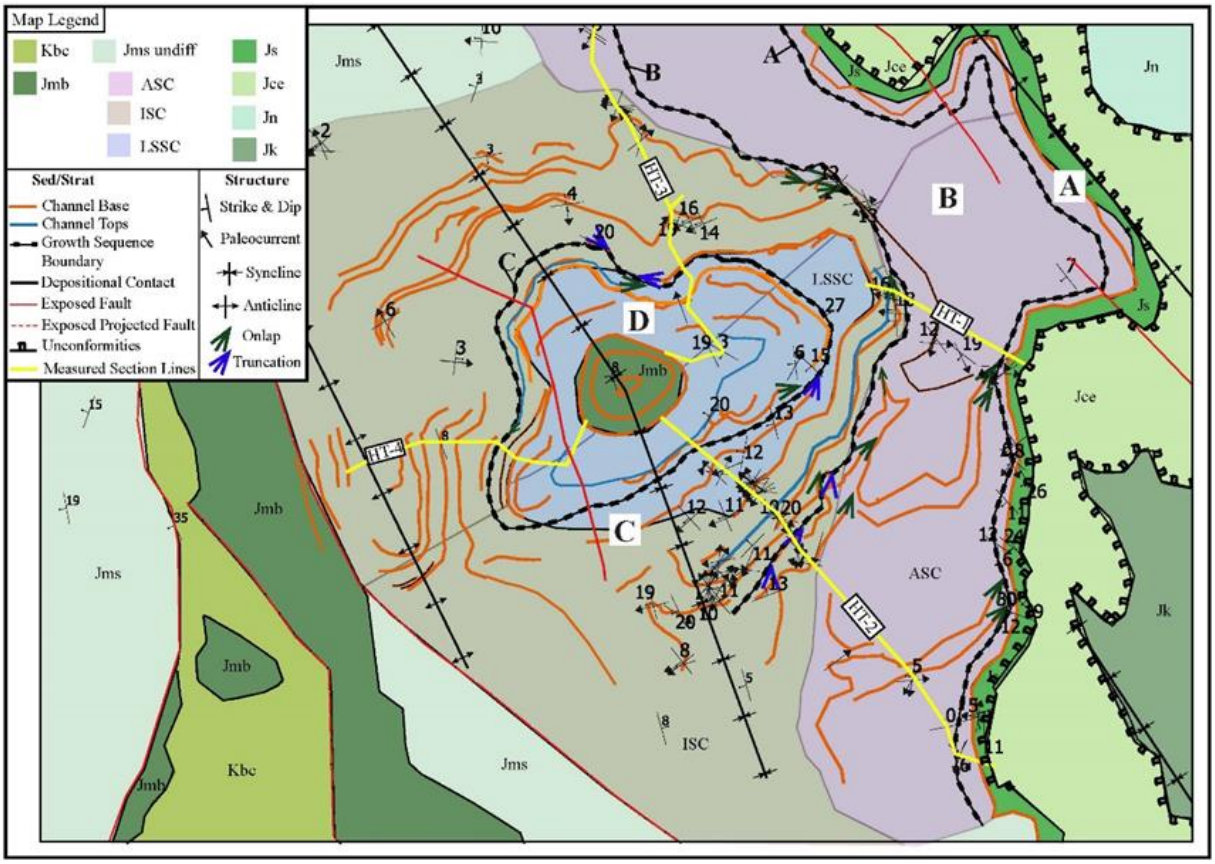

Figure 4.4: Detailed geologic map of the Hat area

Showing the mapped extent of each stratigraphic unit, detailed Salt Wash Member stratigraphy (ASC, ISC, and LSSC), channel bases, channel tops, salt tectonic growth sequences (A, B, C, D), growth sequence boundaries (A, B, C), depositional contacts, exposed faults, unconformities, and measured section lines (HT-1, HT-2, HT-3, HT-4). Onlap and truncation of channels onto growth package boundaries are highlighted by green and blue arrows respectively. Data on map also includes strike and dips, paleocurrents, and syncline and anticline fold axis. Location in Figure 4.1.

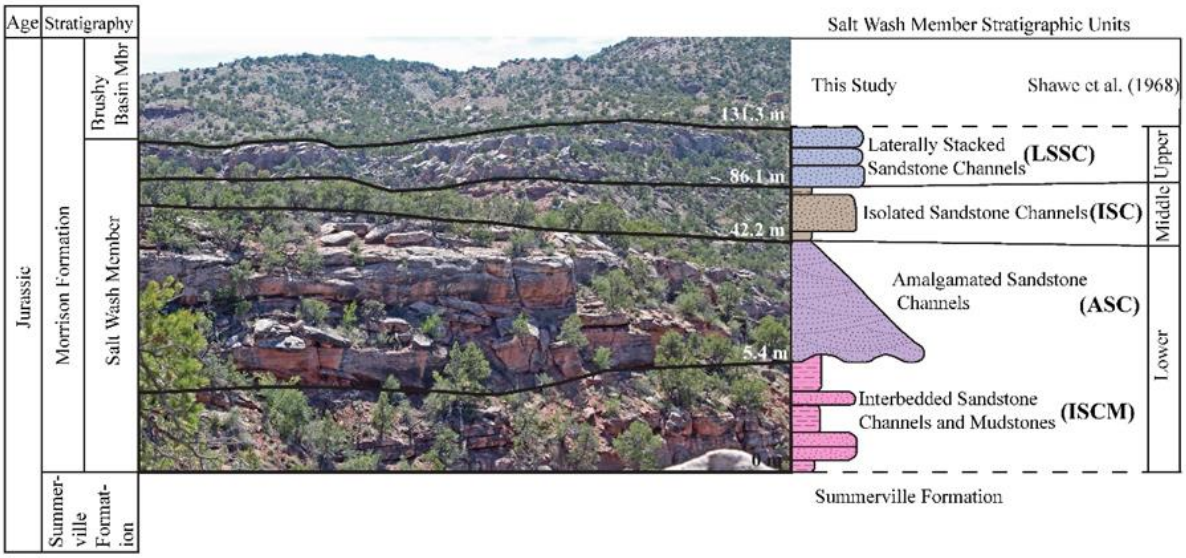

Figure 4.5: Outcrop photo of complete section of the Salt Wash Member

Photo taken at Grassy Hill on the SW side of Little Gypsum Valley. Gypsum Valley identified in this study. The column on the right side identifies units described in this study and correlation to Shawe et al. (1968). Their lower unit contains ISCM and ASC, Middle unit is ISC, and Upper Unit is LSSC. The approximate thickness of the Salt Wash Member at this location is 131.3 meters thick**.**

Figure 4.6: Type 1 Channel Fill

All pictures are of amalgamated sandstone channels at the base of 'The Hat' structure. A. Amalgamated Sandstone Channels at 'The Hat' with lithofacies Sh- subhorizontally laminated sandstone, Scr- Ripple cross stratified sandstone, St- trough crossbedded sandstone B. Outcrop of amalgamated internally scoured chanel fill. The thickness of the amalgamated channel package is 18 meters. C. Outcrop photo of amalgamated channels. Person in the photo is 6' 4".

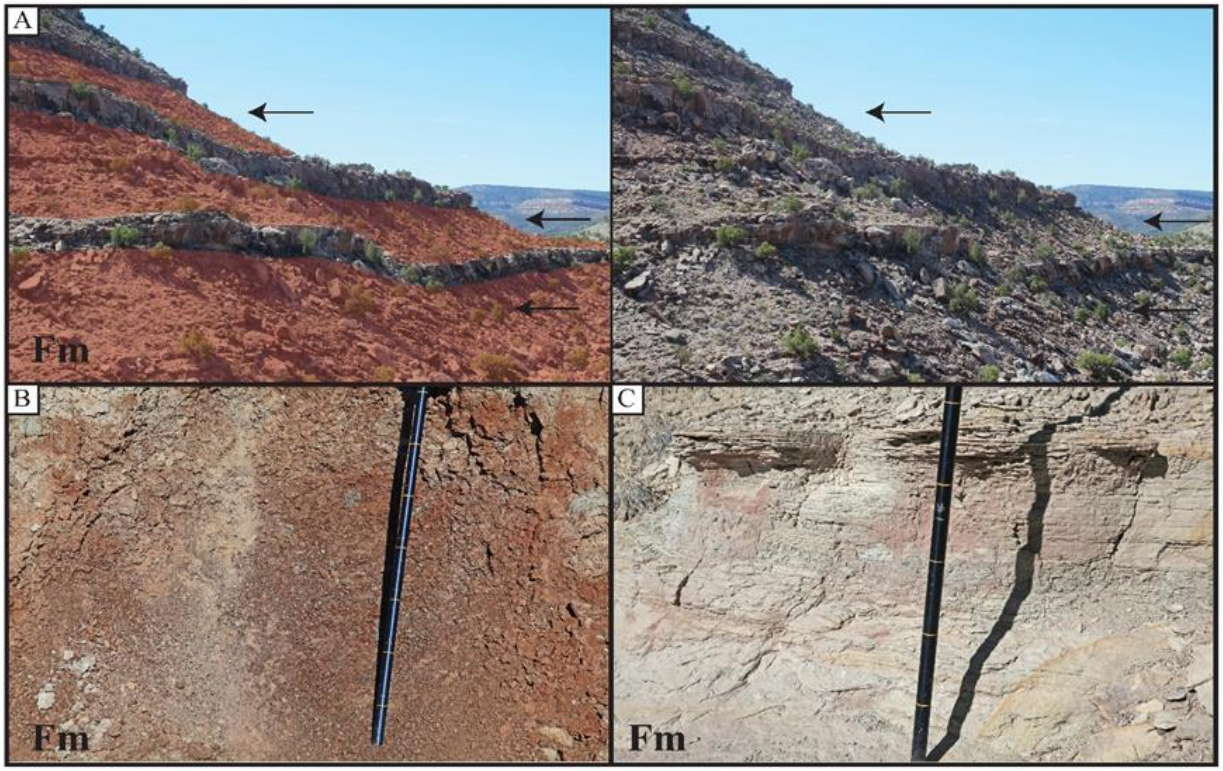

Figure 4.7: Floodplain facies assemblage

A. Isolated channel sandstones interbedded with reddish brown to greenish grey mudstones and siltstones. Arrows highlighting mudstones and siltstones form slopes between meandering channel sandstones. The thickness of the mudstones in the outcrop are 1-28 meters. Mudstones are lithofacies Fm. B. Reddish brown mudstone/siltstones. Scale in the photo is a Jacob Staff. Each yellow mark is 10 centimeters. C. Greenish Gray Mudstones/Siltstones. All photos taken on the southside of 'the Hat' structure.

Figure 4.8: Type 2 Channel Fill

A. Lateral accretion sets in type 2 channel facies. Person in photo is 1.5 meters. B. Dominate subhorizontal bedding. Person in photo is 6'4". C. Channel with massive to subhorizontal bedding. Jacob staff is used as scale in photo and is 1.5 meters.

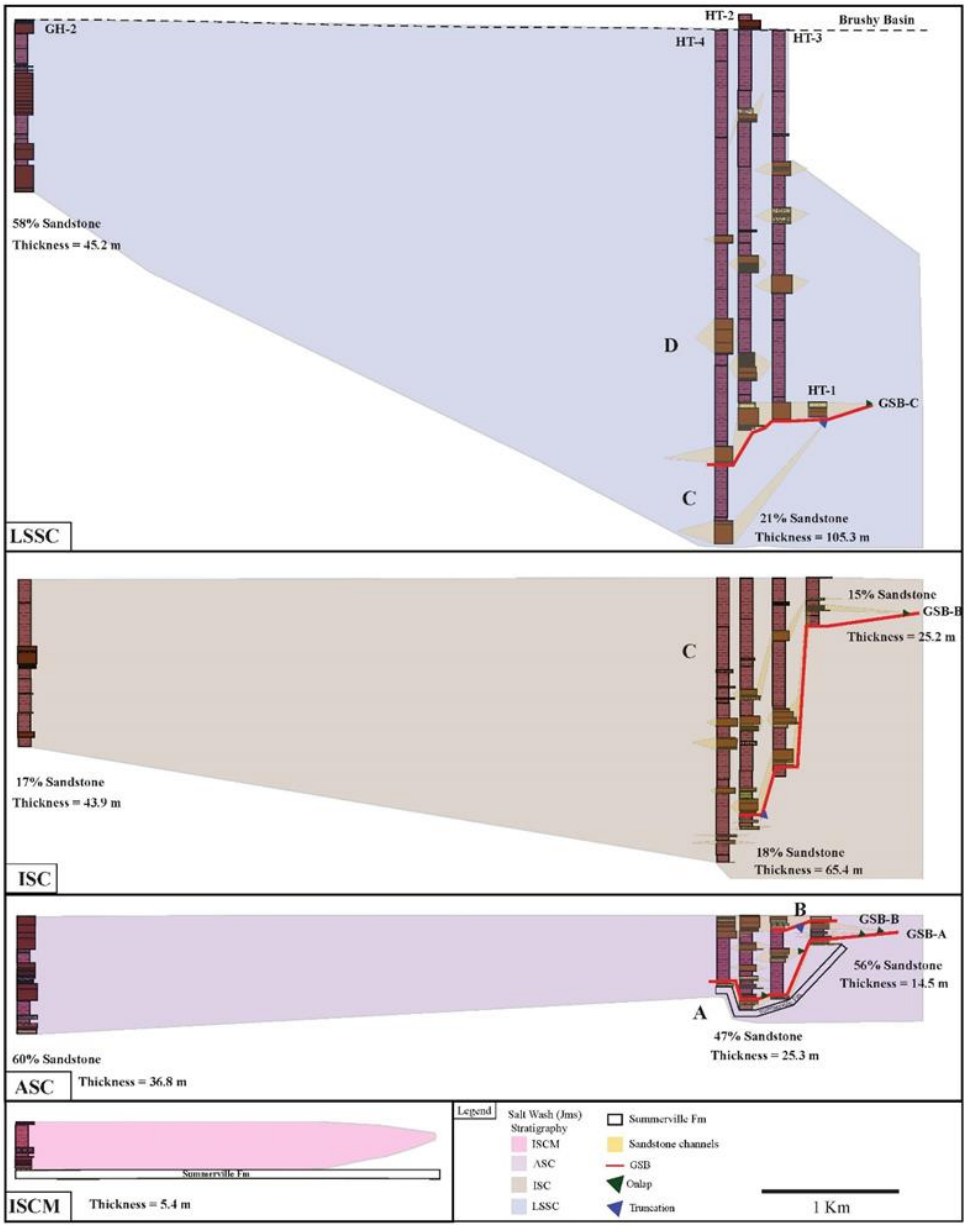

Figure 4.9: Correlation of measured sections at Grassy Hill to the four composite stratigraphic sections measured at the Hat.

Measured sections are hung on the top of each stratigraphic interval defined in Figure 5. Sandstones (yellow) are correlated based on relationships mapped in the field. If channels are not correlated, then they are likely to pinch out. Figure also includes correlation of growth sequence boundaries in red that are defined by onlap (green arrows) and truncation (blue arrows) of channels. The stratigraphic relationship of the Summerville Formation is shown at both the Hat and at Summerville Formation.

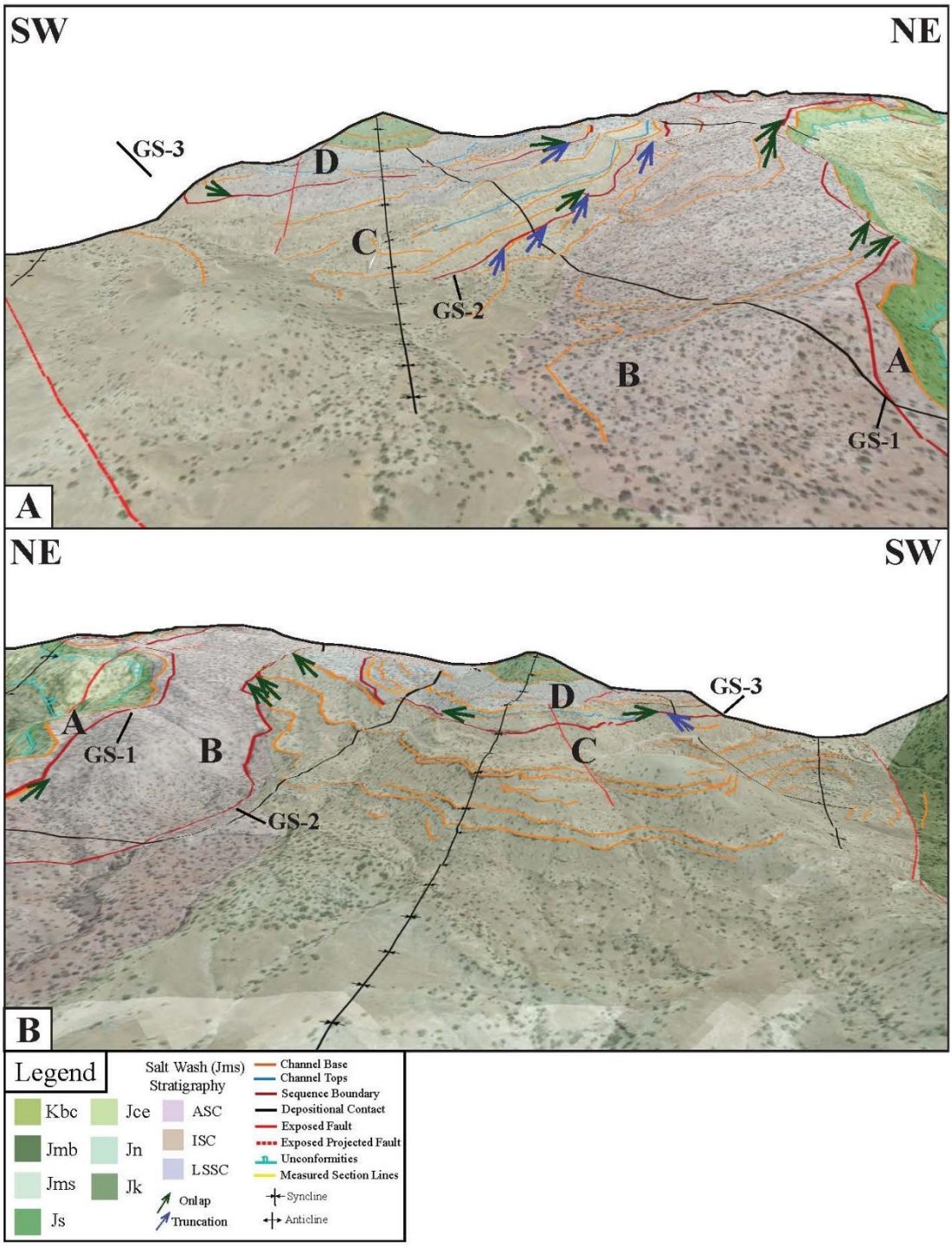

Figure 4.10: Panoramic images of 'the Hat' syncline.

A. Is the view from the southside of 'the Hat'. B. Is the view of the structure from the north.

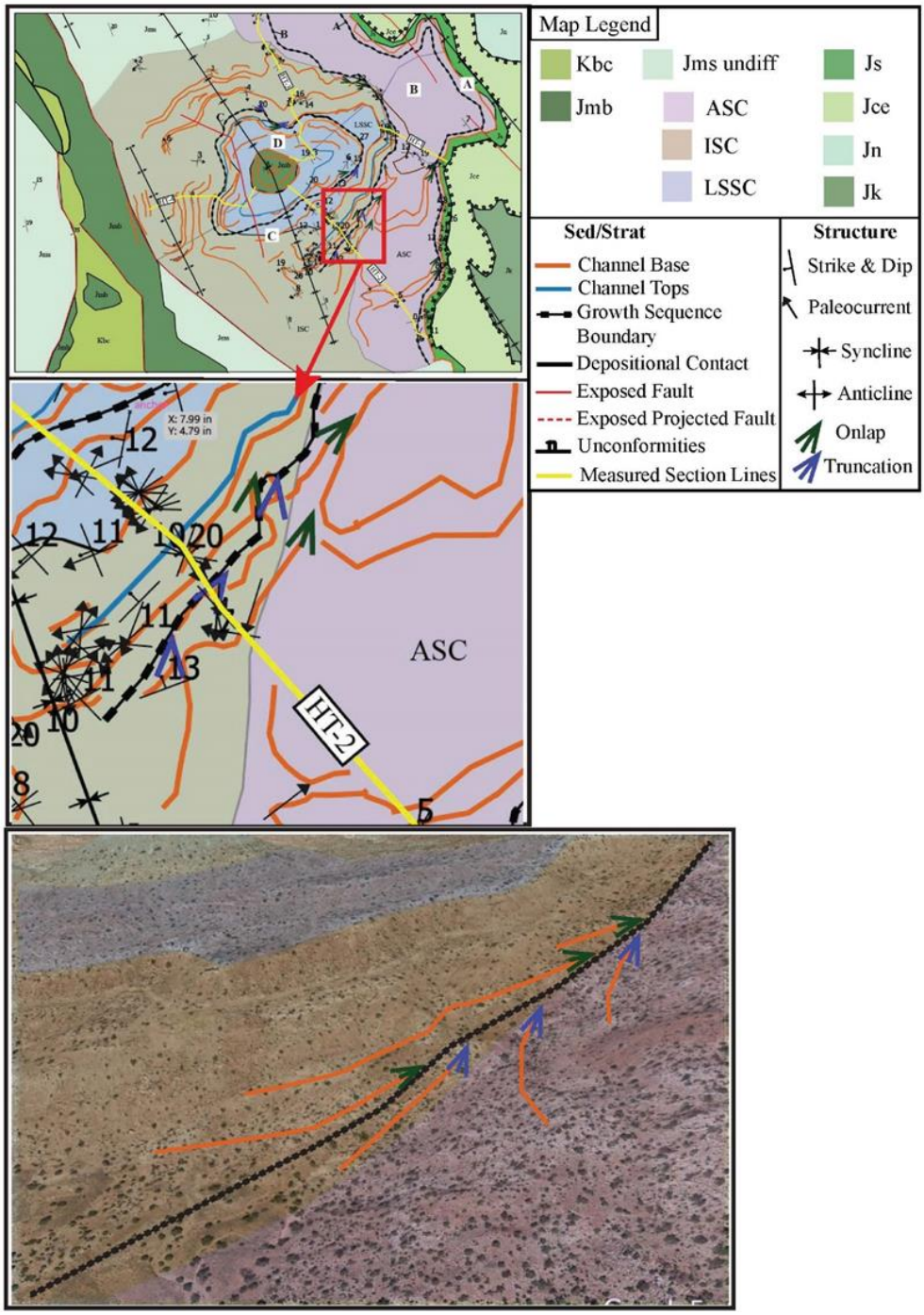

Figure 4.11: Growth Sequences

A. Geologic Map of the Hat highlighting location of where growth sequence boundary does not follow stratigraphic boundaries. B. Close up of area. C. Google Earth photo of outcrop where this is apparent.

References

Andrie, J.R., Giles, K.A., Lawton, T.F., and Rowan, M.G., 2012, Halokinetic-sequence stratigraphy, fluvial sedimentology and structural geometry of the Eocene Carroza Formation along La Popa salt weld, La Popa Basin, Mexico: Geological Society, London, Special Publications, v. 363, p. 59–79, doi:10.1144/SP363.4.

Banham, S.G., and Mountney, N.P., 2013a, Controls on fluvial sedimentary architecture and sediment-fill state in salt-walled mini-basins: Triassic Moenkopi Formation, Salt Anticline Region, SE Utah, USA: Basin Research, v. 25, p. 709–737, doi:10.1111/bre.12022.

Banham, S.G., and Mountney, N.P., 2013b, Evolution of fluvial systems in salt-walled mini-basins: A review and new insights: Sedimentary Geology, v. 296, p. 142–166, doi:10.1016/j.sedgeo.2013.08.010.

Blum, M.D., and Törnqvist, T.E., 2000, Fluvial responses to climate and sea-level change: a review and look forward: Fluvial responses to climate and sea-level change: Sedimentology, v. 47, p. 2–48, doi:10.1046/j.1365-3091.2000.00008.x.

Cater, F.W., 1970, Geology of the Salt Anticline Region in Southwestern Colorado: , p. 84.

Cater, F.W., and Craig, L.C., 1970, Geology of the Salt Anticline region in southwestern Colorado, with a section on stratigraphy.: Geol. Quad. U.S. Geol. Survey PP-637, 84 p.

Craig, L.C., 1955, Stratigraphy of the Morrison and Related Formations, Colorado Plateau Region: A Preliminary Report: U.S. Government Printing Office, 50 p.

Cross, T.A., 1986, Tectonic Controls of Foreland Basin Subsidence and Laramide Style Deformation, Western United States - Foreland Basins - Wiley Online Library:, https://onlinelibrary.wiley.com/doi/abs/10.1002/9781444303810.ch1 (accessed September 2019).

DeCelles, P.G., 2004, Late Jurassic to Eocene evolution of the Cordilleran thrust belt and foreland basin system, western U.S.A.: American Journal of Science, v. 304, p. 105–168, doi:10.2475/ajs.304.2.105.

DeCelles, P.G., and Currie, B.S., 1996, Long-term sediment accumulation in the Middle Jurassic–early Eocene Cordilleran retroarc foreland-basin system: Geology, v. 24, p. 591, doi:10.1130/0091-7613(1996)024<0591:LTSAIT>2.3.CO;2.

DeCelles, P.G., Lawton, T.F., and Mitra, G., 1995, Thrust timing, growth of structural culminations, and synorogenic sedimentation in the type Sevier orogenic belt, western United States: Geology, v. 23, p. 699, doi:10.1130/0091-7613(1995)023<0699:TTGOSC>2.3.CO;2.

Dickinson, W.R., and Gehrels, G.E., 2008, Sediment delivery to the Cordilleran foreland basin: Insights from U-Pb ages of detrital zircons in Upper Jurassic and Cretaceous strata of the

Colorado Plateau: American Journal of Science, v. 308, p. 1041–1082, doi:10.2475/10.2008.01.

Dickinson, W.R., and Lawton, T.F., 2003, Sequential intercontinental suturing as the ultimate control for Pennsylvanian Ancestral Rocky Mountains deformation: Geology, v. 31, p. 609–612, doi:10.1130/0091-7613(2003)031<0609:SISATU>2.0.CO;2.

Dickinson, W.R., and Lawton, T.F., 2001, Tectonic setting and sandstone petrofacies of the Bisbee basin(USA–Mexico): Journal of South American Earth Sciences, v. 14, p. 475–504, doi:10.1016/S0895-9811(01)00046-3.

Elston, D., and Landis, E., 1960, Pre-Cutler unconformities and early growth of the Paradox Valley and Gypsum Valley salt anticlines, Colorado, *in* Short papers in the geological sciences: US Geol. Survey Prof. Paper 400B, p. B261–B265.

Escosa, F.O., Rowan, M.G., Giles, K.A., Deatrick, K.T., Mast, A.M., Langford, R.P., Hearon, T.E., and Roca, E., 2018, Lateral terminations of salt walls and megaflaps: An example from Gypsum Valley Diapir, Paradox Basin, Colorado, USA: Basin Research, doi:10.1111/bre.12316.

Ge, H., Jackson, M.P.A., and Vendeville, and B.C., 1997, Kinematics and Dynamics of Salt Tectonics Driven by Progradation: AAPG Bulletin, v. 81, p. 398–423.

Hazel, J.E., 1994, Sedimentary response to intrabasinal salt tectonism in the Upper Triassic Chinle Formation: US Geological Survey Bulletin 2000-F, 30 p.

Heller, P.L., Bowdler, S.S., Chambers, H.P., Coogan, J.C., Hagen, E.S., Shuster, M.W., Winslow, N.S., and Lawton, T.F., 1986, Time of initial thrusting in the Sevier orogenic belt, Idaho-Wyoming and Utah: Geology, v. 14, p. 388, doi:10.1130/0091-7613(1986)14<388:TOITIT>2.0.CO;2.

Heller, P.L., and Paola, C., 1989, The paradox of Lower Cretaceous gravels and the initiation of thrusting in the Sevier orogenic belt, United States Western Interior: GSA Bulletin, v. 101, p. 864–875, doi:10.1130/0016-7606(1989)101<0864:TPOLCG>2.3.CO;2.

Hite, R.J., and Buckner, D.H., 1981, Stratigraphic Correlations, Facies Concepts, and Cyclicity in Pennsylvanian Rocks of the Paradox Basin: , p. 13.

Kjemperud, A.V., Schomacker, E.R., and Cross, T.A., 2008, Architecture and stratigraphy of alluvial deposits, Morrison Formation (Upper Jurassic), Utah: AAPG Bulletin, v. 92, p. 1055–1076, doi:10.1306/03250807115.

Landis, E.R., Shoemaker, E.M., and Elston, D.P., 1961, Early and late growth of the Gypsum Valley salt anticline, San Miguel County, Colorado: Short papers in the geologic and hydrologic sciences: US Geol. Survey Prof. Paper, p. C131–136.

Langford, R., Giles, K.A., Thompson, J.A., and Rowan, M.G., 2018, Shoulder Formation in the Paradox Basin: A Record of Progressive Diapir Narrowing and Minibasin Expansion,

http://www.searchanddiscovery.com/abstracts/html/2018/ace2018/abstracts/2855342.html (accessed June 2019).

Lawton, T.F., and Buck, B.J., 2006, Implications of diapir-derived detritus and gypsic paleosols in Lower Triassic strata near the Castle Valley salt wall, Paradox Basin, Utah: Geology, v. 34, p. 885–888.

Lawton, T.F., González-León, C.M., Lucas, S.G., and Scott, R.W., 2004, Stratigraphy and sedimentology of the upper Aptian–upper Albian Mural Limestone (Bisbee Group) in northern Sonora, Mexic: Cretaceous Research, v. 25, p. 43–60, doi:10.1016/j.cretres.2003.09.003.

Matthews, W.J., Hampson, G.J., Trudgill, B.D., and Underhill, J.R., 2007, Controls on fluviolacustrine reservoir distribution and architecture in passive salt-diapir provinces: Insights from outcrop analogs: AAPG bulletin, v. 91, p. 1367–1403.

Mullens, T.E., and Freeman, V.L., 1957, Lithofacies of the Salt Wash Member of the Morrison Formation, Colorado Plateau: Geological Society of America Bulletin, v. 68, p. 505–526, doi:10.1130/0016-7606(1957)68[505:LOTSWM]2.0.CO;2.

Owen, A., Jupp, P.E., Nichols, G.J., Hartley, A.J., Weissmann, G.S., and Sadykova, D., 2015a, Statistical Estimation of the Position of An Apex: Application To the Geological Record: Journal of Sedimentary Research, v. 85, p. 142–152, doi:10.2110/jsr.2015.16.

Owen, A., Nichols, G.J., Hartley, A.J., and Weissmann, G.S., 2015b, Vertical trends within the prograding Salt Wash distributive fluvial system, SW USA: Basin Research, p. n/a-n/a, doi:10.1111/bre.12165.

Owen, A., Nichols, G.J., Hartley, A.J., Weissmann, G.S., and Scuderi, L.A., 2015c, Quantification of a Distributive Fluvial System: The Salt Wash DFS of the Morrison Formation, SW U.S.A.: Journal of Sedimentary Research, v. 85, p. 544–561, doi:10.2110/jsr.2015.35.

Peterson, F., 1984, Fluvial sedimentation on a quivering craton: Influence of slight crustal movements on fluvial processes, upper Jurassic Morrison formation, western Colorado plateau: Sedimentary Geology, v. 38, p. 21–49, doi:10.1016/0037-0738(84)90073-3.

Prochnow, S.J., Atchley, S.C., Boucher, T.E., Nordt, L.C., and Hudec, M.R., 2006, The influence of salt withdrawal subsidence on palaeosol maturity and cyclic fluvial deposition in the Upper Triassic Chinle Formation: Castle Valley, Utah: Sedimentology, v. 53, p. 1319–1345.

Ronson, R.B., 2018, Facies Changes Associated with Formation of an Extensive Salt Shoulder by the Coastal and Eolian Carmel and Entrada Formations, Gypsum Valley, Colorado [M.S.]: The University of Texas at El Paso, 142 p., https://search.proquest.com/docview/2111273760/abstract/B4ECC5C697AE4A86PQ/1 (accessed June 2019).

Rowan, M.G., Giles, K.A., Hearon IV, T.E., and Fiduk, J.C., 2016, Megaflaps adjacent to salt diapirs: AAPG Bulletin, v. 100, p. 1723–1747, doi:10.1306/05241616009.

Shawe, D.R., 1968a, Geological investigations in the Slick Rock district, San Miguel and Dolores Counties, Colorado: G.P.O.

Shawe, D.R., 1968b, Petrography of sedimentary rocks in the Slick Rock district, San Miguel and Dolores Counties, Colorado: U.S. Geol. Survey Prof. Paper 576-B, 34 p.

Shoemaker, E.M., Case, J.E., and Elston, D.P., 1958, Salt Anticlines of the Paradox Basin, *in* Guidebook to the Geology of the Paradox Basin, Ninth Annual Field Conference, Utah Geological Survey, p. 39–59, http://archives.datapages.com/data/uga/data/008/008001/39_ugs80039.htm (accessed November 2017).

Stokes, W.L., 1944, Morrison formation and related deposits in and adjacent to the Colorado Plateau: Geological Society of America Bulletin, v. 55, p. 951–992, doi:10.1130/GSAB-55-951.

Stokes, W.L., and Phoenix, D.A., 1948, Geology of the Egnar-Gypsum Valley area, San Miguel and Montrose Counties, Colorado: US Geological Survey Oil and Gas Investigations Map OM-93.

Trudgill, B.D., 2011, Evolution of salt structures in the northern Paradox Basin: controls on evaporite deposition, salt wall growth and supra-salt stratigraphic architecture: Basin Research, v. 23, p. 208–238, doi:10.1111/j.1365-2117.2010.00478.x.

Turner, C.E., and Peterson, F., 2004, Reconstruction of the Upper Jurassic Morrison Formation extinct ecosystem—a synthesis: Sedimentary Geology, v. 167, p. 309–355, doi:10.1016/j.sedgeo.2004.01.009.

Tyler, N., and Ethridge, F.G., 1983, Depositional setting of the Salt Wash Member of the Morrison Formation, Southwest Colorado: Journal of Sedimentary Research, v. 53, p. 67–82, doi:10.1306/212F8157-2B24-11D7-8648000102C1865D.

Venus, J.H., Mountney, N.P., and McCaffrey, W.D., 2015, Syn-sedimentary salt diapirism as a control on fluvial-system evolution: an example from the proximal Permian Cutler Group, SE Utah, USA: Basin Research, v. 27, p. 152–182, doi:10.1111/bre.12066.

Vogel, J.D., 1960, Geology and ore deposits of the Klondike Ridge area, Colorado: U.S. Geological Survey], Open-File Report USGS Numbered Series 60–145, http://pubs.er.usgs.gov/publication/ofr60145 (accessed February 2019).

Weissmann, G.S., Hartley, A.J., Nichols, G.J., Scuderi, L.A., Olson, M., Buehler, H., and Banteah, R., 2010, Fluvial form in modern continental sedimentary basins: Distributive fluvial systems: Geology, v. 38, p. 39–42, doi:10.1130/G30242.1.

Yingling, V.L., and Heller, P.L., 1992, Timing and record of foreland sedimentation during the initiation of the Sevier orogenic belt in central Utah: Basin Research, v. 4, p. 279–290, doi:10.1111/j.1365-2117.1992.tb00049.x.

Chapter 5: Conclusions

Exposures of the Salt Wash Member of the Morrison Formation and its interaction with the Gypsum Valley Salt Diapir exhibit variations in stacking patterns and fluvial architecture related to variations in diapir rise or subsidence, and to changes in rates of deposition.

1. Fluvial systems of the Salt Wash Member were influenced by movement of the Gypsum Valley Salt Diapir. This observation is supported by changes in thickness, sandstone content, stacking patterns, and paleoflow in each of the stratigraphic units identified in the Salt Wash Member of the Morrison Formation.
    a. Halokinetic subsidence or uplift of salt resulted in either: 1) non-deposition, thinning, or thickening of the unit, 2) removal by erosion truncation or onlap, or 3) facies changes. These relationships are seen within each of the Salt Wash Member stratigraphic units.
    b. In Little Gypsum Valley, paleoflow of the Salt Wash Member is dominantly into the diapir. Throughout deposition of the Salt Wash Member, rapid rates of subsidence in synclines on the crest of the diapir and little associated minibasin subsidence resulted in muddy thickened sections of most of the units of the Salt Wash Member. Subsidence within Little Gypsum Valley is interpreted to be caused by 1) Radial faults that are inactive during Salt Wash deposition, 2) no input of salt from the adjacent Dry Creek and Disappointment minibasins, and 3) dissolution of salt.
    c. In Big Gypsum Valley, paleoflow of the Salt Wash Member were diverted parallel and into the diapir margin. Thinner packages sandstone was deposited along and across the diapir as diapiric rise and subsidence of the Dry Creek and

Disappointment mini basins continued during Salt Wash Member deposition. Continued rise of salt in Big Gypsum Valley during the deposition of the Salt Wash Member is interpreted to be due to 1) radial faults that continued to be active into the Cretaceous and 2) subsidence of the adjacent minibasins that continued to be a source of deep salt for diapir movement.

d. Tapered composite halokinetic sequence boundaries described in the ASC and ISC are evidence of wedge style halokinetic sequences. This suggests that within Big Gypsum Valley overall sediment accumulation rate adjacent to the diapir exceeded diapir rise rate allowing for Salt Wash Member sedimentation to keep up with local accommodation and deposit sediment on top of the diapir when topography is low enough. When the diapir forms a slightly higher topography it becomes a zone of bypass or erosion.

2. The diagenesis of the Salt Wash Member sandstones of the Morrison Formation within Gypsum Valley is a model for understanding how near-salt fluid circulation can modify porosity and permeability of hydrocarbon conduits.

    a. The paragenetic sequence of events is as follows: 1) precipitation of early ferroan dolomite cements, 2) growth of quartz overgrowths filling pore space, 3) compaction, 4) dissolution of early dolomite cements, feldspar, and chert grains forming secondary porosity and enlarged pores, 5) precipitation of calcite and in lesser amounts ferroan calcite that fills secondary pores and fills dissolved grains.

    b. There is no variation in cementation between the different stratigraphic units of the Salt Wash Member.

c. In Big Gypsum Valley higher amounts of ferroan dolomite and dolomite cements are present and are associated with the proximity to major structures, such as radial faults, and the Megaflap on the southwestern margin.

d. Near diapir fluid flow of saline fluids generated from halite dissolution with meteoric water create, enhance, and maintain secondary porosity in the Salt Wash Member that ranges between 28%-62%. Highlighting the importance of this process is to understand the emplacement of hydrocarbon migration conduits.

3. A thickened section of the Salt Wash Member of the Morrison Formation was deposited syndepositionally on the crest of the Little Gypsum Valley diapir forming 'The Hat' syncline.

    a. Subsidence began just after the first fluvial channels of the ASC unit of the Salt Wash Member were deposited.

    b. Relatively slow subsidence of the structure continued as a result of decreased input of salt from Disappointment and Dry Creek minibasins and/or deep dissolution of salt.

    c. Subsidence resulted in the increased thickness of the Salt Wash Member due to an increase in floodplain facies within the ISC and LSSC.

    d. Four growth sequences separated by 3 growth sequence boundaries were identified and mapped across the structure. These boundaries represent periods of subsidence and erosion and they do not follow along stratigraphic unit boundaries. Low rates of deposition are marked by growth sequence boundaries and thickening into the syncline. Higher rates of deposition and slower subsidence are marked by continuous sandstone beds that extend across the syncline.

e. The deposition of the Salt Wash Member on top of the Little Gypsum Valley Salt diapir does not follow the patterns of fluvial interaction with diapirs described in previous studies because channels are not restricted to adjacent minibasins.

Implications

The results from this study contribute to a body of work done by many authors to try and understand the controls on fluvial deposition as it interacts with salt diapirs. This study shows that the interactions between deposition and deformation is not simple and not restricted to minibasins adjacent to salt walls. Fluvial systems deposit a significant amount of sandstone on top of and along the margin of salt walls given that there is accumulation space available for those sandstones to be preserved. Salt movement is complex and not uniform across the top of a salt wall. Salt movement can produce local topographic lows in one part of the salt wall that create accumulation space and topographic highs that can become barriers to flow in a different area. Changes in salt movement can also vary with time and during the deposition of a stratigraphic unit.

The dynamic between deposition and deformation has been described in many different salt basins including the Gulf of Mexico and the North Sea, where there is exploration for oil by petroleum companies. A better understanding of fluvial deposition around salt can lead to better prediction of reservoir distribution and the placement of the other components of the hydrocarbon system (source, migration pathways, trap, and seal) around salt. This is especially important when the basin being studied is not available in outcrop and is being analyzed in the subsurface via seismic data sets. Outcrop analogs like this one allow for better prediction of fluvial patterns and pathways and can give insight to what might be happening below seismic resolution or up against the diapir margin which is traditionally hard to resolve seismically. This

study also contributes to the understanding of the quality of the reservoir deposited around salt diapirs by understanding fluid migration pathways and how that may change the quality of the sandstones that are the reservoir.

Future Work

This work can be continued in the future by conducting more detailed descriptions of deformed areas and by comparing the relationship of other fluvial systems that interact closely with salt diapirs. Documenting the depositional patterns of fluvial systems that fill accommodation space created locally on top of and on the margins of the diapir. What kinds of patterns are similar or different? What do the distribution of sandstones on the diapir margin look like and are the same kinds of patterns of erosion and truncation present with uplift? Are there also growth sequences with deposition over a diapir with continued subsidence and varying rates of deposition?

Appendix

Point Count Data

Sample	Section	Stratigraphic Unit	Distance from GV Axis	Grains	Quartz	Microcrystalline Quartz	Polycrystalline Quartz	Chalcedony	K-Spar	Plagioclase Feldspar	Feldspar Altered	Muscovite	Biotite	Tourmaline	Zircon	Opaque	Glauconite	Lithics	Calcite	Dolomite	Chert	Chert, Altered?	Coarse Grained cherty li	Igneous Rx Frag.	Metamorphic Rx. Frag.	Sed Rx Frag.	Shale	Clay Clast	Ferroan Calcite grain	organic grain?	Siltstone	Hematite Clasts	siltstone with iron oxide	Silty w/ fossils	Dino Bone	Cements	Calcite	Ferroan Dolomite	Dolomite	Qtz Overgrowths	Carbonate cmnt?	Carbonate mud	Hematite Cemnt?	Ferroan Calcite	clay Cement	Filled Fracture	Pyrite Framboids/iron ox	Porosity	Intergranular	Dissolved grain &	Dissolved grains with Ox	Pore Space	TOTAL
BGH-1-18	BGH-1		Distal		205		3	2	1	1											6		2														12			17									17	22				300
BGH-2-18	BGH-1		Distal		196		4		3												3		1					1			1						9	1		18							1		6	54				300
BGH-3-18	BGH-1		Distal		199		5		2			1				1					3				1		1										2					75					2	9		1		302
BGH-4-18	BGH-1		Distal		211		1		5							1					4					1			3	1						14	7	1	22			1	1					12	15				300
BGH-5-18	BGH-1		Distal		223		3		5												2																15	2	1	30			1	3					5	10				300
BGH-6-18	BGH-1		Distal		194		3		1	1											3										1					78	1		2				1					6	6		3		300
BGH-8-18	BGH-1		Distal		179				1	1						1					3																	88		1			1	3					2	20				300
BGH-9-18	BGH-1		Distal																																																		
BGH-10-18	BGH-1		Distal																																																		
BGH-11-18	BGH-1		Distal																																																		
BGH-12-18	BGH-1		Distal																																																		
BGH-13-18	BGH-1		Distal	Carbonate mud																																																
BGV-10-18			Proximal		188				3	2											5								2							14			23			5						19	39				300
BGV-2-17	BGV-1	2	Proximal		162		4		5	1				1							4								3									42	27									20	31				300
BGV-3-18	BGV-1	2	Proximal		172		2	1	2	1																			1									90	20									3	8				300
BGV-4-17	BGV-1	2	Proximal		187		3		4	1							1				5		3															34	34					2				6	20				300
BGV-6-17	BGV-1	3	Proximal		181		3		5												8		3					1	11		6			1					34									16	31				300
BGV-12-18	BGV-1	4	Proximal																																																		
BGV-7-18	BGV-2	3	Proximal		184		3	2	2	1											13								7							1		4	61			2						7	13				300
BGV-8-18	BGV-2	3	Proximal		194		1	1	3	1									1		3								4									25										26	40	1			301
BGV-9-18	BGV-2	3	Proximal		187		3		2										4		5		1				13		1				2					26										12	45				304
BGV-11-18	BGV-2	4	Proximal		148		11		19	7	4								10	5	4			3											31		5	22			17	1					9	4				300
GH-26-17					179		8		4	1						1					2			1	3	4										9			36									41	11				300
GH-1-17	GH-5	2	Proximal		188		1		1	2											11																1		51	9					1				10	25				300
GH-3-17	GH-5	3	Proximal		184		1	1	3	1											7		1		1				12								18			29				4					6	32				300
GH-4-17	GH-5	4	Proximal		205		1	1											1		8		1				1		3								5			35									9	30				300
GH-6-17	GH-4	1	Proximal		182		1		2	4											2		2														6		70				3					5	21	2			300
GH-7-17	GH-4	1	Proximal		218		1	1																			1										48			30			1										300
GH-9-17	GH-4	2	Proximal		164		1	3	7	5	1										7		1						3			3					55			42			1	4					3				300
GH-11-17	GH-4	3	Proximal		196		3	2	3	2									2		3																25		17	8									8	24	7			300
GH-14-17	GH-4	4	Proximal		195		1	1		1							1				5		1						9								9			28									7	41	1			300
GH-16-17	GH-4	4	Proximal		184		5		1												7		3						1			1					15			39			1						23	14	6			300
GH-17-17	GH-4	4	Proximal		153		7	2	1	2											14	1	8	1	1		2		9		1						57		4		6		1					5		23	300
GH-18-17	GH-1	1	Proximal		206		3		6											8	3		1						1									13	18									6	28	7			300
HM-10-17	HM-3	3	Proximal		185		1			1											4								1								13		4	20			2						21	48				300
HM-12-17	HM-3	4	Proximal		185		2		1												7		4				1		9								17			20									25	29				300
HM-20-17	HM-5	2	Proximal		190		1		1												5		6						8								9			33									13	34				300
HM-21-17	HM-5	3	Proximal		193				1	2											5		1				1		3											29									14	51				300
HM-24-18	HM-6	2	Distal		198		7														4		1		1			1	6								11			24									16	30	1			300
HM-25-18	HM-6	2	Distal		208		3			1					1	2					3						2		2								28			46			2	1			1						300
HM-26-18	HM-6	2	Distal		207		2					1															3		2								27			20			1						14	23				300
HM-27-18	HM-6	3	Distal		136		5		1												3		2				1	3	5								139			1					3				1						300
HM-28-18	HM-6	3	Distal		178		6		2	1		1									7		3					1	22								9	2		19			2	38	3				6				300
HM-29-18	HM-6	3	Distal		188		7		1	1											1							1	4								3		1	45			1	6					15	27				300
HM-30-18	HM-6	3	Distal		174		6		2	2											6		3		1				18								4			23				2	1				14	42	2			300
HM-31-18	HM-6	4	Distal		199		6	3	1			1									5		1				3		4								2			43									12	19	1			300
HM-32-18	HM-6	4	Distal		157		7	2	1	1											24		11				1		25								12			28				2					6	23				300
HM-33-18	HM-6	4	Distal		180		3	1	2						1						1								2								66			6								36	1	1			300
HM-34-18	HM-6	4	Distal		217		5		1	2		1																	1											10			1					2	12	48				300
HM-35-18	HM-7	2	Distal		206		1		1	1													1				1		1	1							1	2	1	25			1	16					13	28				300
HM-36-18	HM-7	2	Distal		202				1												3						1		2	2										46			2						3	37	1			300
HM-37-18	HM-7	2	Distal		199		4		4												4						3		1								8		1	10			1						14	51				300
HM-38-18	HM-7	3	Distal		192		6		1												3						1		10								74		1	5			2						1	4				300
HM-39-18	HM-7	3	Distal		197		10		1												4						1		2	3										20			1						12	49				300
HM-40-18	HM-7	4	Distal		192		4	2	1	1											5		1				1		14		1						13			11		1		9					13	31				300
HM-41-18	HM-7	4	Distal		180		7		5												3						1	2	2								9			23			8	2					3	55				300
HM-4-17	HM-2	3	Proximal		151		3		1																				1								120			3									12	6	3			300
HM-5-17	HM-2	3	Proximal		170		4		2												8		1					2	3								9		16	28									13	43	1			300
HM-6-17	HM-2	3	Proximal		215		3								1						7						2										1			18									26	24	3			300
HM-7-17	HM-2	4	Proximal		174		4		2												4		6					1	1								39			44									5	20				300
HT-2-17	HT-3	2	Top		171		4	2	3	5											5		6				1		1								6			24				36	1				28	7				300
HT-6-17	HT-3	2	Top		195		3														7		1					1	6		5						3			13									12	54				300
HT-7-17	HT-3	3	Top		189				3												3						1	6	47		8						6			20				4					12	1				300
HT-8-17	HT-3	3	Top		181		3		1											2	3							2	4		1									38									17	48				300
HT-10-17	HT-3	3	Top		188				3	1											5			1			3				4						51			20				13					9	1	1			300
HT-11-17	HT-3	4	Top		197		3	1	4												5										8						20			11									9	39	3			300
HT-12-17	HT-3	4	Top		206				5	1						1					6		1								11						2		3	1									7	55	1			300
HT-20-17	HT-4	3	Top		182		1	1	3	2			1	1		1					9							4		1							56								35			3				300
HT-23-17	HT-4	4	Top		189																6			3			2		5							31			45			2						1	16				300
MF-11-18	MF-2	2	Proximal		176		4		3												6		1														40			1	23									30	14	2			300
MF-1-18			Proximal	Carbonate mud																																																	0
MF-2-18	MF-1	2	Proximal		194		7	1		1											10		1						6								15		1	32				9					6	15	2			300
MF-3-18	MF-1	2	Proximal	Carbonate mud																																																0
MF-4-18	MF-1	2	Proximal		157		5		1			1									1								1								117			2			2	1	1				10	1				300
MF-5-18	MF-1	3	Proximal		193		5		3	2											1																20		2	38			1	12					14	8	1			300
MF-6-18	MF-1	3	Proximal		197		10		2												4								4								11			1	30			2						19	20				300
MF-7-18	MF-1	3	Proximal		184		9		3	2				1							6		1	1			1		3											62	14			2					2	6	3			300
MF-8-18	MF-1	3	Proximal		204		7		1												5				1												1			7	35									6	32	1			300
MF-9-18	MF-1	3	Proximal		211		8					1									4		1				2		1								9			37									8	16	2			300
MF-10-18	MF-1	3	Proximal		199		2		6												13				1				8								10			31									11	19				300

Stratigraphic Sections

Measured Section 1: Big Gypsum Valley (pg. 1)

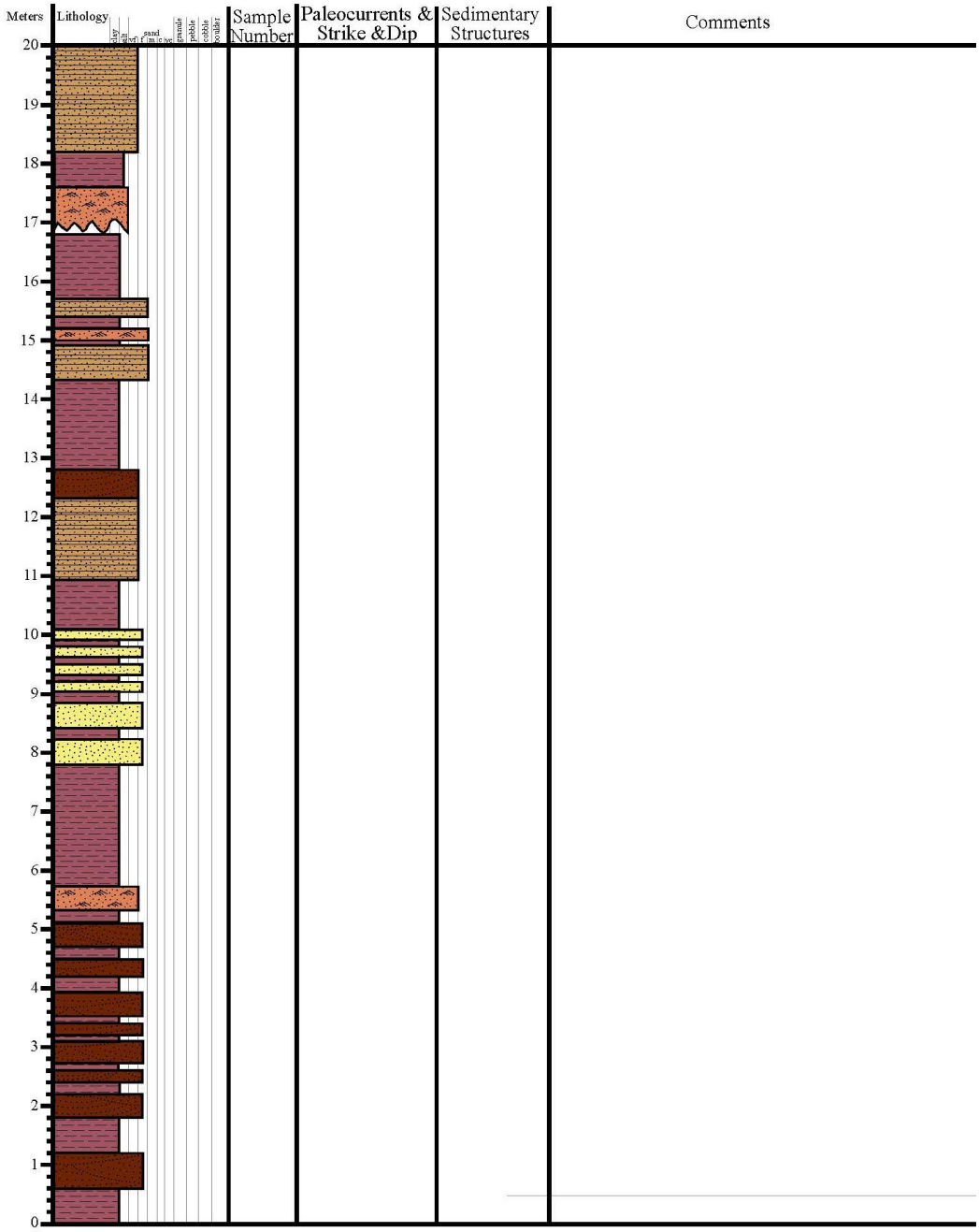

Measured Section 1: Big Gypsum Valley (pg. 2)

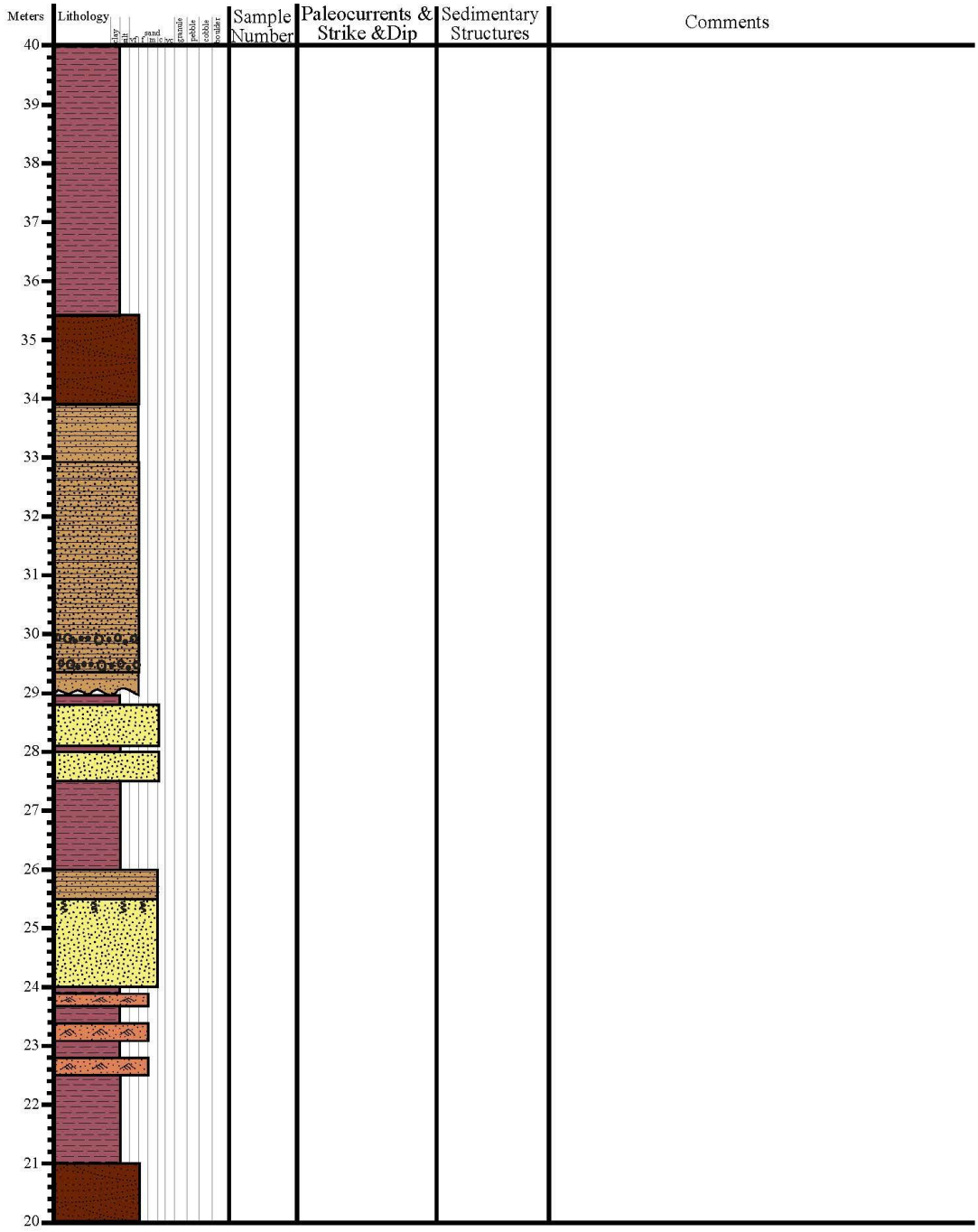

Measured Section 1: Big Gypsum Valley (pg. 3)

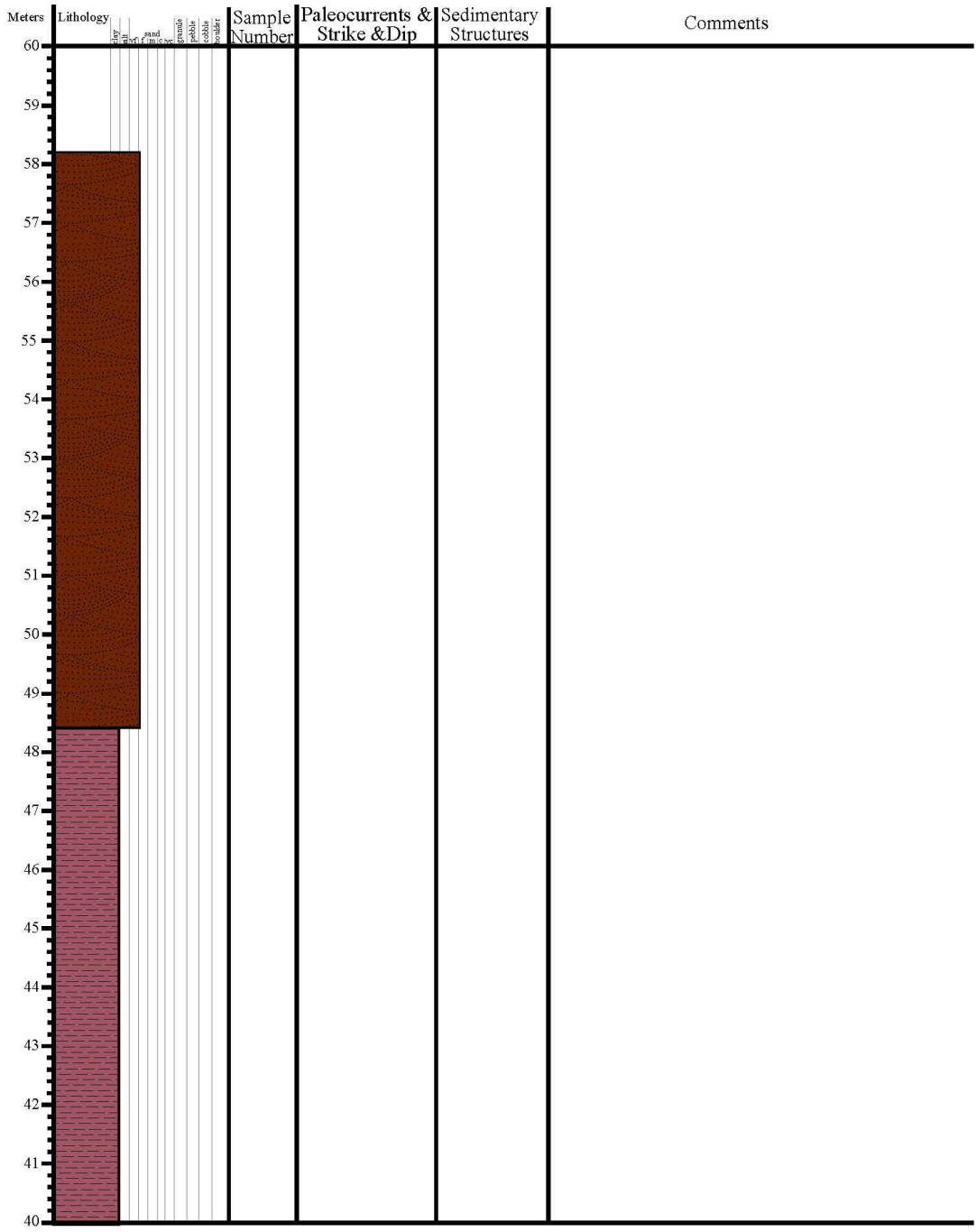

Measured Section 2: Big Gypsum Valley (pg. 1)

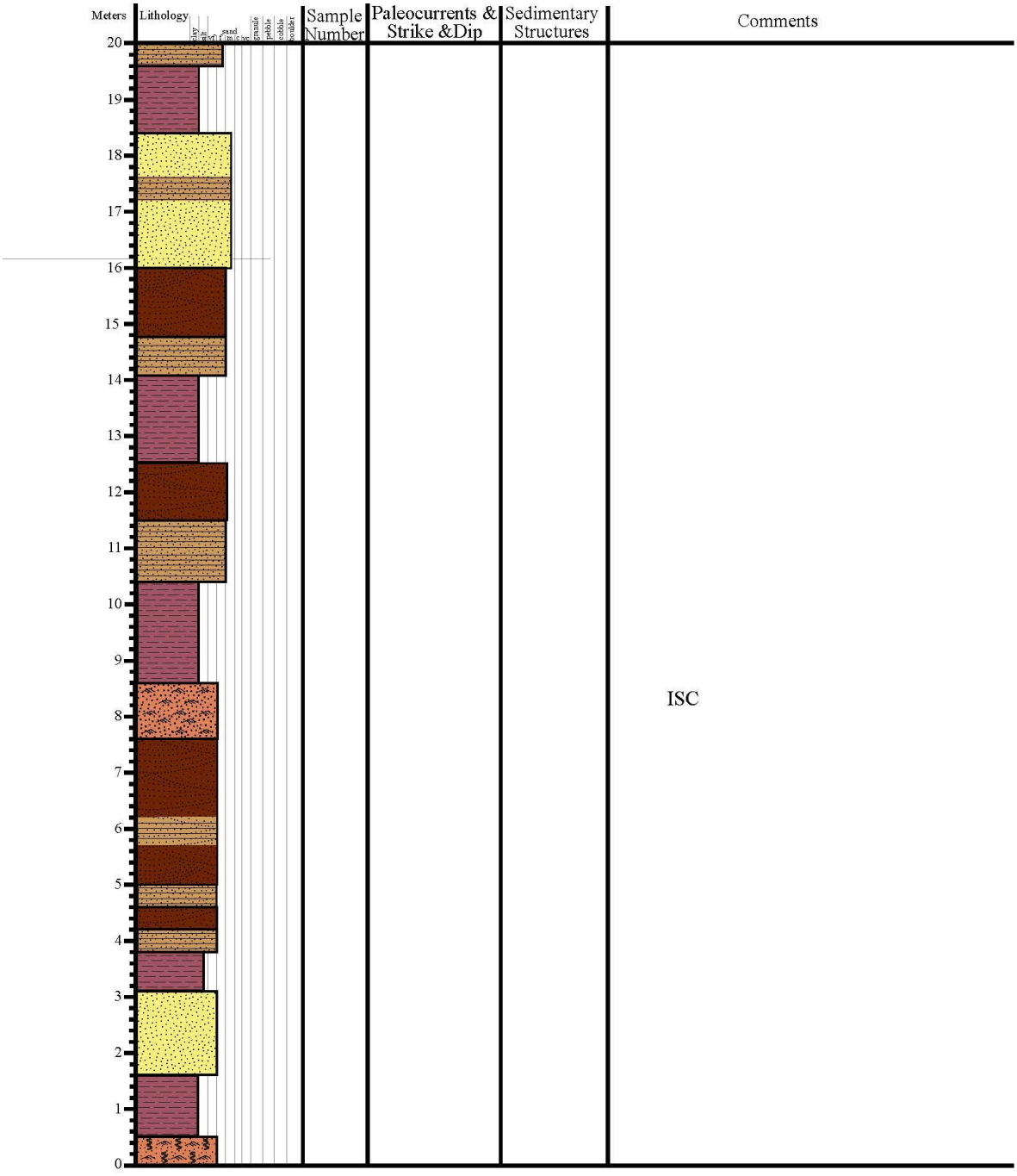

Measured Section 2: Big Gypsum Valley (pg. 2)

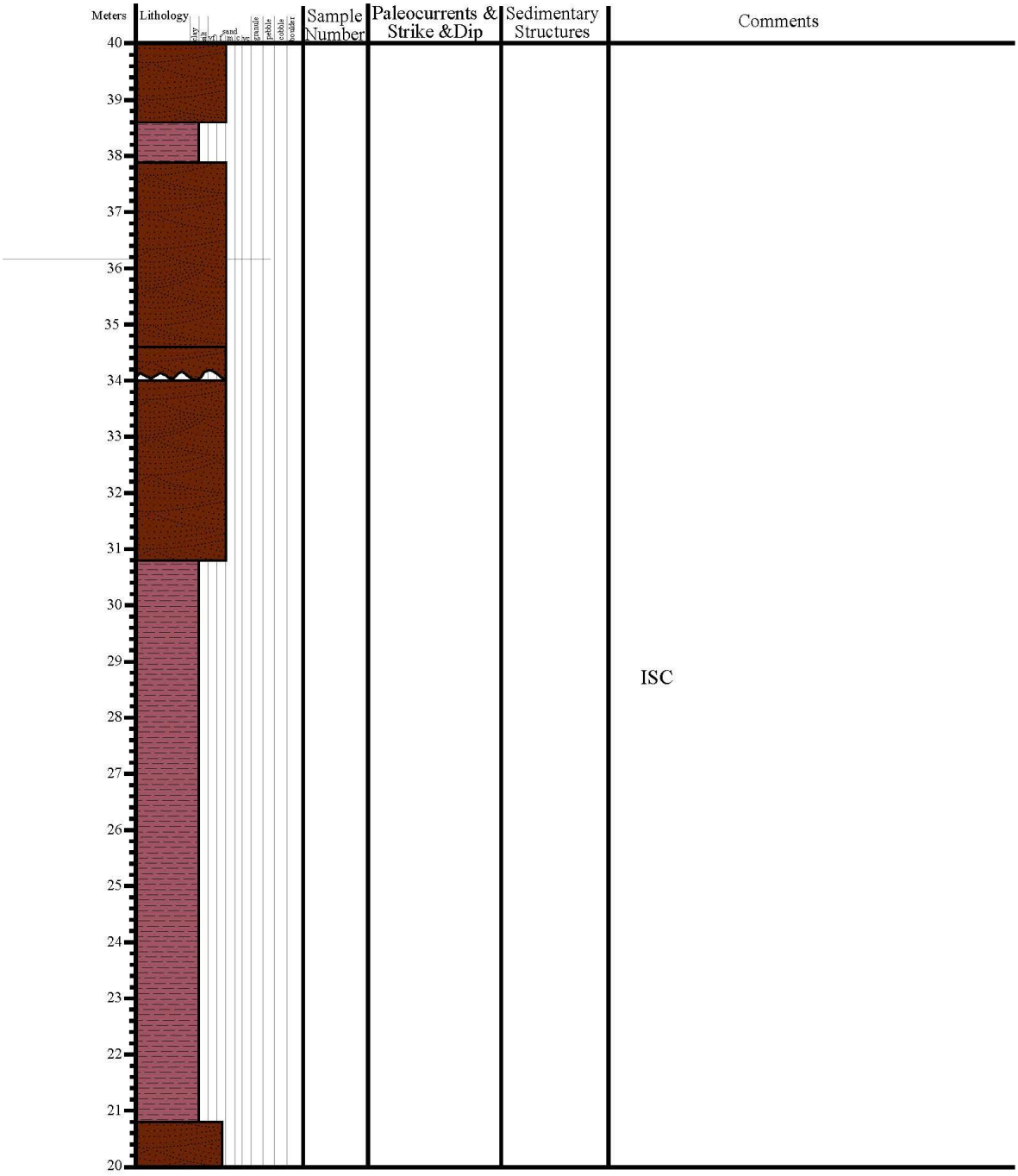

Measured Section 2: Big Gypsum Valley (pg. 3)

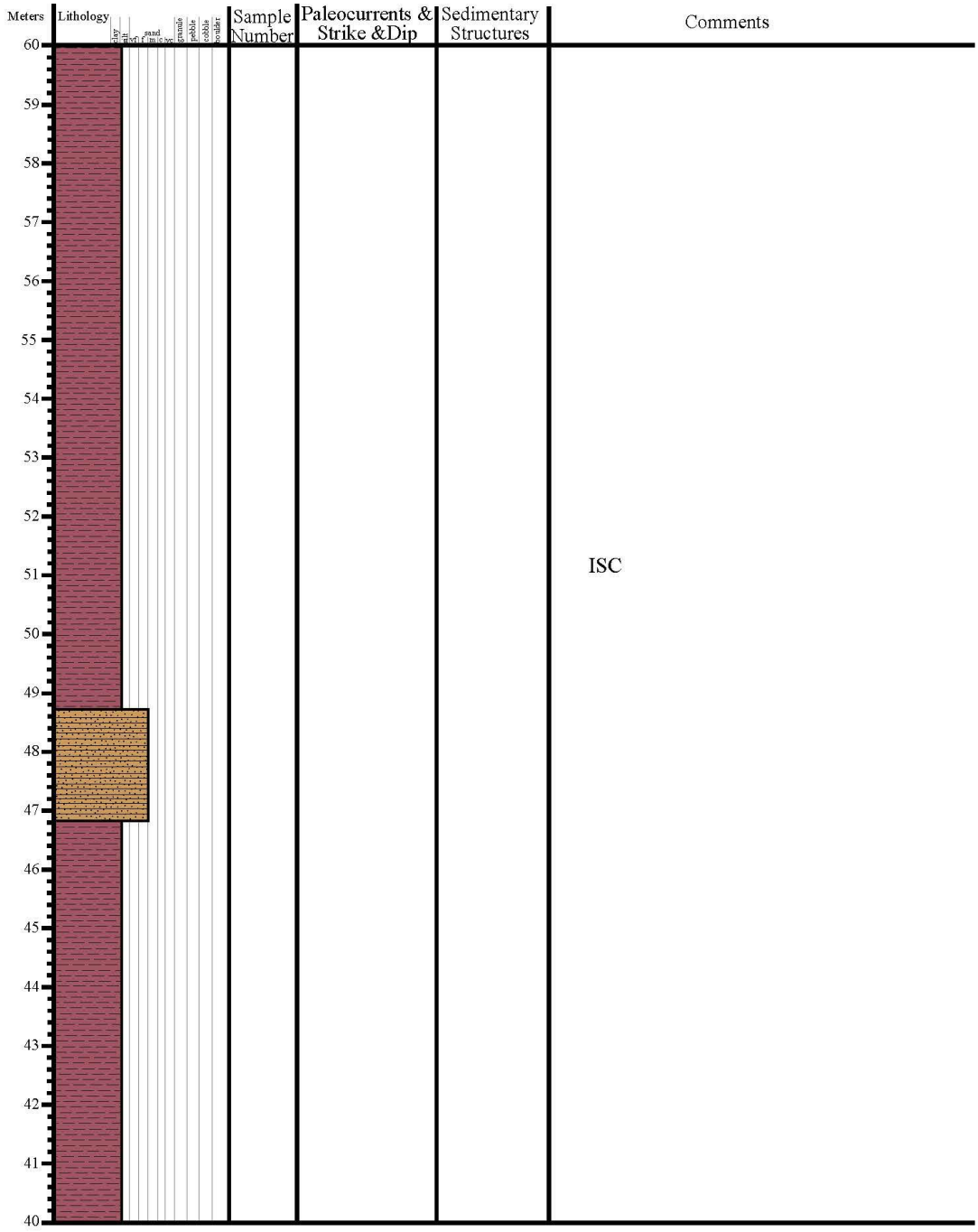

Measured Section 2: Big Gypsum Valley (pg. 4)

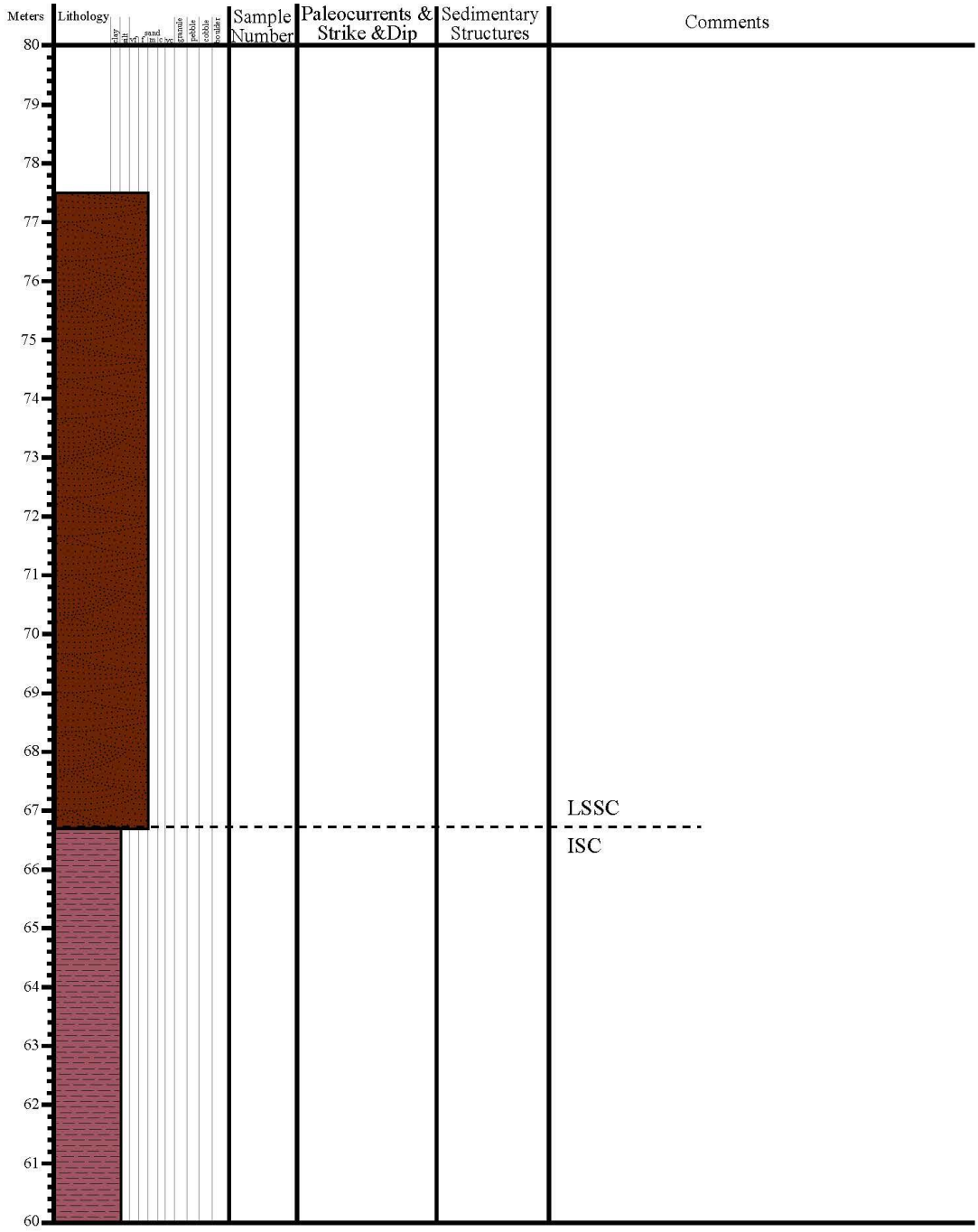

Measured Section 1: Grassy Hill (pg. 1)

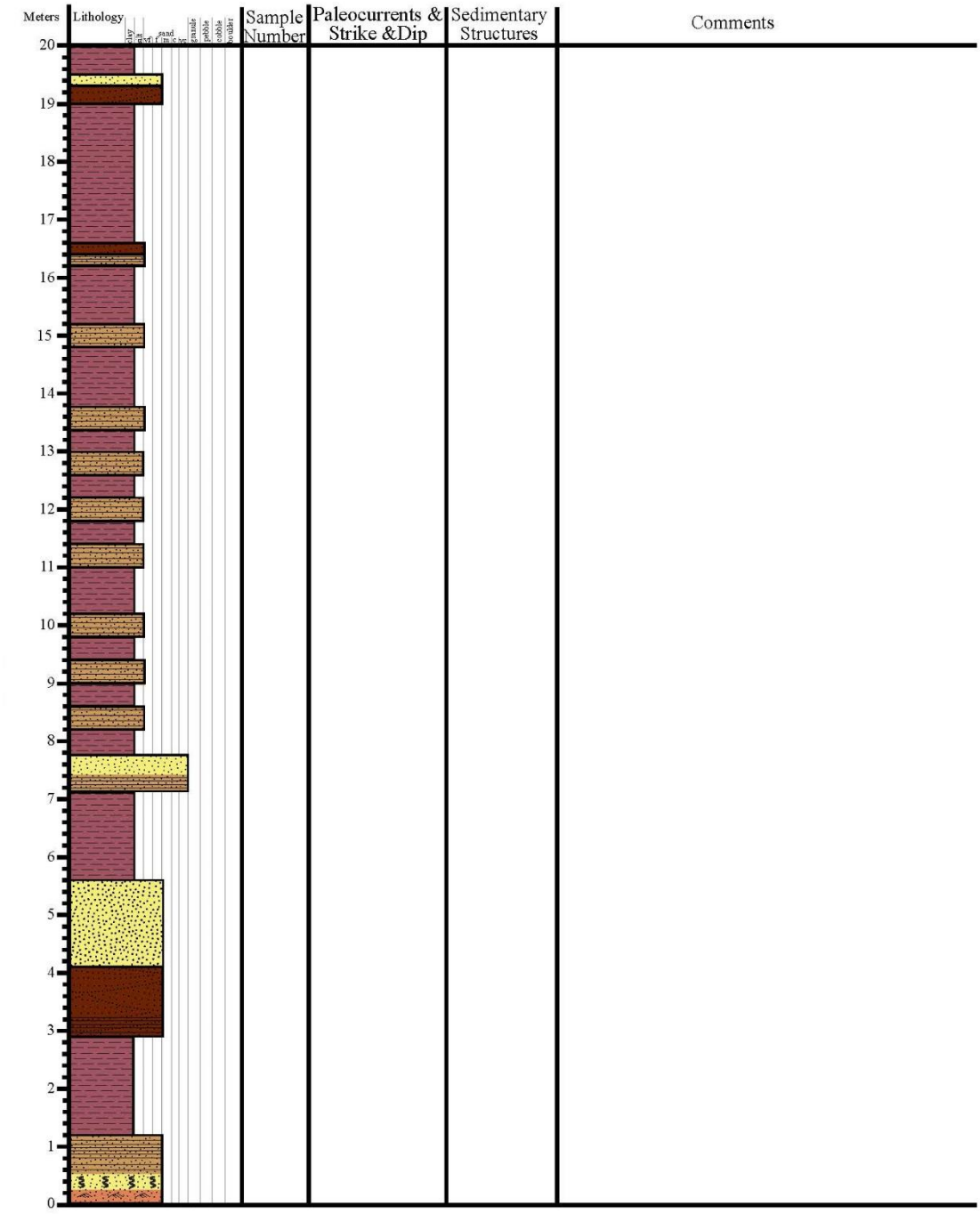

Measured Section 1: Grassy Hill (pg. 2)

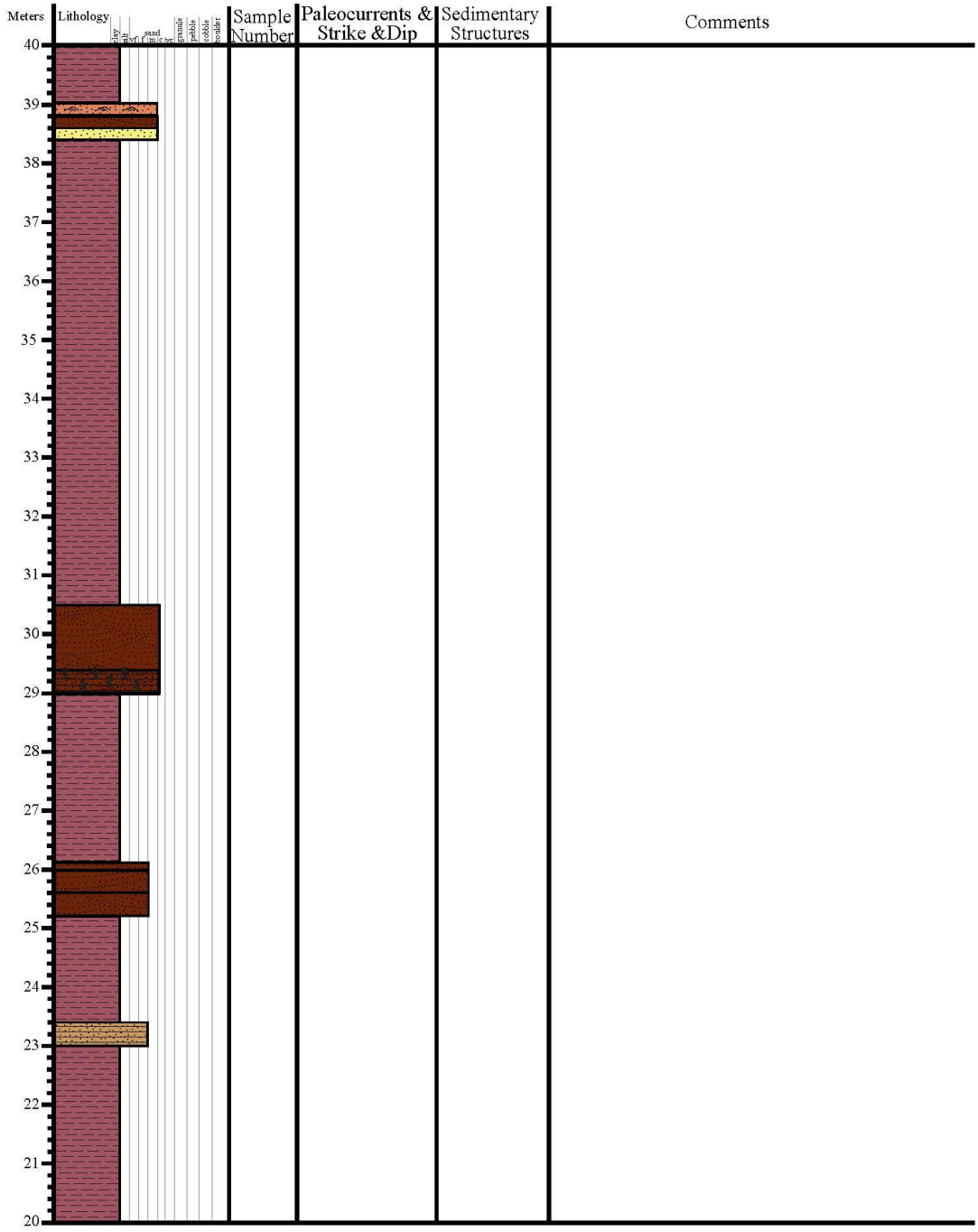

Measured Section 1:Grassy Hill (pg. 3)

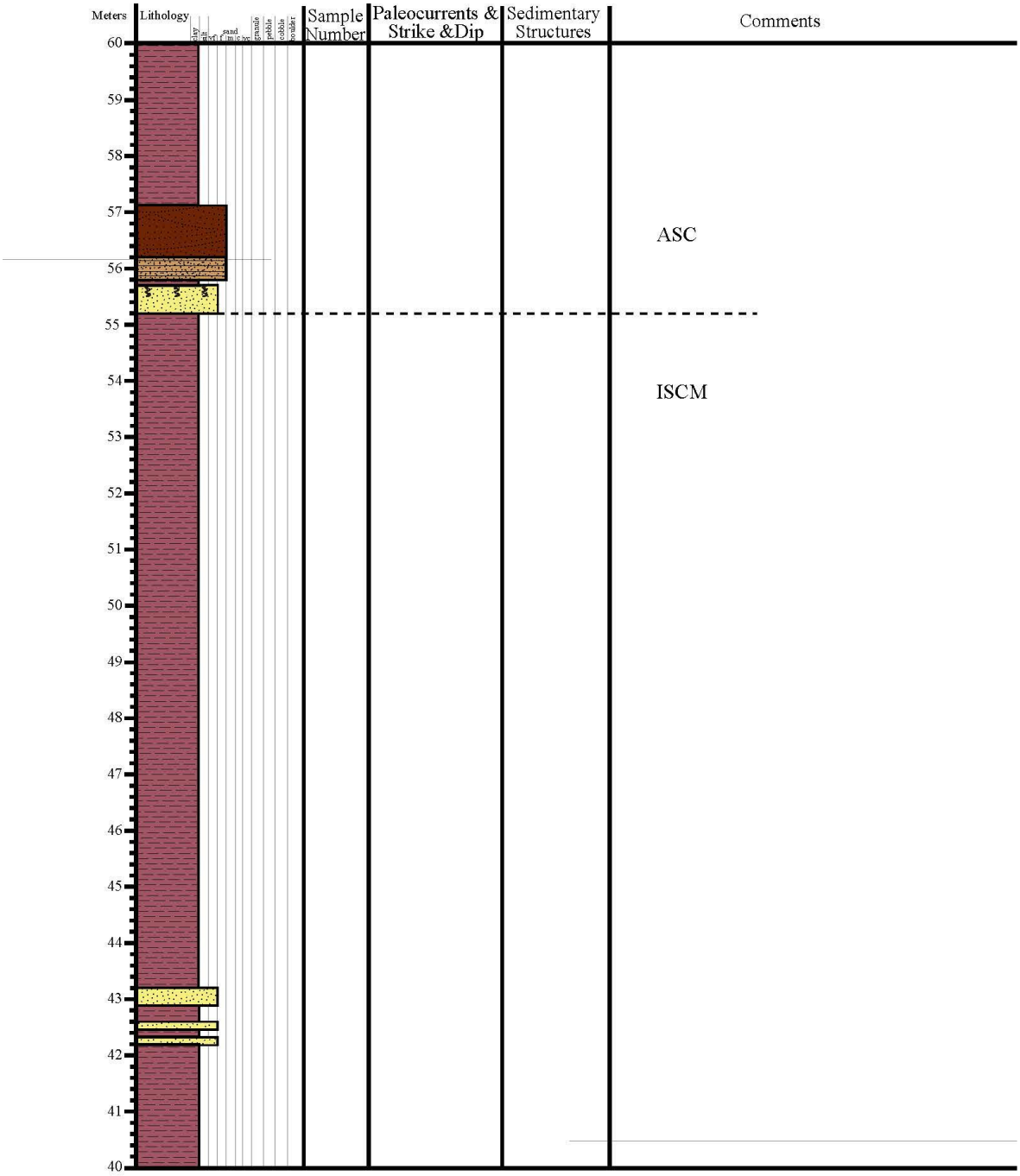

Measured Section 1: Grassy Hill (pg. 4)

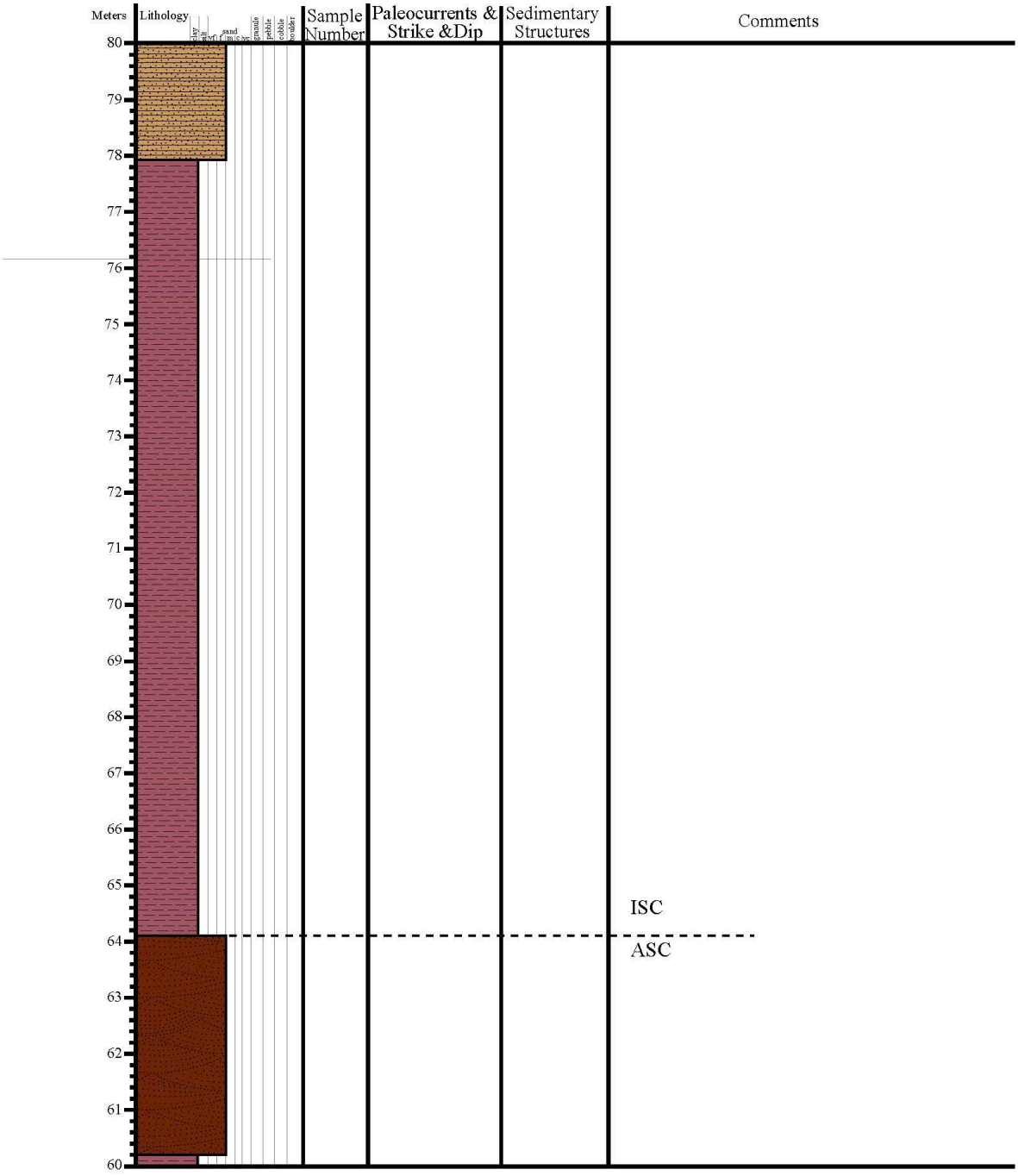

Measured Section 1: Grassy Hill (pg. 5)

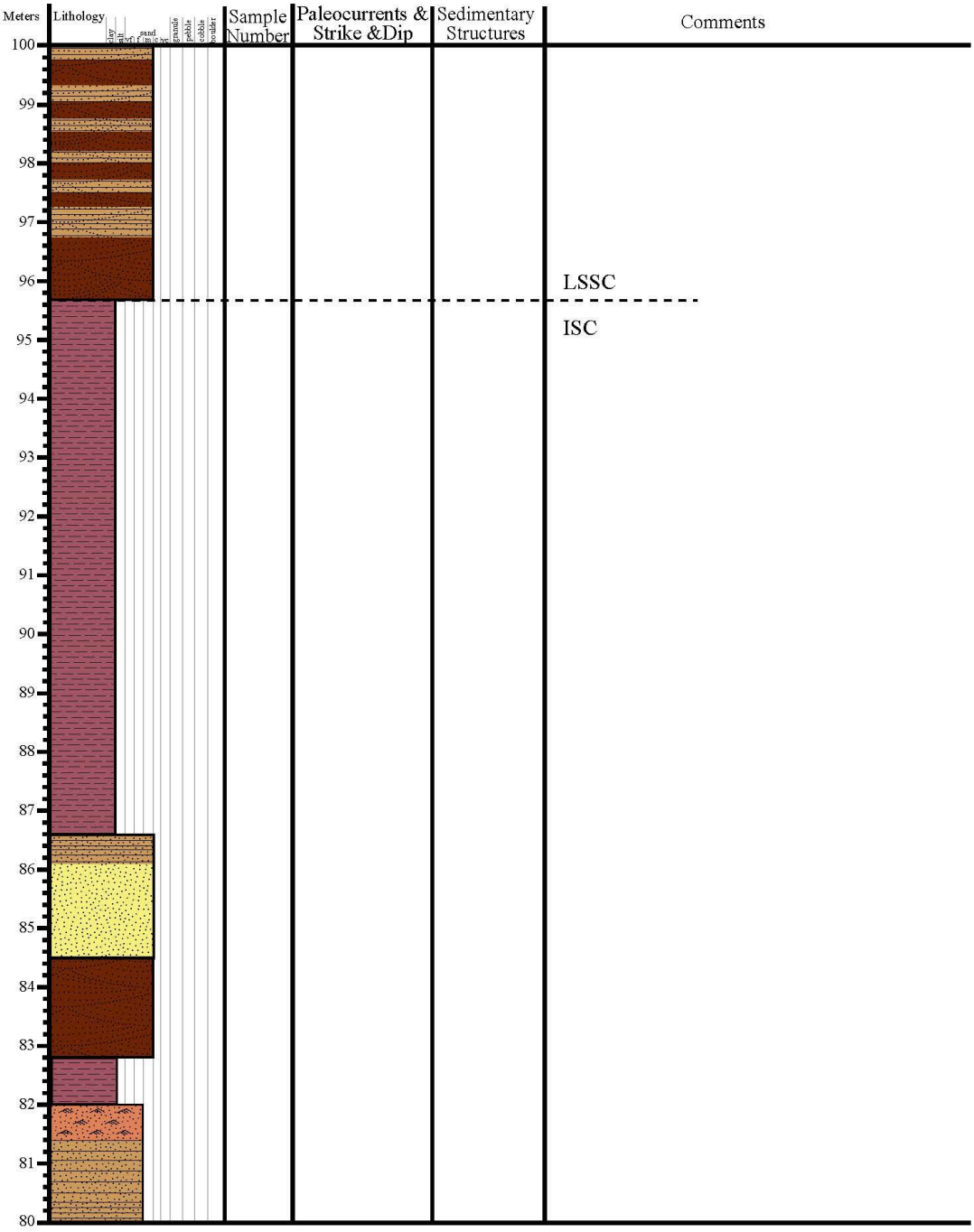

Measured Section 1: Grassy Hill (pg. 6)

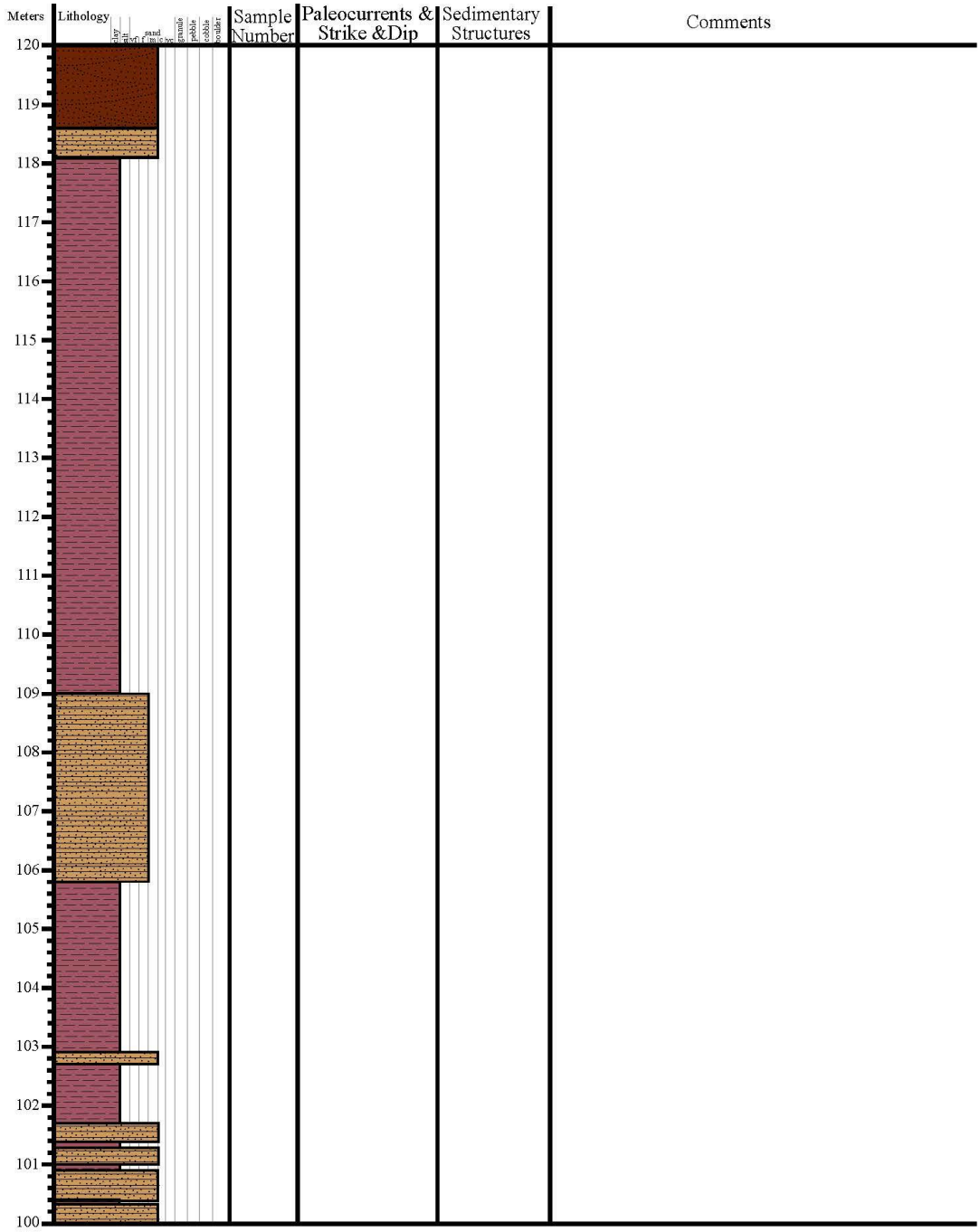

Measured Section 1: Grassy Hill (pg. 6)

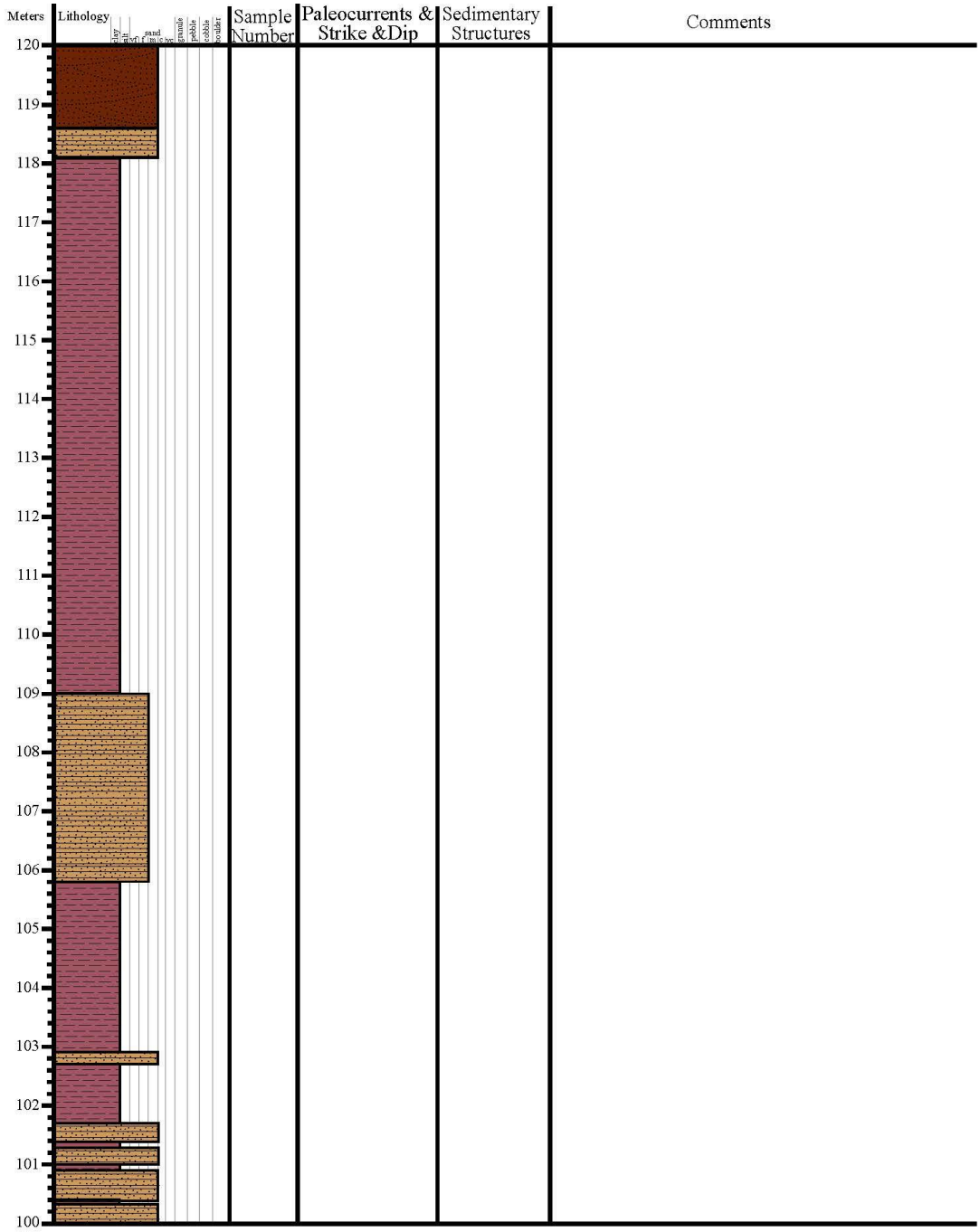

Measured Section 1: Grassy Hill (pg. 7)

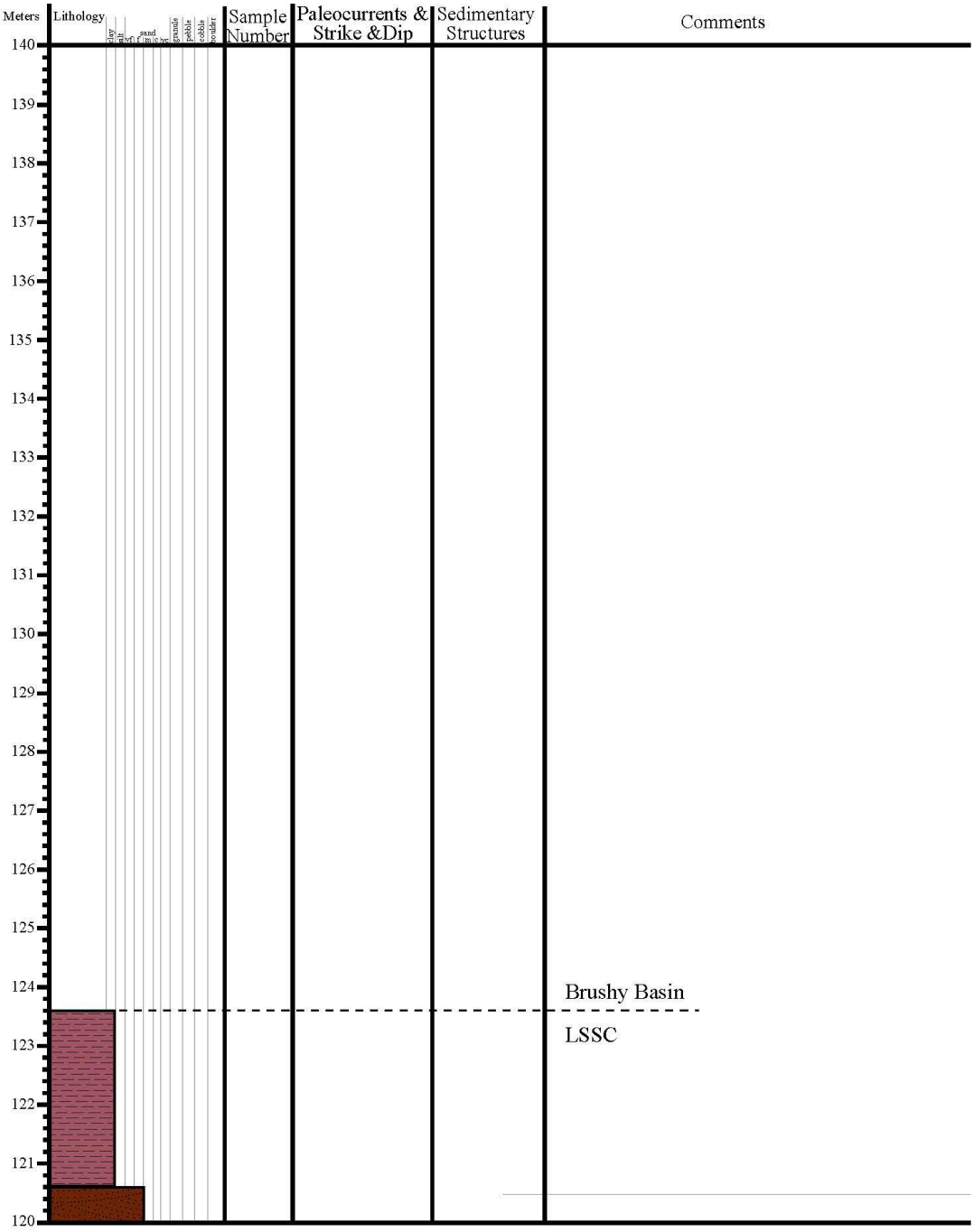

Measured Section 2: Grassy Hill (pg. 1)

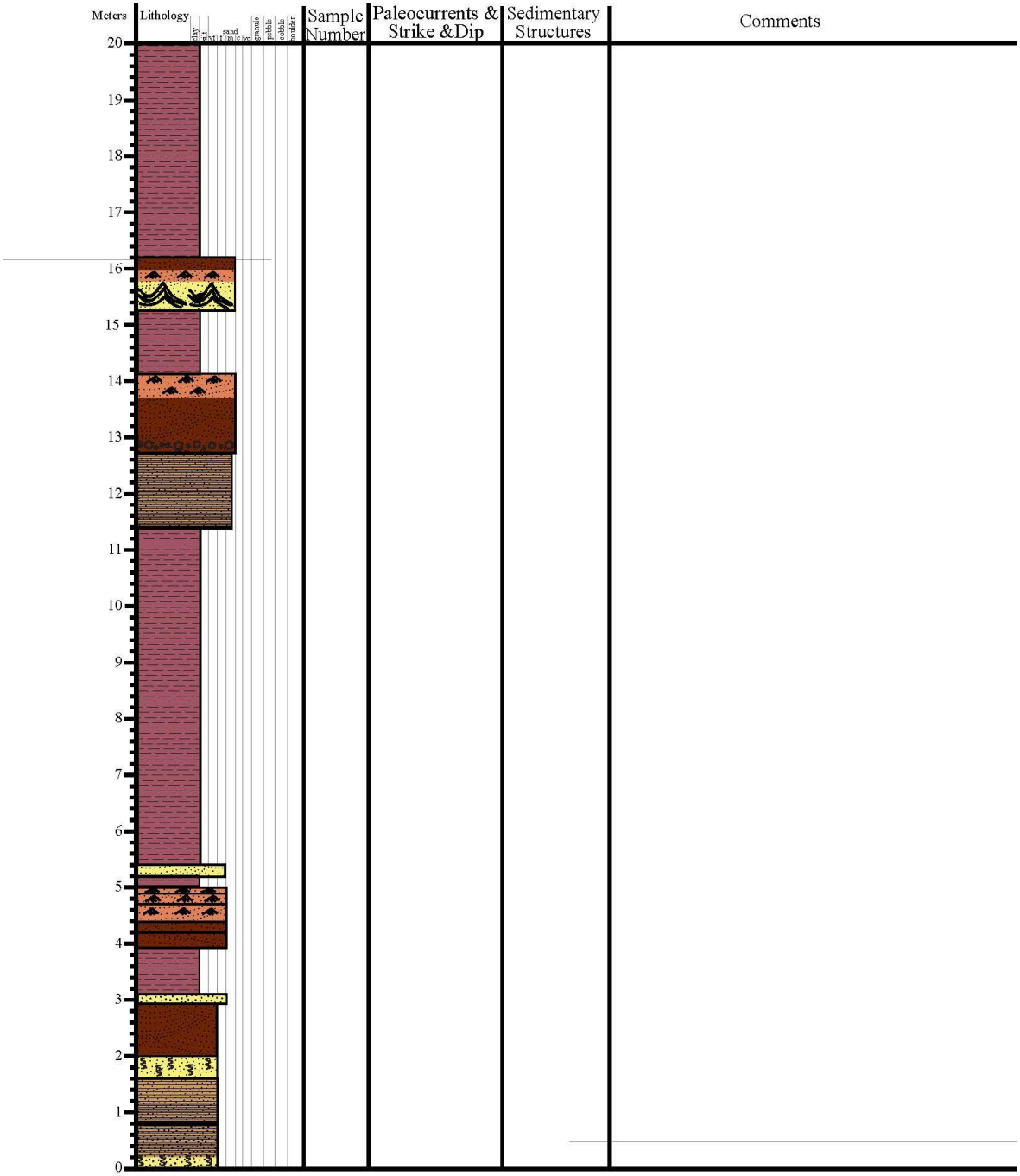

Measured Section 2: Grassy Hill (pg. 2)

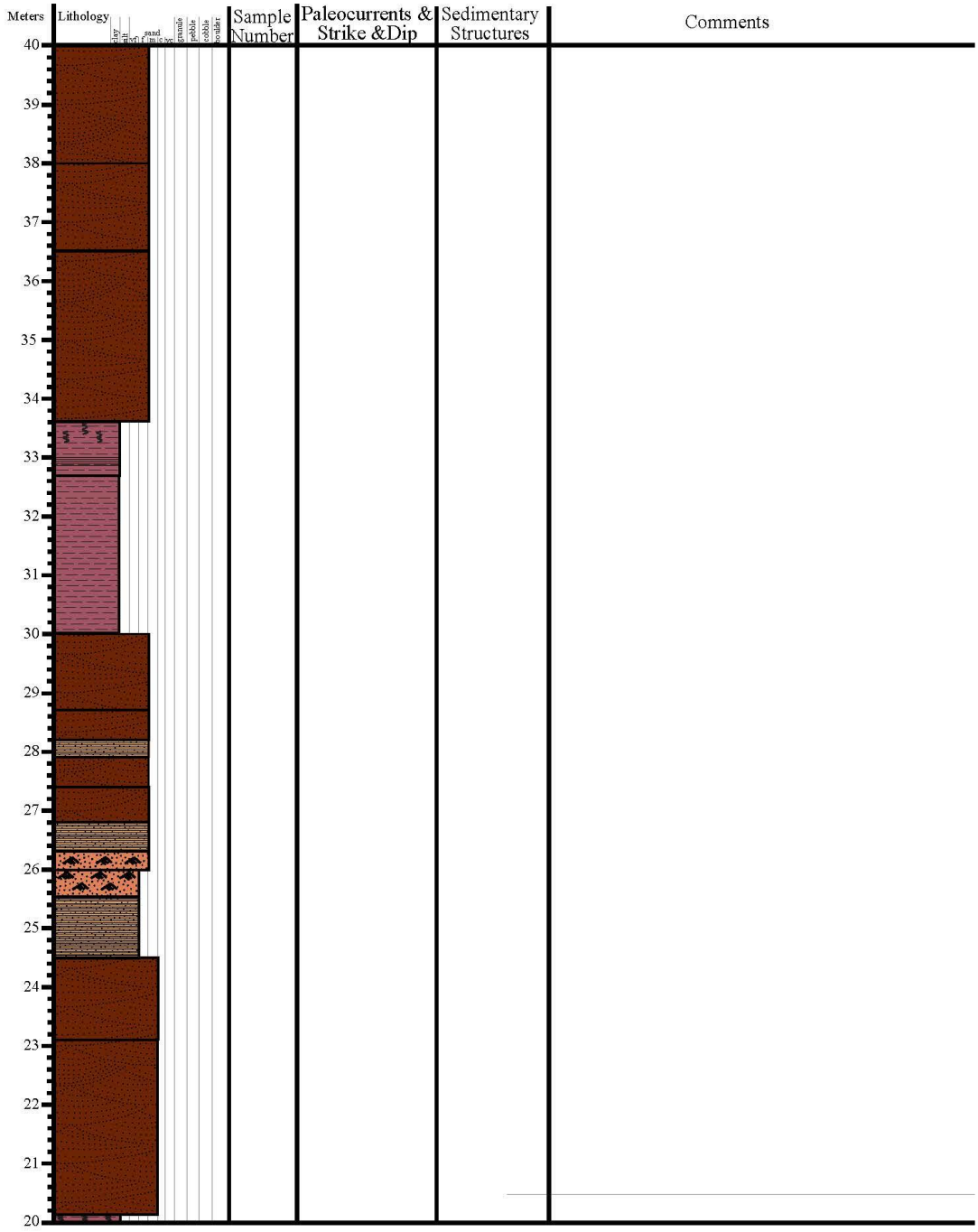

Measured Section 2: Grassy Hill (pg. 3)

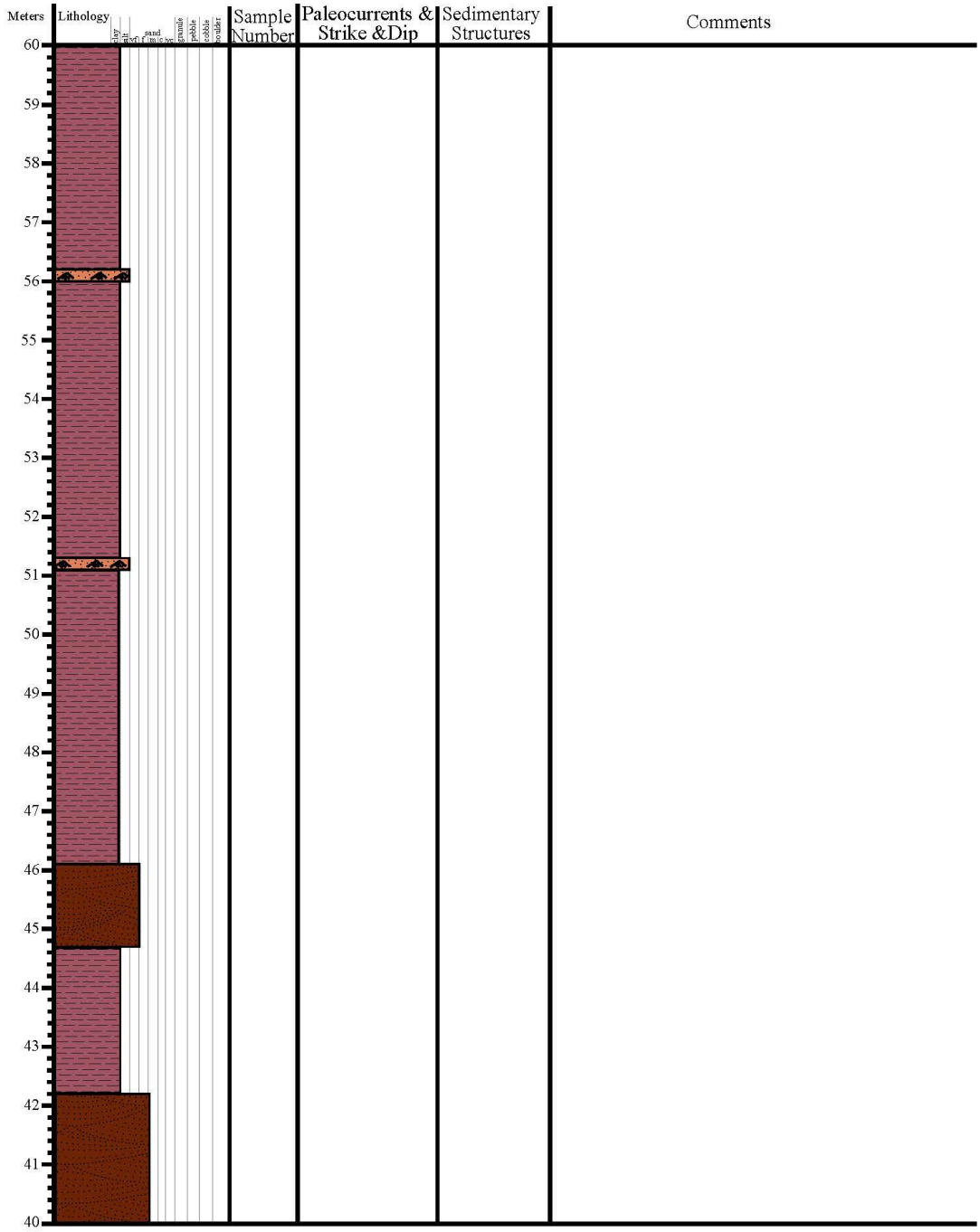

Measured Section 2: The Hat (pg. 4)

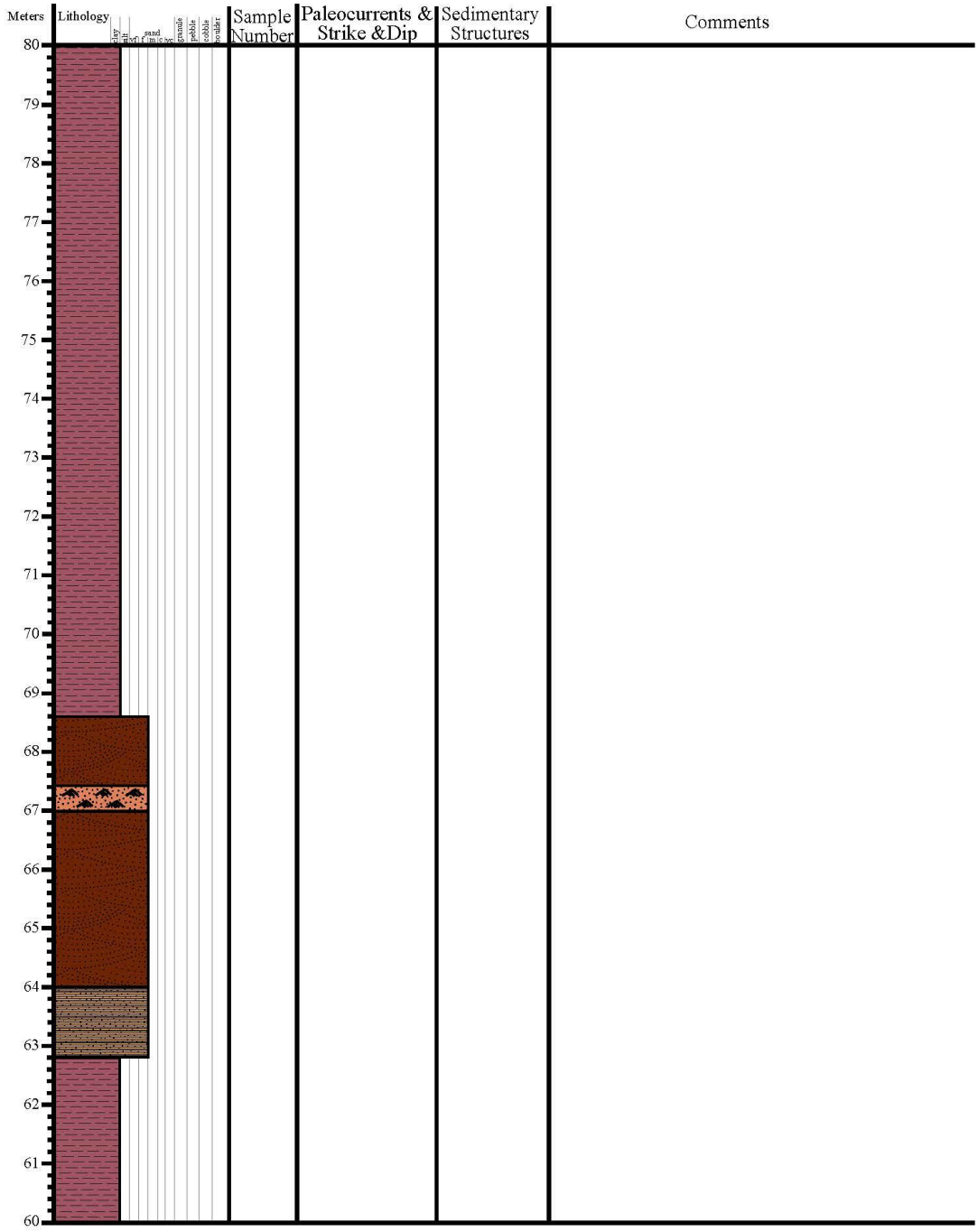

Measured Section 2: Grassy Hill (pg. 5)

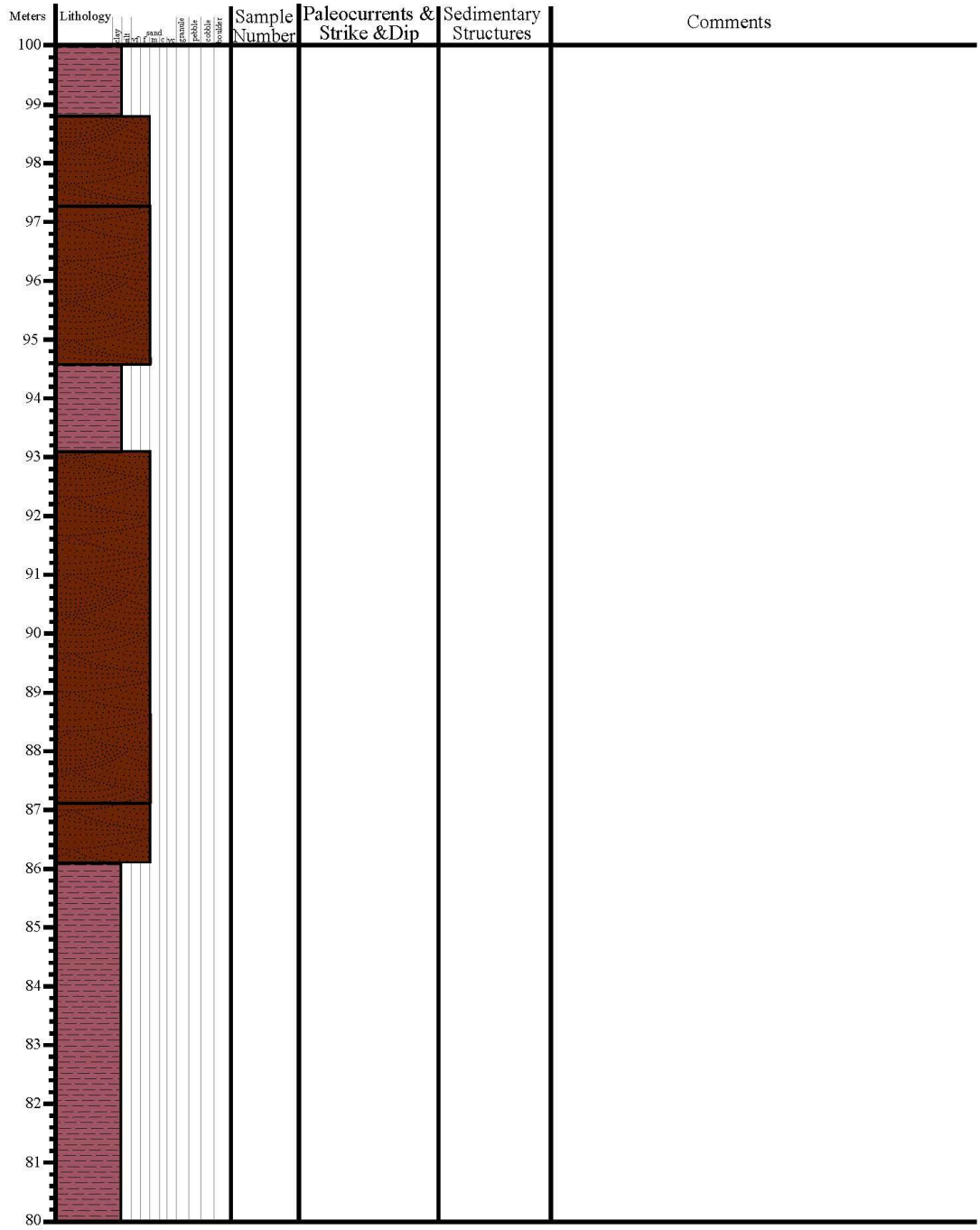

Measured Section 2: Grassy Hill (pg. 6)

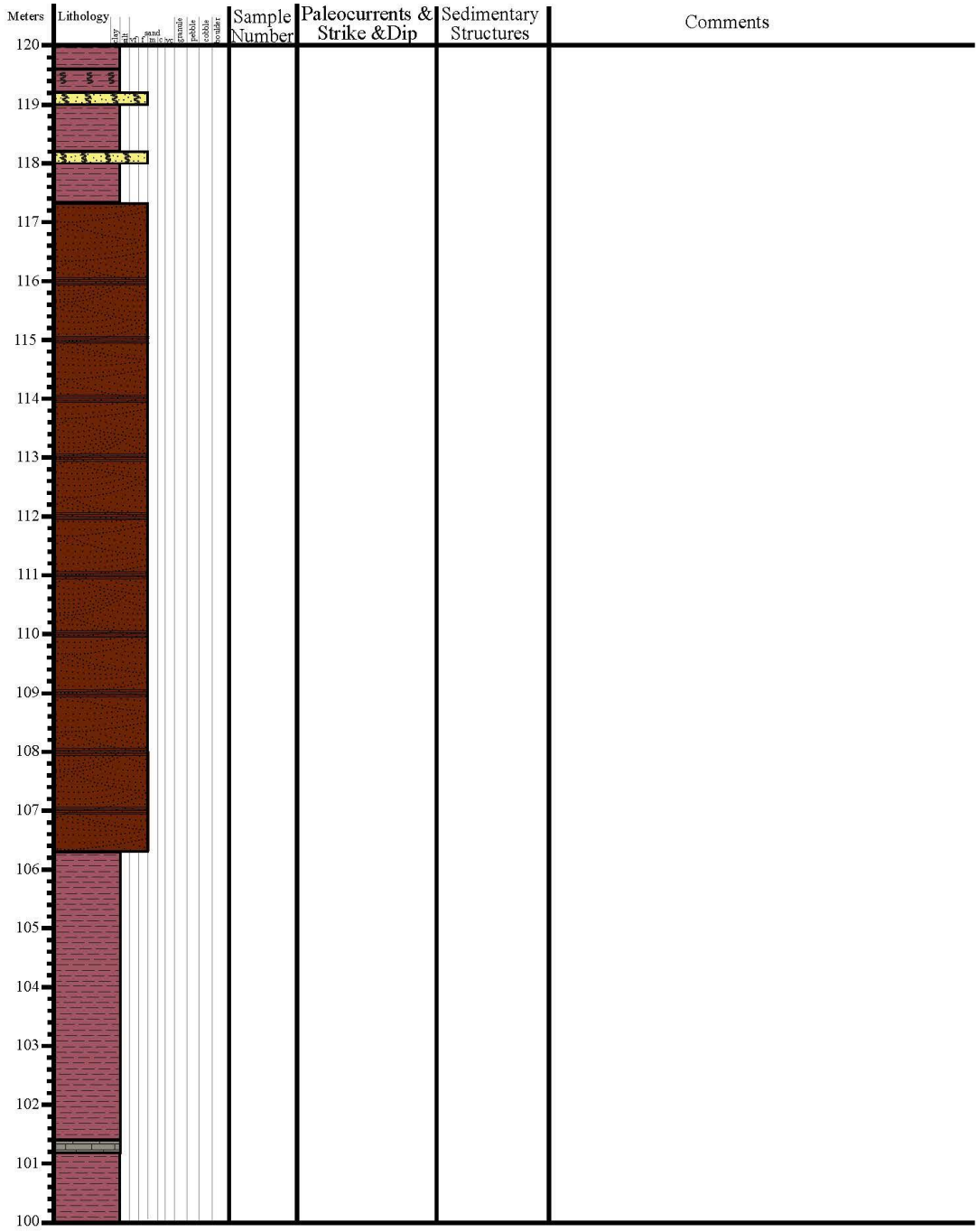

Measured Section 2: Grassy Hill (pg. 7)

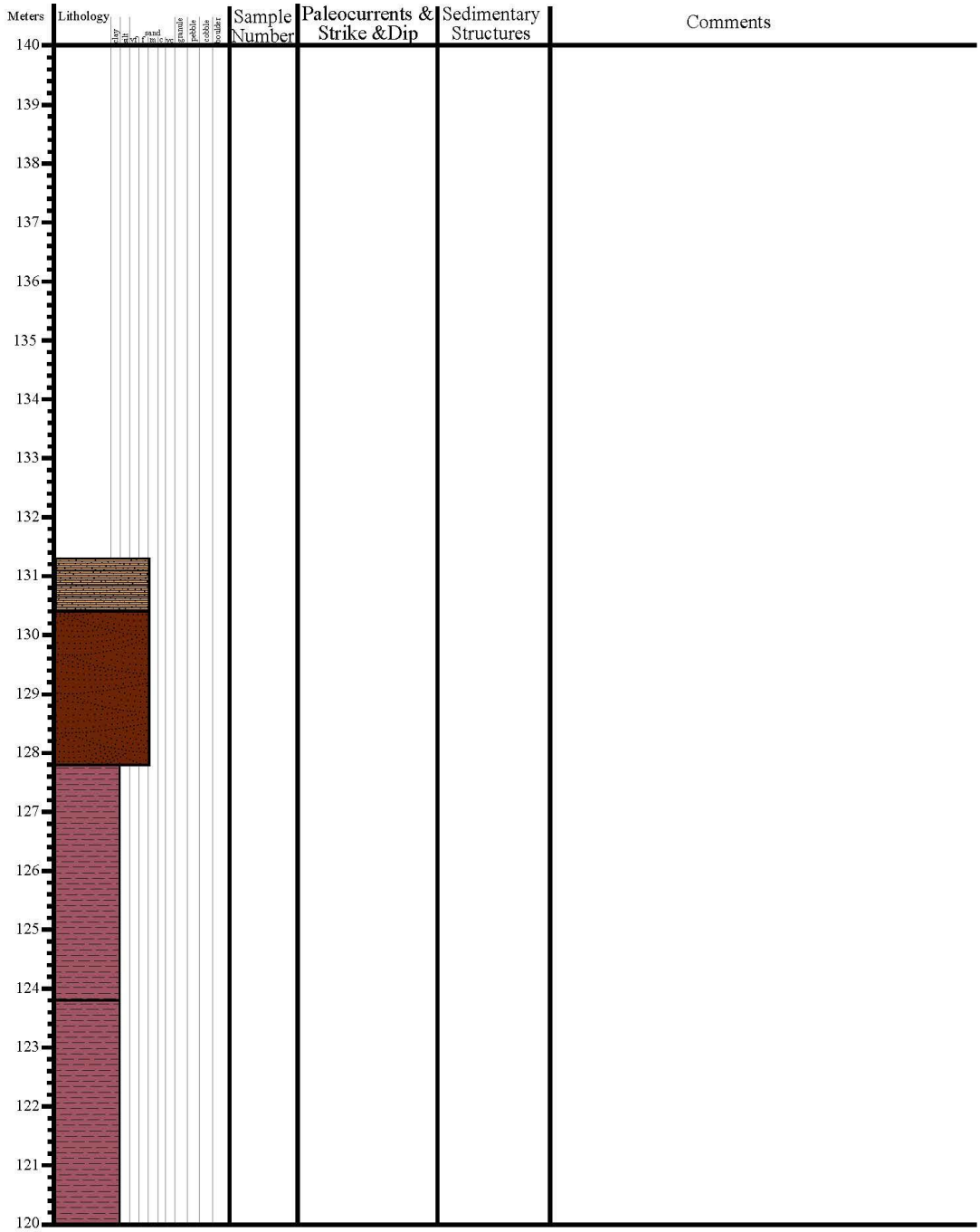

Measured Section 4: Grassy Hill (pg. 1)

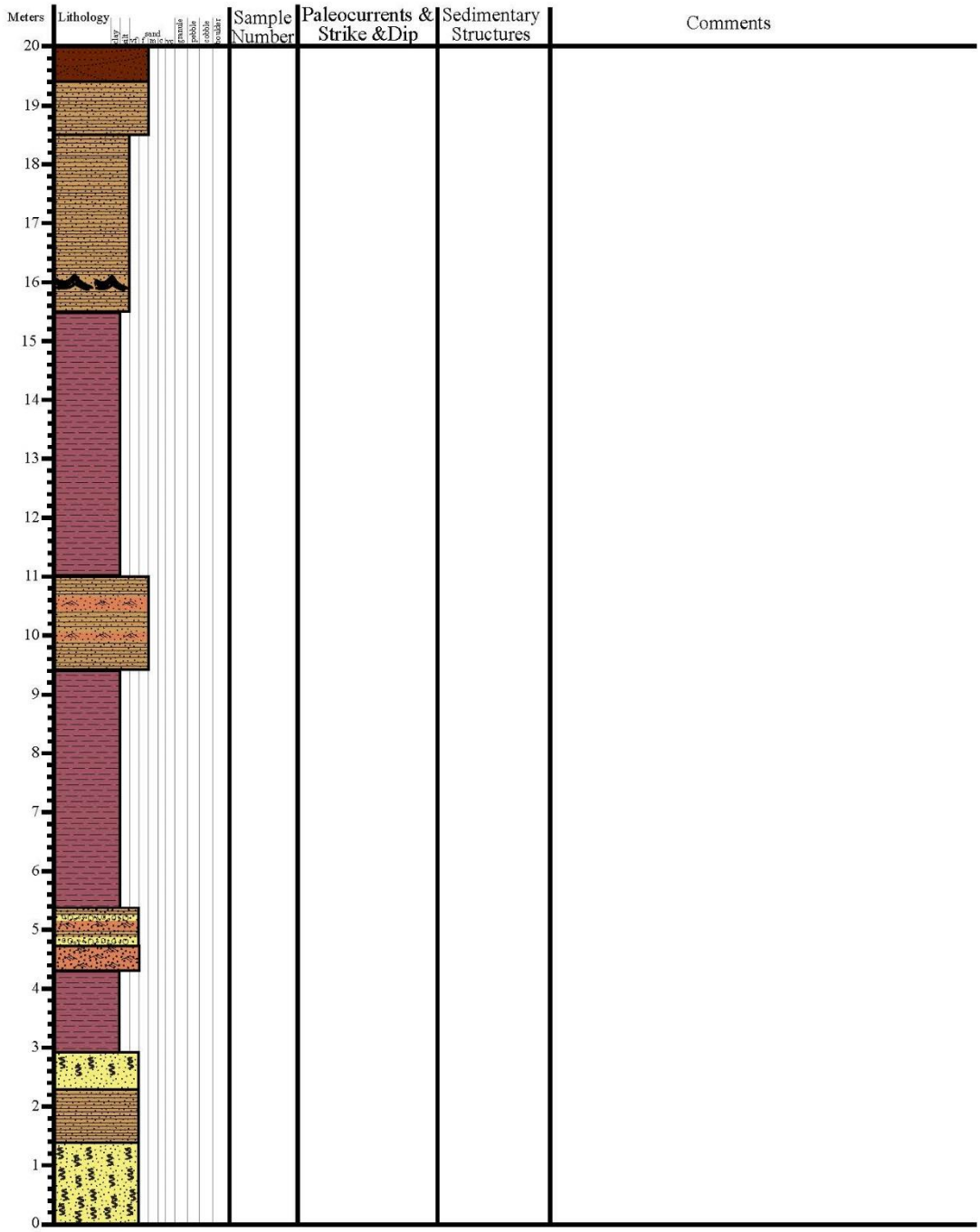

Measured Section 4: Grassy Hill (pg. 2)

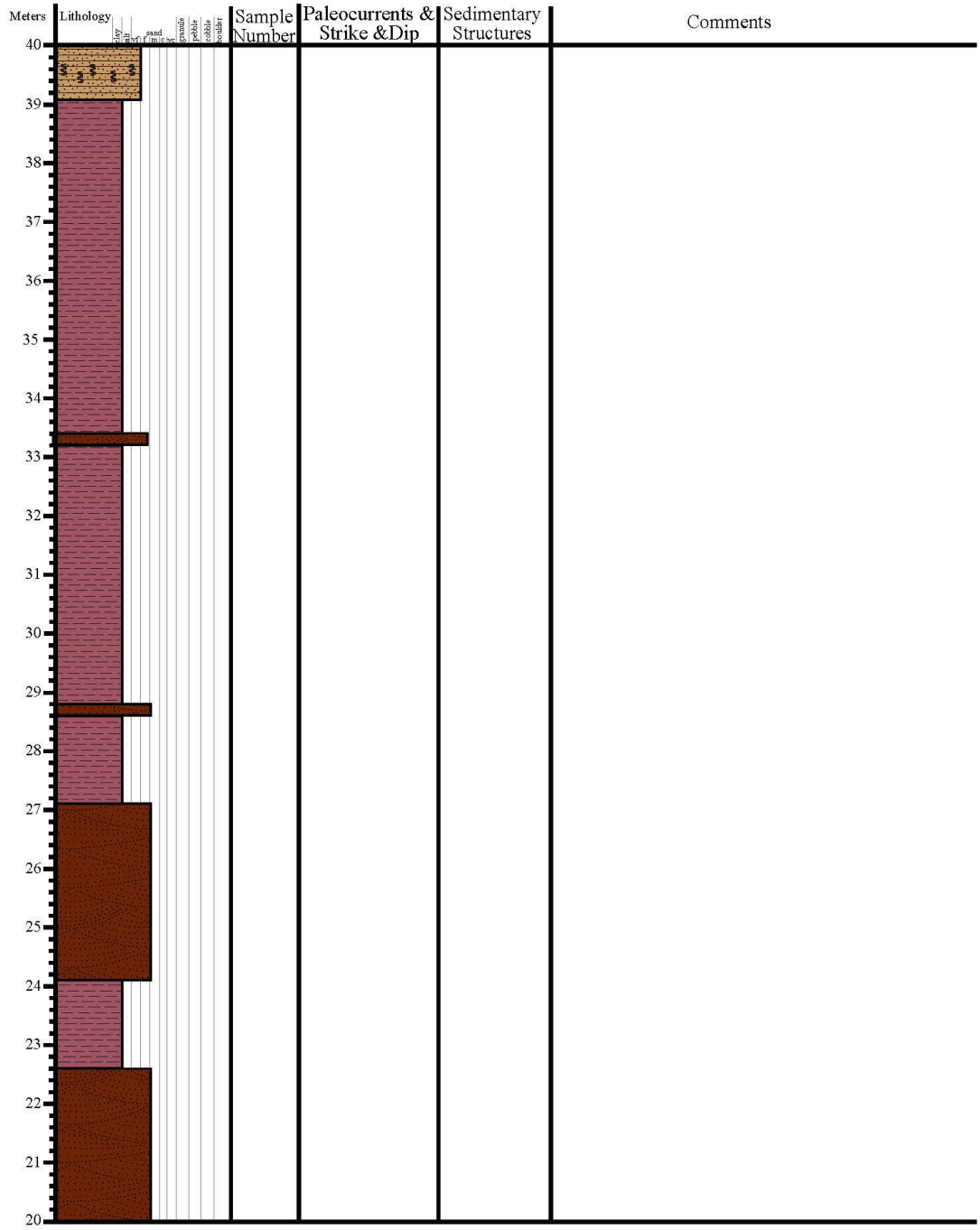

Measured Section 4: Grassy Hill (pg. 3)

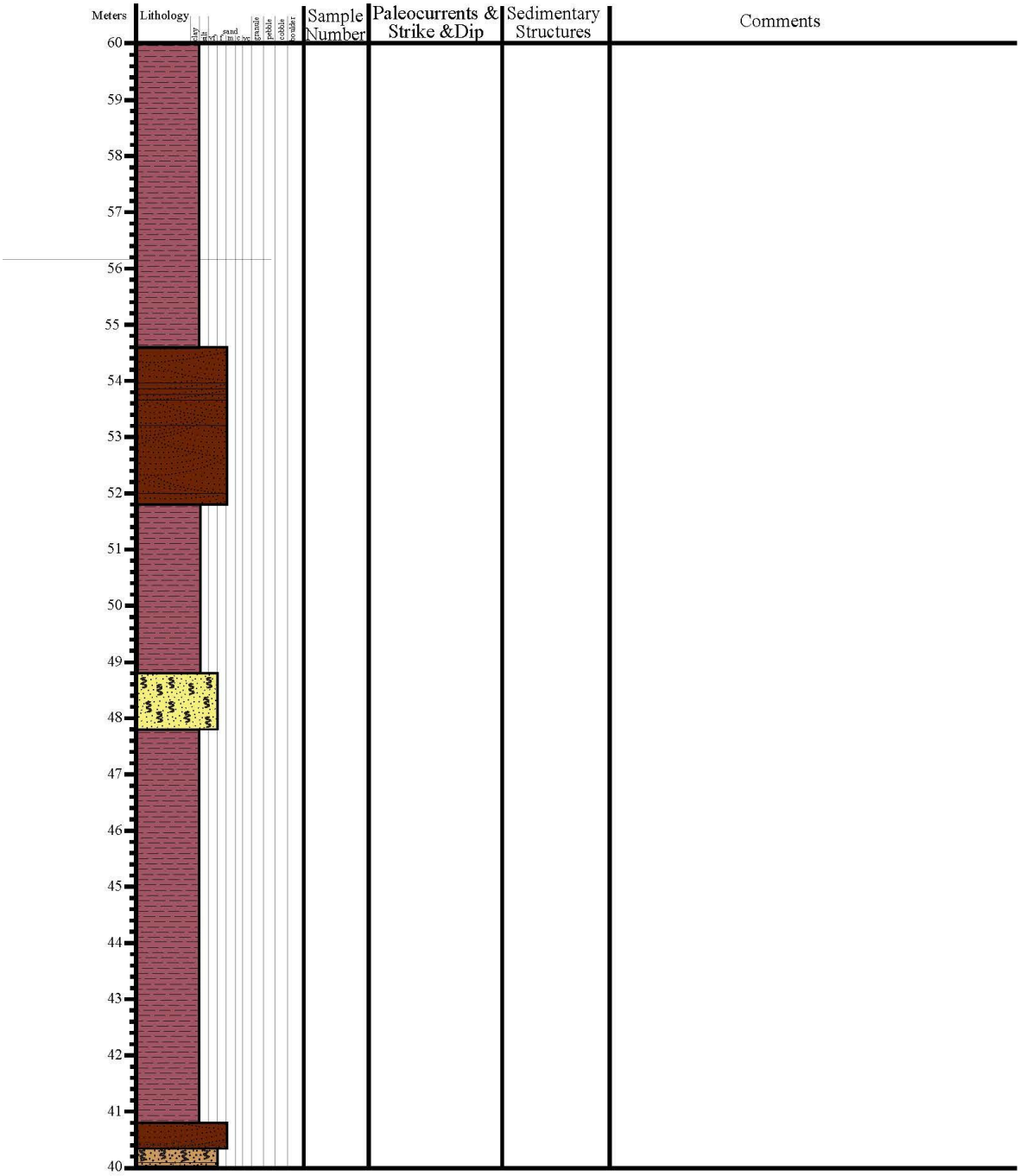

Measured Section 4: Grassy Hill (pg. 4)

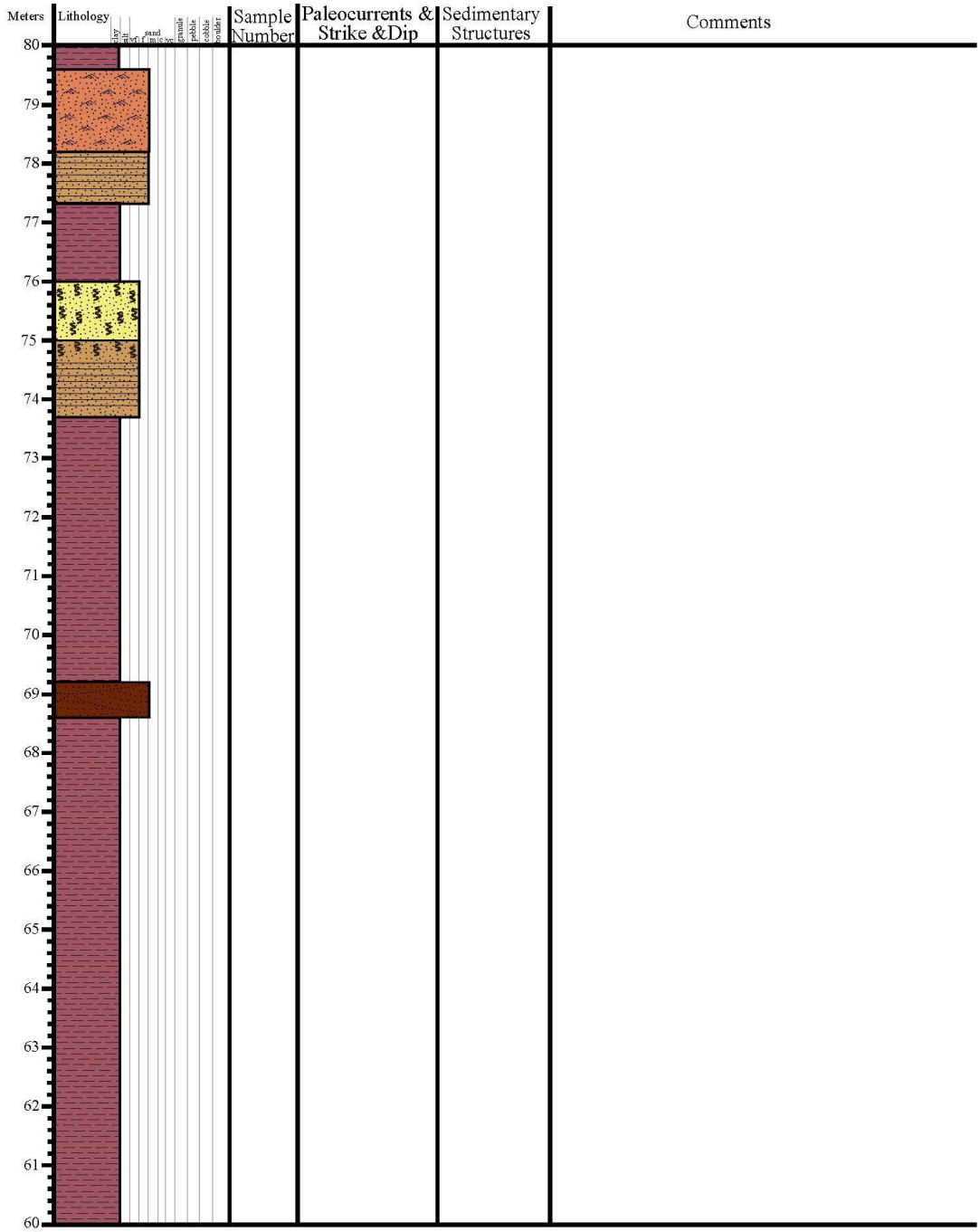

Measured Section 4: Grassy Hill (pg. 5)

Measured Section 4: Grassy Hill (pg. 6)

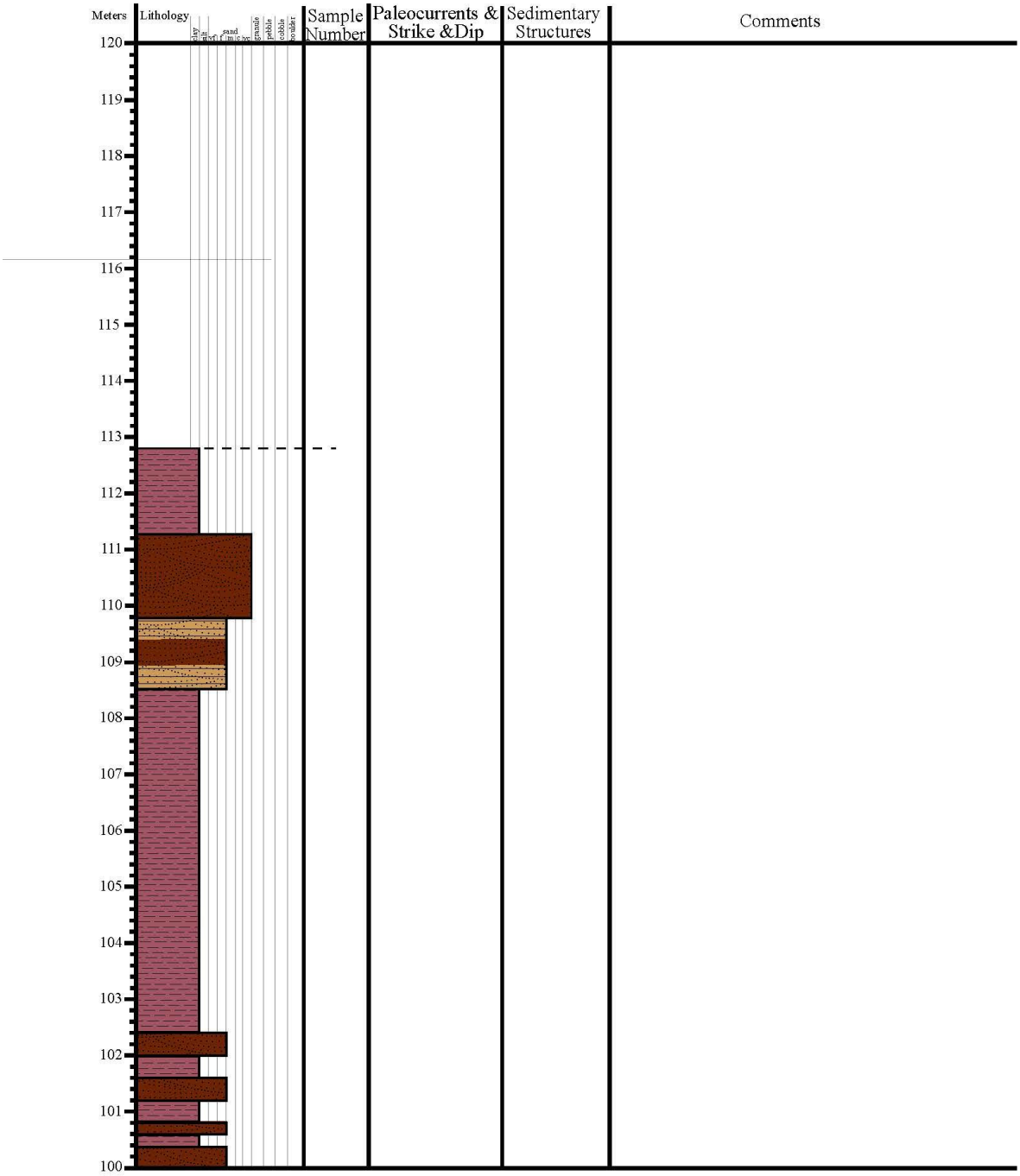

Measured Section 1:MegaFlap (pg. 1)

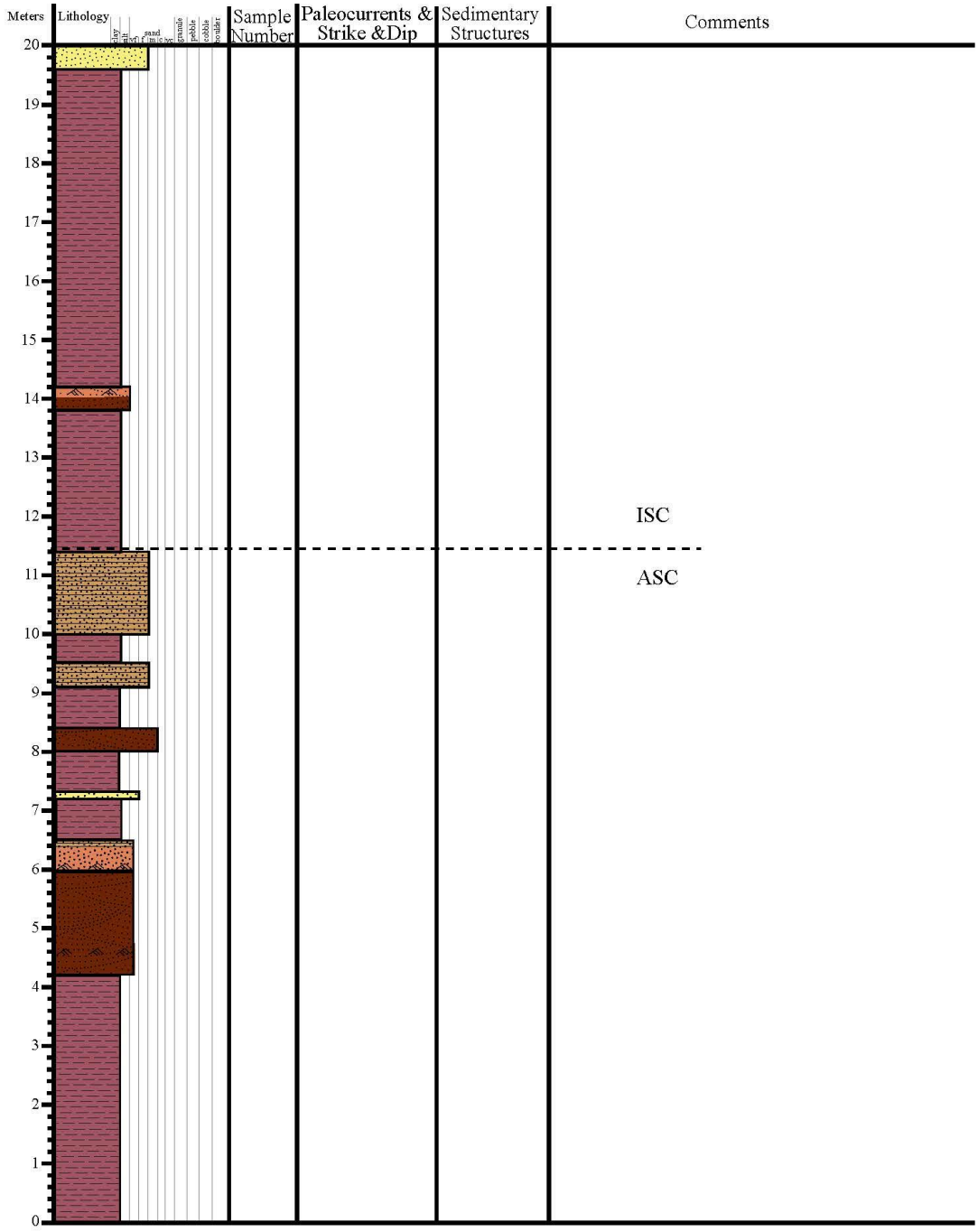

Measured Section 1: MegaFlap (pg. 2)

Measured Section 1: MegaFlap (pg. 3)

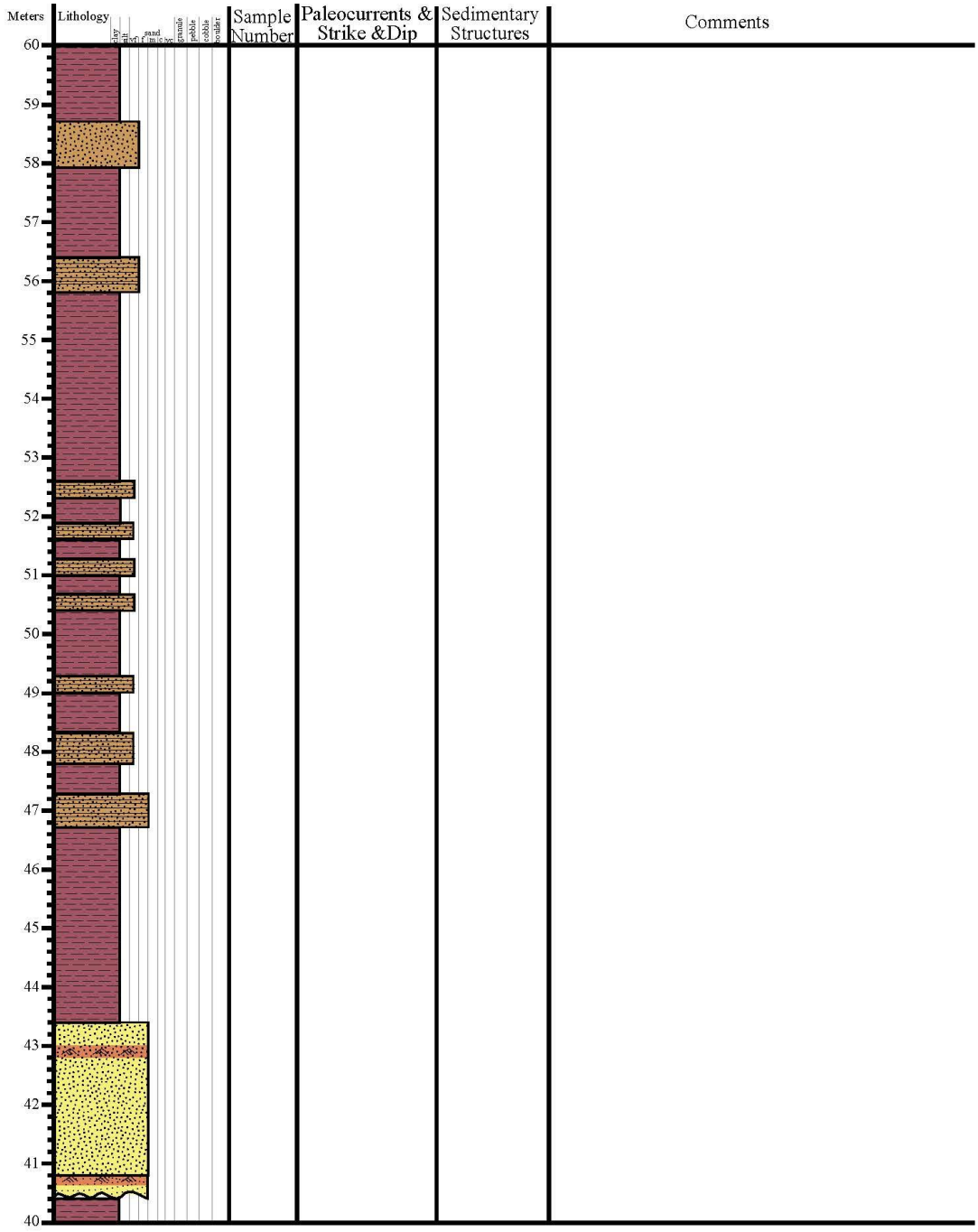

Measured Section 1: MegaFlap (pg. 4)

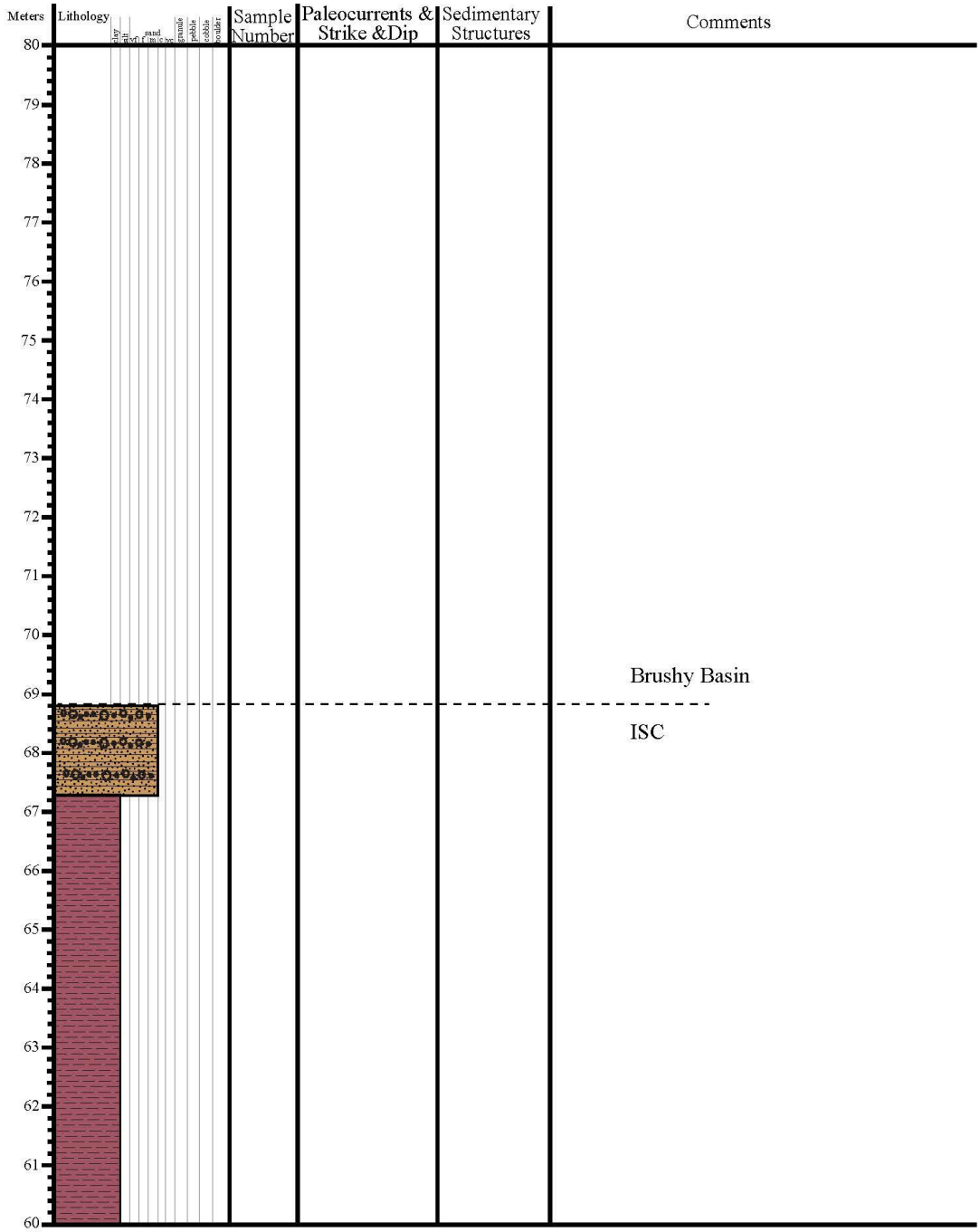

Measured Section 2: MegaFlap (pg. 1)

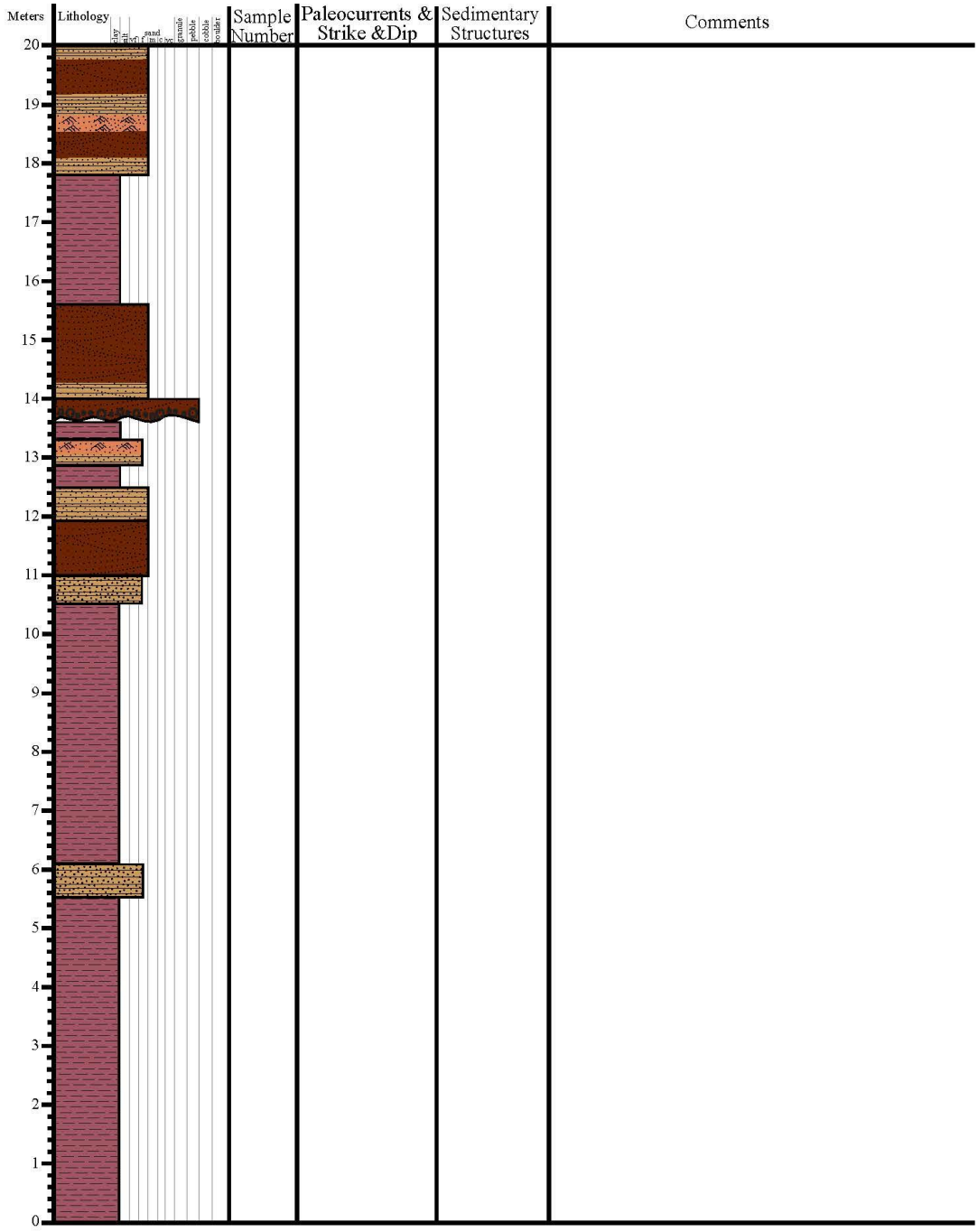

Measured Section 2: MegaFlap (pg. 2)

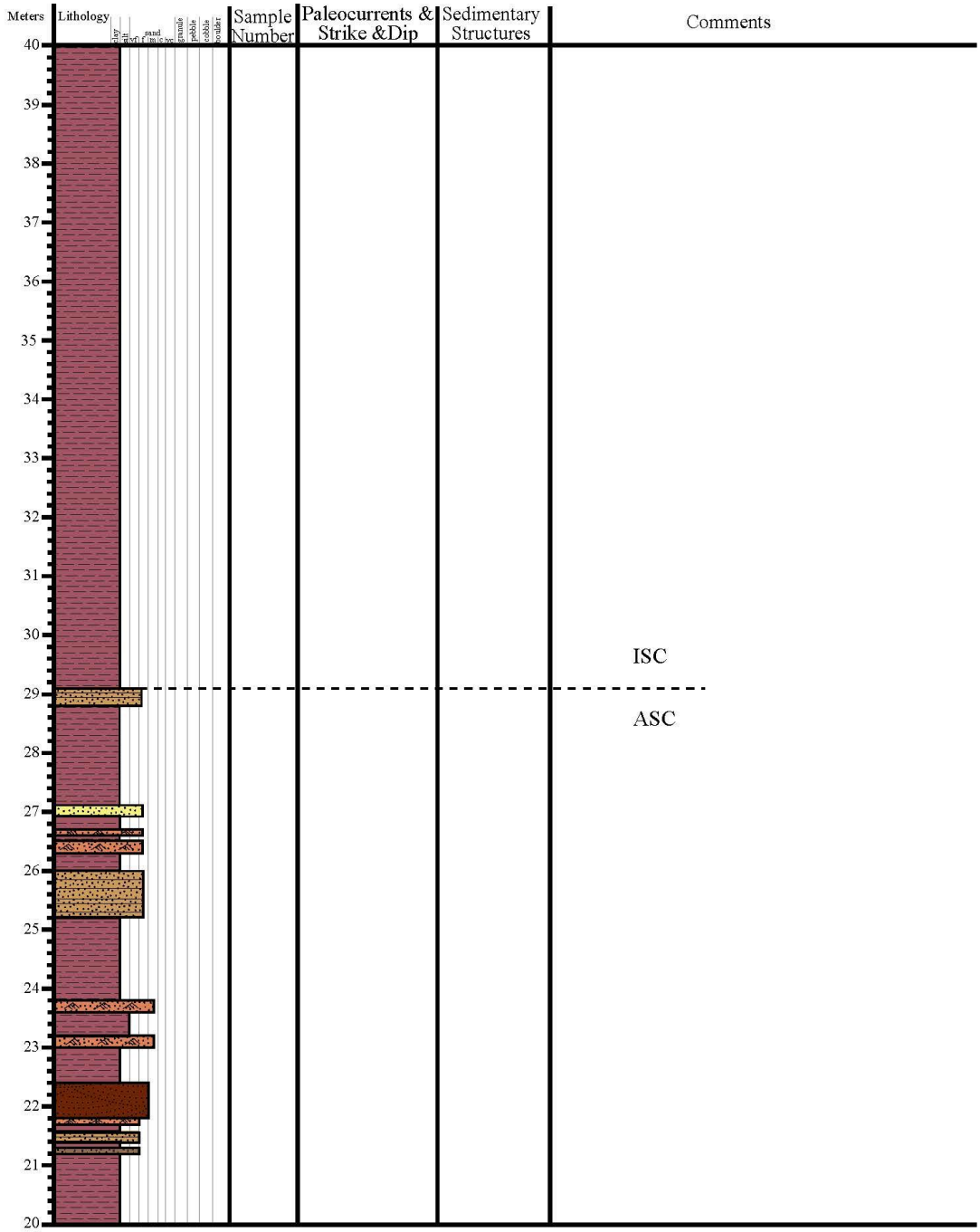

Measured Section 2: MegaFlap (pg. 3)

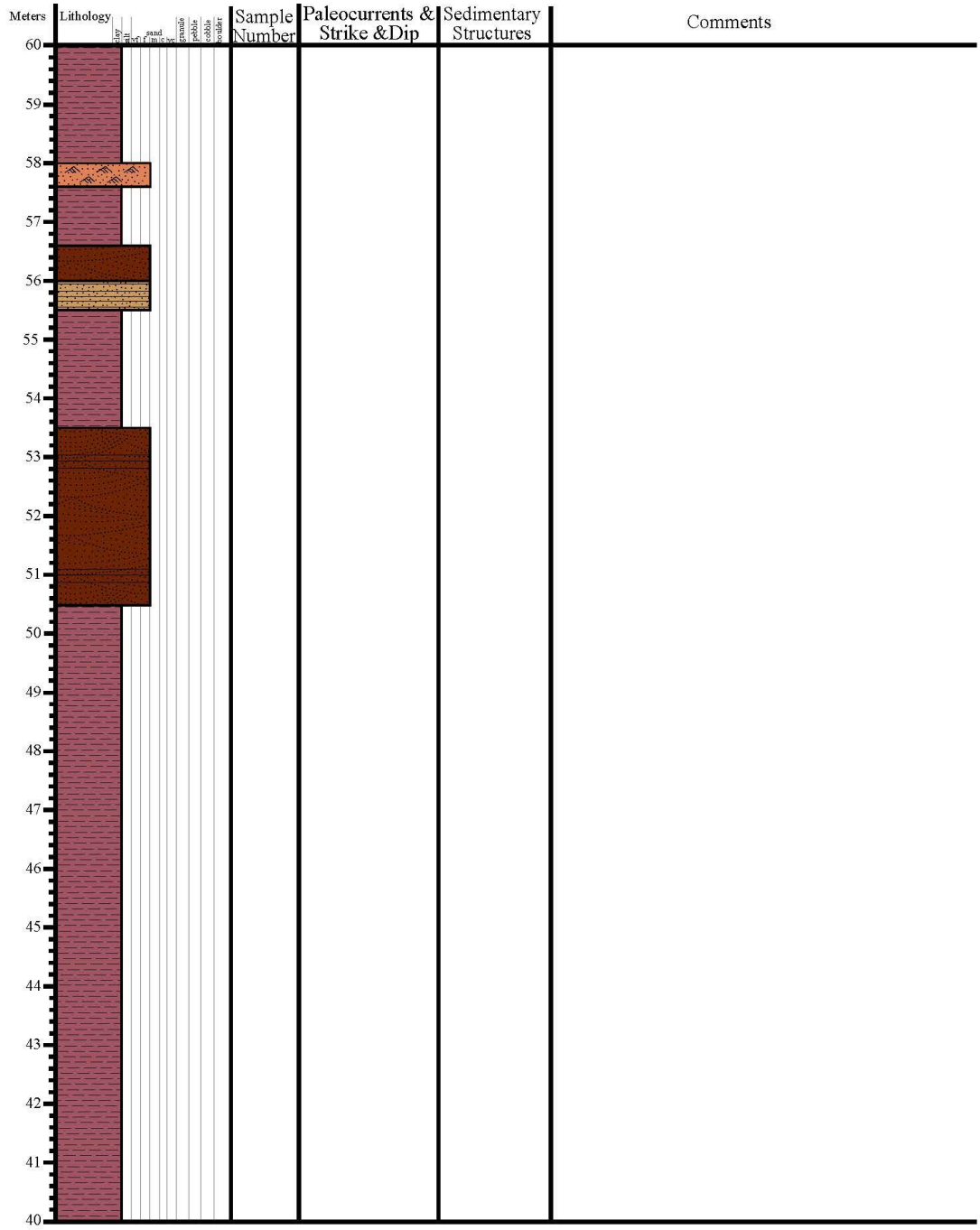

Measured Section 2: MegaFlap (pg. 4)

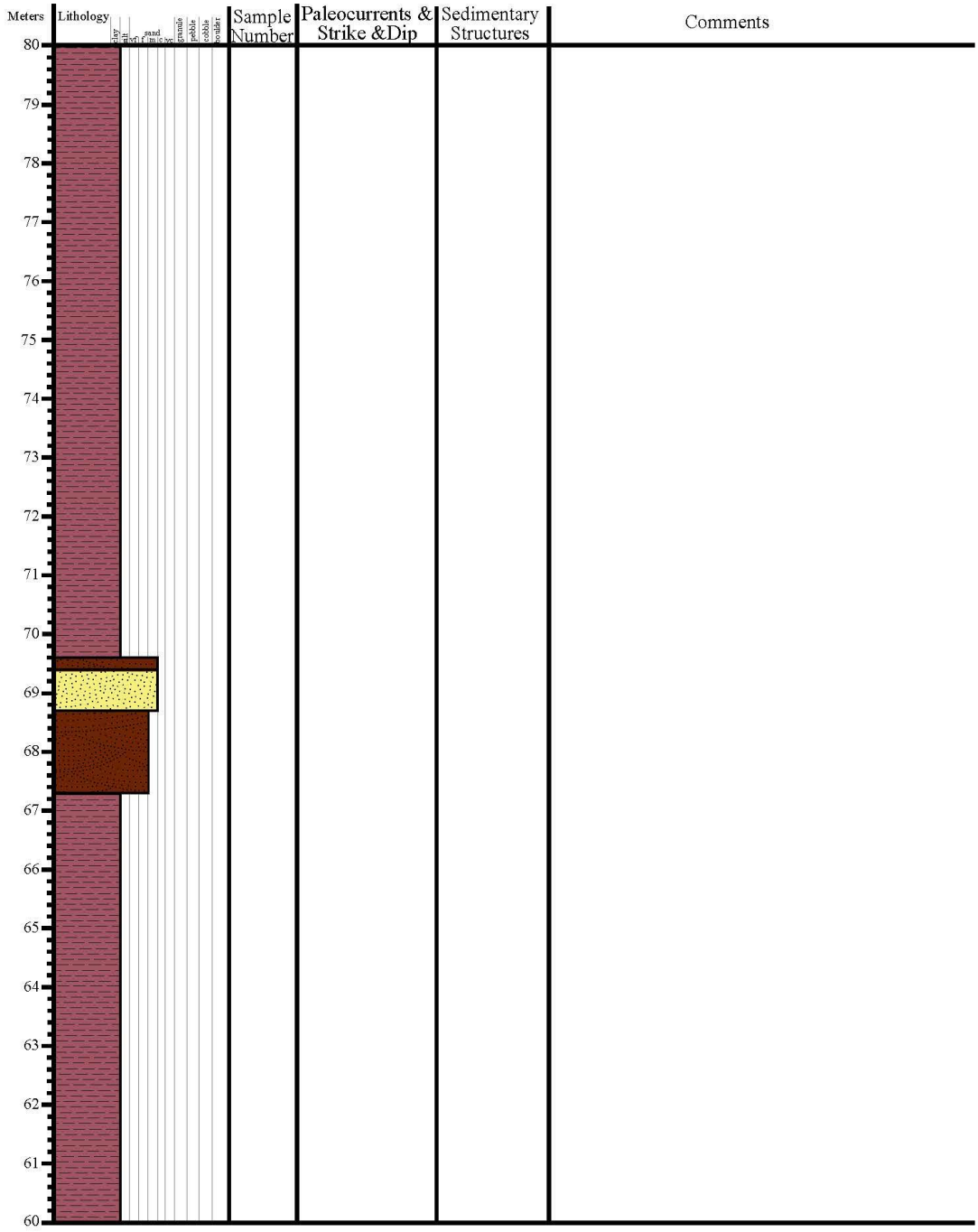

Measured Section 2: MegaFlap (pg. 5)

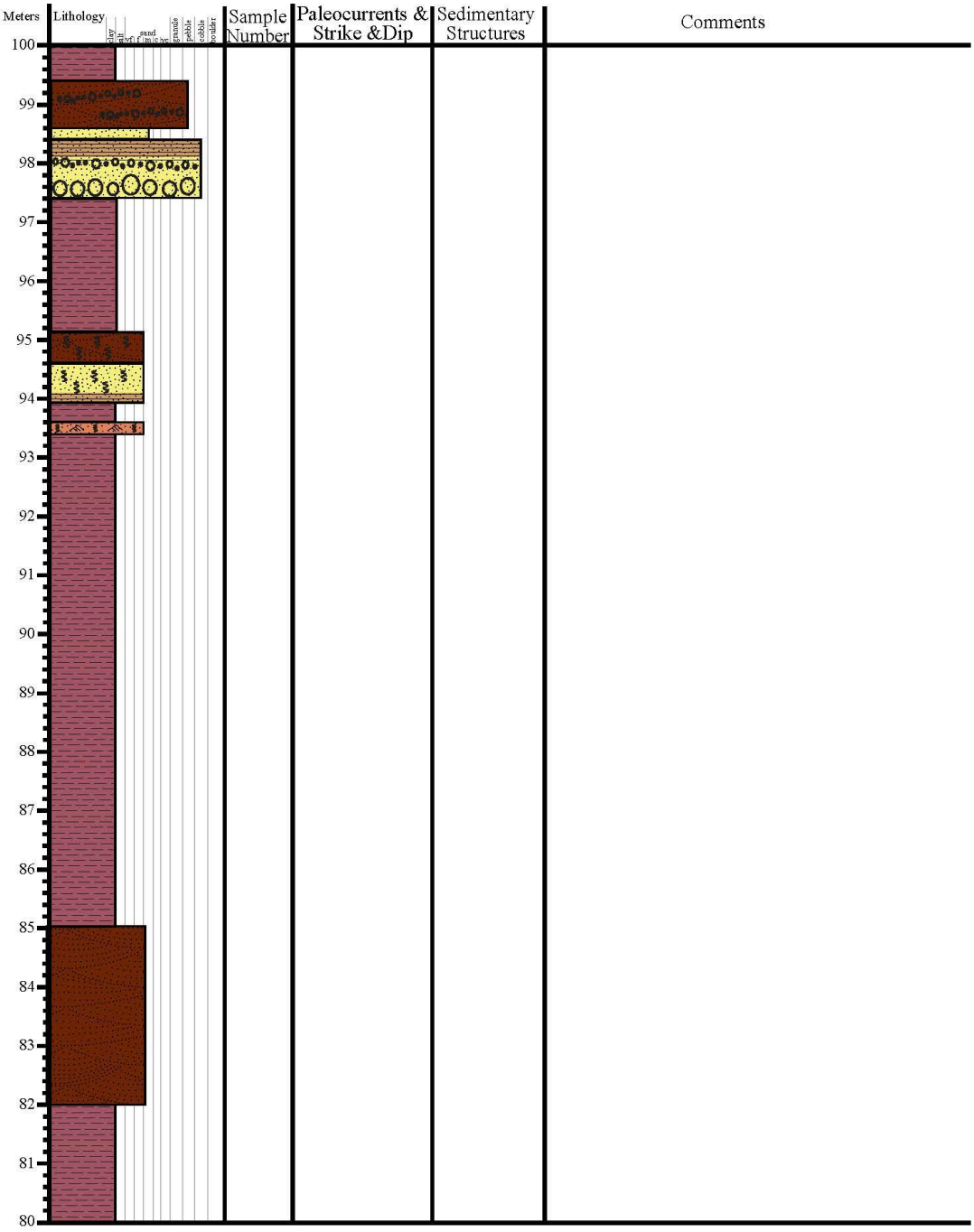

Measured Section 2: MegaFlap (pg. 1)

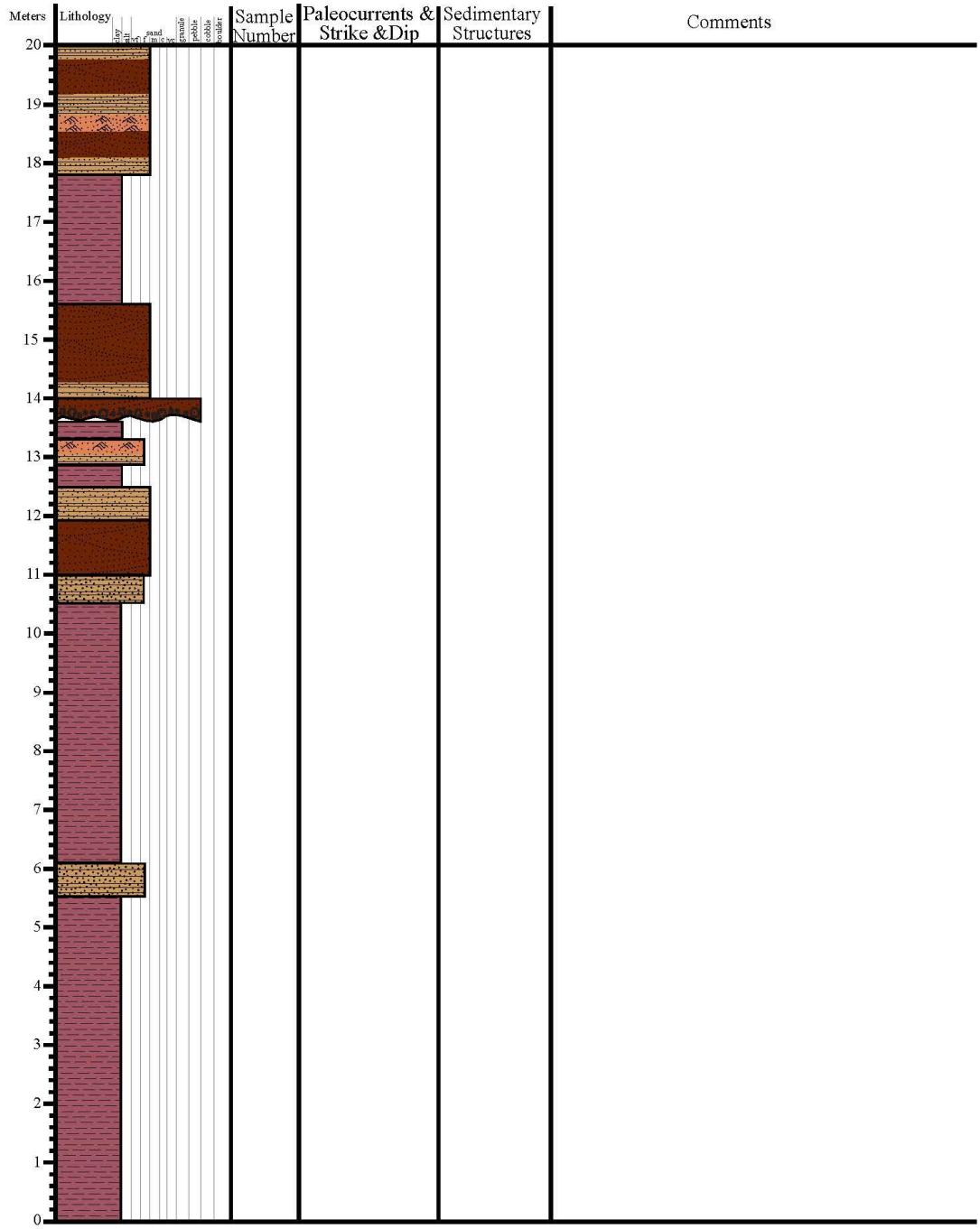

Measured Section 2: MegaFlap (pg. 2)

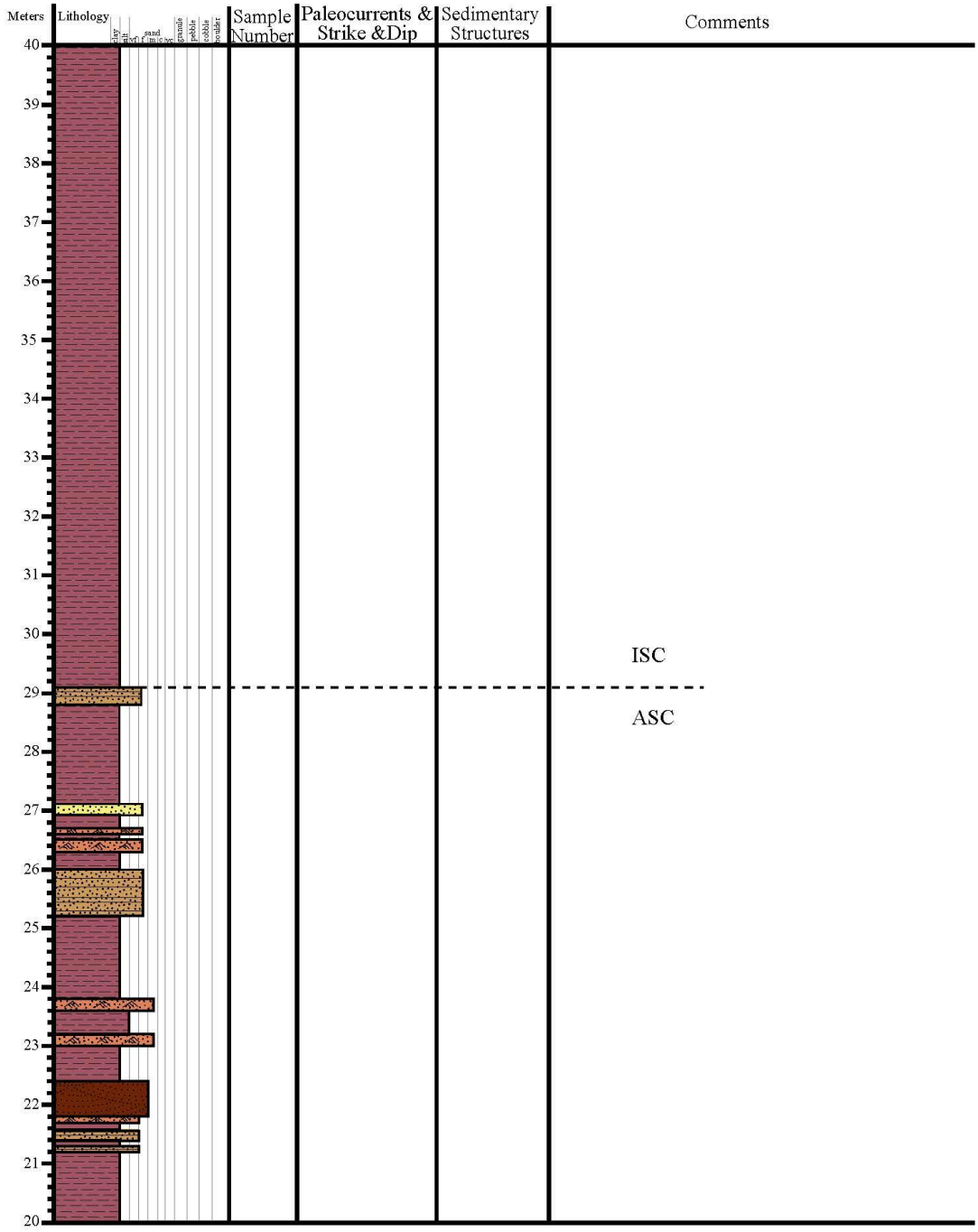

Measured Section 2: MegaFlap (pg. 3)

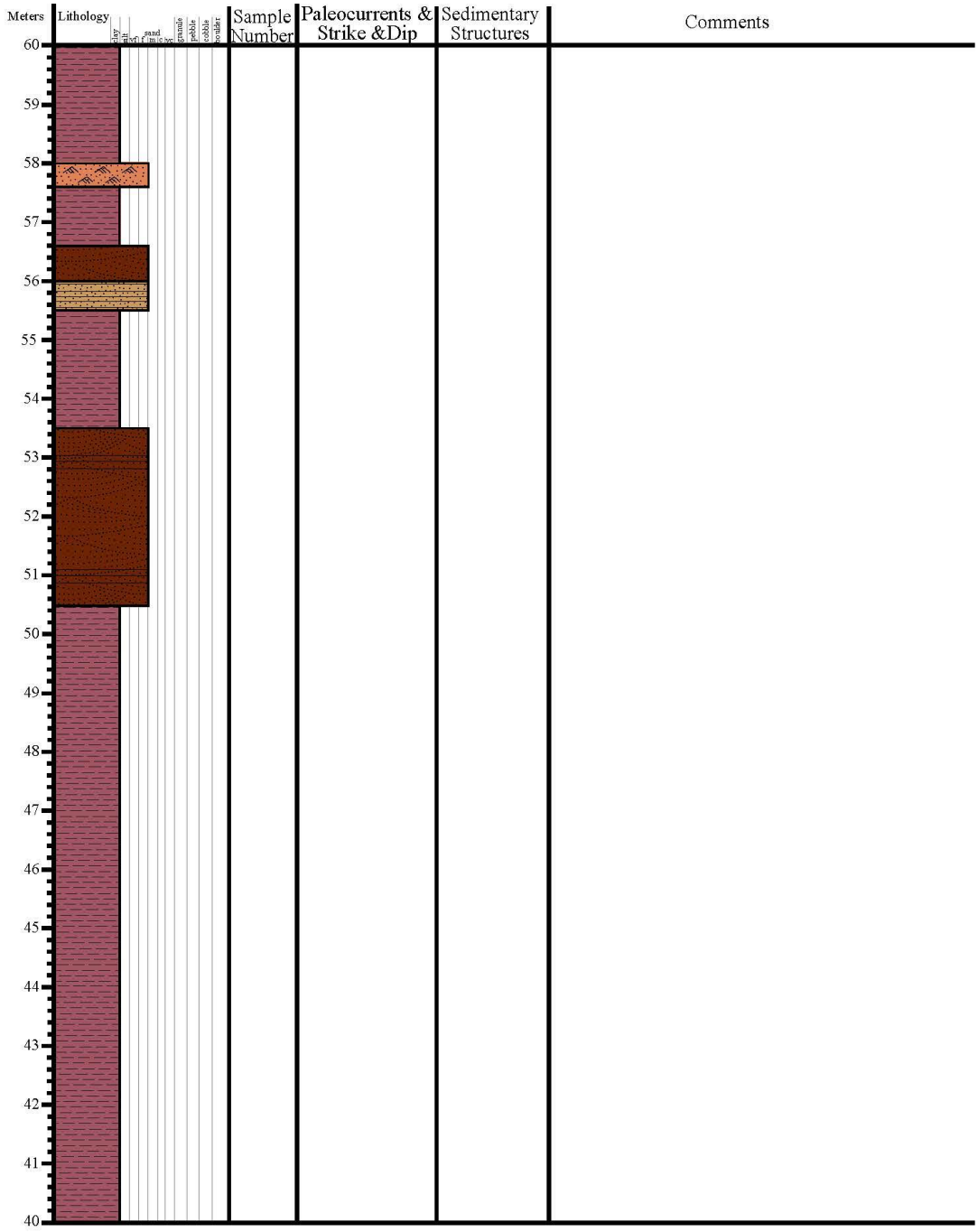

Measured Section 2: MegaFlap (pg. 4)

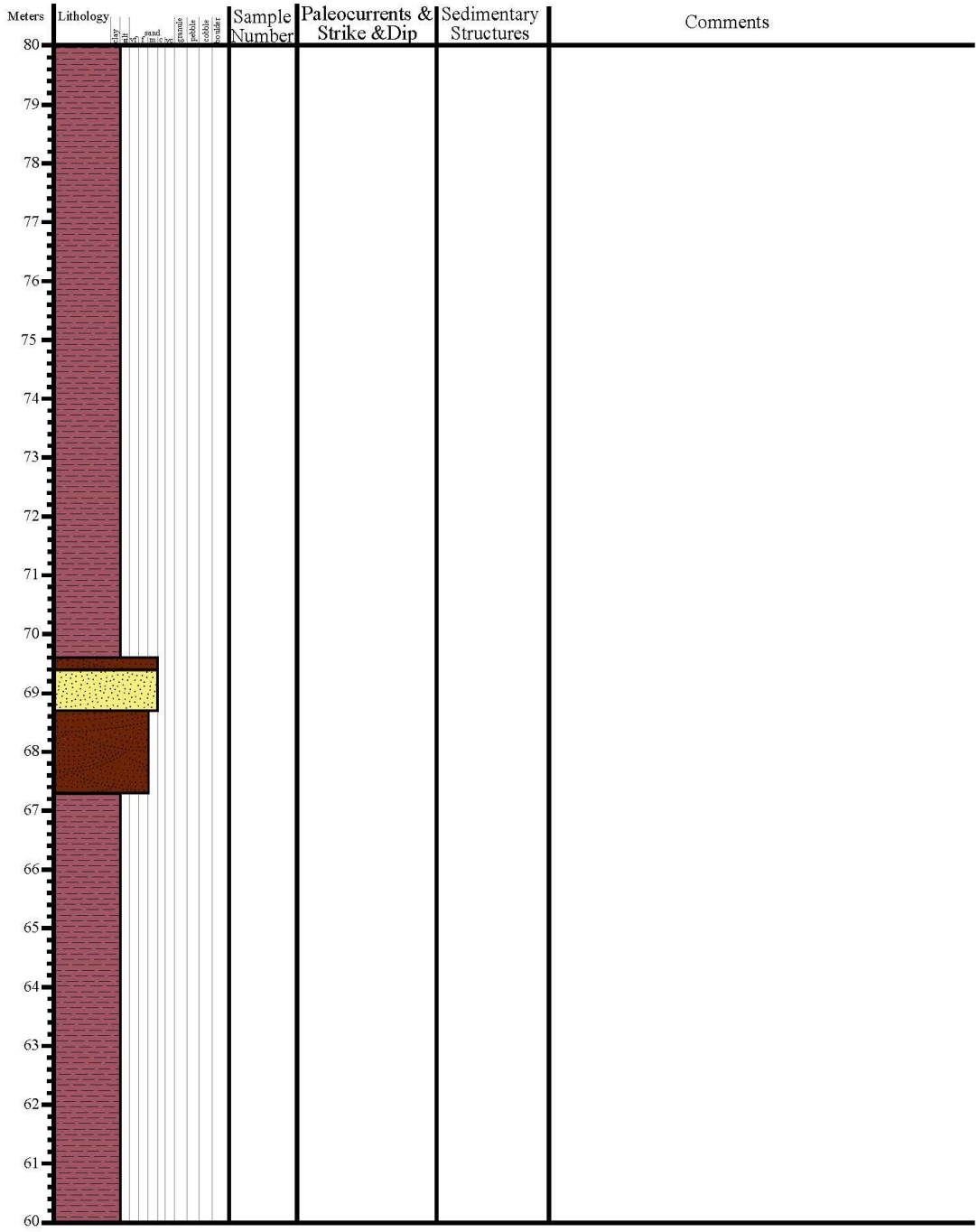

Measured Section 2: MegaFlap (pg. 5)

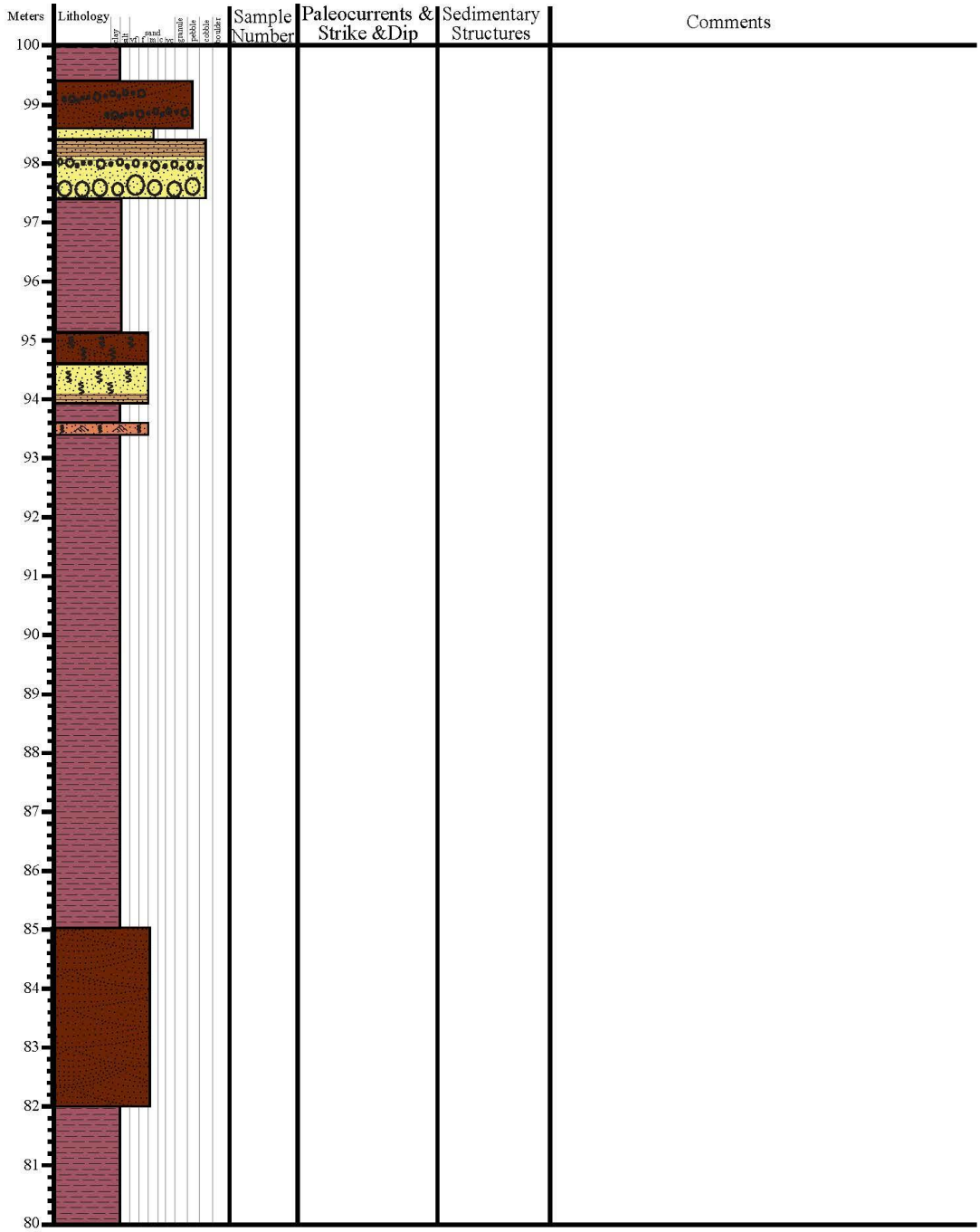

Measured Section 2: MegaFlap (pg. 6)

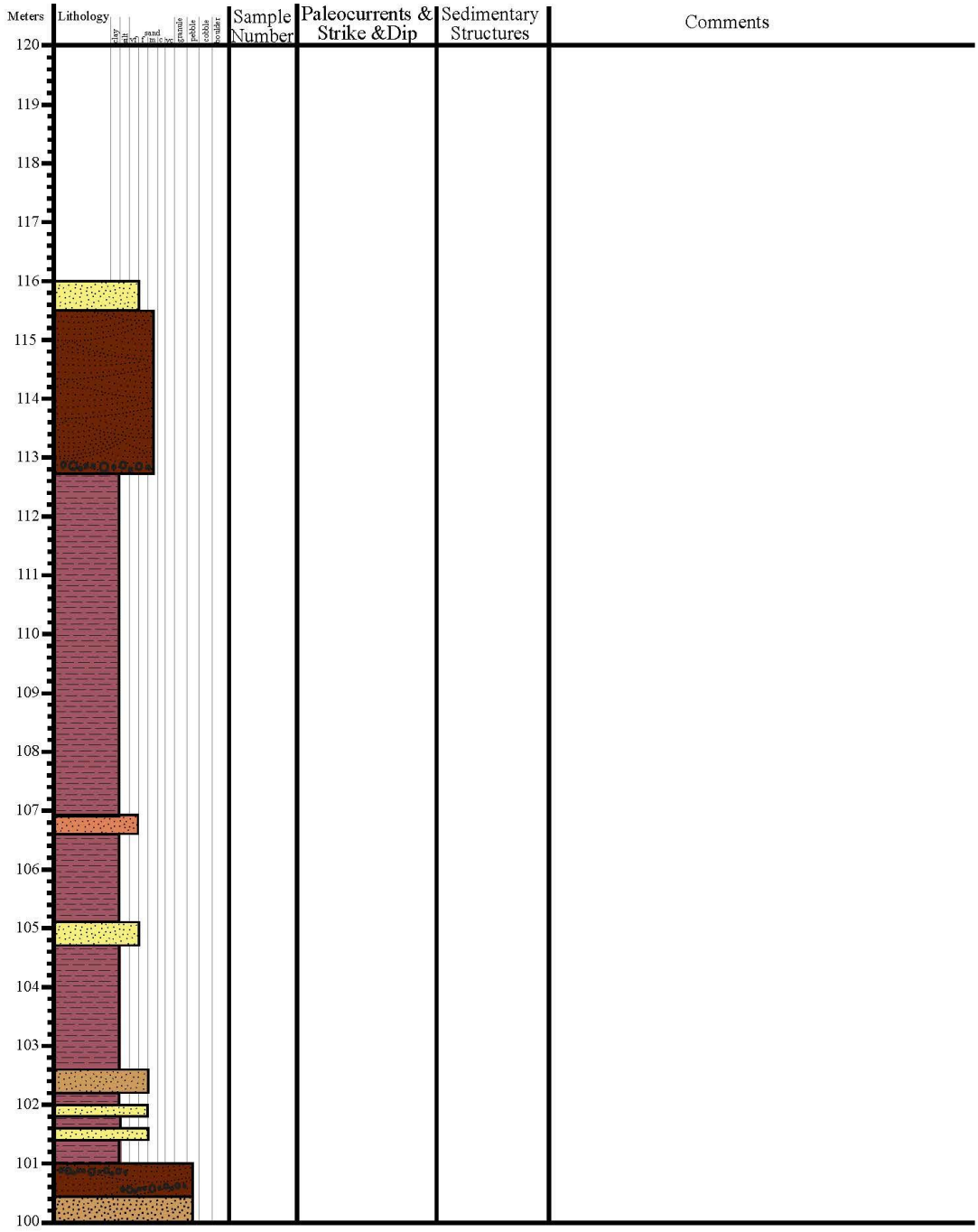

Measured Section 1: Hamm Canyon (pg. 1)

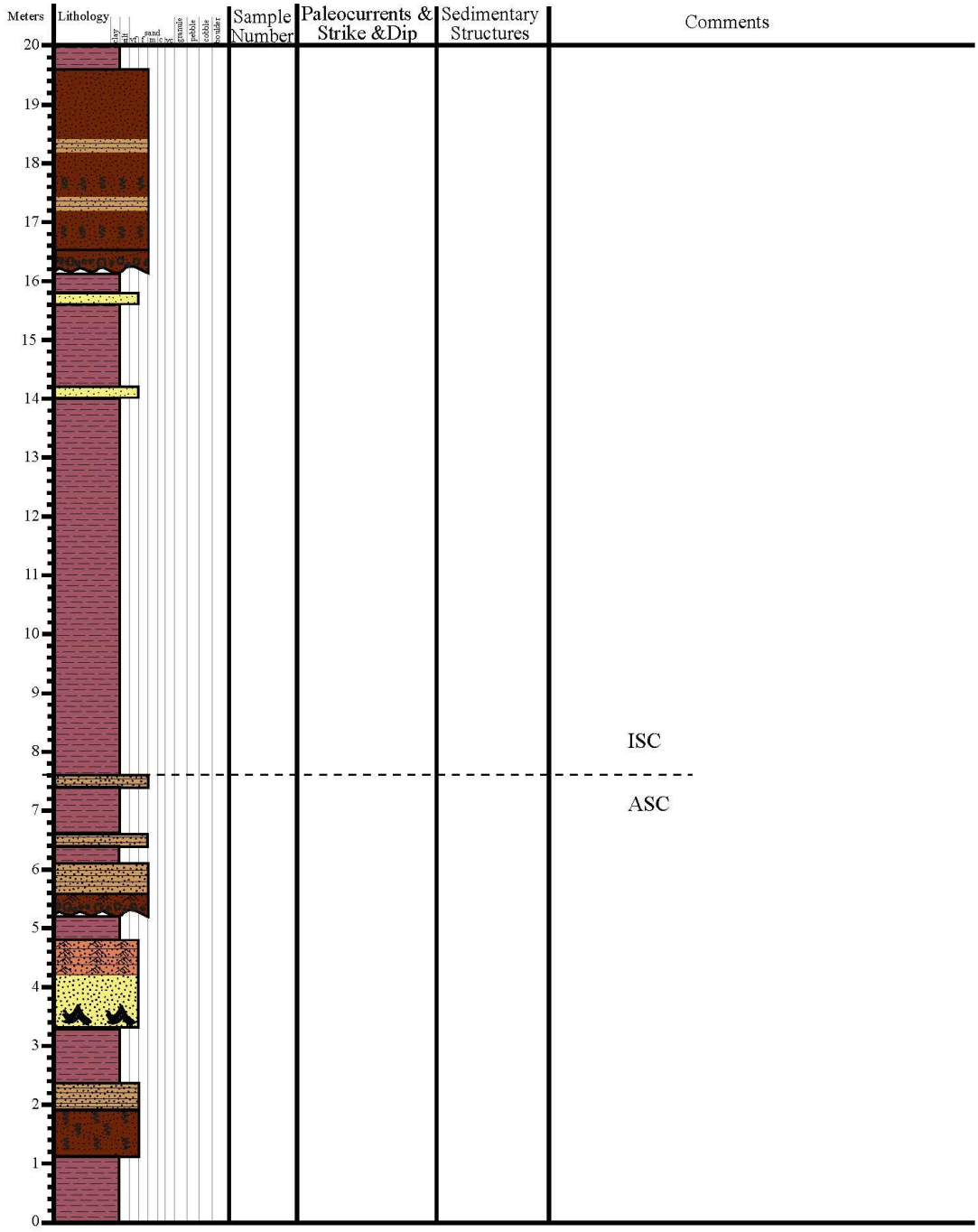

Measured Section 1: Hamm Canyon (pg. 2)

Start
End

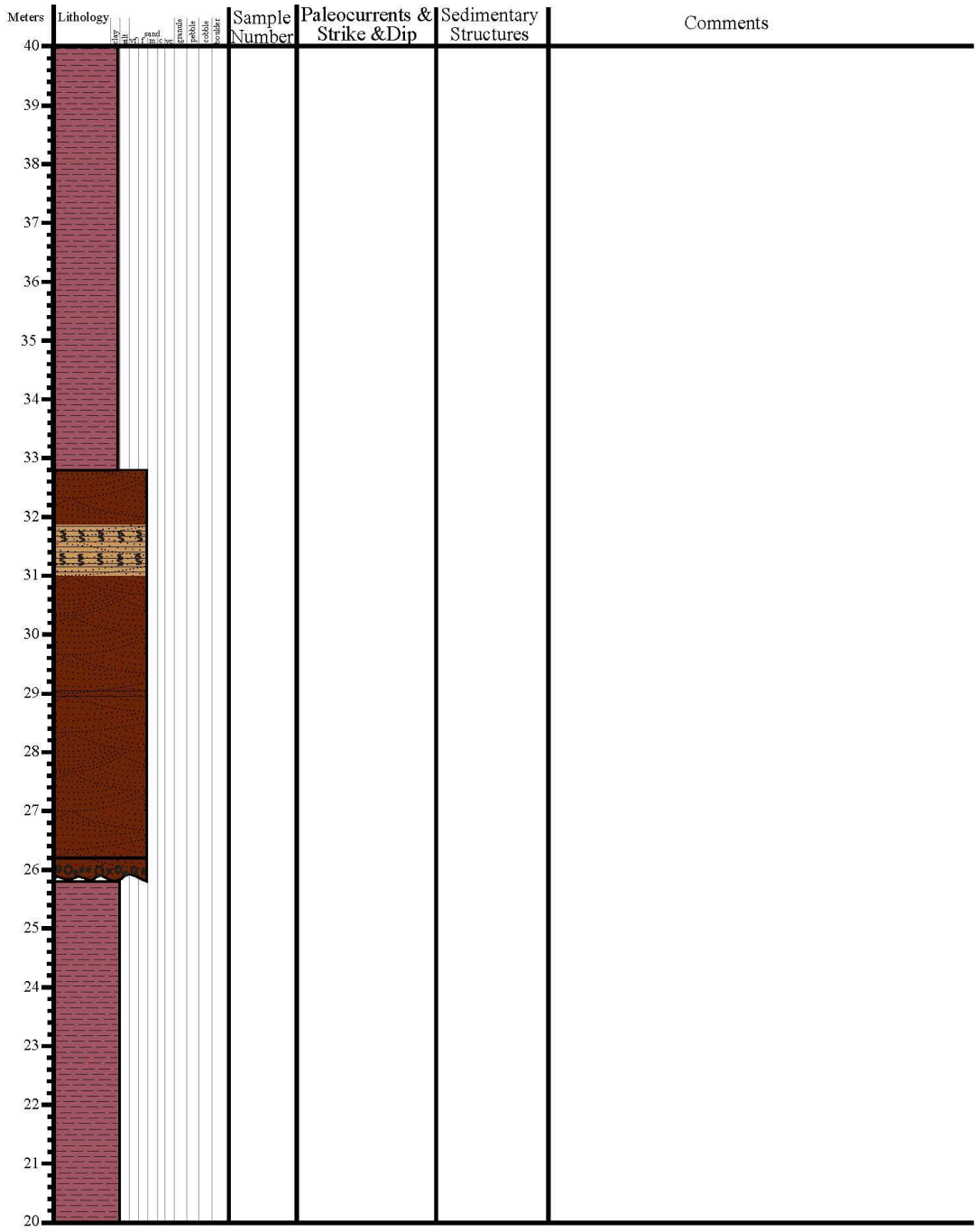

Measured Section 1: Hamm Canyon (pg. 3)

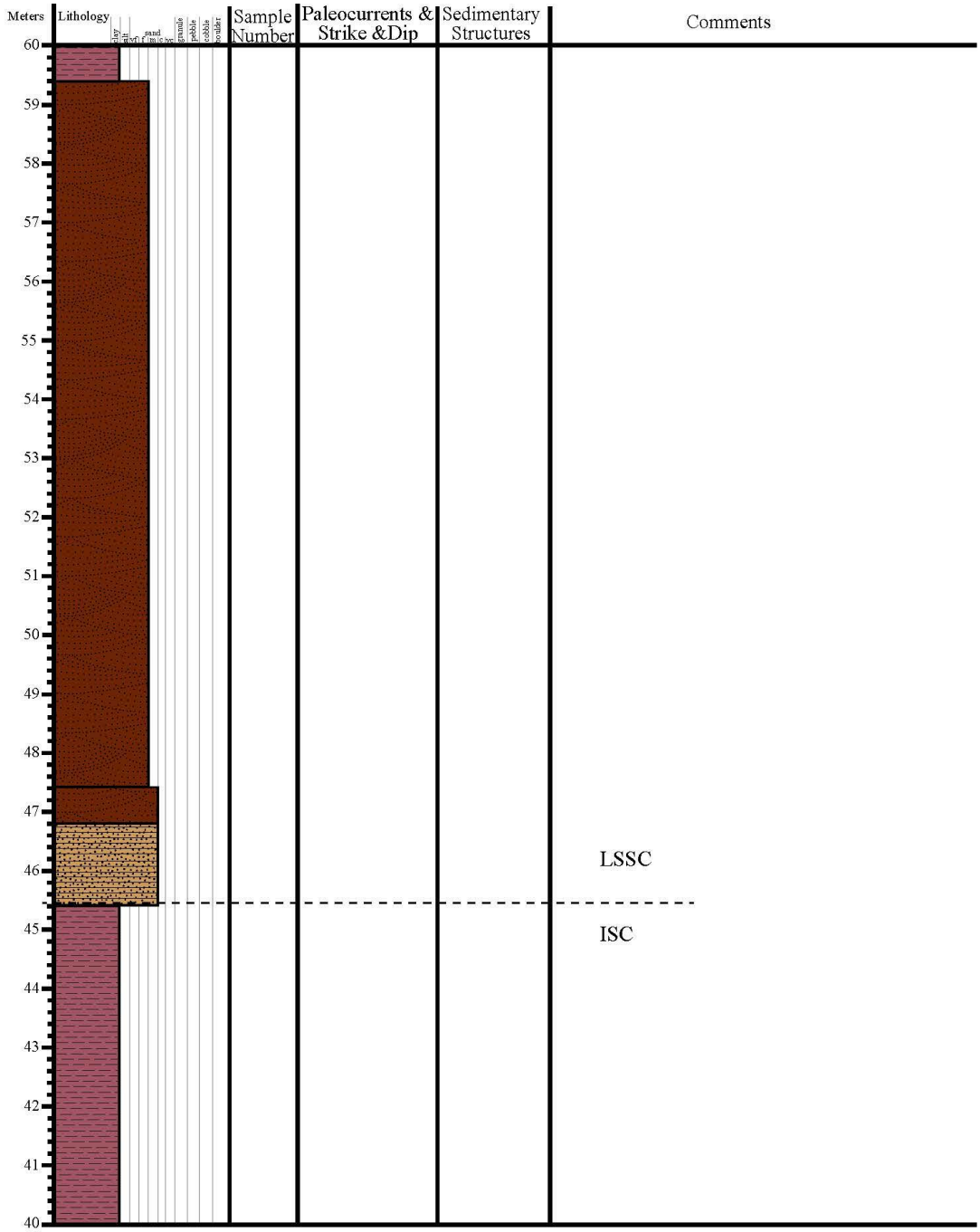

Measured Section 1: Hamm Canyon (pg. 4)

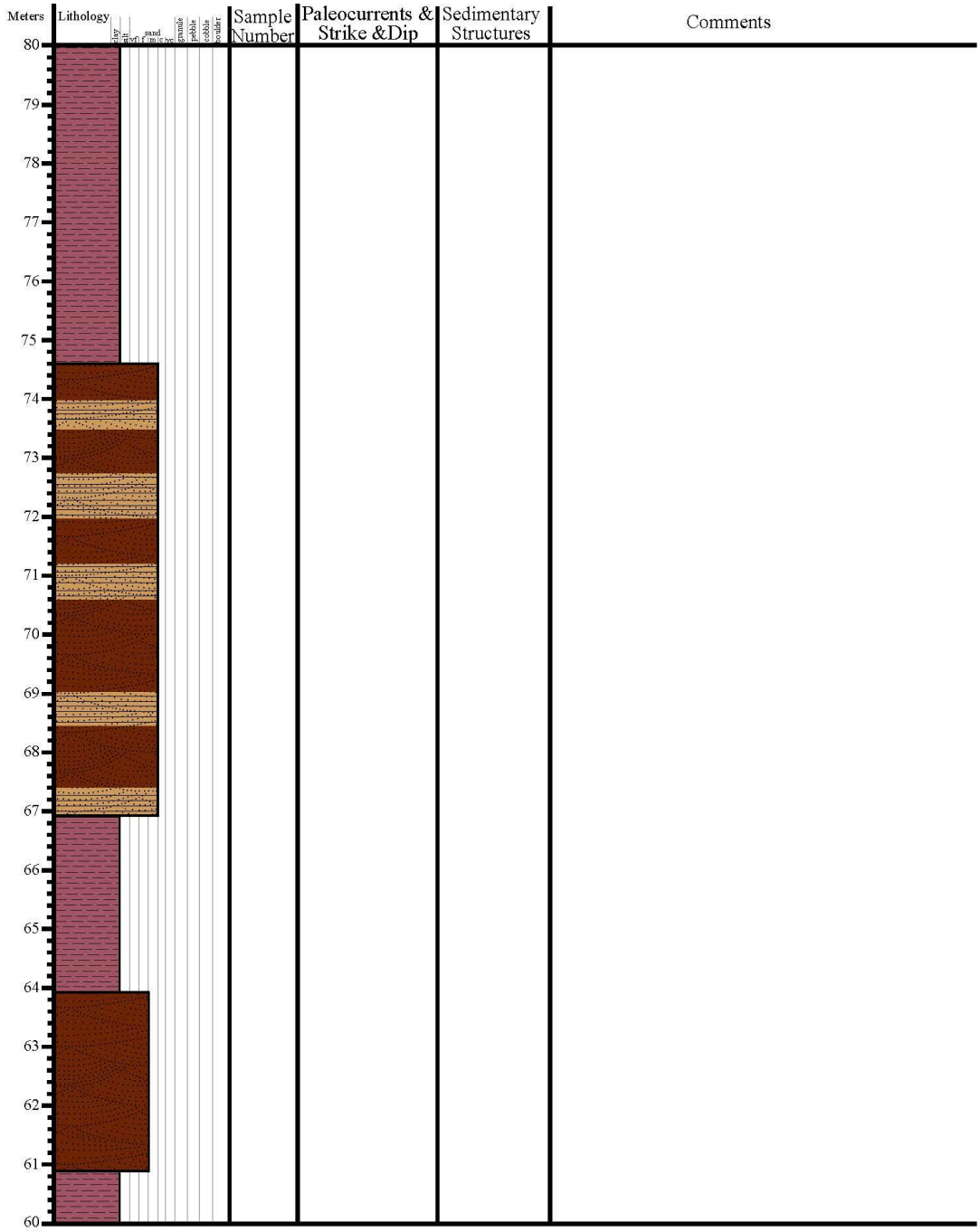

Measured Section 1: Hamm Canyon (pg. 5)

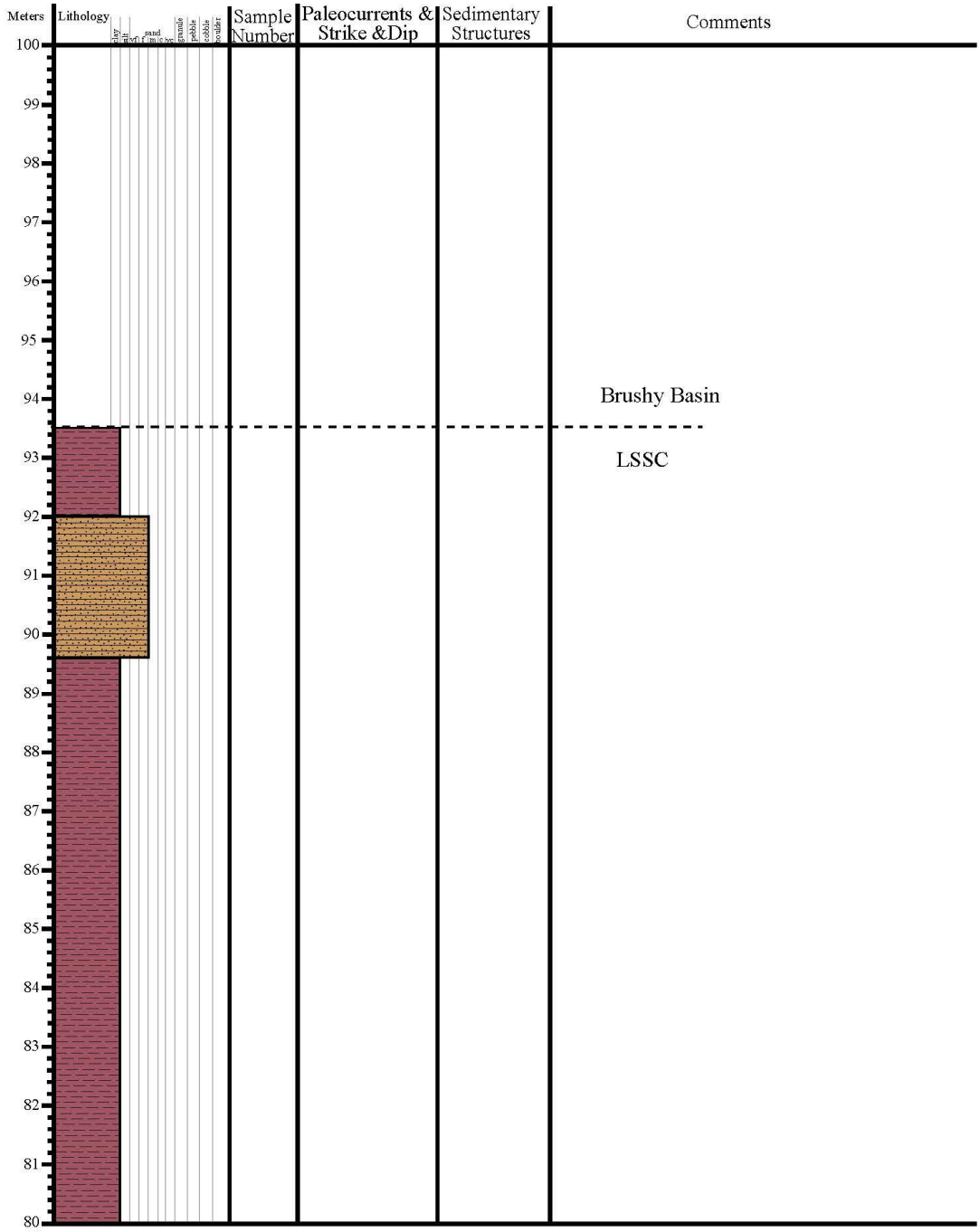

Measured Section 2:Hamm Canyon (pg. 1)

Measured Section 2: Hamm Canyon (pg. 2)

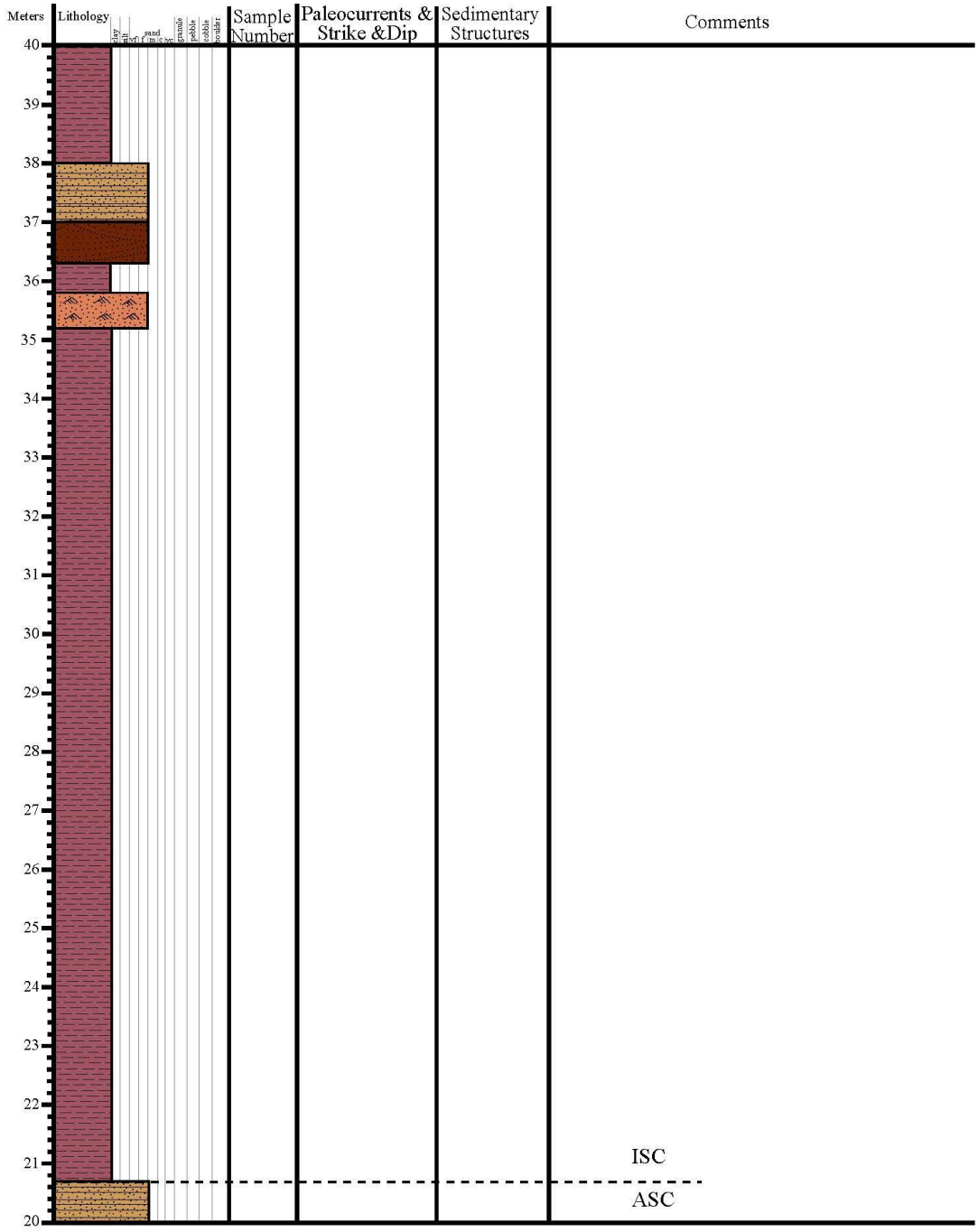

Measured Section 2: Hamm Canyon (pg. 3)

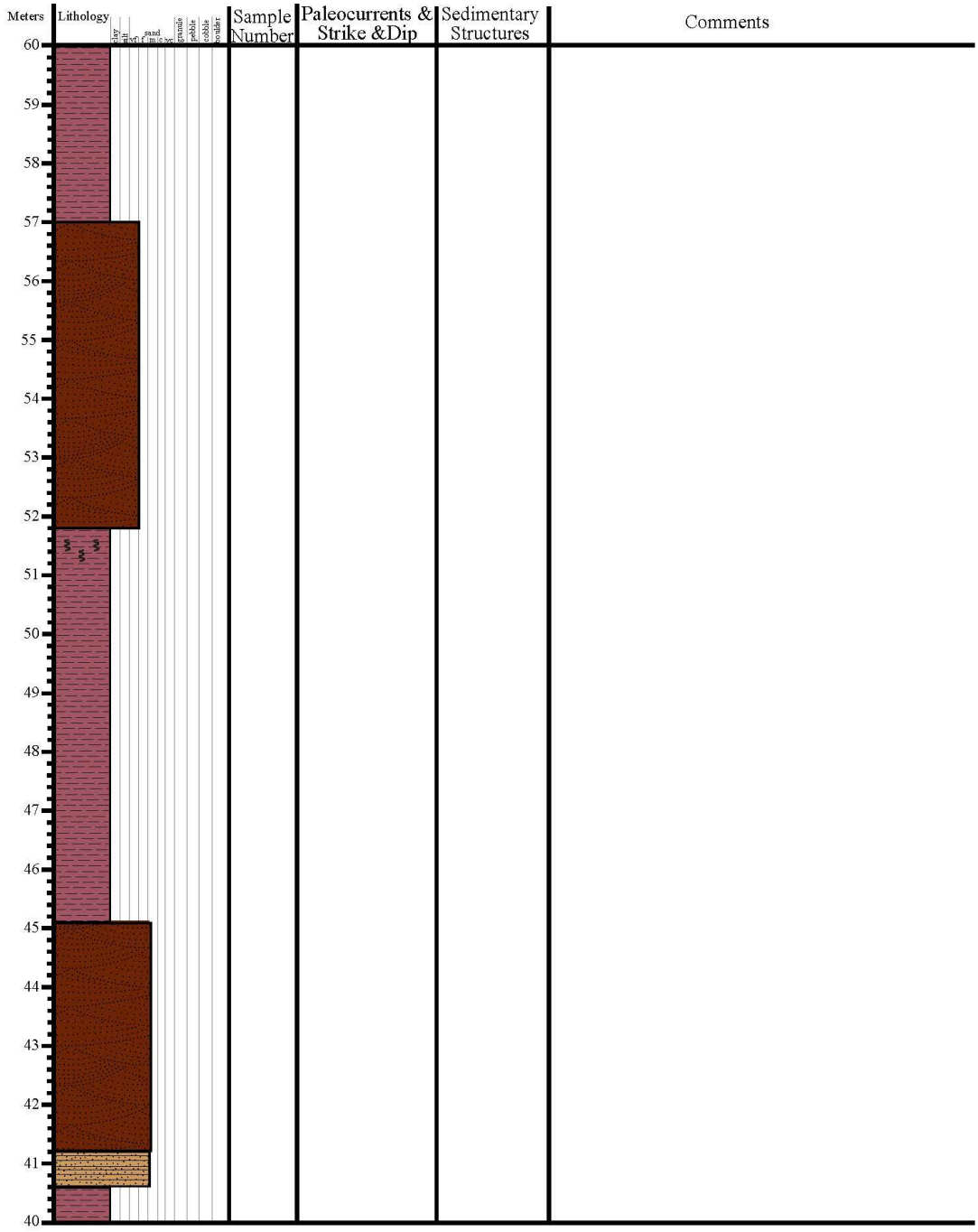

Measured Section 2: Hamm Canyon (pg. 4)

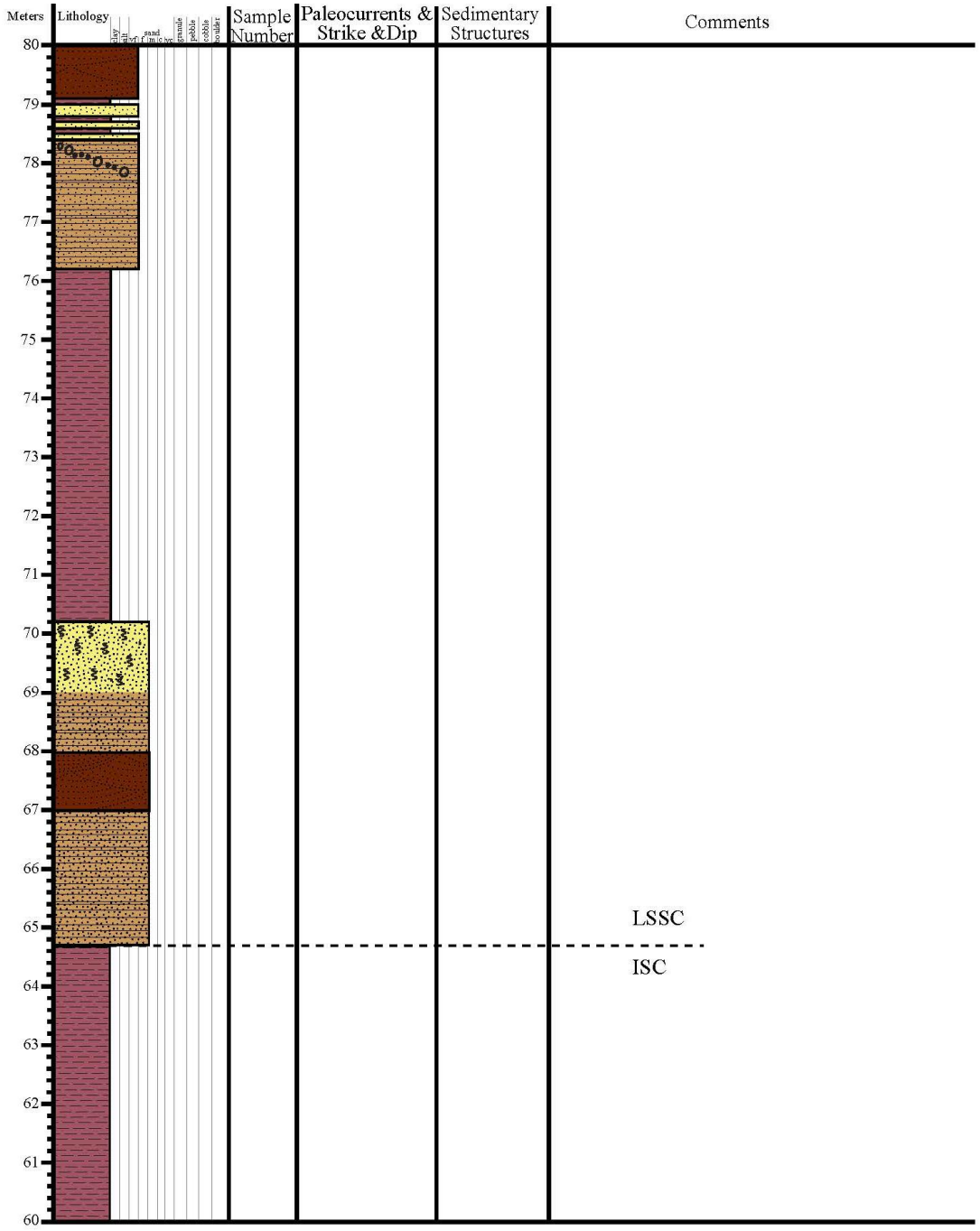

Measured Section 2: Hamm Canyon (pg. 5)

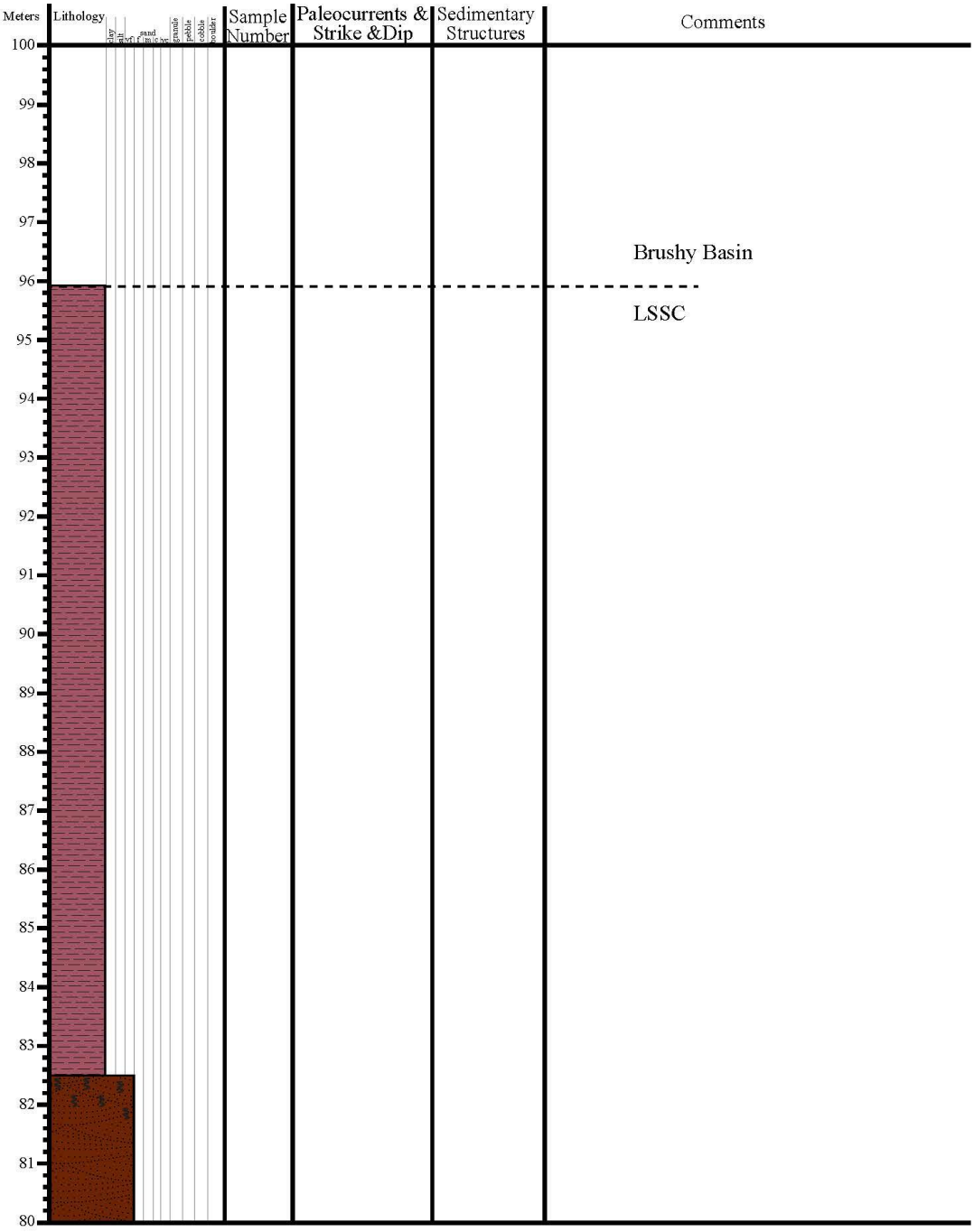

Measured Section 3: Hamm Canyon (pg. 1)

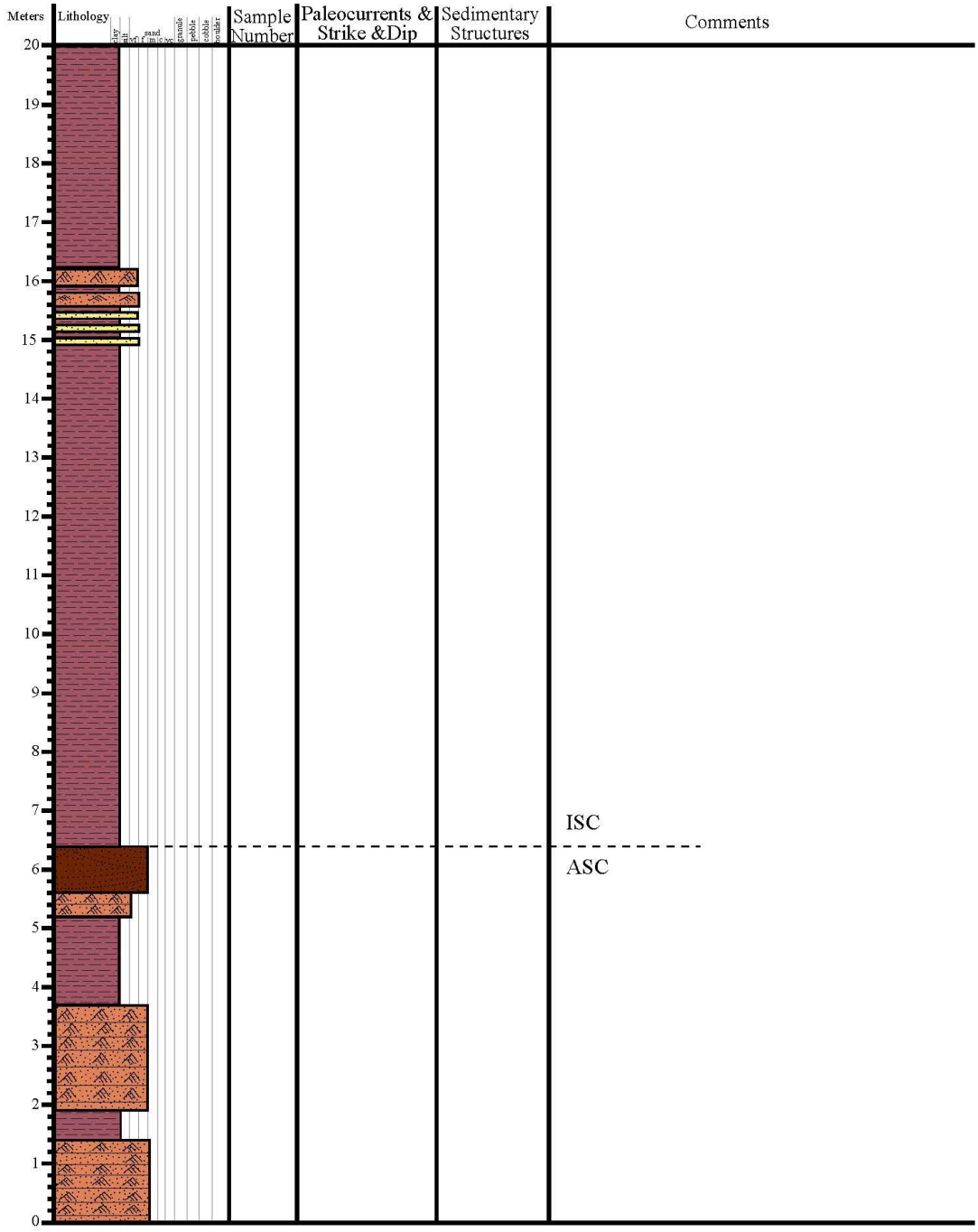

Measured Section 3: Hamm Canyon (pg. 2)

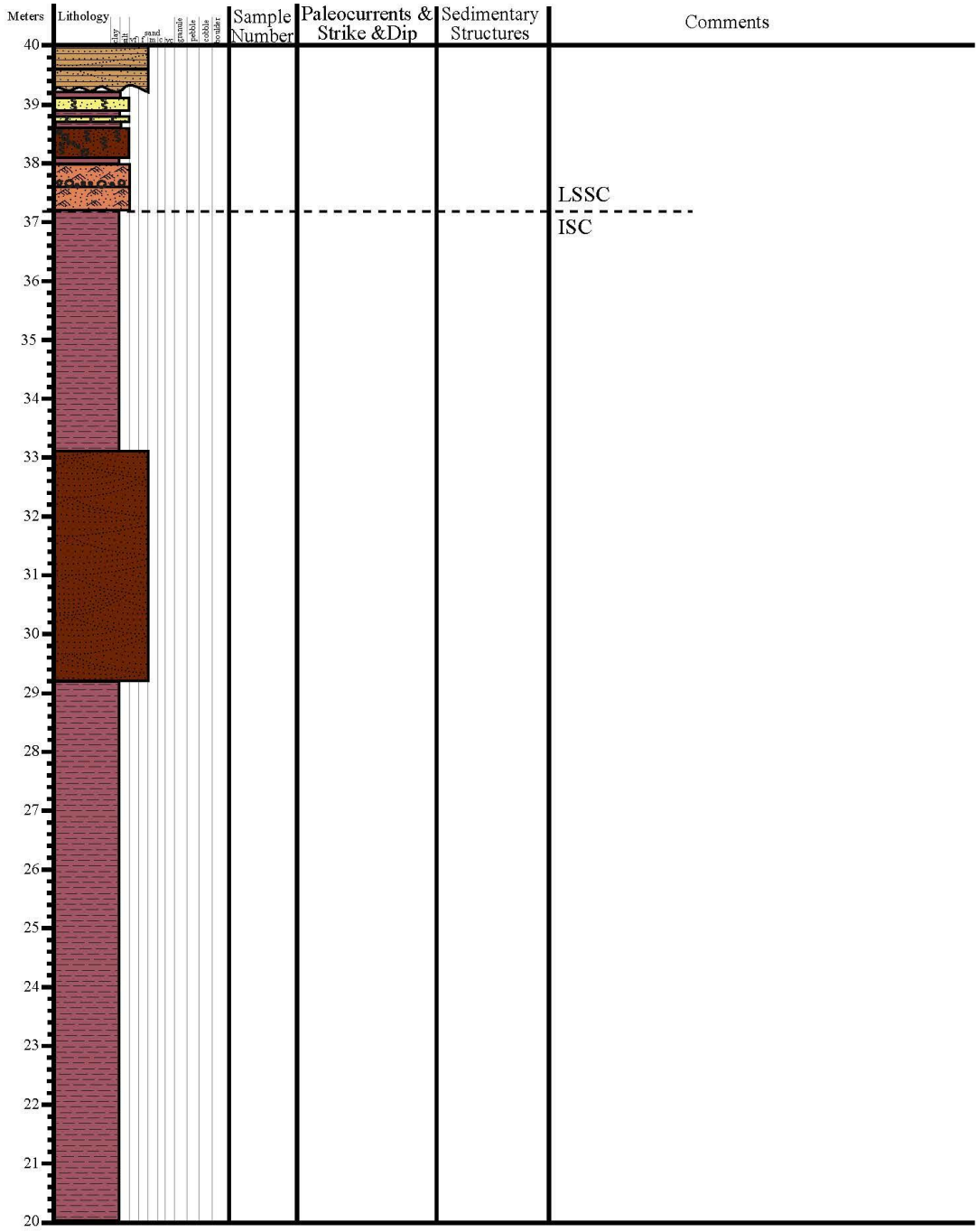

Measured Section 3: Hamm Canyon (pg. 3)

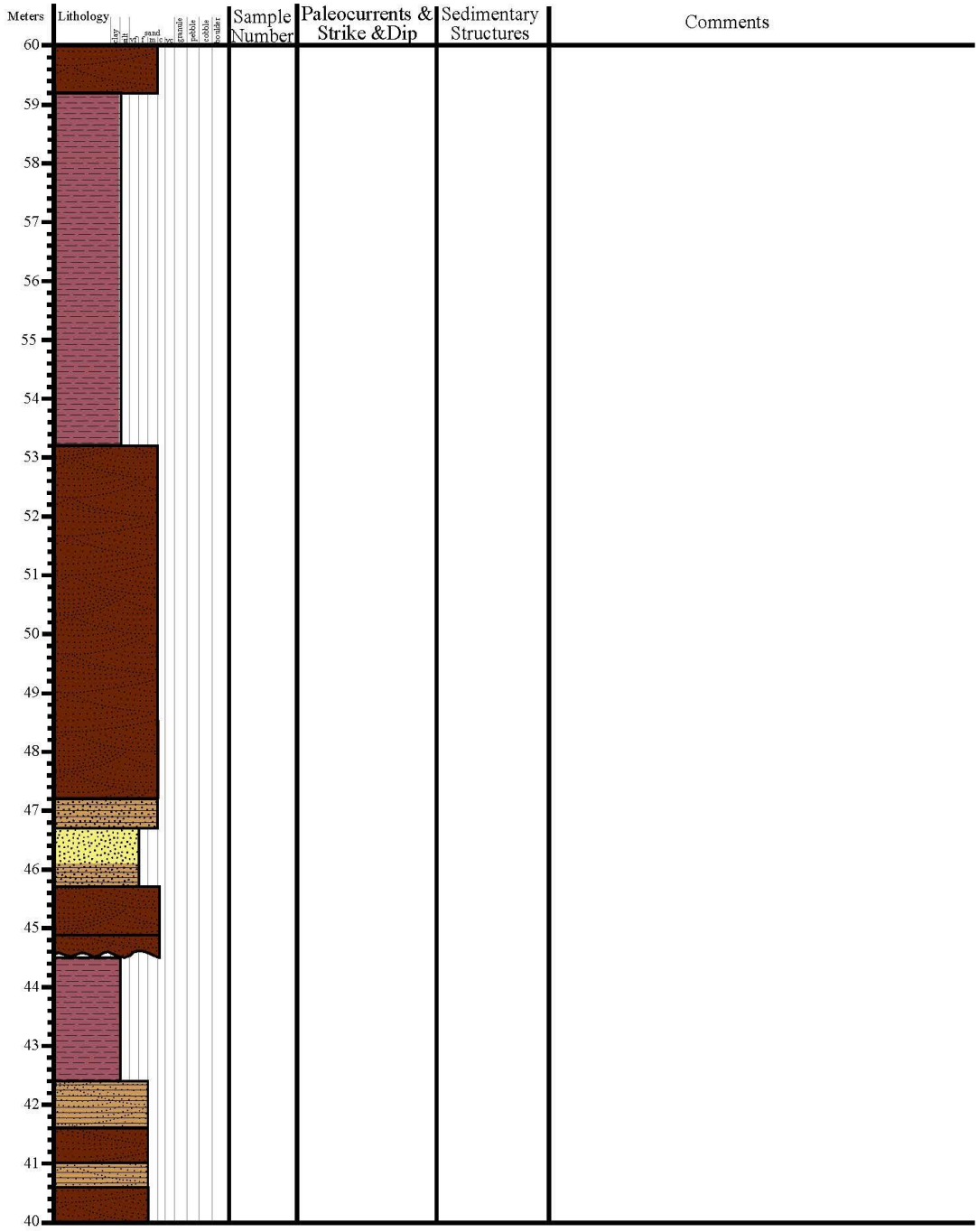

Measured Section 3: Hamm Canyon (pg. 4)

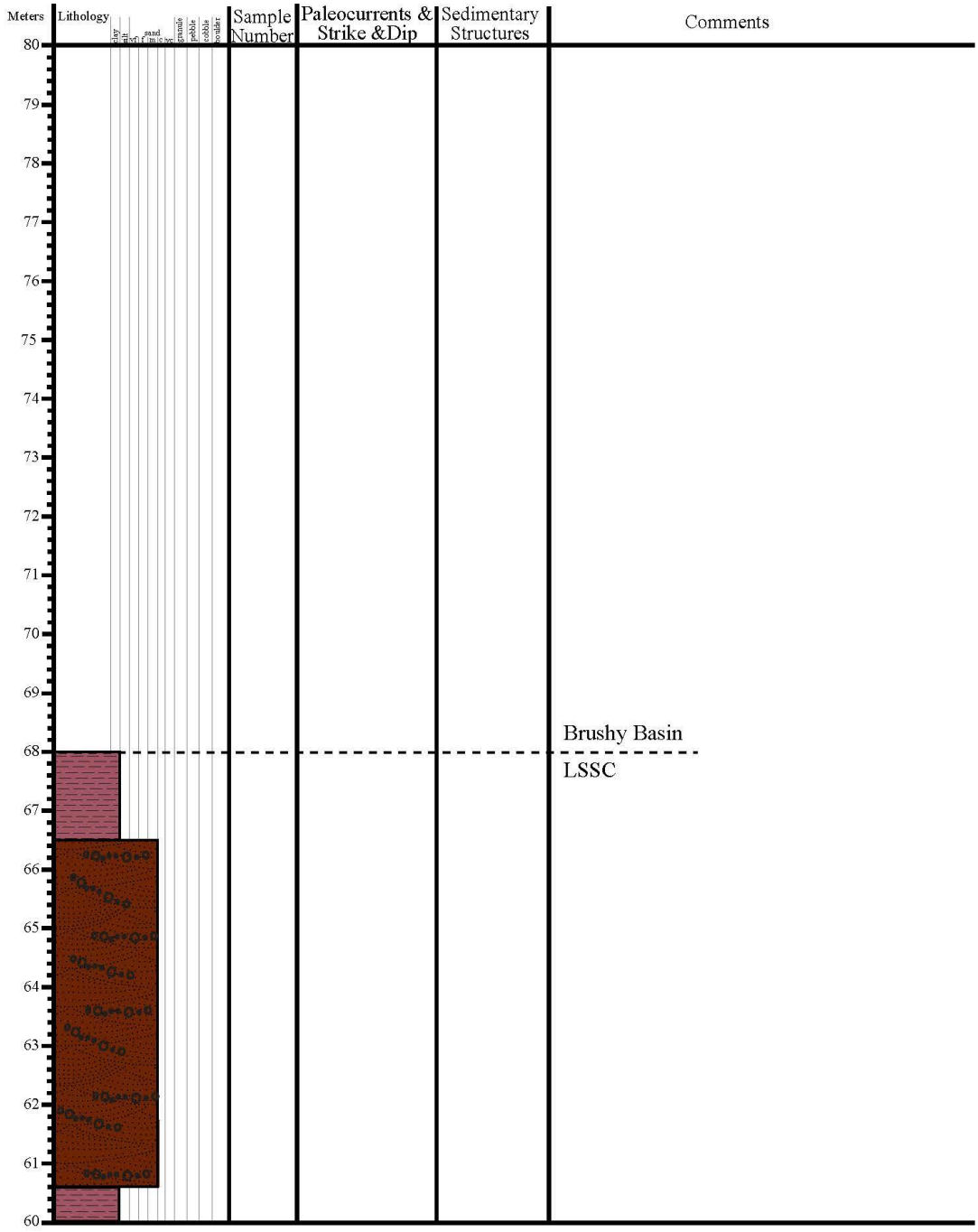

Measured Section 5:Hamm Canyon (pg. 1)

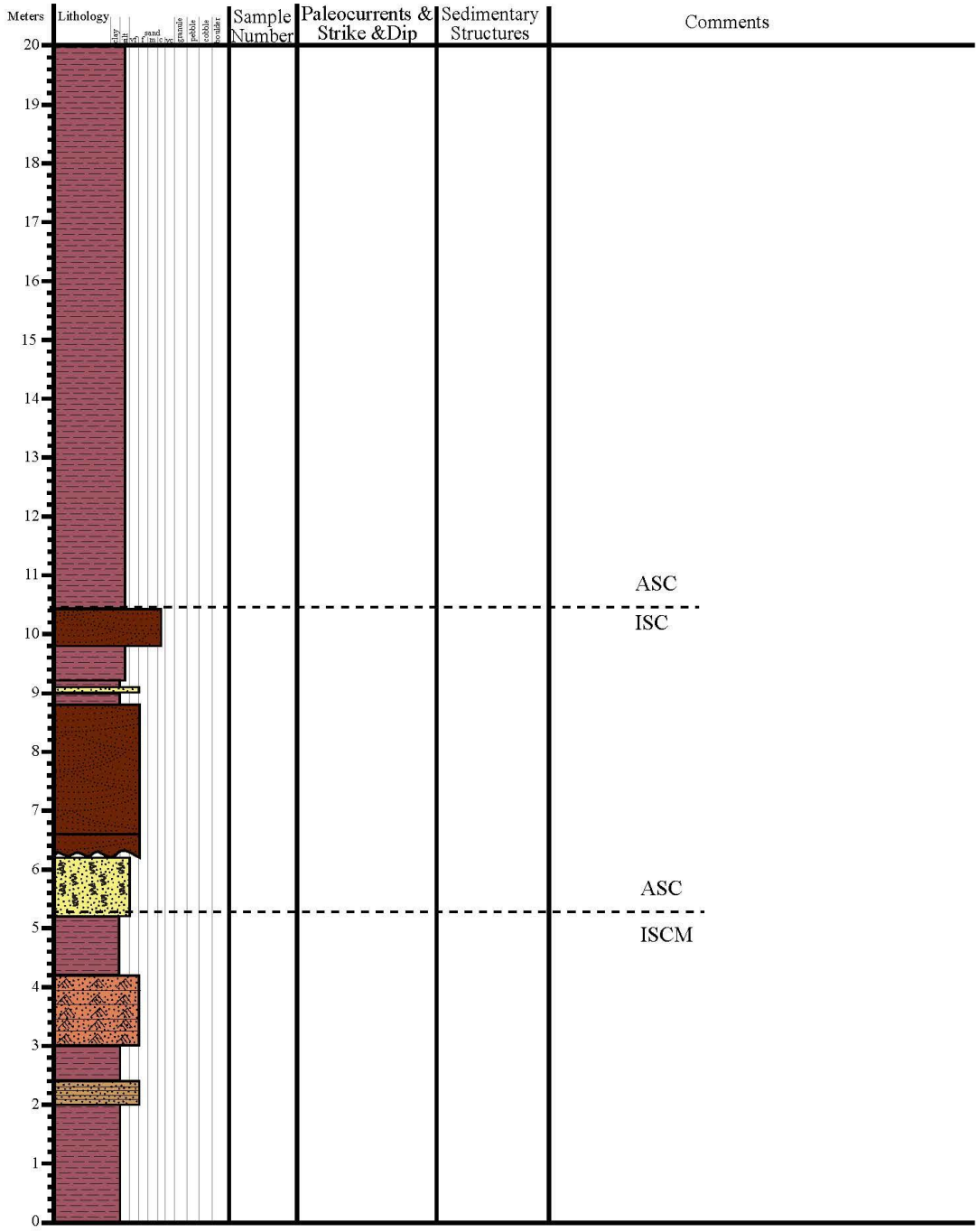

Measured Section 5: Hamm Canyon (pg. 2)

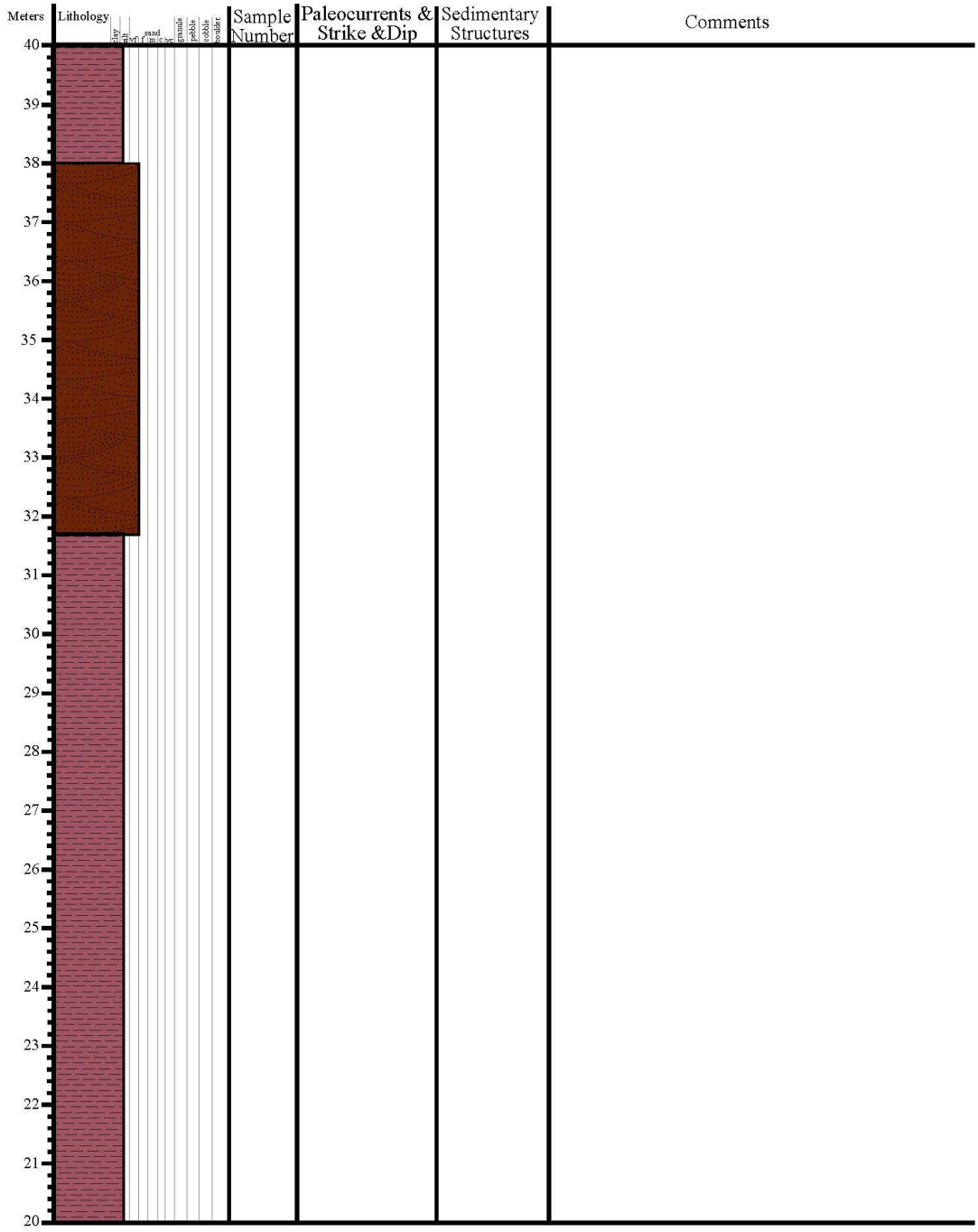

Measured Section 5: Hamm Canyon (pg. 3)

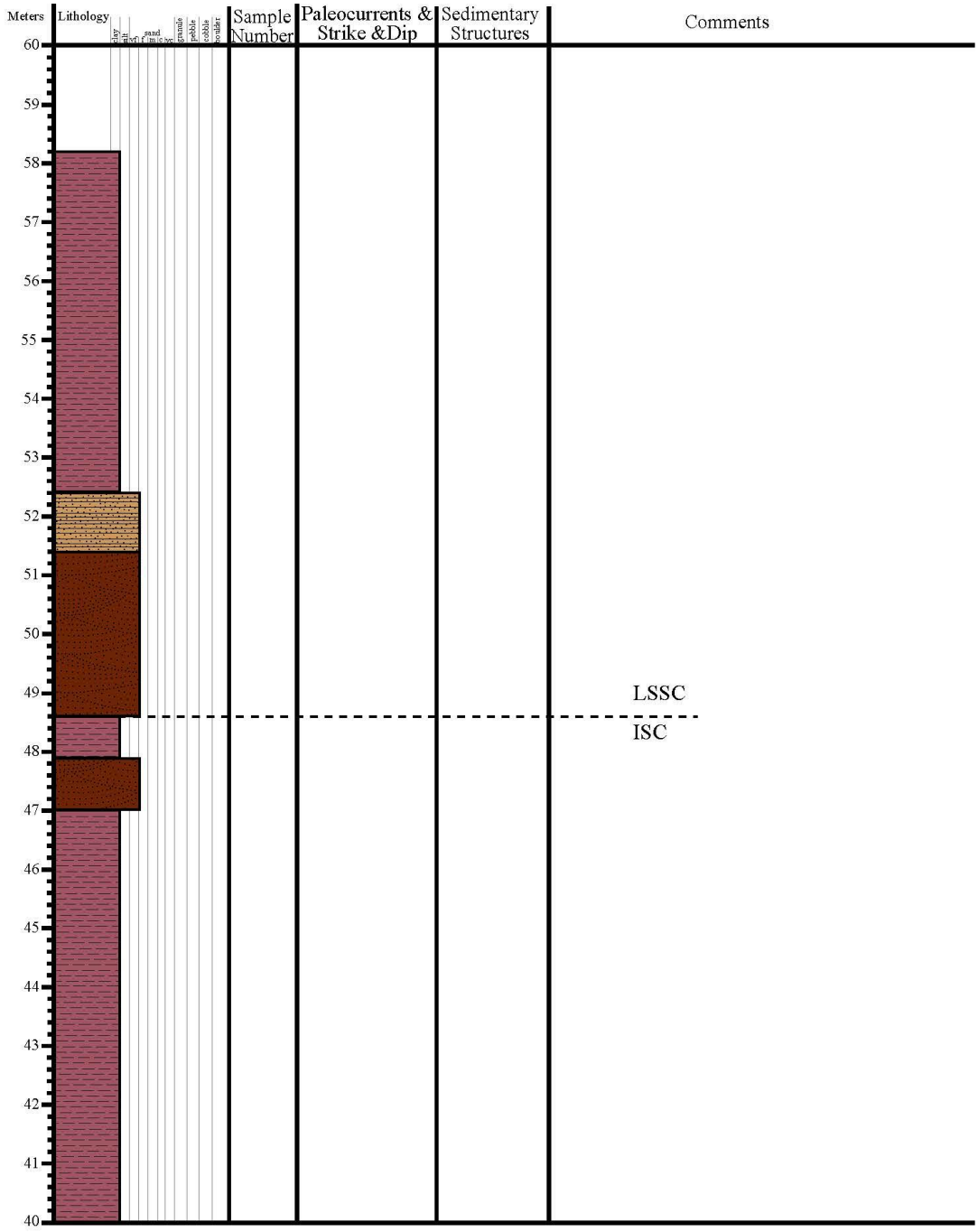

Measured Section 1: The Hat (pg. 1)

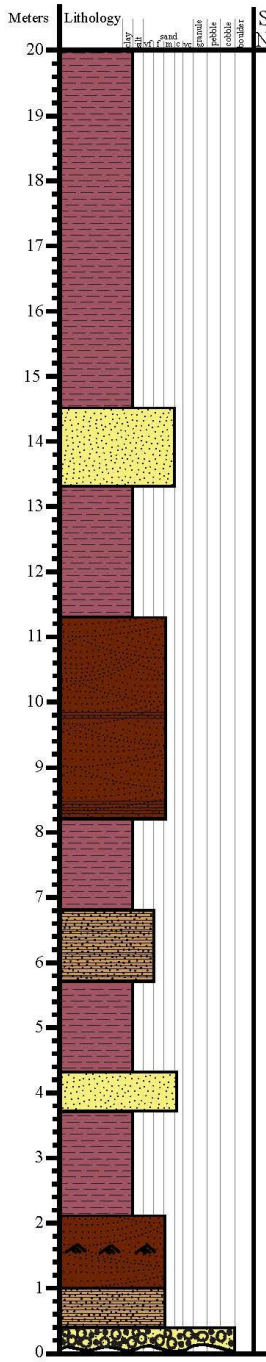

Sample Number	Paleocurrents & Strike &Dip	Sedimentary Structures	Comments
	155°, 160°, 115°	Laminated to trough x-strata	
	105°, 175°, 170°		
	165 15° SW	Ripples, trough x-strata	
1		Laminated	8cm clasts in a upperfine sandy matrix, poorly sorted clasts are angular, limestone. clasts are also granule and pebble sized. Sand grains are subrounded.

Measured Section 1: The Hat (pg. 2)

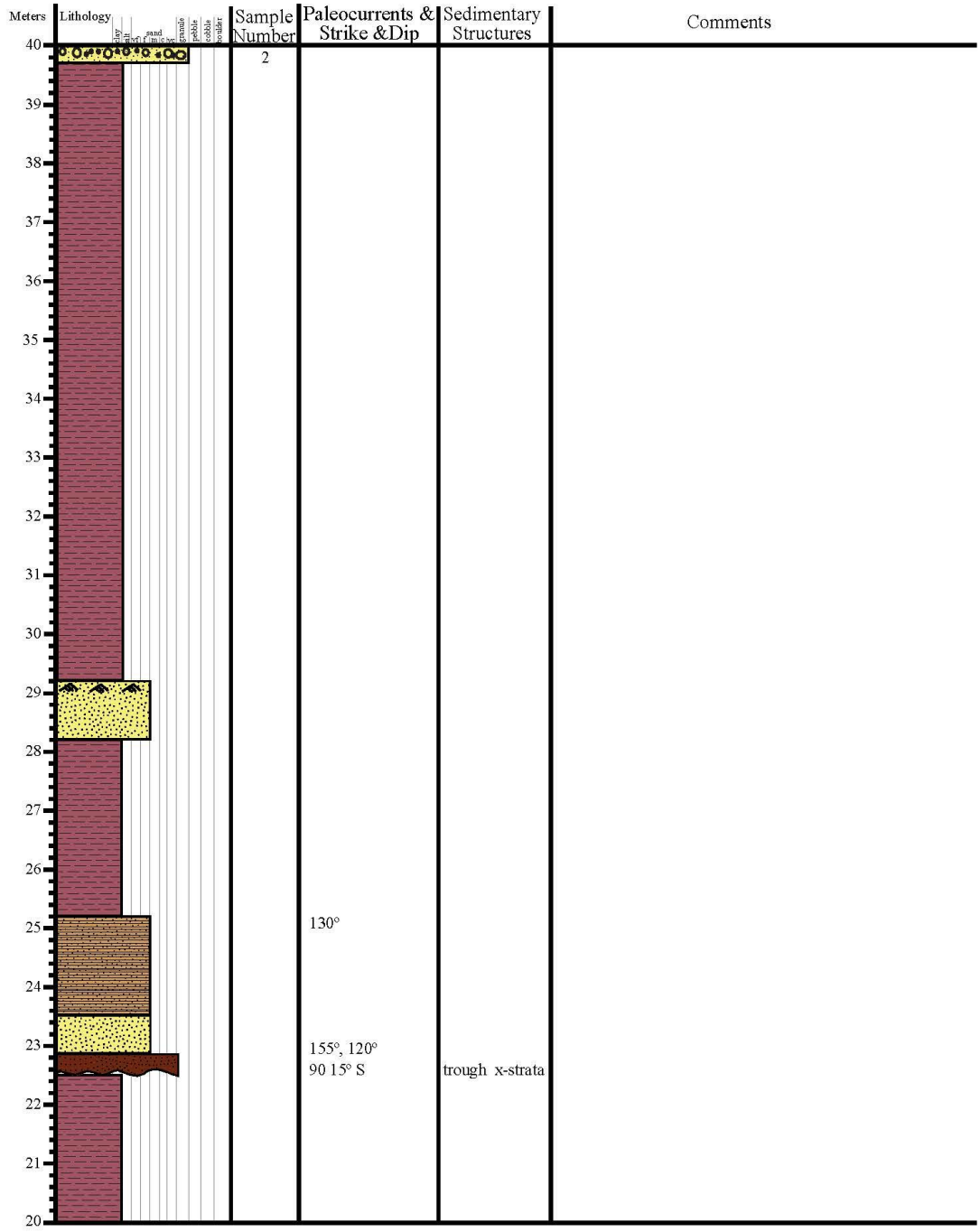

Measured Section 1: The Hat (pg. 3)

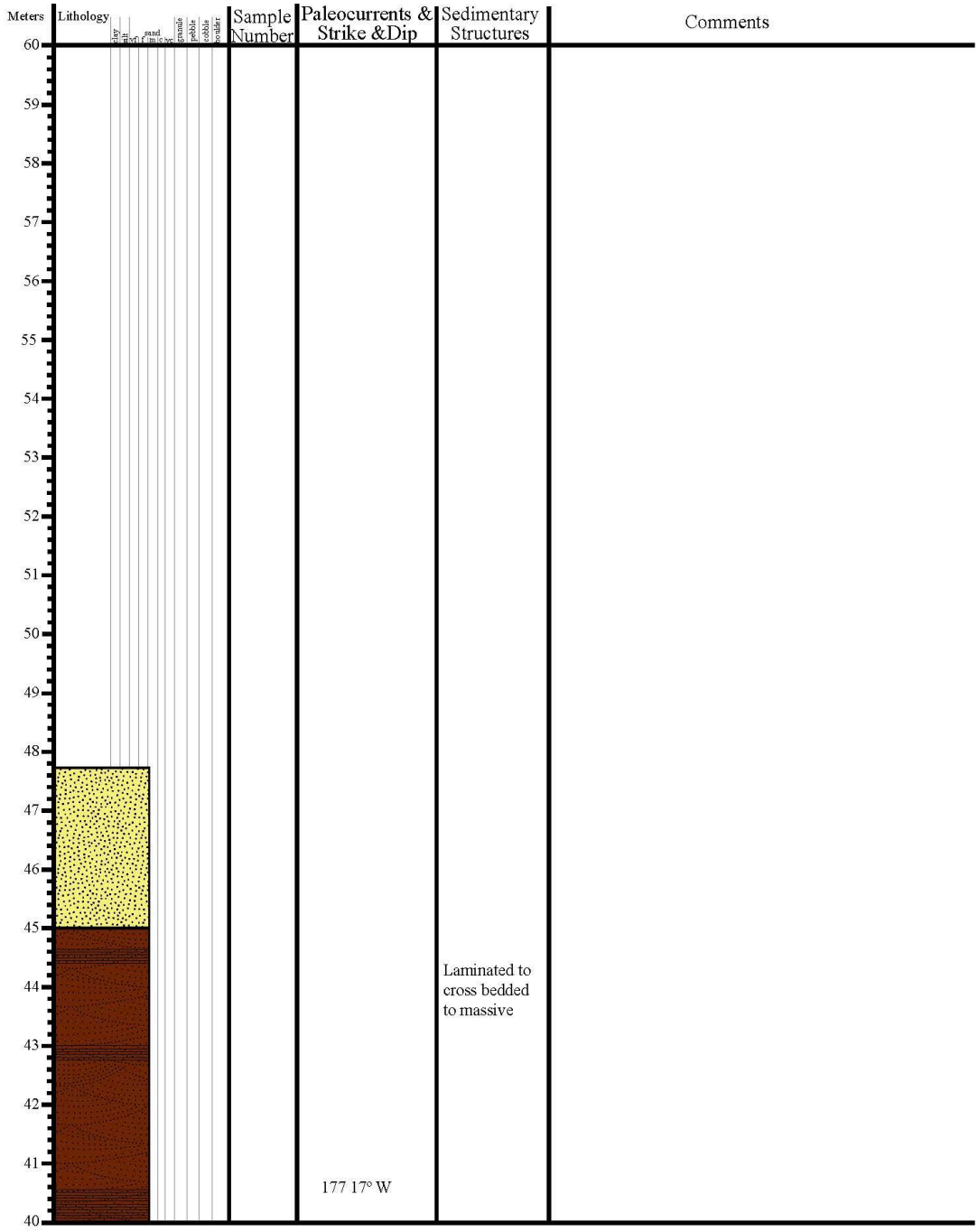

Measured Section 2: The Hat (pg. 1)

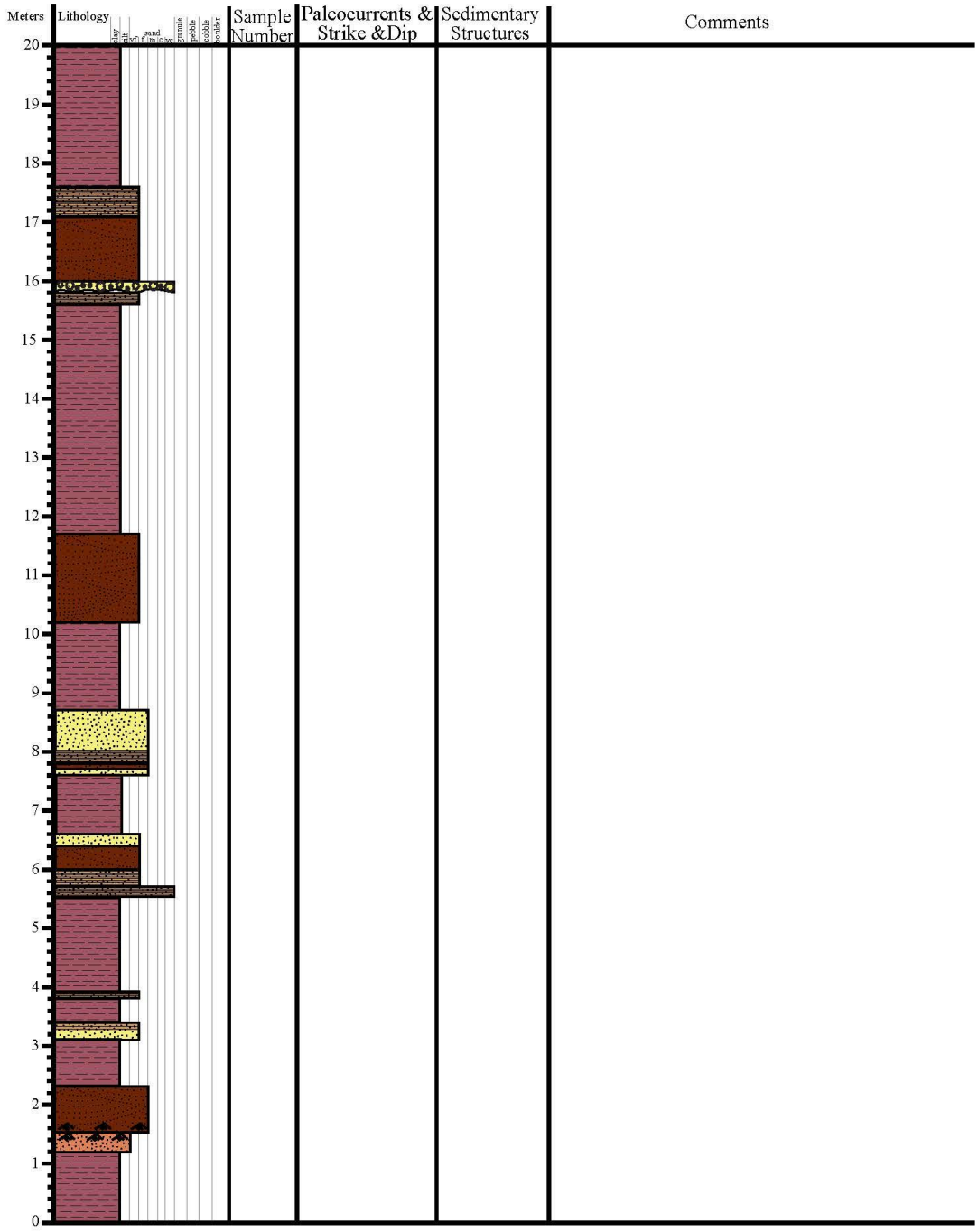

Measured Section 2: The Hat (pg. 2)

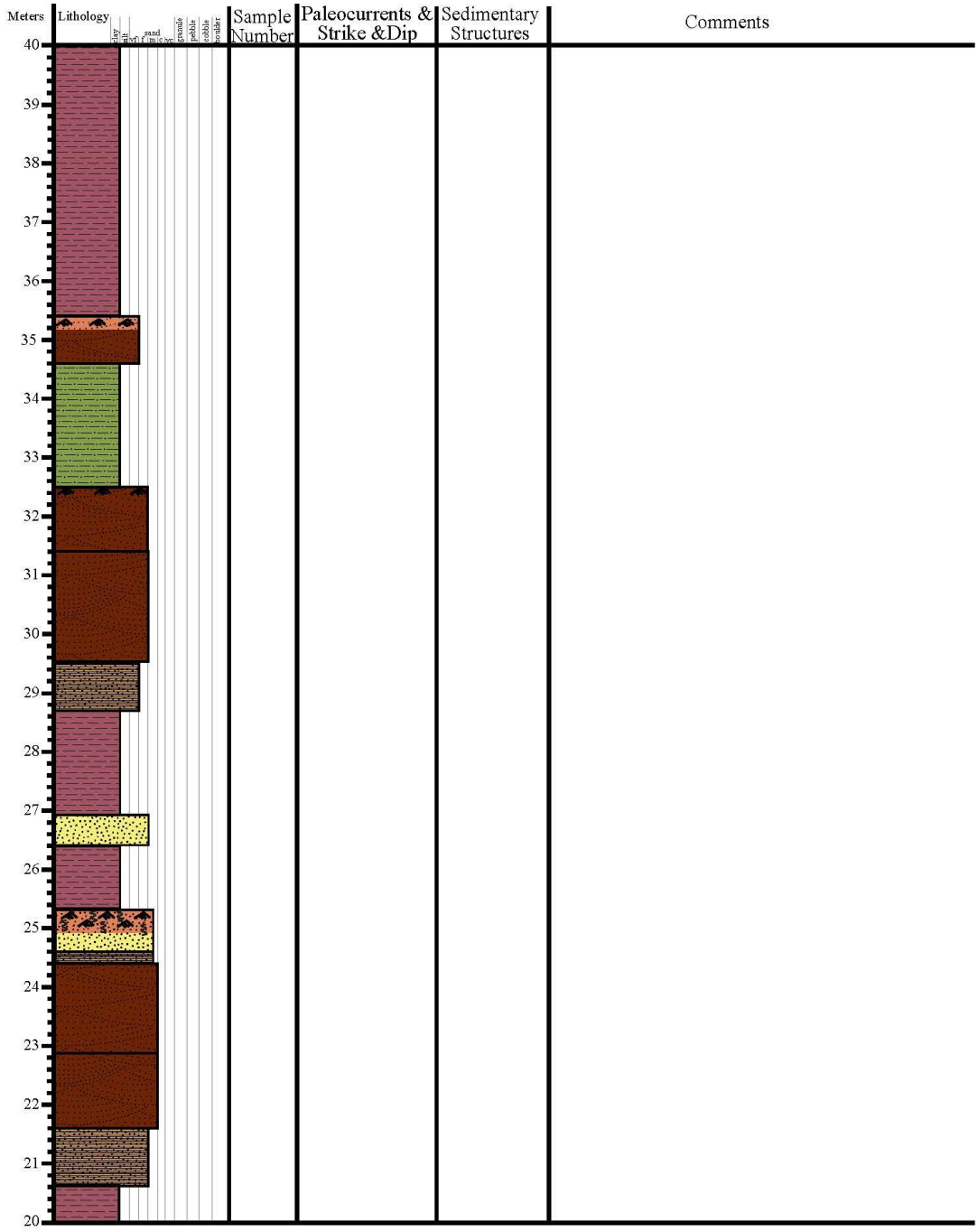

Measured Section 2: The Hat (pg. 3)

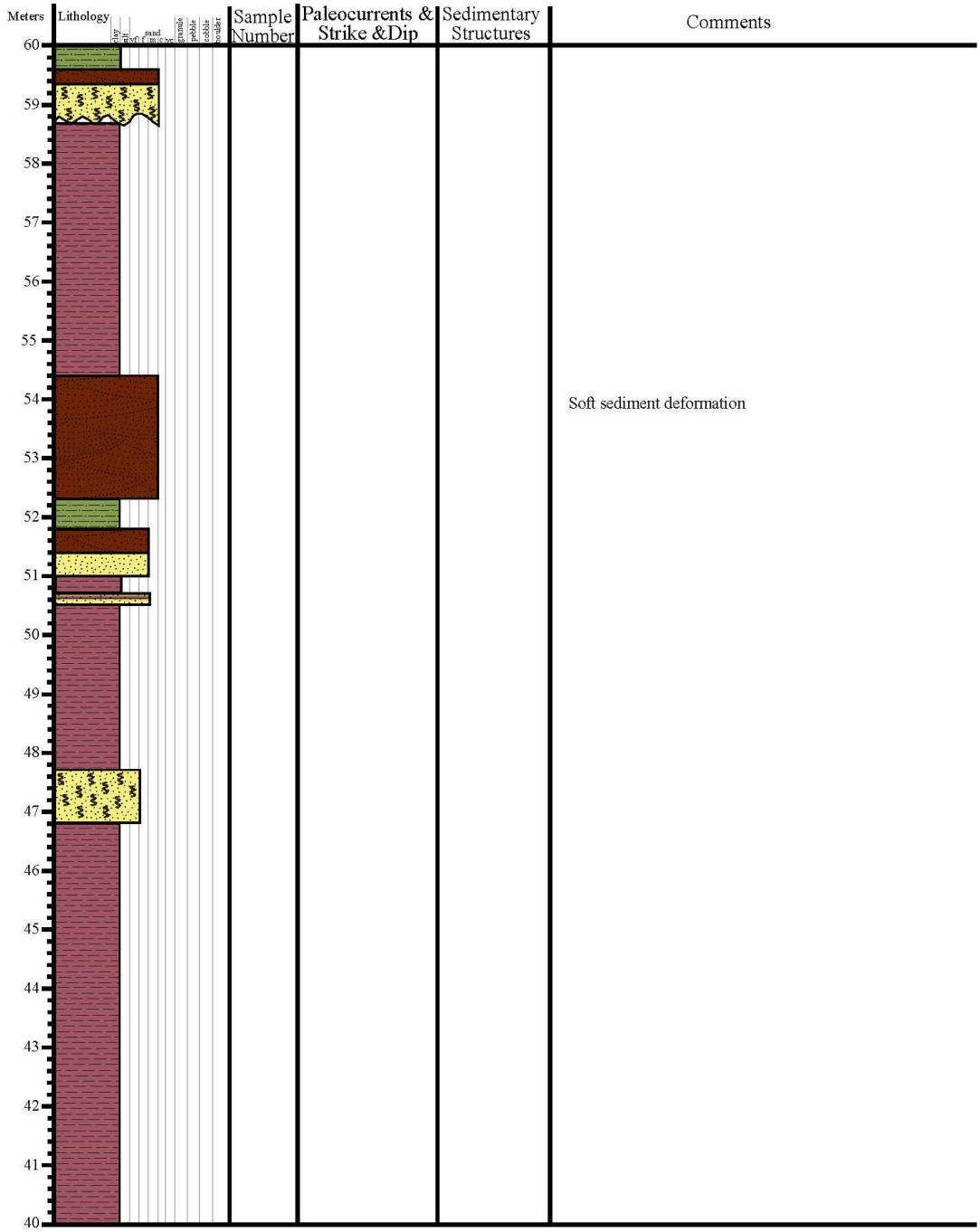

Measured Section 2: The Hat (pg. 4)

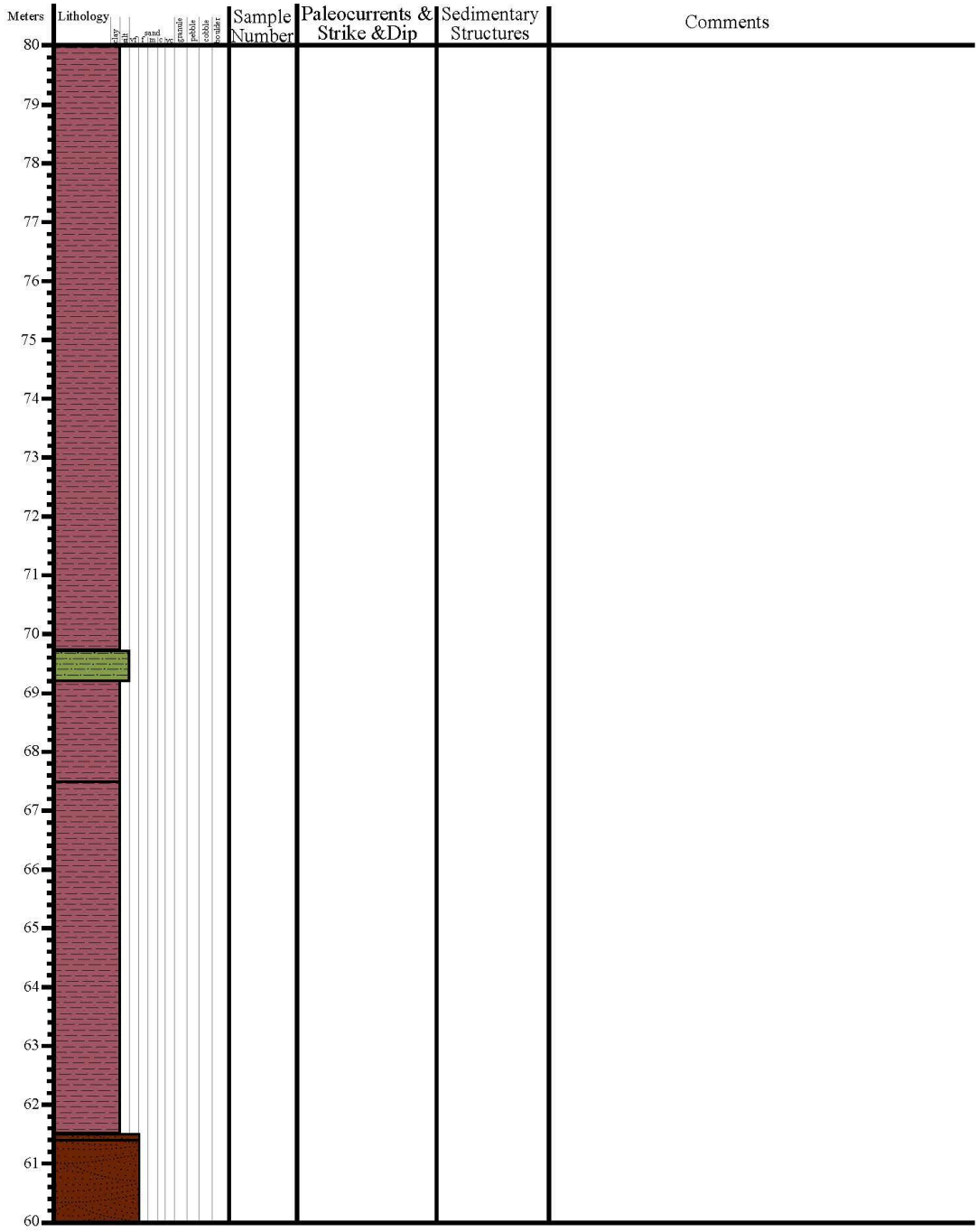

Measured Section 2: The Hat (pg. 5)

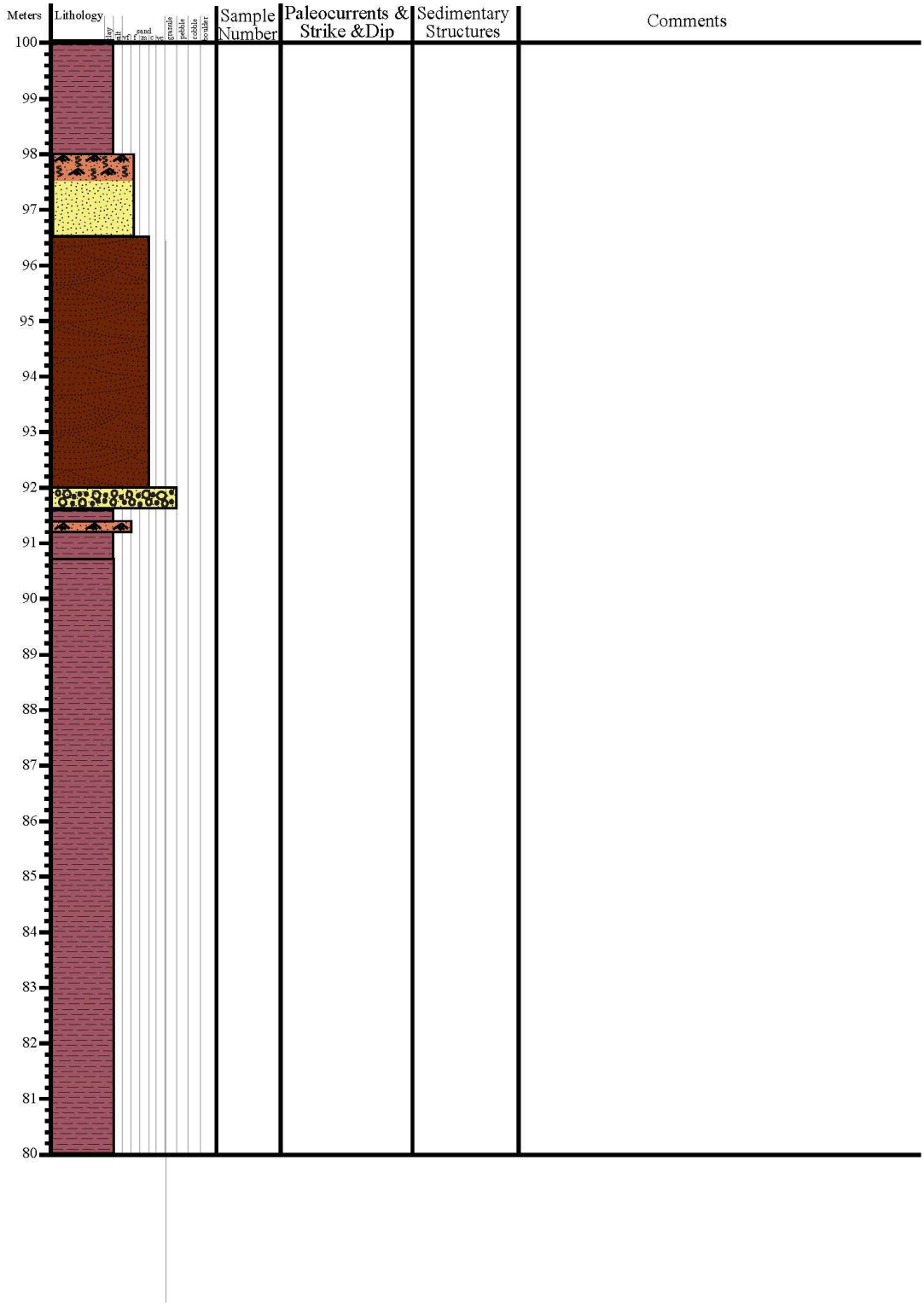

Measured Section 2: The Hat (pg. 6)

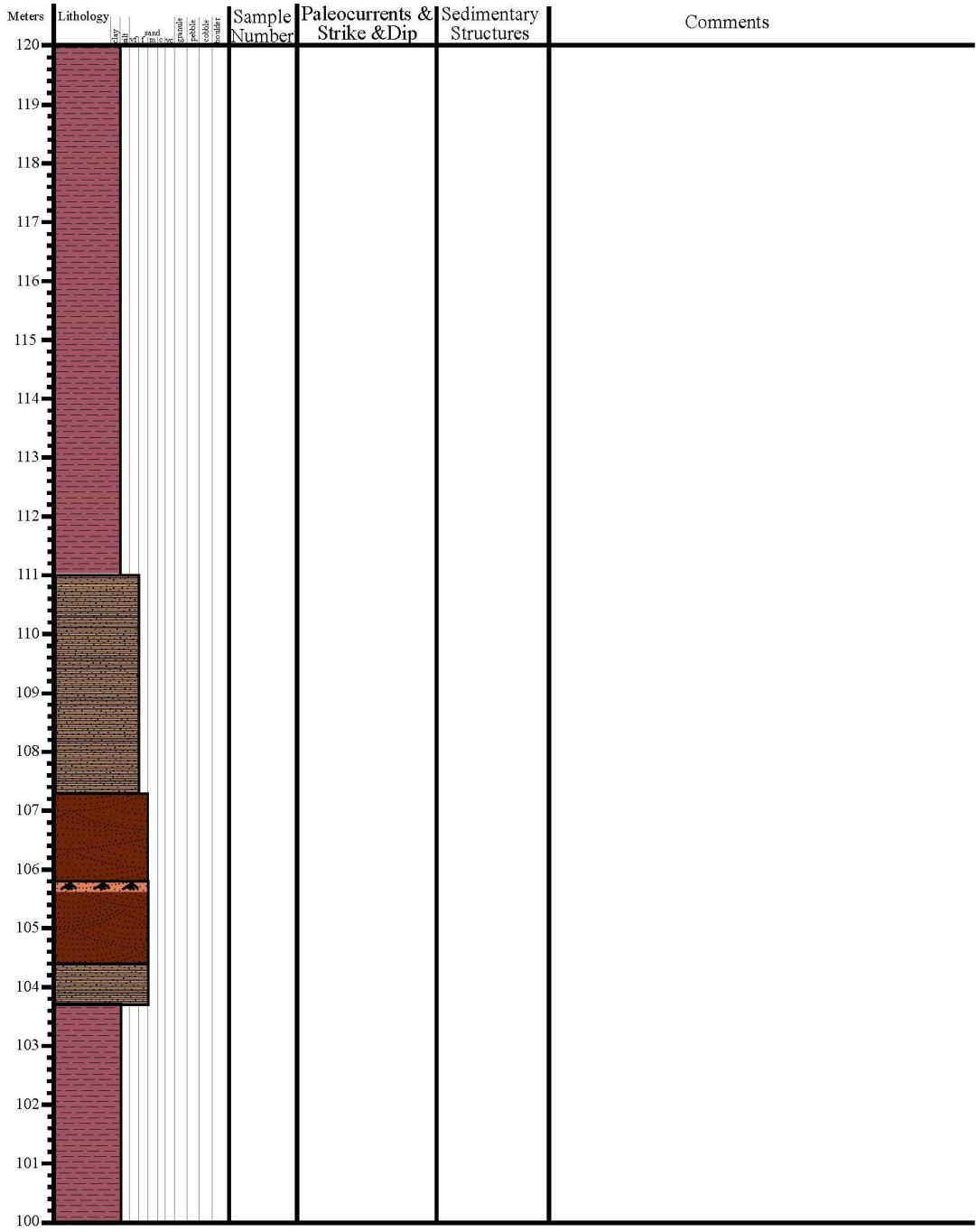

Measured Section 2: The Hat (pg. 7)

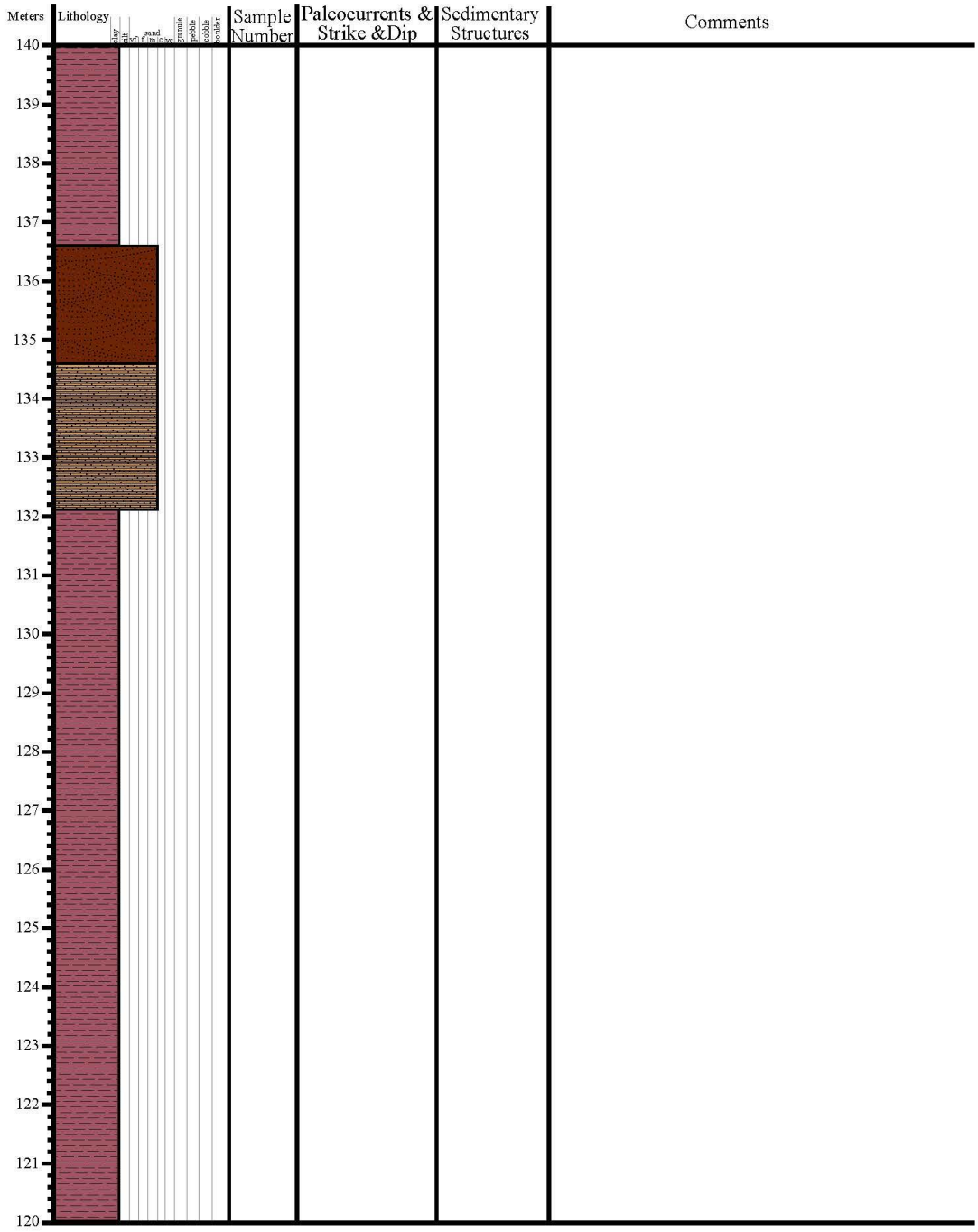

pg #

Measured Section 2: The Hat (pg. 8)

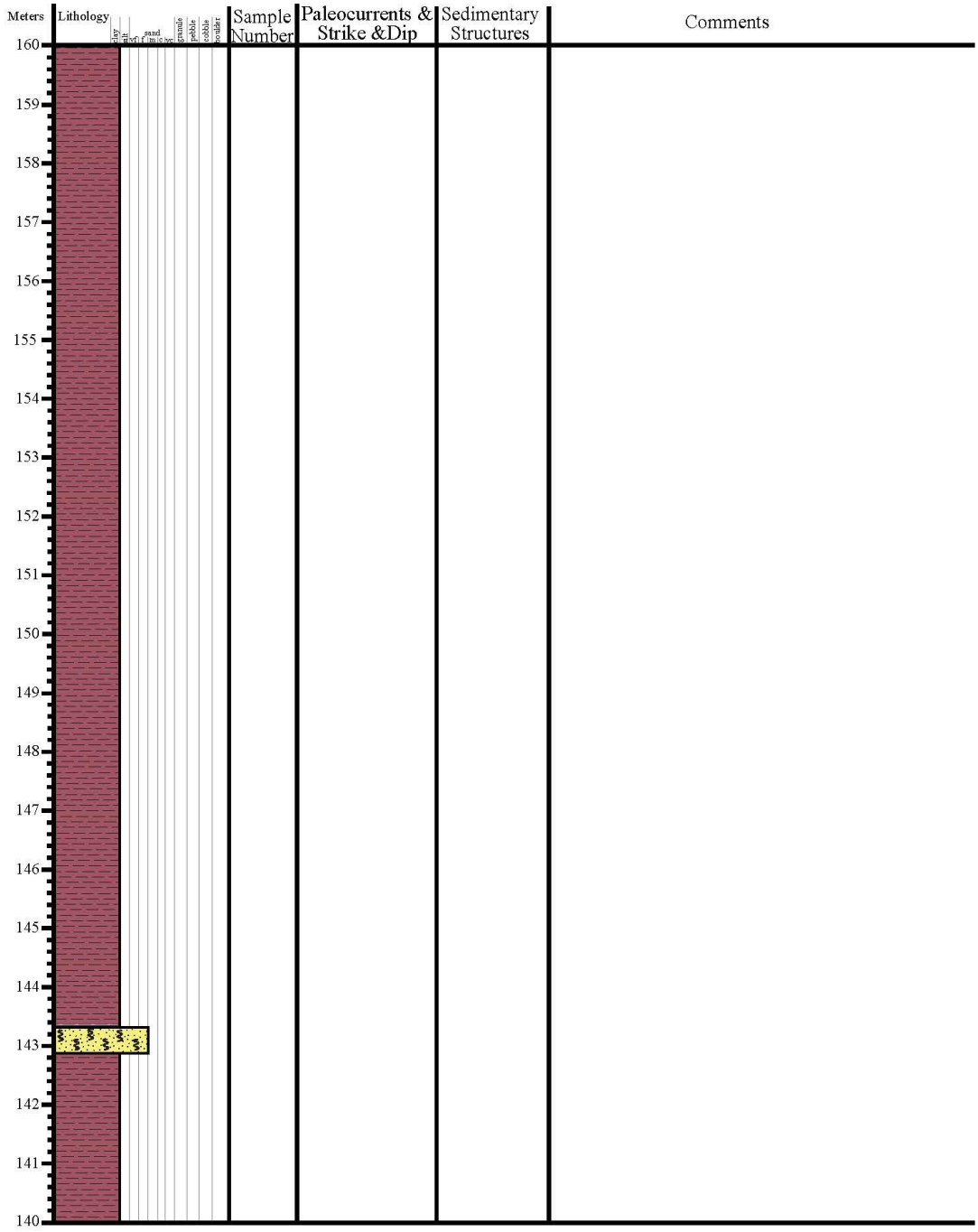

Measured Section 2: The Hat (pg. 9)

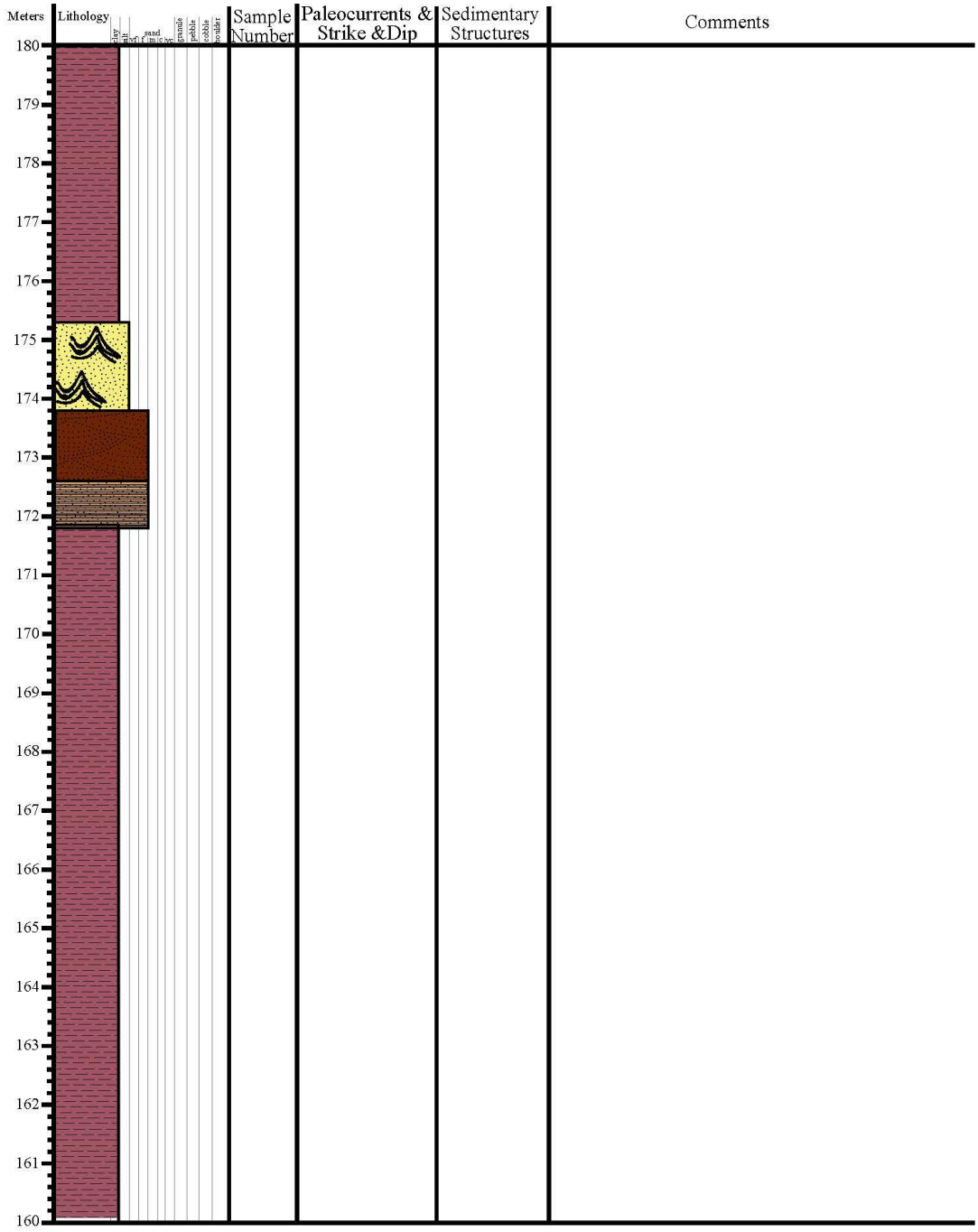

Measured Section 2: The Hat (pg. 10)

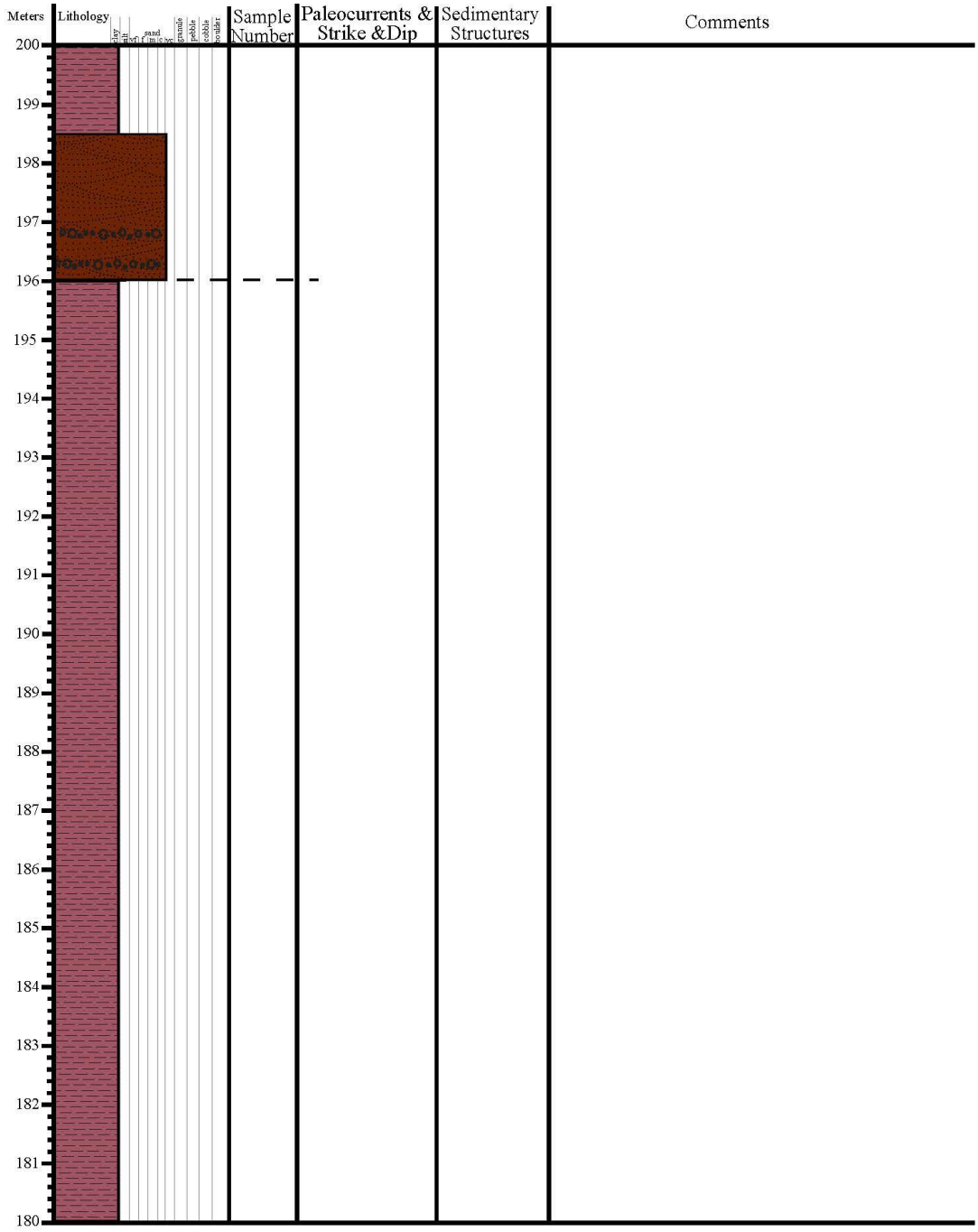

Measured Section 2: The Hat (pg.11)

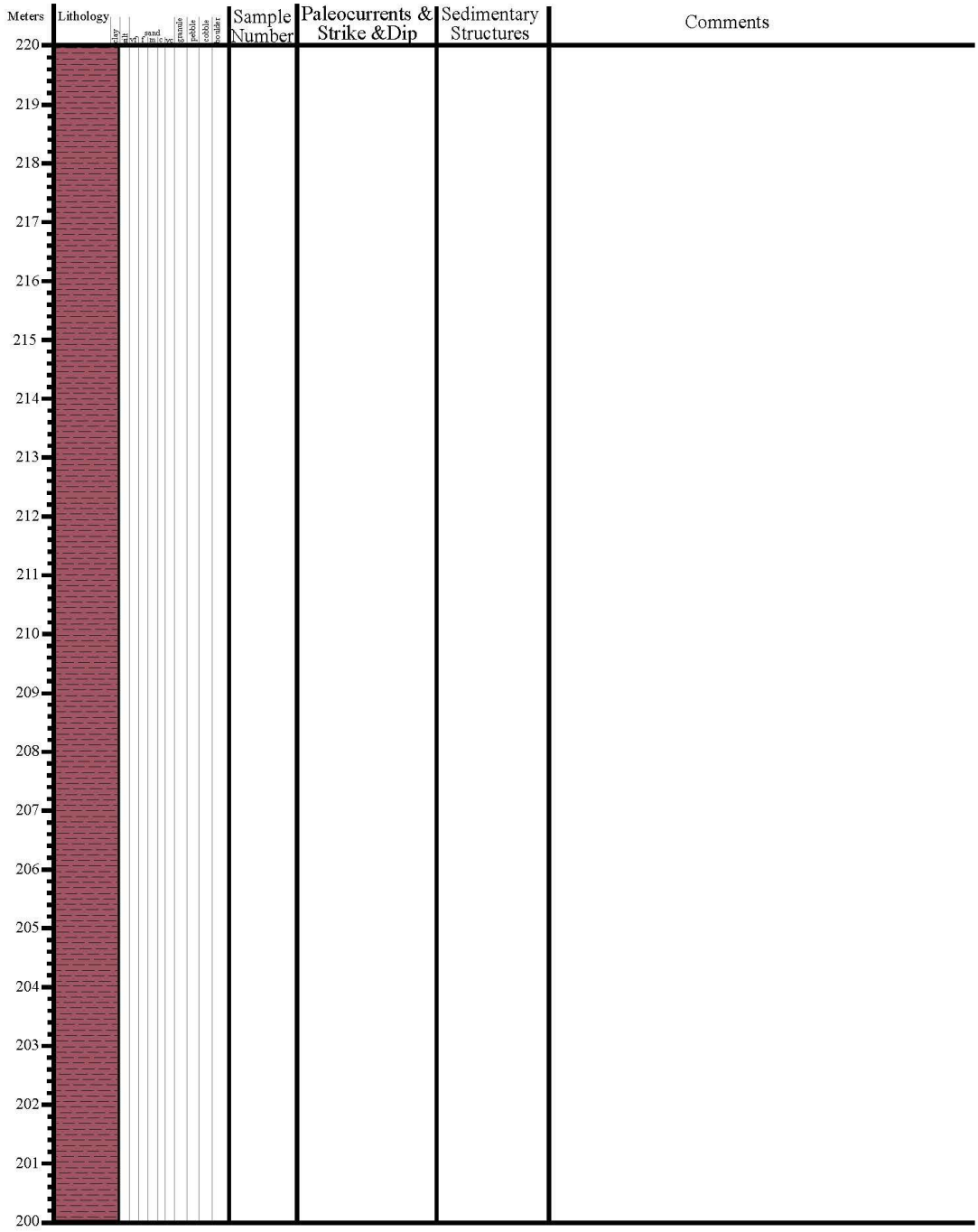

Measured Section 2: The Hat (pg. 12)

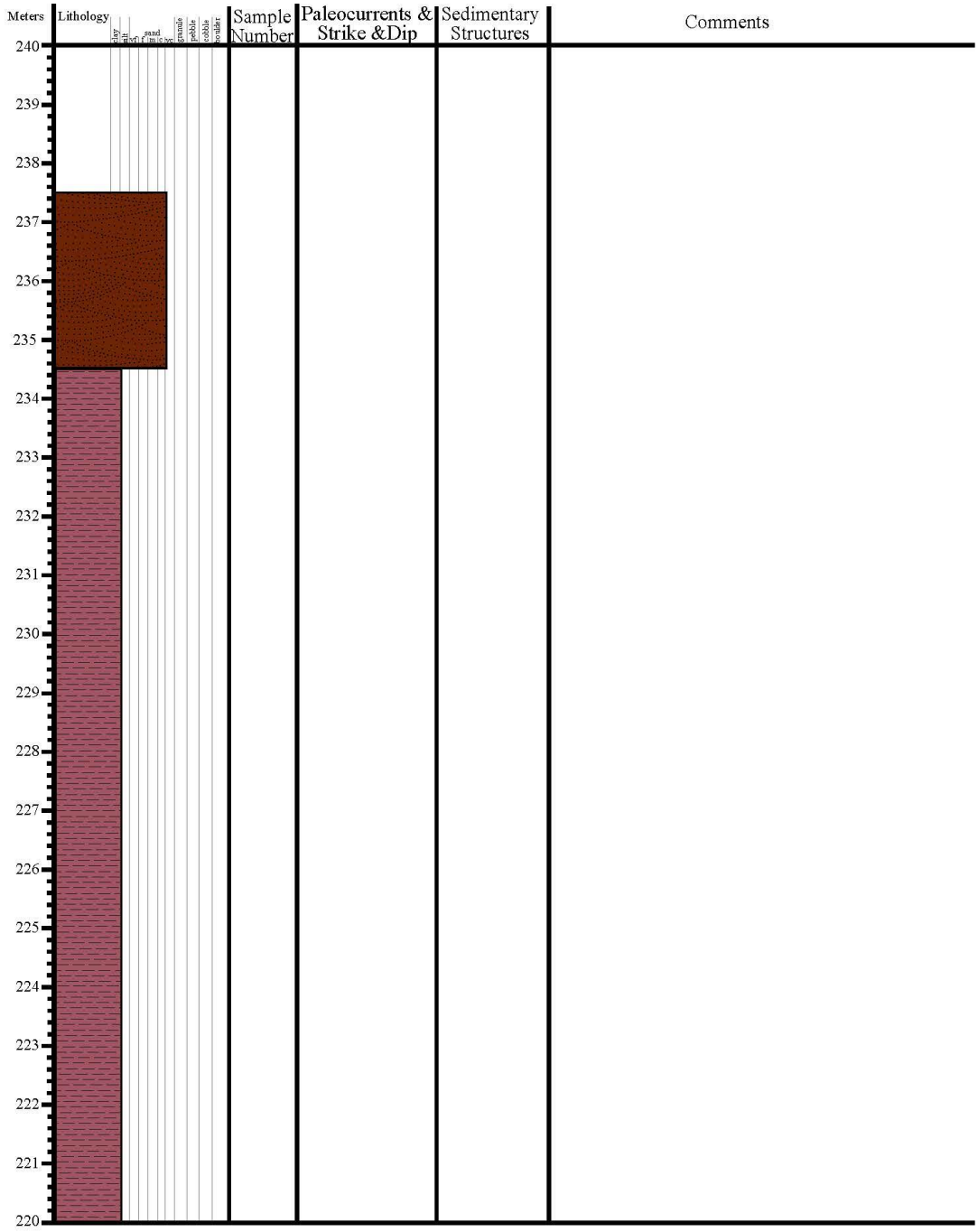

Measured Section 3: The Hat (pg. 1)

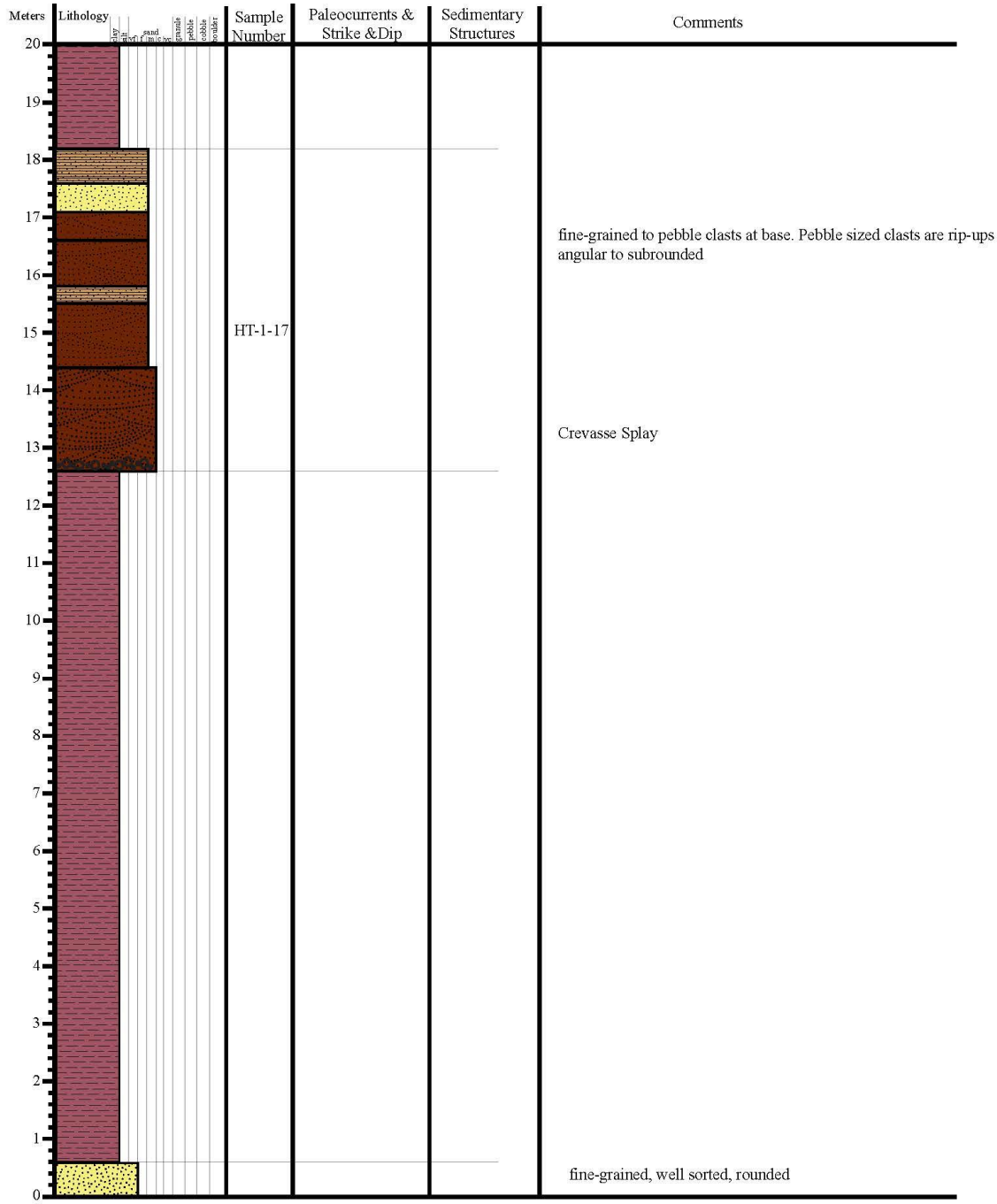

Measured Section 3: The Hat (pg. 2)

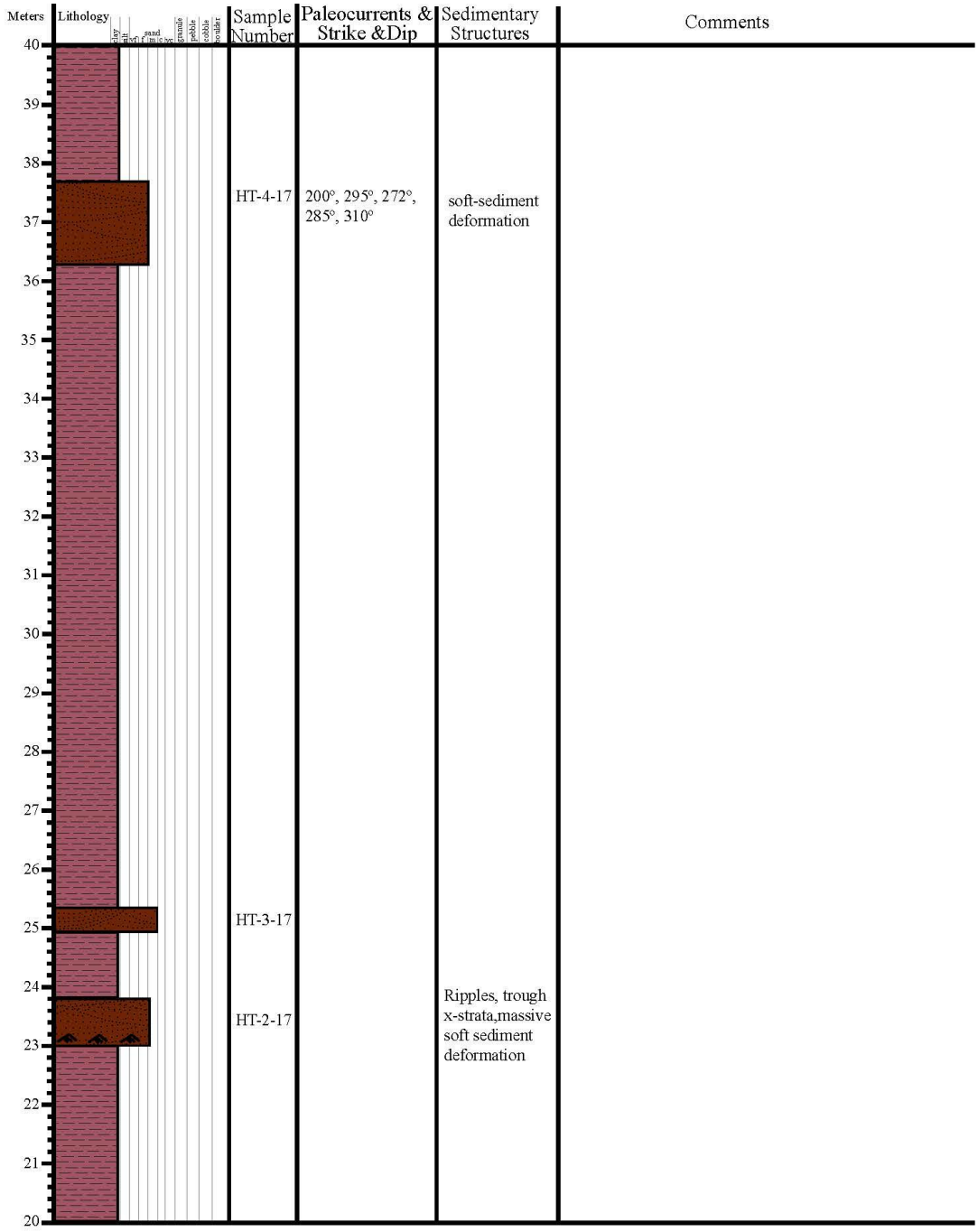

Measured Section 3: The Hat (pg. 3)

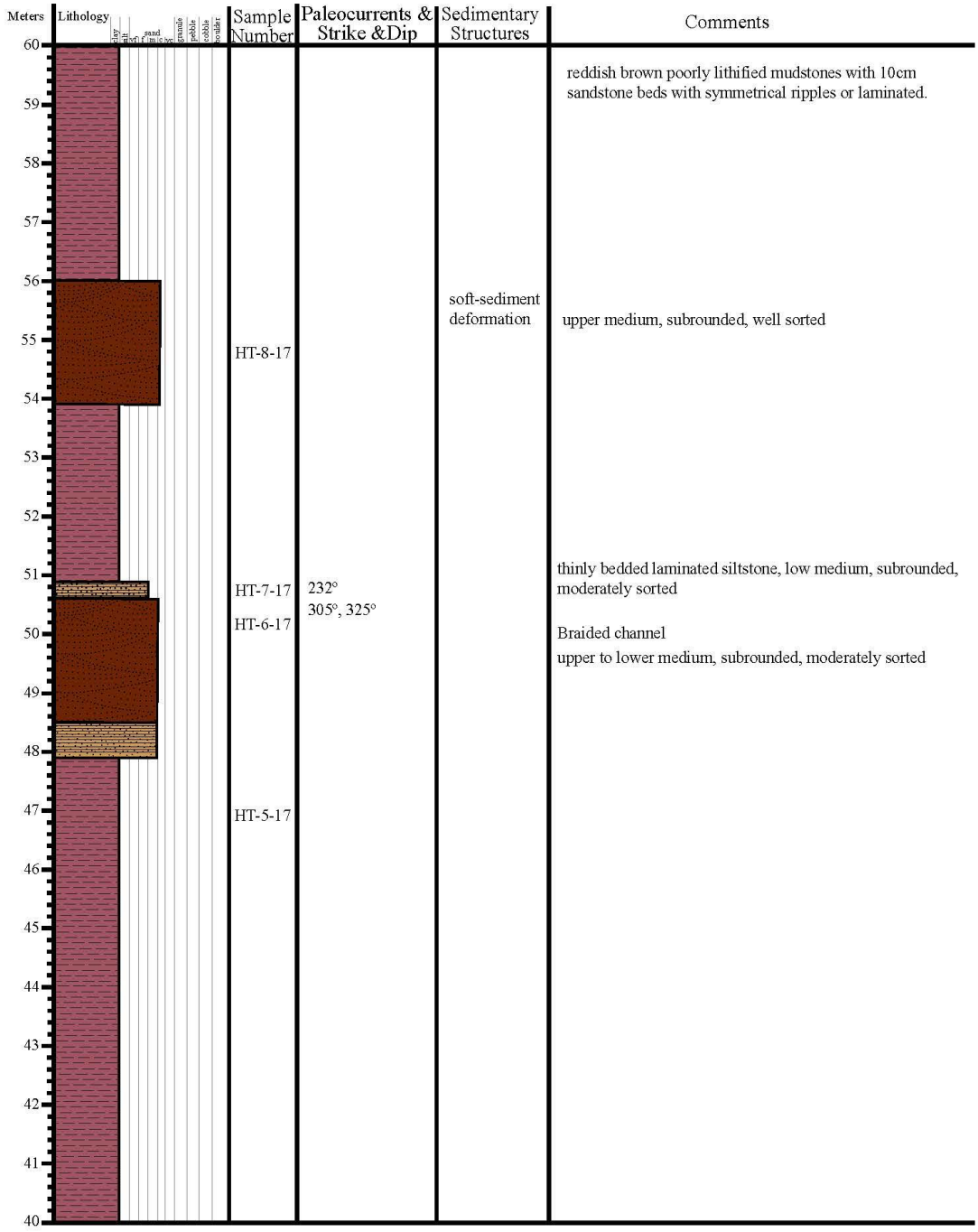

Measured Section 3: The Hat (pg. 4)

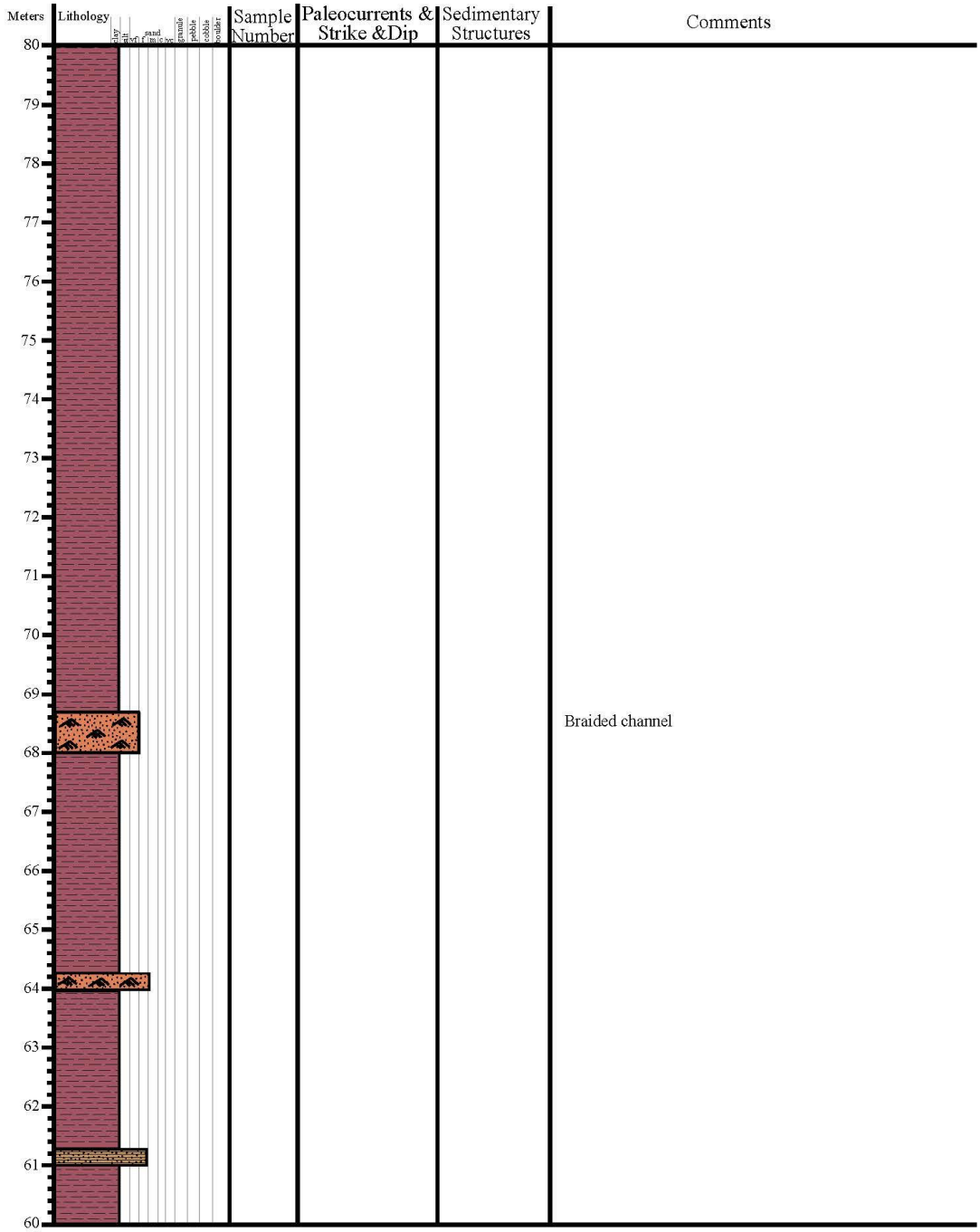

Measured Section 3: The Hat (pg. 5)

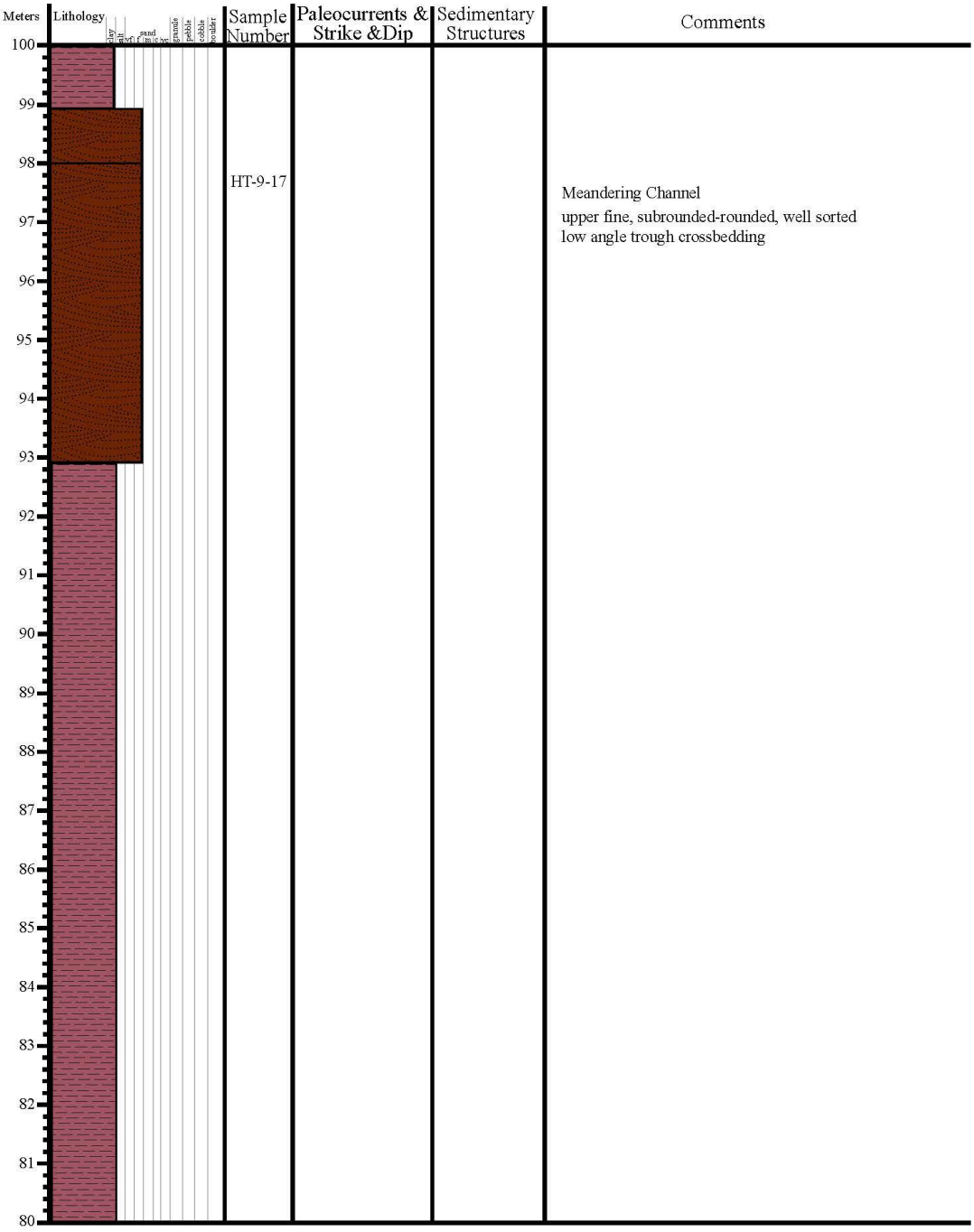

Measured Section 3: The Hat (pg. 6)

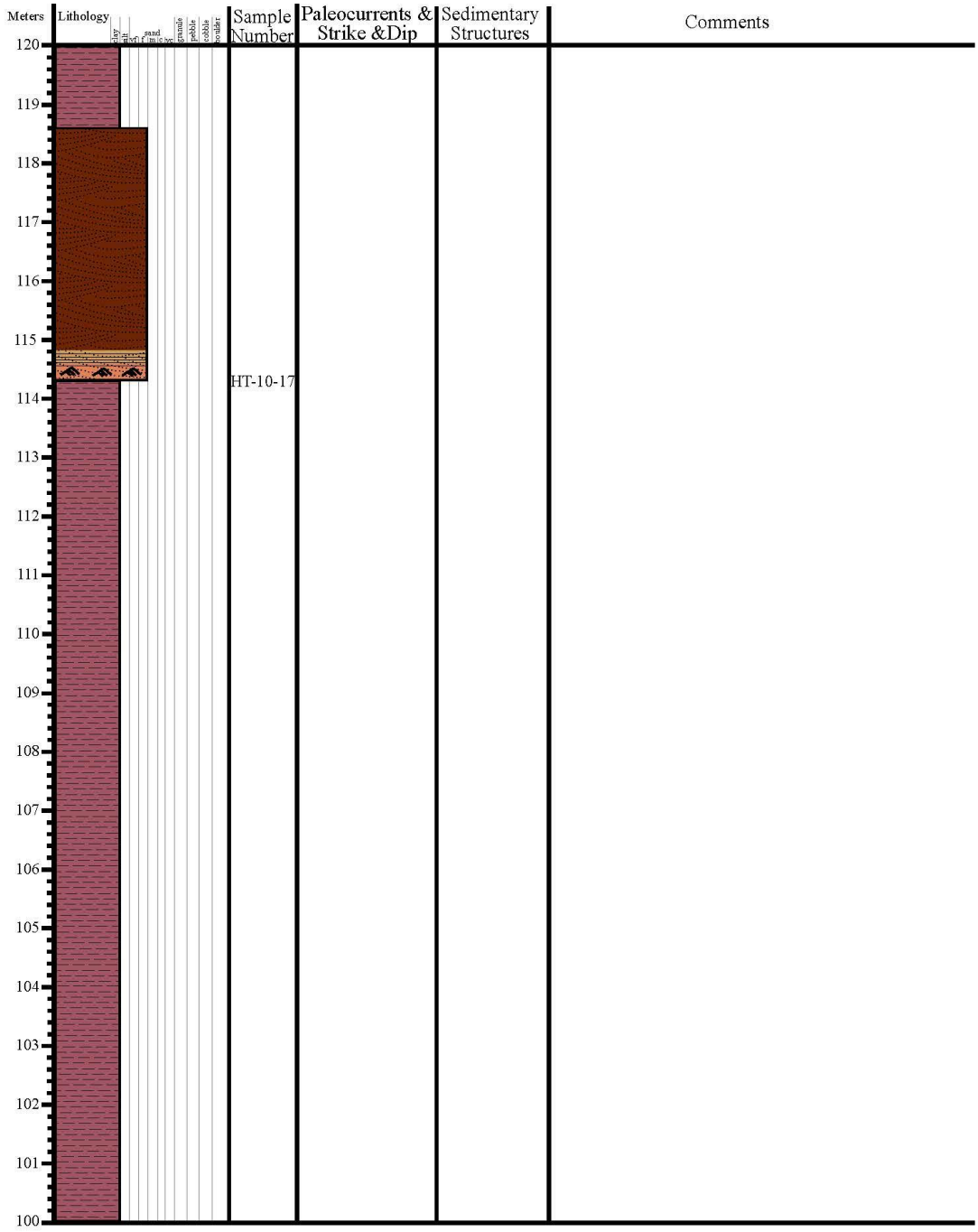

Measured Section 3: The Hat (pg. 7)

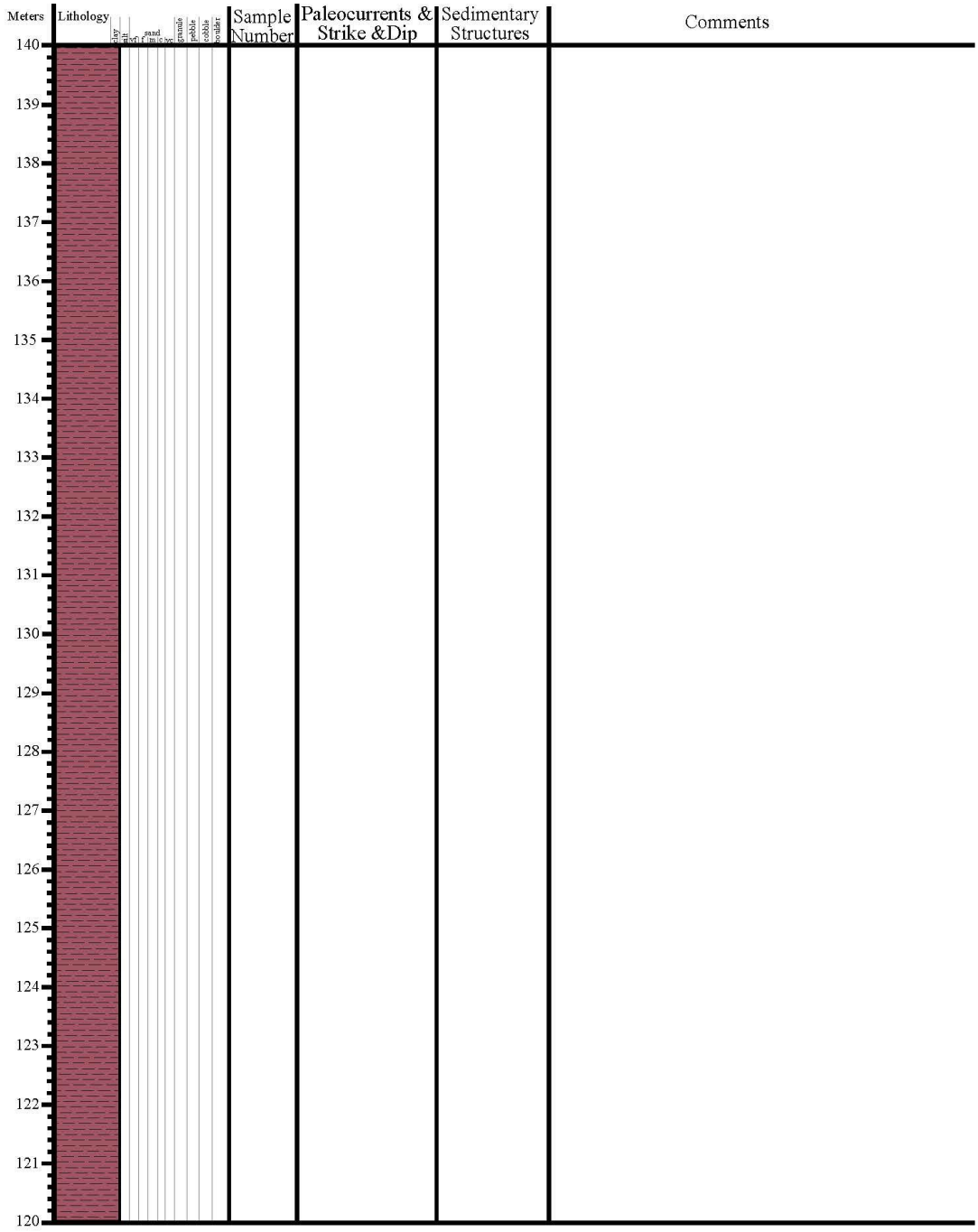

Measured Section 3: The Hat (pg. 8)

Start
End

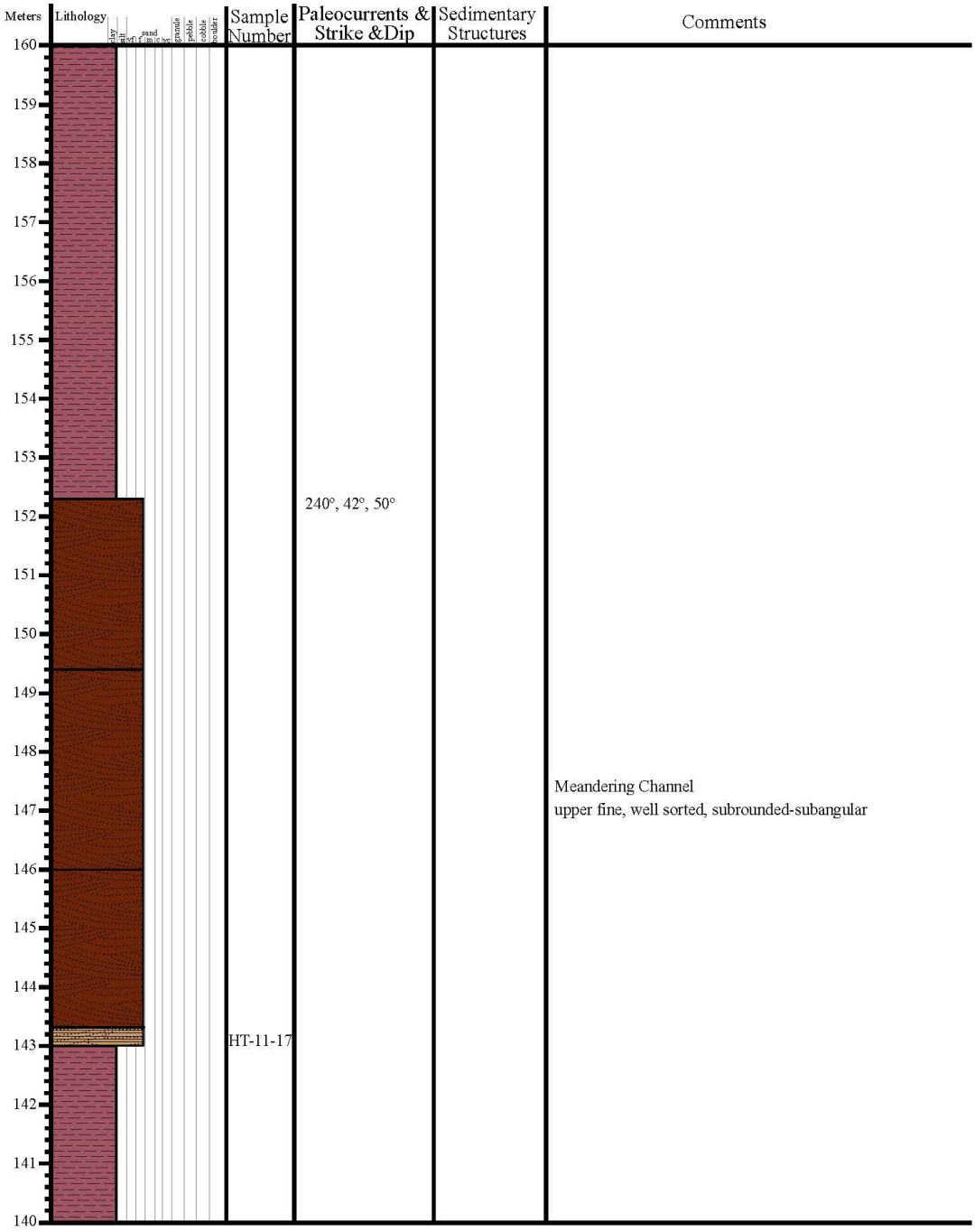

Measured Section 3: The Hat (pg. 9)

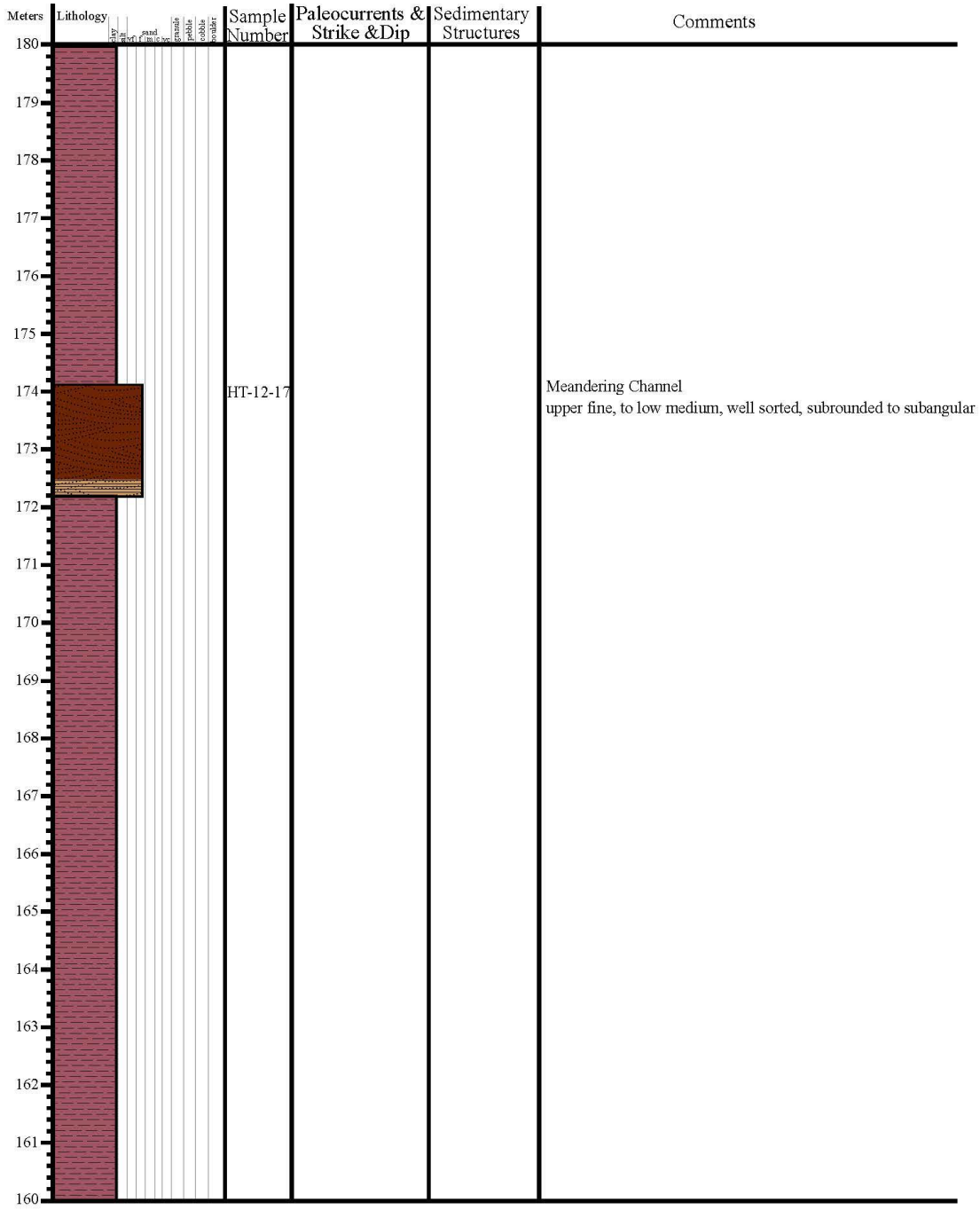

Measured Section 3: The Hat (pg. 10)

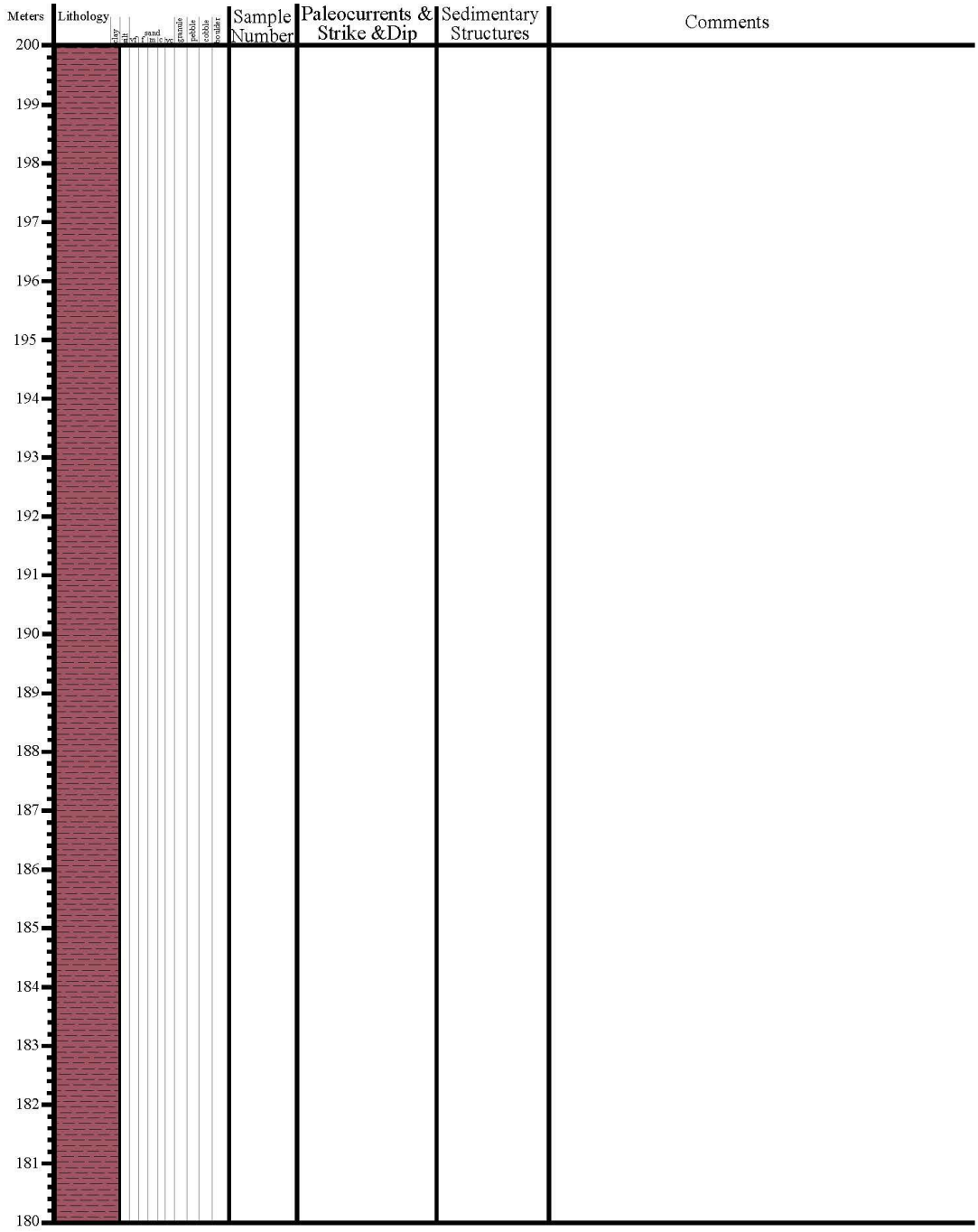

Measured Section 3: The Hat (pg. 11)

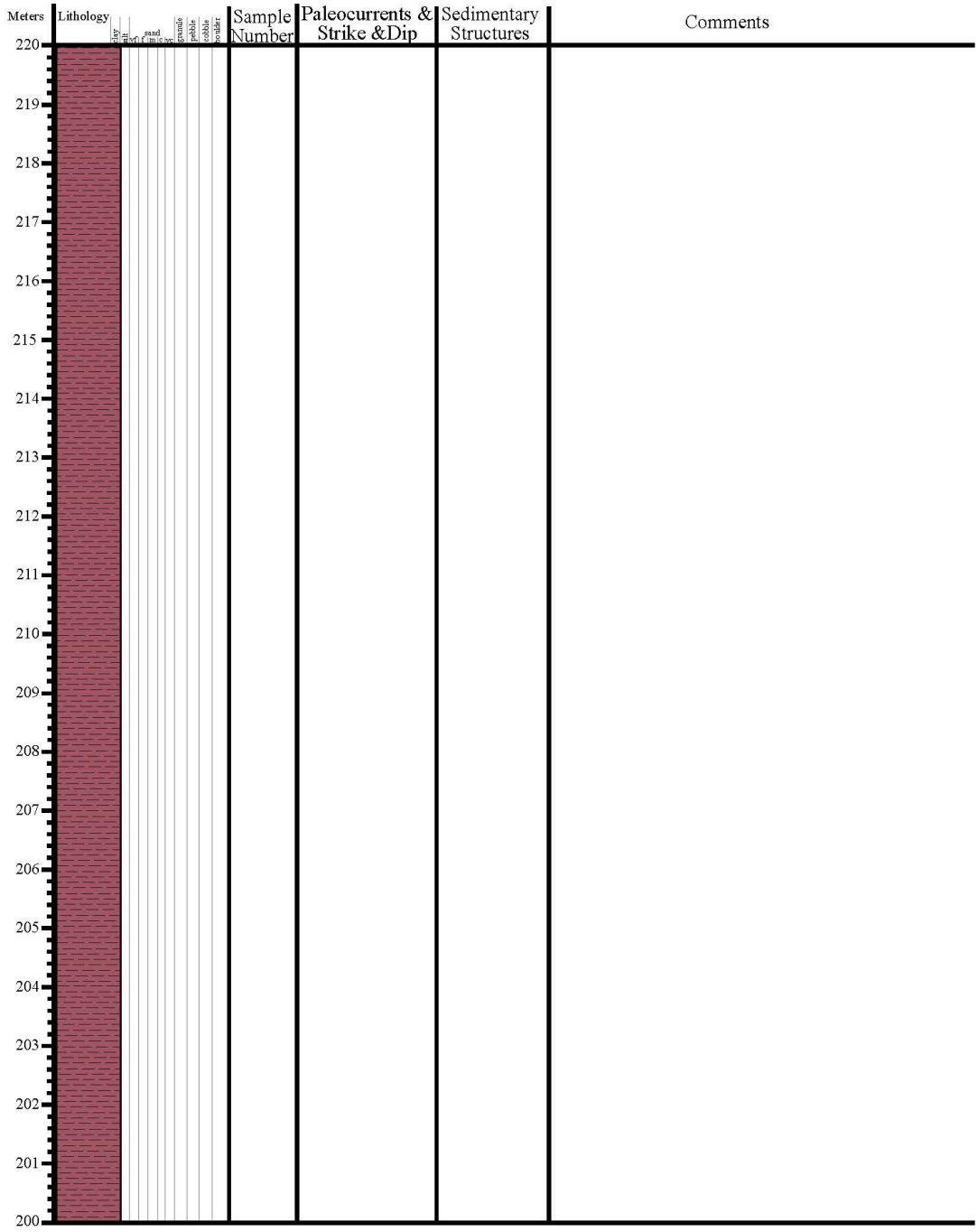

Measured Section 3: The Hat (pg. 12)

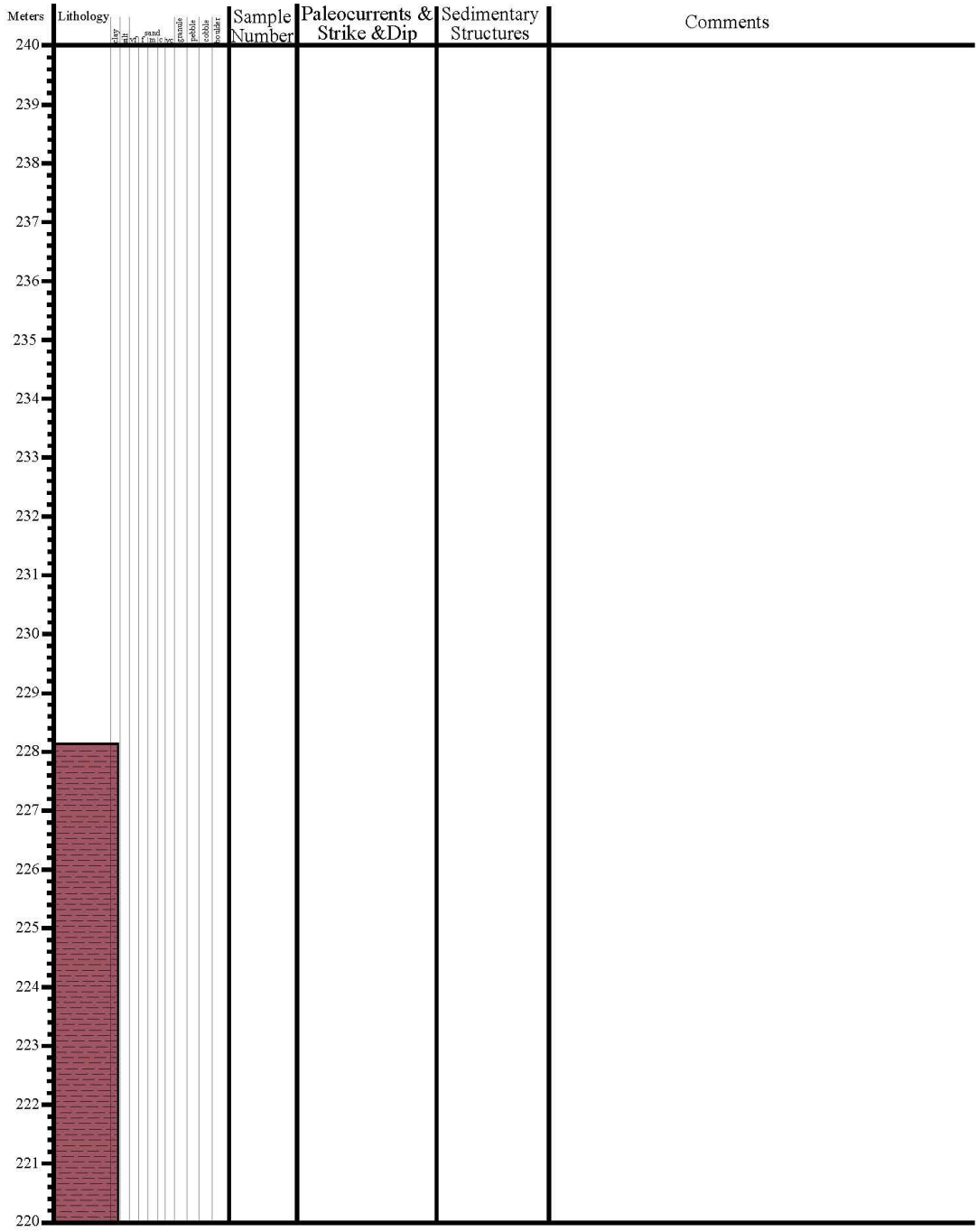

Measured Section 4: The Hat (pg. 1)

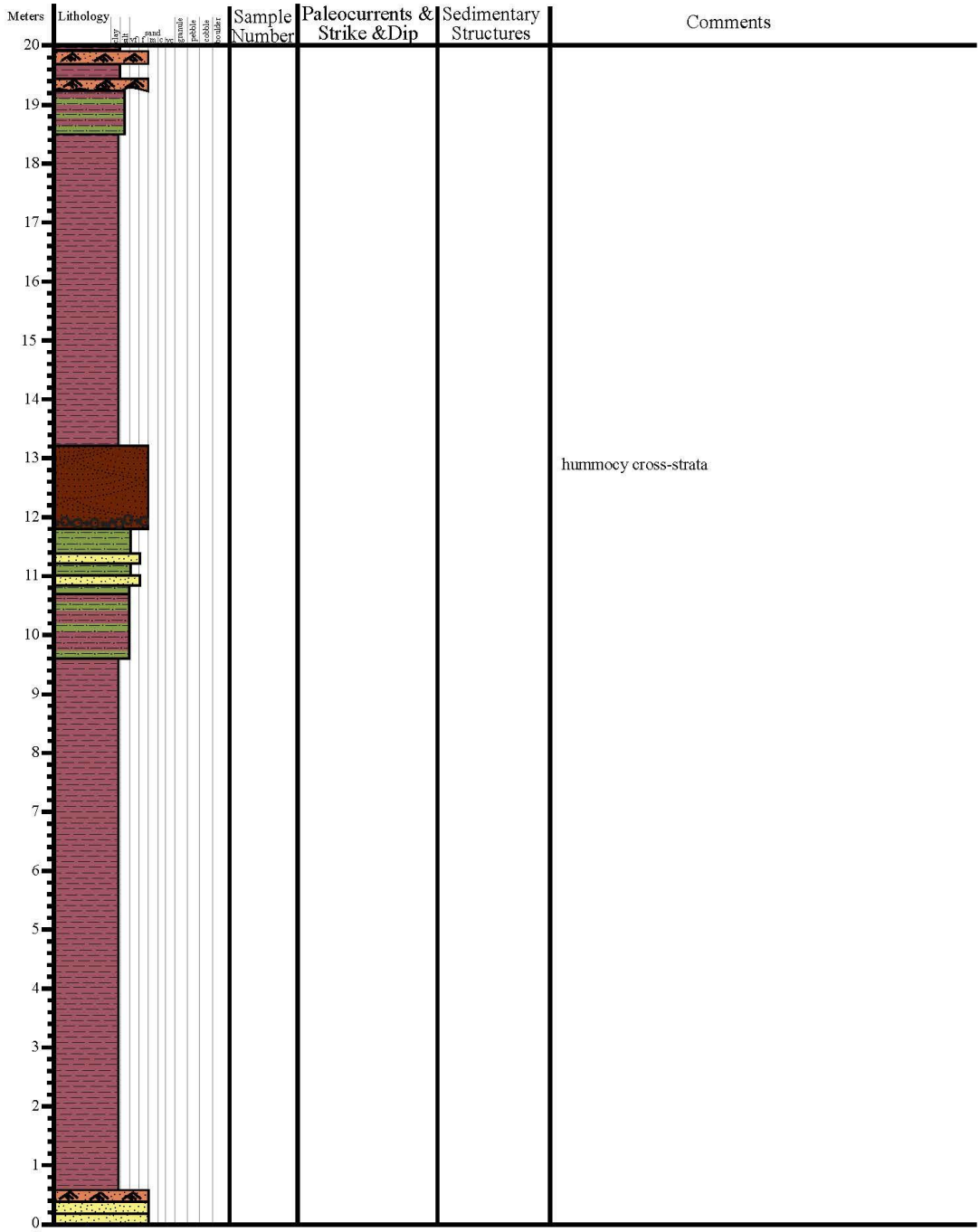

Measured Section 1: The Hat (pg. 2)

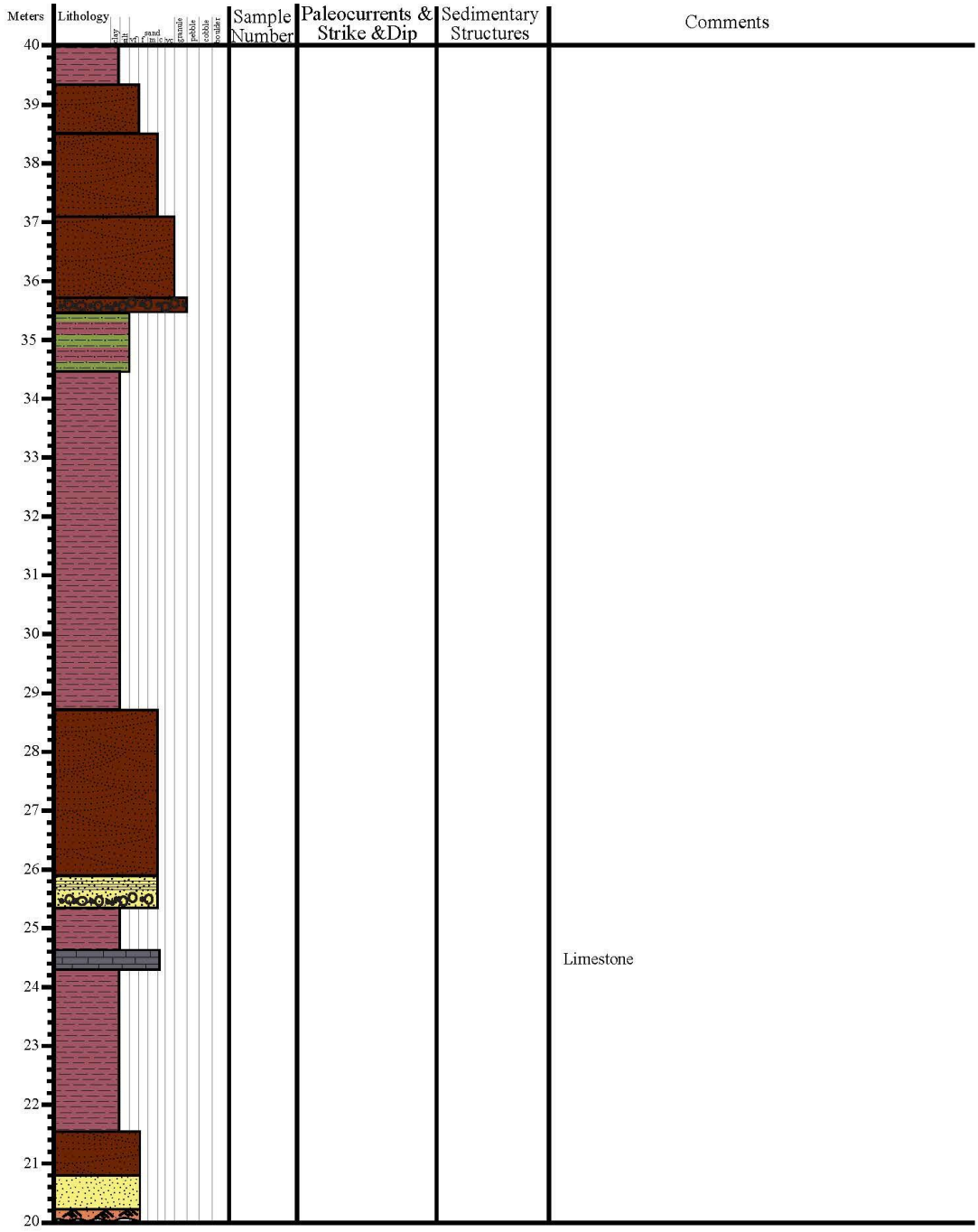

pg #

Measured Section 4: The Hat (pg. 3)

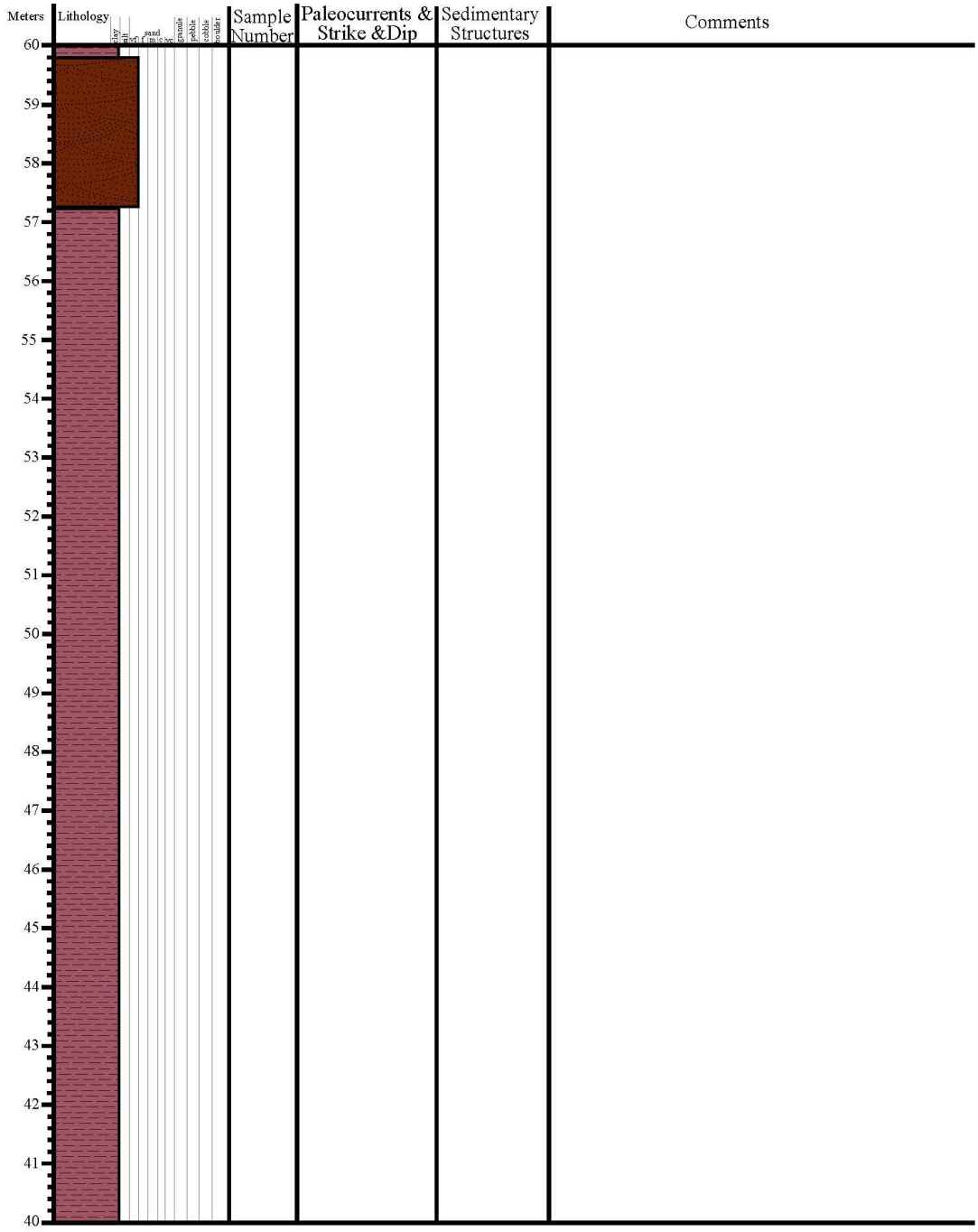

Measured Section 4: The Hat (pg. 4)

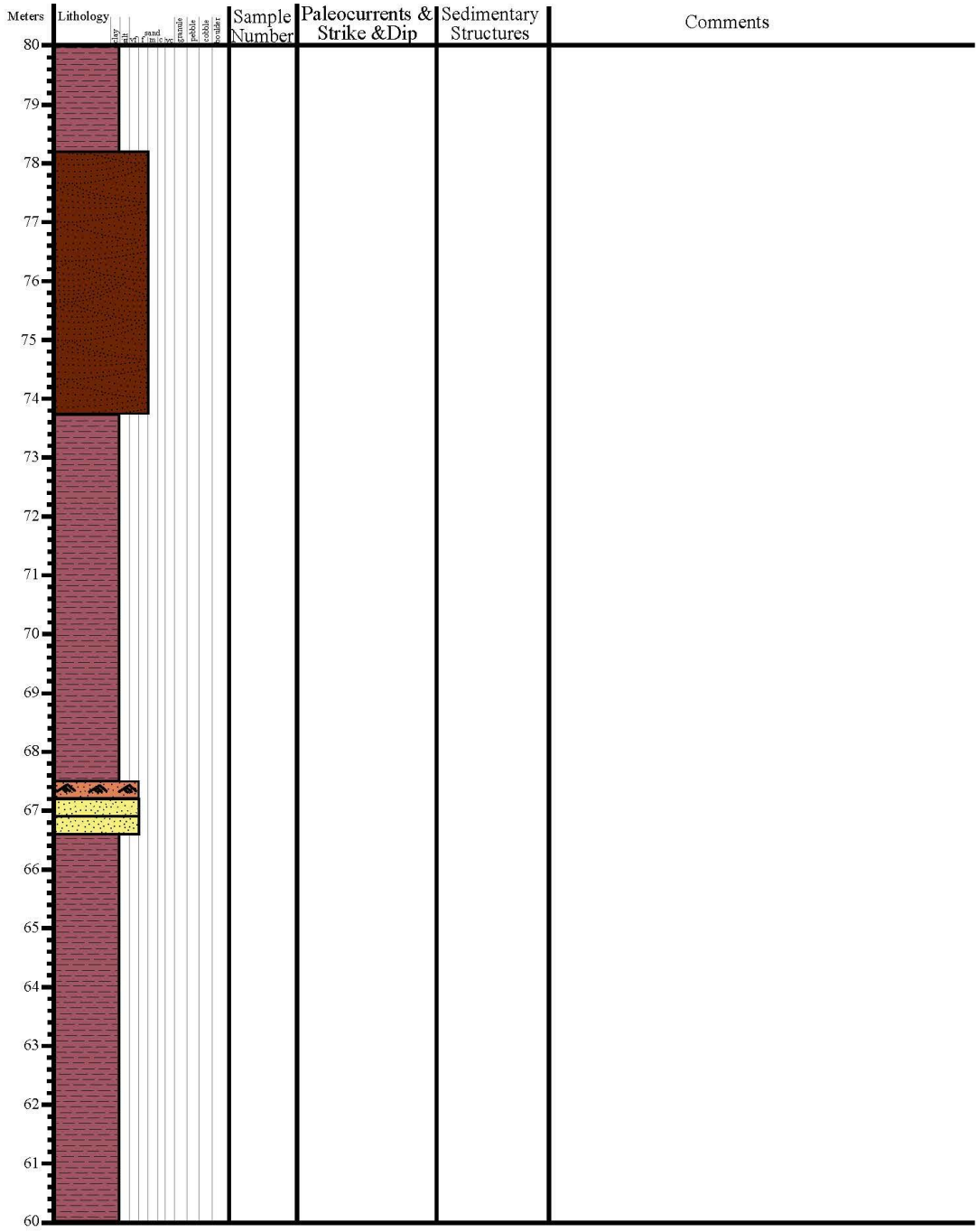

Measured Section 4: The Hat (pg. 5)

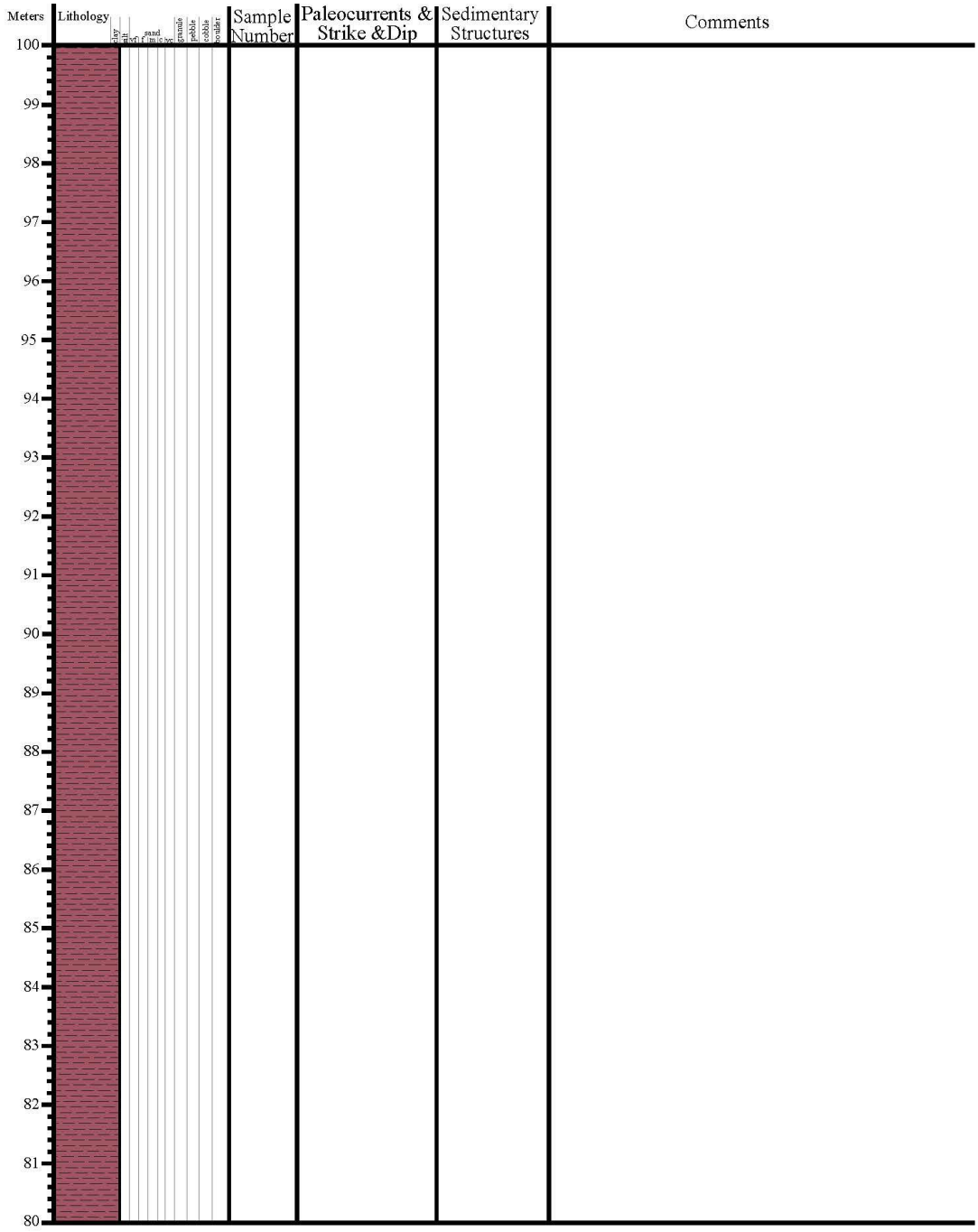

Measured Section 4: The Hat (pg. 6)

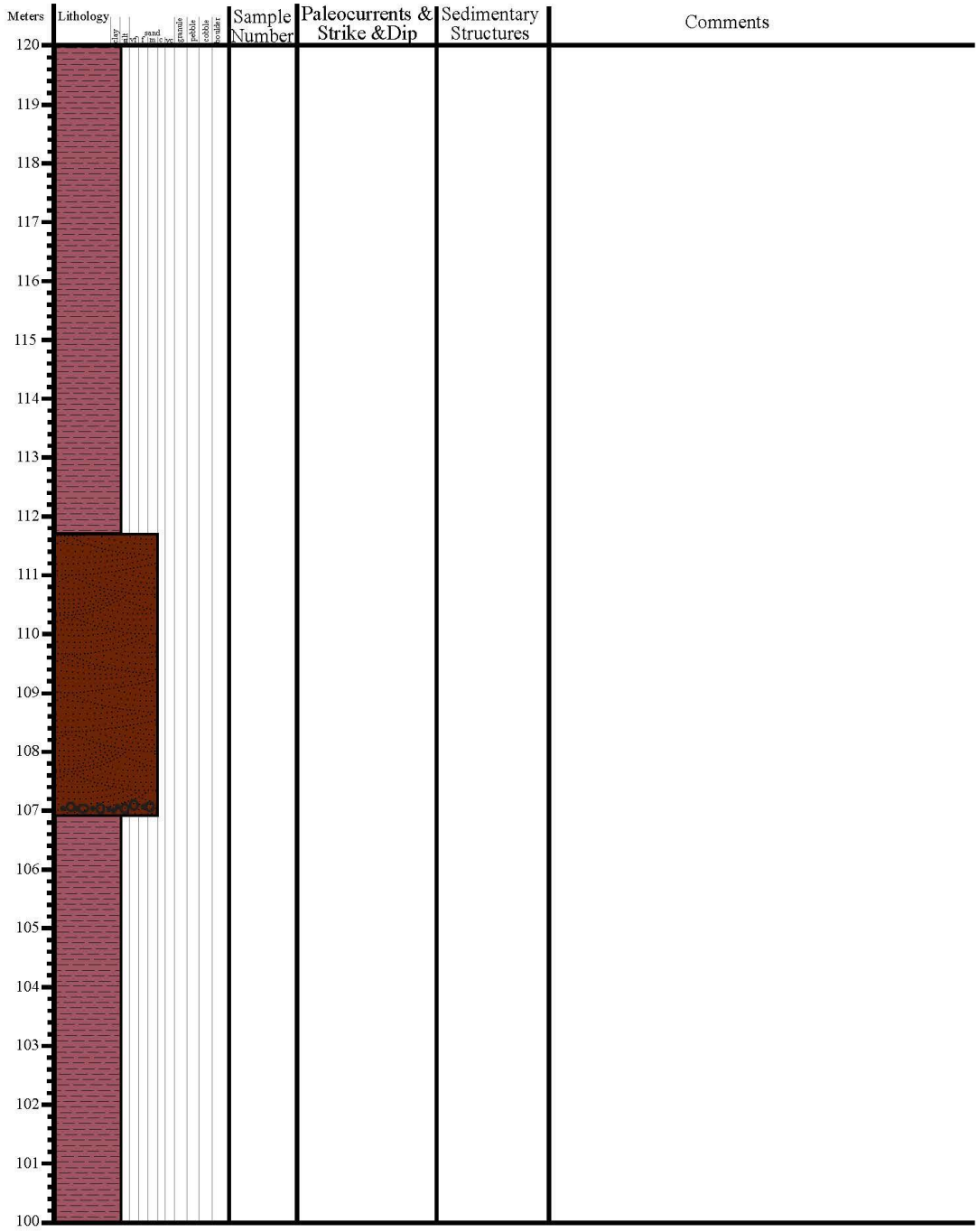

Measured Section 4: The Hat (pg. 7)

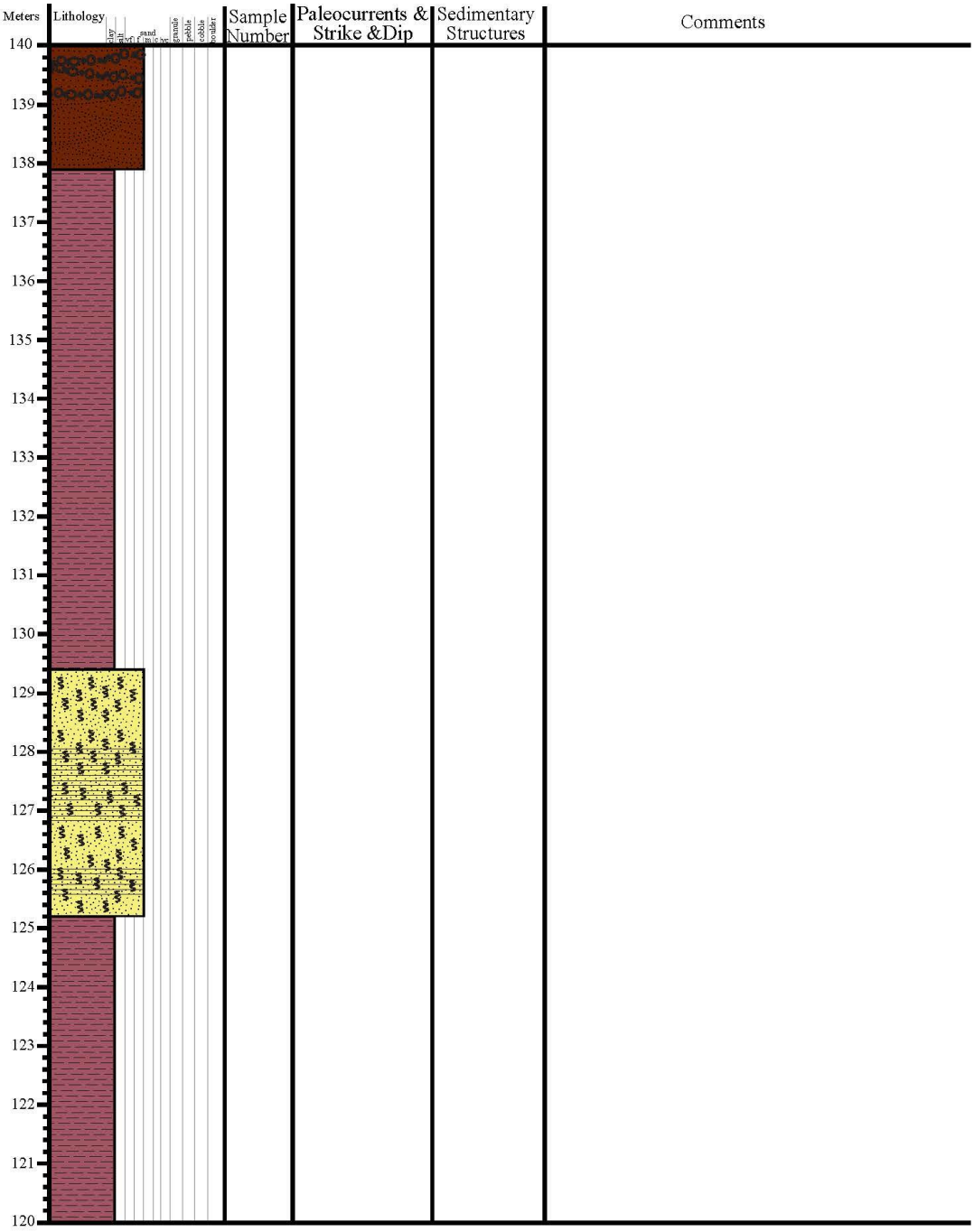

Measured Section 4: The Hat (pg. 8)

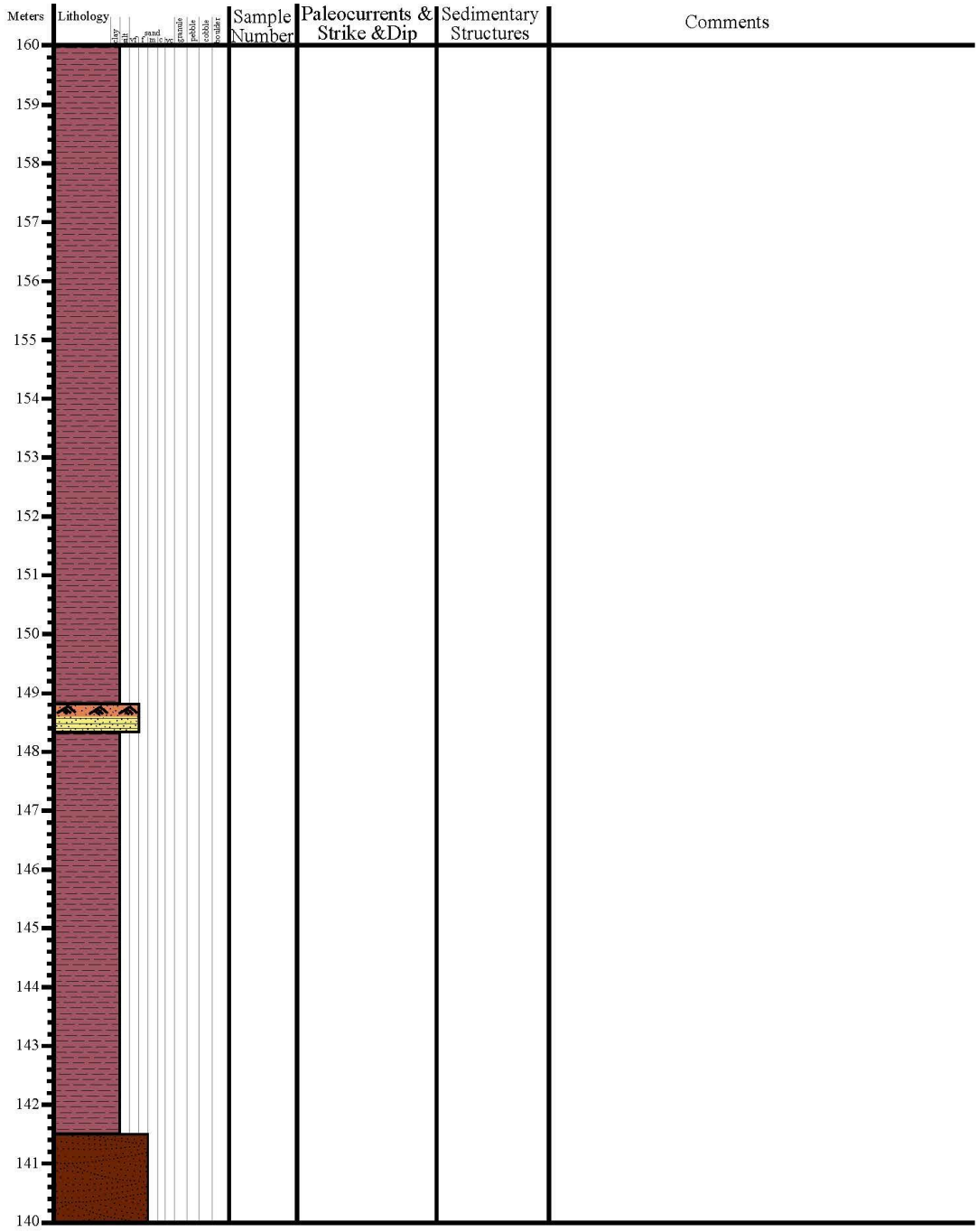

Measured Section 4: The Hat (pg. 9)

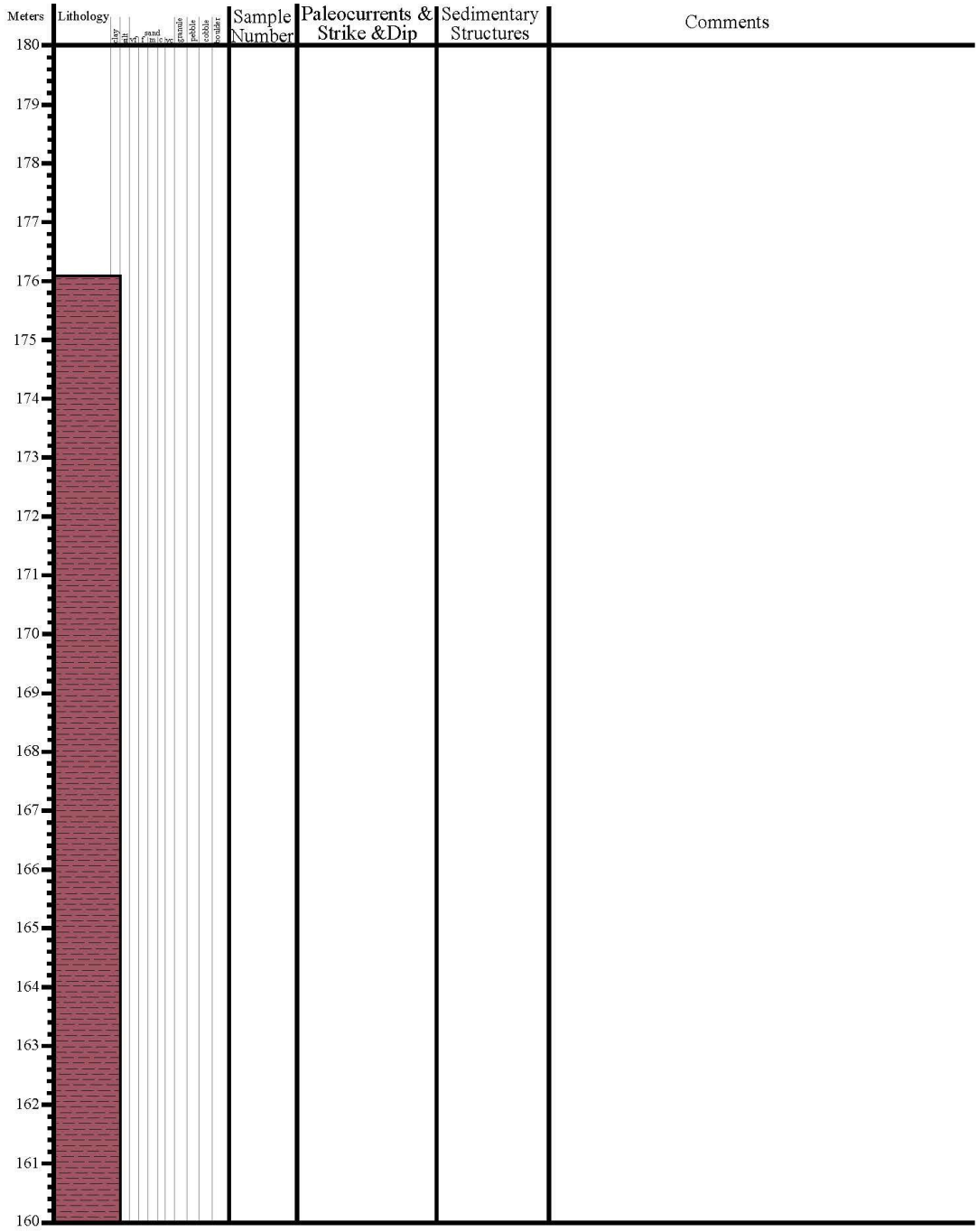

Vita

Claire Henry Bailey was born and raised in San Francisco, California. It was in San Francisco at the end of her freshman year of high school she discovered her interest in geology. As a high school student, she participated in an NSF funded program called SF-ROCKS where she completed a research project focused on earthquakes and presented this research at the Fall 2003 AGU annual meeting held in San Francisco, CA. Her participation in the SF-ROCKS program throughout high school inspired her to pursue an undergraduate degree in geology at San Francisco State University. During her undergraduate experience she participated in the NSF funded research experience for undergraduates (REU) at the Saint Anthony Falls Laboratory at the University of Minnesota and Louisiana State University. During this she discovered her passion for sedimentology and stratigraphy. After graduating with a B.S. in geology from San Francisco State she moved on to a M.S. in geology at California State University Northridge where she received full funding through the NSF Bridge to Doctorate program. In Northridge her masters focused on the provenance of sandstones of the Canterbury Basin in South Island New Zealand. After completing her M.S. she started a PhD in geology at The University of Texas at El Paso. During her time at UTEP she was a teaching assistant for introductory environmental science and geology labs. She was also an NSF GK-12 fellow where she worked with biology and chemistry high school teachers. She received several other scholarships and grants from West Texas Geologic Society, SIPES, AAPG SWS, the Geologic Society of America, and ExxonMobil. She was the 2018 recipient of the Bruce Davidson Memorial award for service to her department. She was the president of the El Paso Geologic Society while they hosted the AAPG SWS meeting in El Paso, served as delegate for the society, was nominated by EPGS and received a distinguished service award from the SWS AAPG. Contact Information: Claireb415@gmail.com